Design, synthesis, and biochemical evaluation of guanidine-based derivatives targeting protein kinases

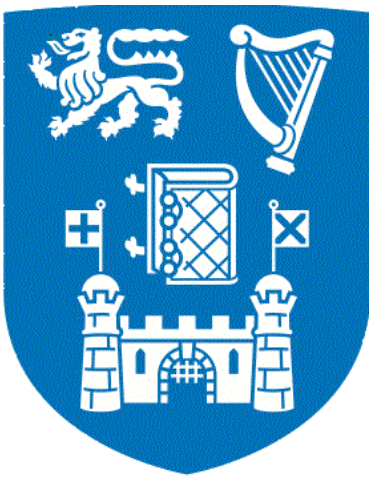

A thesis presented to the University of Dublin for the degree of Doctor of Philosophy

Helene Bikorimana Mihigo, BSc

Under the supervision of Prof. Isabel Rozas

School of Chemistry

Trinity College Dublin

2023

Declaration

This work comprises a doctoral thesis submitted for the consideration of Trinity College Dublin.

I declare that this thesis has not been submitted as an exercise for a degree at this or any other university and it is entirely my own work, with due acknowledgement and reference given to the work of others, where appropriate.

I agree to deposit this thesis in the University's open access institutional repository or allow the Library to do so on my behalf, subject to Irish Copyright Legislation and Trinity College Library conditions of use and acknowledgement.

……

Helene Bikorimana Mihigo, BSc.

2023

Trinity College Dublin

Acknowledgements

First I would like to thank my supervisor professor Isabel Rozas, for the big opportunity that she gave me, for the constant support, both academically and personal, she gave me throughout my time in Trinity College Dublin.

A big thank you to the Rozas group members, past and present, Aaron, Jagdeep and Fillipo for their expert advices. I would like to thank the Rozas group members and my friends who have been with me throughout this experience, Yemi, Nikolina and Simon. Dr. Cristina Trujillo for being a great listener and an even better teacher. Thank you to Prof. David Grayson for his expert advice on organic synthesis. Thank you also to Prof. Daniela Zisterer (School of Biochemistry and Immunology, TCD) whose collaboration allowed me to step into the biological world and a special thanks to Dr. Rebecca Amet, who took the time to teach me everything I know about Biochemistry. Thank you also to all the 'biochemistry girls' of the 6th floor, who have always been helping me with all of my main cell related problems.

I would also like to thank Dr John O'Brien, and Dr Manuel Ruether for their NMR assistance, and Dr Gary Hessman for the Mass spectroscopy.

And finally last but not least, thank you to my late dad, David who supported me from the beginning of my academic career to his last say, and my sister, Angelique, who has held my hand (and drove me every where during throughout the pandemic) through every milestone of my life including this one as well as all of my familiy.

Dedicated to my late dad, David, and to my sisters Angelique, Michelle, and Danielle.

Abstract

Kinases are some of the most intensively pursued classes of drug targets with approximately 243 distinct kinase inhibitors making it to human trials and most of these compounds are being investigated for the treatment of cancer. However, it has been found that deregulation of kinase function is also implicated in other disorders, including immunological, neurological, metabolic, and infectious diseases. Hence, development of small-molecule kinase inhibitors for the treatment of health disorders is still a medical unmet need.

During the last 12 years Rozas' group has developed a series of guanidine-based compounds that inhibit the MAPK pathway. The first series of compounds studied, which have structural similarities to commercial protein kinase inhibitor Sorafenib, were found to inhibit the kinase B-Raf at an allosteric site. Subsequent series of derivatives were synthesised and biochemically tested, finding that these exert anticancer activity by means of a different mode of action, i.e. they do not inhibitor B-Raf. Further biochemical studies performed by our collaborators in the TBSI (Prof. D. Zisterer, School of Biochemistry and Immunology, TCD) indicate that the possible target is the STAT3/JAK2 pathway.

Throughout the present project new guanidine-based derivatives will be synthesized pursuing two different objectives. On the one hand, in a structure-based drug design strategy, derivatives of the first lead compound will be computationally studied in an in-house model of ATP-containing B-Raf, and other B-Raf crystal structures. On the other hand, in a ligand-based drug design strategy new derivatives will be prepared to further confirm the target of the second series of compounds previously prepared and together with those will be evaluated in cell lines with active STAT3/JAK2; furthermore, computational studies will be carried out to confirm that the new lead and its derivatives cannot allosterically inhibit B-Raf, but it can inhibit protein kinase involved in the STAT3/JAK2 pathway.

Abbreviations

ADP: Adenosine diphosphate

AGC: PKA, PKC, PKG

AnV: Annexin V

AP-1: Activator protein 1

APAF-1: Apoptotic protease activating factor-1

Akt: Protein kinase B

ATP: Adenosine triphosphate

Bcl-2: B-cell lymphoma 2

BINAP: 2,2'-bis(diphenylphosphino)-1,1'-binaphthyl

CADD: Computer-aided drug design

CAMK: Calcium/calmodulin-dependent protein kinase

CCl_4: Carbon tetrachloride

CH_2Cl_2: Dichloromethane

$CHCl_3$: Chloroform

CK1: Casein kinase 1

CMGC: CDK, MAPK, GSK3, Cdc2

CNS: Central nervous system

CRC: Colorectal cancer

Cs_2CO_3: caesium carbonate

CuI: Copper (II) Iodide

DFT: Density functional theory

DMF: dimethylformamide

DMSO: Dimethyl sulfoxide

EDCI: 1-Ethyl-3-(3-dimethylaminopropyl)carbodiimide

EGFR: Epidermal growth factor receptor

ERK: Extracellular signal–regulated kinase

EtOAc: Ethylacetate

FDA: Food and Drug Administration

GAPDH: Glyceraldehyde 3-phosphate dehydrogenase

GSK3: Glycogen synthase kinase 3

HCl: Hydrochloric acid

HCT116: Human colon cancer cell line

HDAC: histone deacetylase

HDI: human development index

HeLa: Henrietta Lacks

HgCl2: Mercury (II) chloride

HL-60: Human promyelocytic leukemia cells

HPLC: High-performance liquid chromatography

IC50: Concentration of an inhibitor where the response (or binding) is reduced by half

IL: interleukin

IMHB: Intra molecular hydrogen bond

JAK: Janus kinase

K_2CO_3: Potassium carbonate

LBDD: Ligand-based drug design

MAPK: Mitogen-activated protein kinase

MCF-7: Michigan cancer foundation-7

Mcl-1: Induced myeloid leukemia cell differentiation protein

MEK: Mitogen-activated protein kinase

MeOH: Methanol

MM: Multiple myeloma

mTOR: Mechanistic target of rapamycin

NaH: Sodium hydride

NaO^tBu: Sodium *tert*-butoxide

NCI: National Cancer Institute

NEt_3: Triethylamine

NMR: Nuclear magnetic resonance

$Pd_2(dba)_3$: Tris(dibenzylideneacetone)dipalladium(0)

PDGF: Platelet-derived growth factor

PI: Propidium iodide

PI3K: Phosphoinositide 3-kinase

PKA: protein kinase A

PKI: Protein kinase inhibitors

PS: Phosphatidylserine

Raf: Rapidly accelerated fibrosarcoma

RTK: Receptor tyrosine kinase

SAR: Structure activity relationship

SBDD: Structure-based drug design

SMKI: Small molecules kinase inhibitors

S_NAR: Nucleophilic aromatic substitution

$SnCl_2 \cdot 2H_2O$: Tin (II) chloride dihydrate

$SOCl_2$: Thionyl chloride

STAT: Signal transducer and activator of transcription

STE: Homologs of yeast Sterile

TFA: Trifluoroacetic acid

TFAA: Trifluoroacetic anhydride

TGFα/β: Tumour growth factor α/β

THF: Tetrahydrofuran

TKL: Tyrosine kinase-like

TLC: Thin-layer chromatography

TR-FRET: Time resolved fluorescence resonance energy transfer

VEGF: Vascular endothelial growth factor

Xantphos: 4,5-Bis(diphenylphosphino)-9,9-dimethylxanthene

Table of Contents

Chapter 1- Introduction

1.1. Cancer: general overview and statistics

Cancer is the second leading cause of death and according to the World Health Organization (WHO) it has been estimated that 19.3 million cases and 10 million deaths occurred in 2020 based on 185 countries and 36 different cancers. One in five people develop cancer in their lifetime.[1] Projections estimate that by 2040 there will be 28.4 million new cancer cases. Most will occur in low and middle income countries due to low human development index (HDI), a ranking based on country's life expectancy, education, and per capita income. Key issues in low HDI countries include lack of accessible diagnosis and treatment. For example, in 2017 26 of 35 of low income countries reported having services available to the general public.[2]

For males of all ages the most common cancers diagnosed are lung (14.3%), prostate (14.1%) and colorectum (10.6%). In females the most common cancers are breast (24.5%), colorectal (9.4%) and lung (8.4%), making breast cancer the most commonly diagnosed cancer worldwide (Figure 1.1.1).

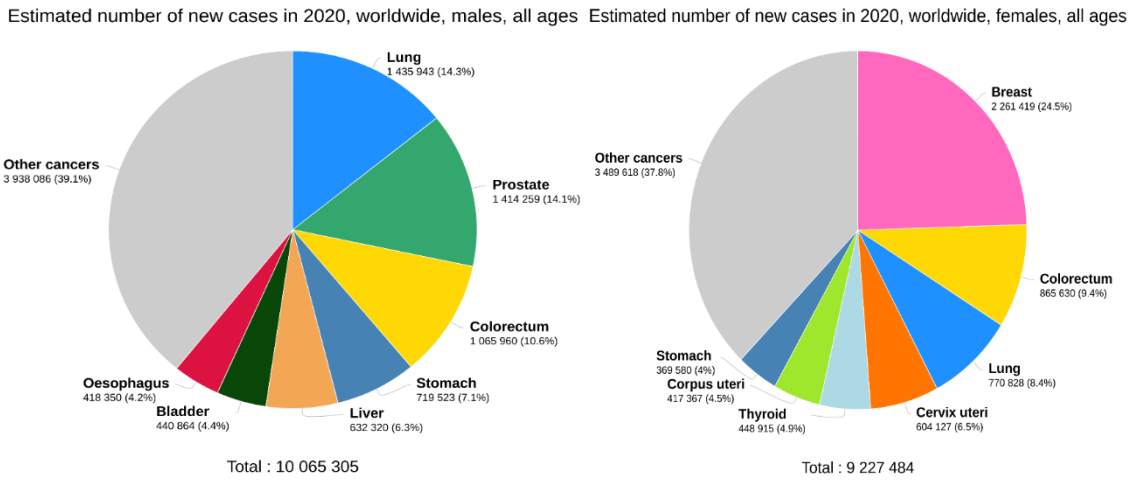

Figure 1.1.1. Estimated world cancer incidence proportions by major sites, in men, and in
women, 2020.[1]

Among men, lung cancer had the highest mortality rate reflecting its high incidence rate. Other cancers with a high mortality rate include liver (10.4%), colorectal (9.3%) and stomach (9.1%) cancers. Among woman, breast cancer has the highest mortality rate (15.5%), followed by lung, colorectal and cervix/uteri, which cause deaths among females in an estimated 13.7%, 9.5% and 7.7%, respectively (Figure 1.1.2).

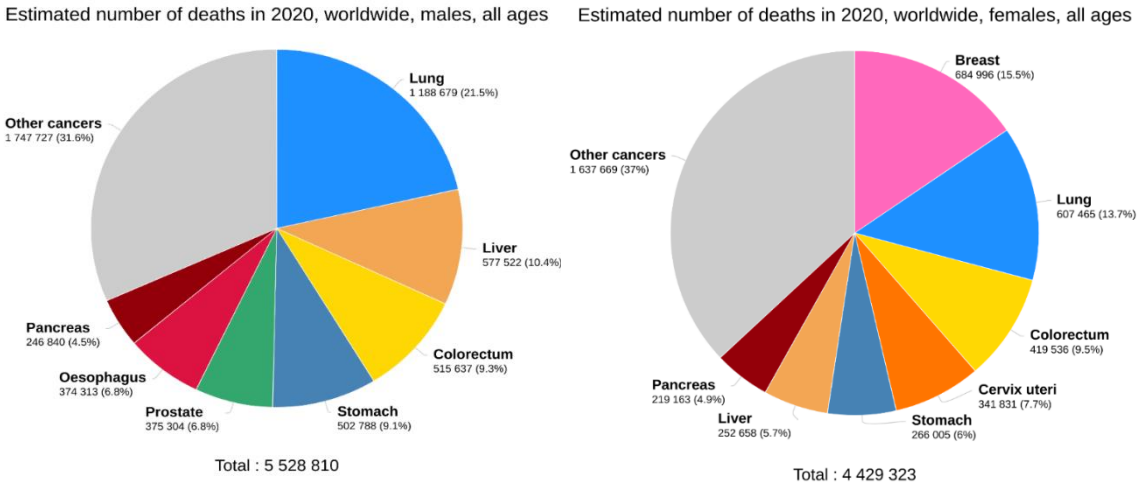

Figure 1.1.2. Estimated world cancer mortality proportions by major sites, in men, and in
women, 2020.[1]

1.2. Cancer and its hallmarks

In order for cells to be considered as cancerous they have to acquire the following traits: self-sufficiency in growth signals, insensitivity to growth-inhibitory (i.e. antigrowth) signals, evasion of programmed cell death (i.e. apoptosis), limitless replicative potential, sustained angiogenesis and tissue invasion and metastasis (Figure 1.2.1). [3]

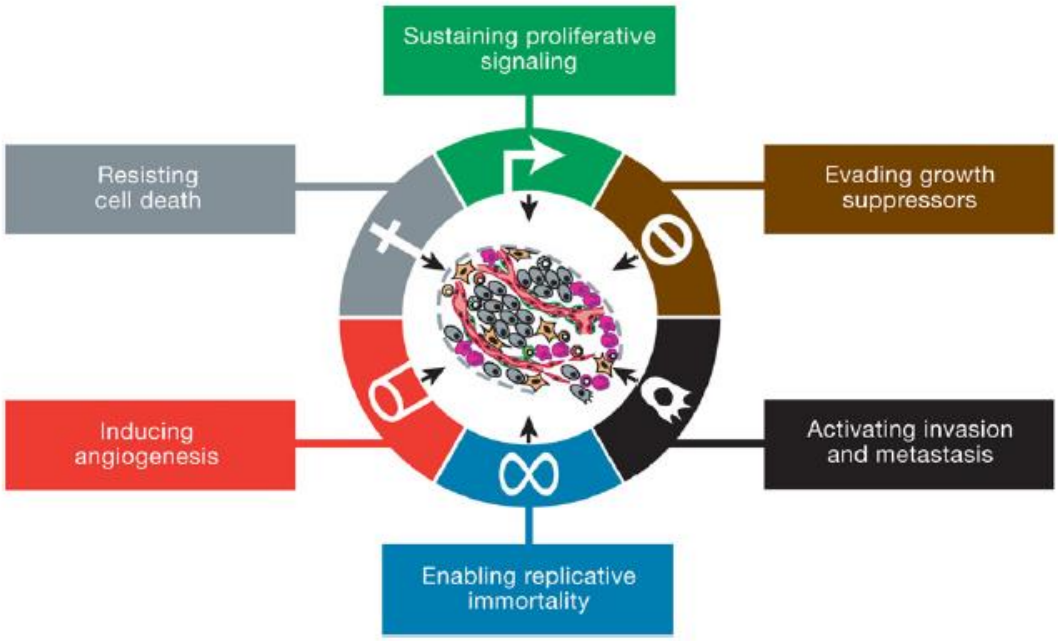

Figure 1.2.1. Hallmarks of cancer.[3]

1.2.1. Sustaining proliferative signalling

Mitogenesis is the induction (triggering) of mitosis, typically via a mitogen. A mitogen is a protein/peptide which induces cell division or enhances the rate of cell division. Mitogens trigger signal transduction pathways involving mitogen-activated protein kinases (MAPK), which leads to mitosis. Typically, normal cells undergo mitogenesis before they go into an active proliferative state. Cancers cells find a way around undergoing mitogenesis by mimicking normal growth signalling. By disrupting this homeostasis, the cells become immortal.[4] One way in which they can achieve immortality is by synthesising growth factors such as tumor growth factor α (TGFα).

TGFα) activates signalling pathways required for cell development, proliferation, and differentiation. It also causes transmembrane receptor overexpression such as receptor tyrosine kinase (RTK) or integrins, which are extracellular matrix receptors.[5,6]

One of the machineries used by cancerous cells is the MAPK pathway (SOS-Ras-Raf-MAPK pathway). This pathway plays a critical role in receiving and processing signals given by growth factors and integrins. In about 25% of tumours it has been found that the Ras proteins are altered to release mitogenic signals to cells.[7]

1.2.2. Cell death

Cell death occurs in different ways. Major mechanisms of cells death include apoptosis, necrosis, and autophagy. Apoptosis is a highly conserved process of programmed cell death which occurs in healthy cells and is key in maintaining cellular homeostasis. Thus, cancer cells must find a way to evade this predetermined method of cell arrest.[8,9]

The process of apoptosis involves a diverse range of signals, both extra- and intra-cellular. There are three successive stages which ensure that this process occurs without damage to healthy cells: (i) initiating cell death by either intrinsic or extrinsic pathways, depending on the starting stimuli, (ii) killing the cell by activation of intracellular proteases and (iii) removal of the dead cell by engulfment of the apoptotic cells by macrophages.

Both the intrinsic and extrinsic pathways result in the activation of caspases, a family of cysteine proteases. There are several caspases with a variety of functions. Caspases 2, 3, 6, 7, 8, 9 and 10 are apoptotic caspases, while caspases 1, 4, 5, 11 and 12 are pro-inflammatory. Caspases activate one another during caspase cascade, and they have been found to cleave a number of other substrates both in the nucleus and cytoplasm of cells. There are two categories of apoptotic caspases, initiator (caspases 8 and 9), or effector (caspases 3,6 and 7). Initiator caspases cleave effector caspases, which in turn cleave cellular substrates leading to cell death.[10]

The extrinsic pathway of apoptosis (Figure 1.2.2.1) is initiated by ligands such as TNF-α, lymphotoxin-α or TNF-related apoptosis-inducing ligand (TRAIL) binding to 'death

receptors' on the membrane surface. These receptors are members of the tumour necrosis factor (TNF) receptor gene family, and they consist of about 20 proteins (e.g. CD120a, CD120b, CD95/FAS, Trail R1 or Trail R2). Once the receptor-ligand complex has been formed adapter proteins such as the fas-associated protein with death domain (FADD) are recruited and the initiator caspase (procaspase 8) is activated to active caspase 8. Following this activation, effector procaspase 3 is cleaved to caspase 3, which then leads to apoptosis. It has also been found that caspase 8 can initiate the mitochondrial pathway by cleaving Bid to tBid, which then moves to the mitochondria membrane and carries out apoptosis as discussed below.[11,12]

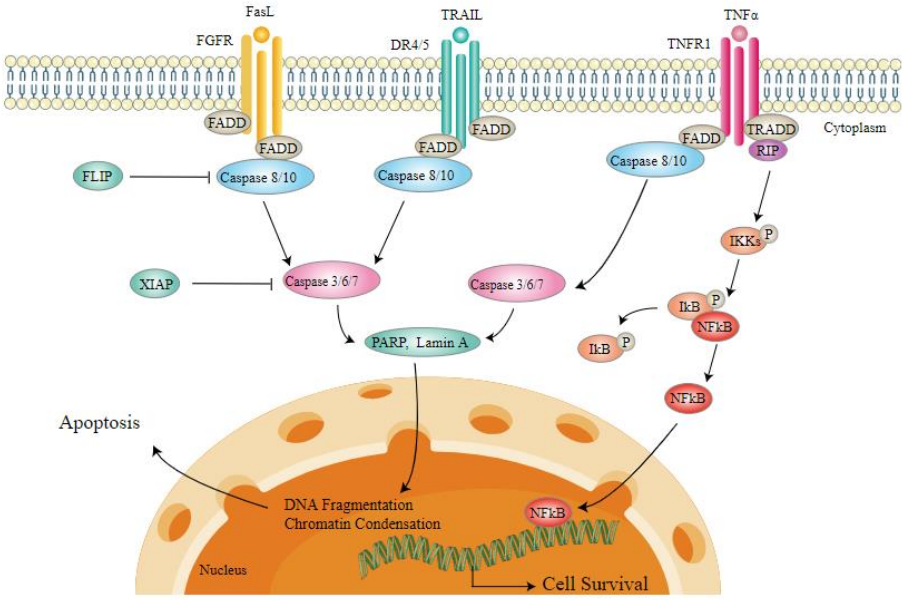

Figure 1.2.2.1. Extrinsic pathway of apoptosis.[13]

In the intrinsic pathway (Figure 1.2.2.2) the activation of apoptosis is linked to the permeabilization of the mitochondria. This pathway is activated due to a number of stimuli such as DNA damage. Following DNA damage regulatory proteins belonging to the B-cell Lymphoma 2 (Bcl-2) family proteins whose role is to regulate apoptosis (pro- and anti-apoptotic proteins) are activated/inactivated.[14] Pro-apoptotic proteins include BIM, PUMA, BAD, BID, BIK, BAX, BAK and NOXA. Antiapoptotic proteins include Bcl-2, Bcl-XL, Bcl-W and Mcl-1. The pro-apoptotic proteins BAX and BAK oligomerise on the

outer mitochondrial membrane, which leads to the mitochondrial membrane losing its integrity. Loss of mitochondrial membrane integrity initiates the apoptotic process. Proteins which would normally be found in between the mitochondrial membrane (e.g. cytochrome c) bind to the apoptotic protease activating factor 1 (APAF-1) to form the apoptosome. This leads to conformational changes in the APAF-1, specifically in the caspase recruitment domains that recruit the initiator procaspase 9 which is cleaved to caspase 9.[15] Once cleaved, caspase 9 activates effector caspases 3 and 7, which go on to cleave proteins responsible for cell death.[16]

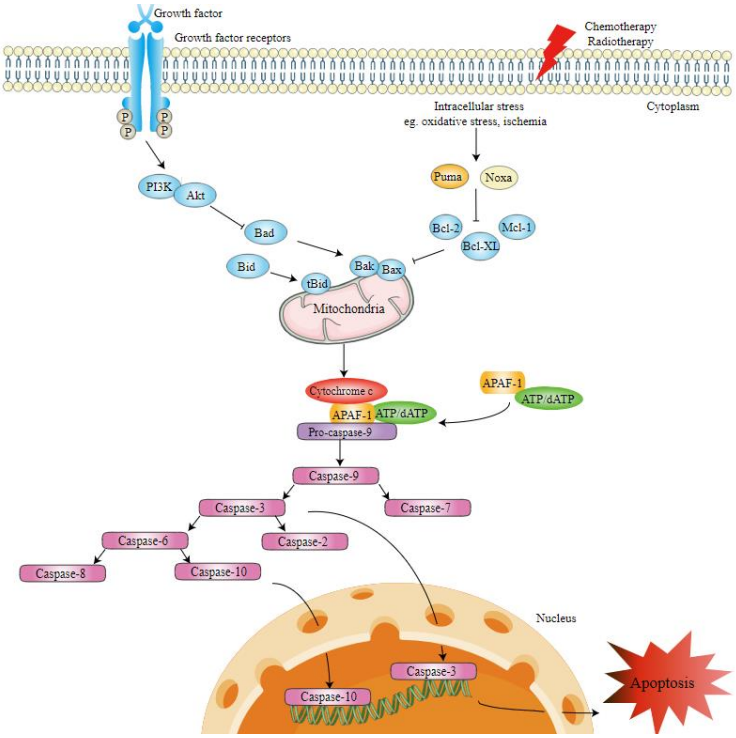

Figure 1.2.2.2. intrinsic pathway of apoptosis.[13]

1.3. Anticancer agents

There are six major groups of anticancer agents: biological, hormonal, DNA-interactive, anti-tubulin, tumour-targeting and molecularly targeted. Each have different targets and mechanisms of action. For the current project only DNA-interactive agents and molecularly targeted agents will be discussed.

1.3.1. DNA interacting agents

There are several ways in which anticancer drugs interact to or interfere with DNA which determines their classification (Table 1.3.2.1). For example, drugs that bind to proteins (DNA polymerases and transcription factors) which bind to DNA, such as histone deacetylase inhibitors (HDAC inhibitors), inhibitors of c-Myc, or STAT3 inhibitors. Another group comprises of drugs which bind to DNA through non-covalent interactions. Such non-covalent interactions include binding to the DNA minor/major grooves by hydrogen bonding interactions or intercalating between the base pairs of the DNA double strand.

As double stranded DNA coils and develops, it forms the minor and major grooves. These are different in size and contain different binding elements. When a ligand binds to any of the grooves similar non-covalent interactions are observed. The different sizes of these grooves and their binding elements allow for ligand selectivity.[17] For example, large molecules and proteins can bind to the major groove whereas small molecules favour the minor groove. Binding of ligands to the grooves has catastrophic effects for DNA as it interferes with the interactions between DNA and DNA binding proteins (e.g. transcription factors), leading to cell cycle arrest and subsequently apoptosis.

Structurally speaking the DNA intercalators and groove binders are different. Intercalators are usually flat, rigid, and aromatic molecules. Contrasting DNA

intercalating agent traits, groove binders usually take on a more flexible shape and are typically cationic in nature. The most common interactions established by these DNA binding agents are hydrogen bonds and electrostatic interactions.

Table 1.3.2.1. DNA interacting agents.[18]

Non-covalent binding agents		**Covalent DNA-adducts and direct DNA damage**
Groove binding agents	**DNA intercalators**	
Berenil	Aminoacridines	Busulfan
Bisbenzimadoles	Arylaminoalcohols	Camptothecin
Bleomycin	Coumarins	Chlorambucil
Chloroquine	Cystodytin J	*Cis*-platinum
Chromomycin A3	Diplamine	Clomesone
Diamidine-2-phenylindole	YO-1 and YOYO-1	Cyclodisone
Distamycin A	Daunomycin	Ionizing radiation
Guanyl bisfuramidine	Quinolines and quinoxalines	Nitrogen mustard
Mithramycin	Ethidium bromide	Nitrosoureas: 1,3-bis (2-chloroethyl)-1-nitrosourea; 1-(2-chloroethyl)-3-cyclohexyl-nitrosourea; 1-(2-chloroethyl)3-(2,6-dioxo-3-piperidyl)-1-nitrosourea
Netamycin	Proflavine	
Netropsin	Echinomycin	
Pentamidine	Chlorpheniramine	
Pilcamycin	Methapyrilene	
SN6999	Tamoxifen	
SN7167	Bis-naphthalimide	Oxidative-stress agents
Hoechst 33258	Doxorubicin	UV radiation
	M-AMSA	Busulfan

	Indoles	Camptothecin
		Cis-platinum

1.3.2. Molecular targeted agents

Classical chemotherapy treatments consisting of DNA interacting agents many disadvantages. Lack of selectivity is the largest pitfall, killing cancerous cells and additionally healthy cells simultaneously leading to many undesirable side effects. Selectivity issues may be overcome by designing drugs which bind to a specific part of a particular target involved in tumour growth. This approach can include targeting abnormally expressed proteins unique to cancer cells which are not expressed in same form in healthy cells. The use of targeted therapies is expanding and may include protein kinase inhibitors (discussed in section 1.7), or monoclonal antibodies. Considering that many cancerous cells have mutations in specific kinases, targeted therapies are very relevant with potential for selectivity toward cancer cells only, thereby minimising disadvantageous side effects. About 30% of tumours have been found to have RAS oncogene mutations, with up to 50% of multiple myeloma patients having RAS mutations. Therefore therapies which target kinases pathways specifically are essential.[19]

1.4. Protein kinases

1.4.1. Features of protein kinases

Protein kinases (PKs) are responsible for the communication between the extracellular and intracellular environments of the cell. This communication is responsible for cell growth, metabolism, proliferation, migration, differentiation and transcription.[20] The message is transmitted through the phosphorylation of serine, threonine or tyrosine residues of a cascade of protein kinases, by means of adenosine triphosphate (ATP) as

seen in Scheme 1.4.1.1. Thus, the phosphate is covalently bound to the hydroxyl group of the appropriate residue of the substrate protein.

Scheme 1.4.1.1. Protein kinase/phosphatase "phospho" transfer/elimination reaction**.**

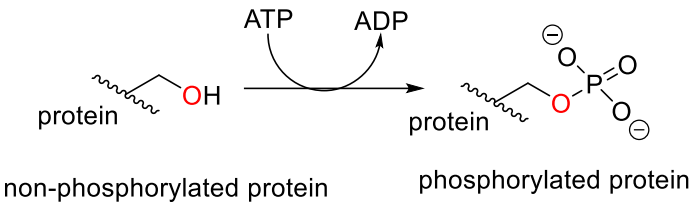

There are several kinase families which play different roles in the cell. Each family is usually involved in one or more different pathways and regulates different cellular functions. Currently, over 500 human kinases are known and the complete set of human kinases is known as the kinome (Figure 1.4.1.1). [21] The kinome represents different groups of kinases grouped by their structural and functional relationships, and by their catalytic domain.

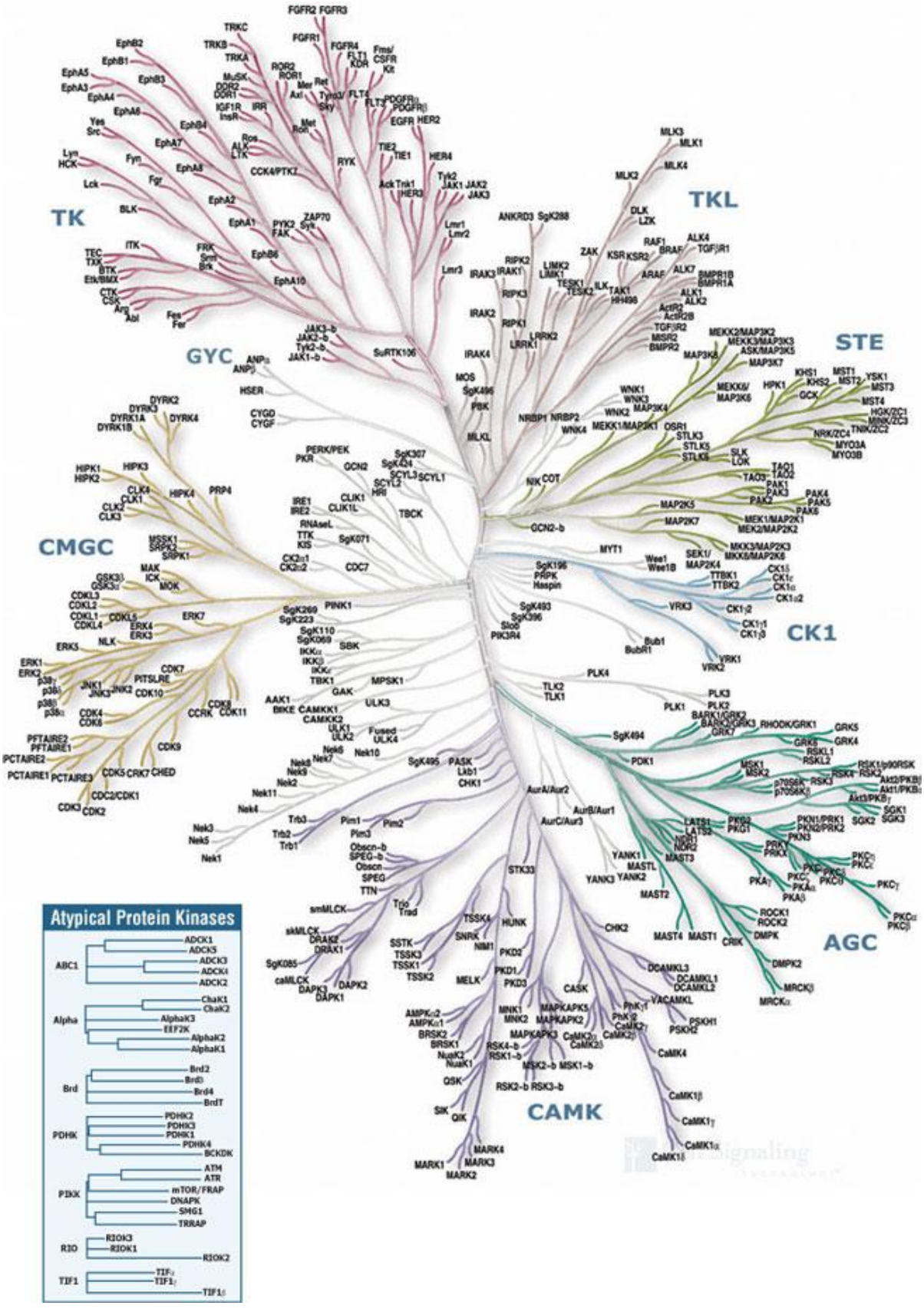

Figure 1.4.1.1. The human kinome.

Table 1.4.1.1. Different groups of human kinases

Subgroup	**Families**
AGC	• PKA • PKG • PKC
CAMK	• CAMKI • CAMKII • CAMKIII • Calcium/calmodulin-dependent protein kinase
CK1	• CK1(casein kinase 1)
CMGC	• Cyclin dependent kinases-CDKs • Mitogen activated protein kinases-MAPKs • Glycogen synthase kinase3-GSK3 • Cdc2-line kinases-CLK families
STE	• Homologs of yeast sterile 7, sterile 11, sterile 20 kinases
TK	• Tyrosine kinases
TKL	• Tyrosine kinase-like
GYC	• CK2

These kinase subgroups are organised based on the protein residue which they phosphorylate, for example TKs only phosphorylate the tyrosine residues, whereas all of the other kinases phosphorylate serine/threonine (Table 1.4.1.1). Kinases from different subgroups can also phosphorylate one another, for example MEK of the STE subgroup phosphorylates ERK of the CMGC group.

1.4.2. Structure of protein kinases

PKs comprise of different moieties, the N-terminal lobe (N-lobe) and the C-terminal (C-lobe). These two lobes form a cleft which acts as the docking site of ATP. This cleft is made up of two hydrophobic spines, the R (regulation) and C (catalytic) spines, which consist of non-linear motifs.[22] There are other conserved regions PKs which are needed for activation, the Asp-Phe-Gly (DFG), the His-Arg-Asp (HRD) and the Ala-Pro-Glu (APE) motifs. These conserved motifs were identified with the protein sequence, but the crystallisation of the first PK, PKA, revealed the way in which a kinase recognises its substrate for phosphorylation.[23] For this reason, PKA will be used to discuss the different motifs of PKs as well as their activation.

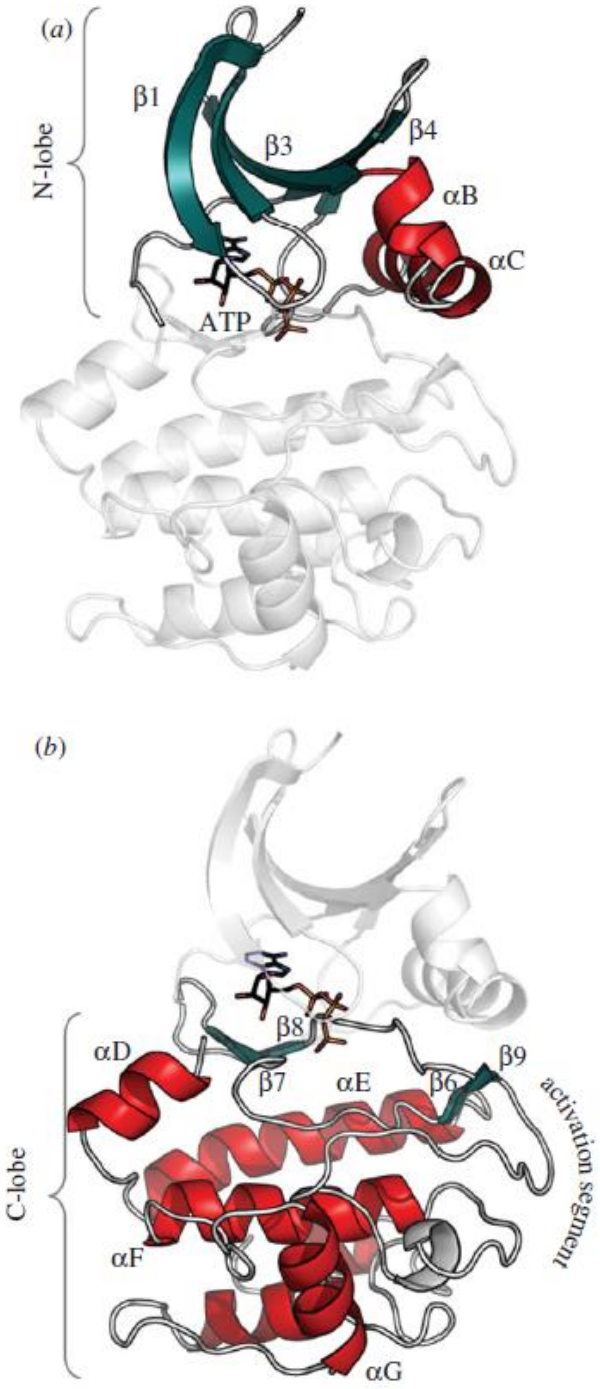
(a)
N-lobe
β1
β3
β4
αB
αC
ATP
(b)
C-lobe
αD
β8
β7
αE
β6
β9
activation segment
αF
αG

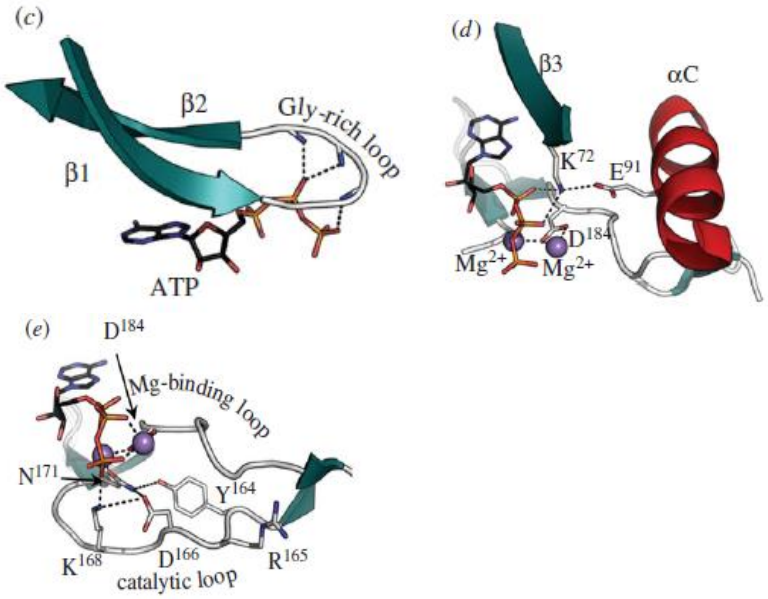

Figure 1.4.2.1. Protein kinases general structure

The N-lobe (Figure 1.4.2.1.a) consist of five β-sheets coupled to a helical sub-domain consisting of the C-helix. The αC-β4 loop is the only part of the N-lobe anchored to the C-lobe (Figure 1.4.2.1.b), which consists of two conserved motifs, the glycine rich loop and the β3. The glycine rich loop is the most flexible moiety of the lobe and is found between β1 and β2. It folds over ATP positioning the γ phosphate in place for catalysis (Figure 1.4.2.1.c). The glycine loop is followed by a conserved valine (Val57 in PKA) which makes hydrophobic contact with the base of ATP.

The β3 is important as it contains a conserved residue, lysine (Lys72 in PKA), which couples the phosphates of ATP to the αC-helix (Figure 1.4.2.1.d). Although β3 belongs to the N-lobe it occupies the space between the two lobes, hence it serves as a signal integration motif as it connects the different parts of the protein. The conserved glutamate (Glu91 in PKA) can also be found in the C-helix, forming a salt bridge with Lys72 in the β3-strand which is considered to be a hallmark of the activated state.

As mentioned, the C-lobe mainly consists of helices. The stable helical subdomain is the core of the kinase and is the surface for protein substrate interaction. Structurally, most of the helices are hidden from solvent and only one is solvent exposed.[24] Phosphate transfer from ATP to the protein substrate is carried out by the catalytic machinery

consisting the β-strands 6-9, which flank the DFG (Asp-Phe-Gly) motif where D (Asp184 in PKA) is needed for recognizing the ATP-bound Mg^{2+} (Figure 1.4.2.1.e).

The regulatory R-spine regulates the state of the kinase (active or inactive). The spine is made up of four hydrophobic residues: two in the N-lobe (Leu106 in β5 and Leu95 in the C-helix), Phe185 of the DFG motif in the activation loop and Tyr164 in the catalytic loop. This spine is assembled as a consequence of phosphorylation of the activation loop. When the spine is complete (i.e. in the DFG-in conformation) Phe185 is flipped leaving Asp184 exposed to interact with the ATP bound magnesium ions, thus adopting the active conformation of the kinase. In the DFG-out conformation the spine is broken, and the kinase is rendered inactive.

Just like the R-spine, the catalytic spine (C-spine) contains non-consecutive residues and is completed by the adenine ring of ATP.[22] It also consists of residues from both the N-lobe (Val57 in β4 and Ala70 in β3, which are directly docked onto the adenine ring) and the C-lobe (Leu172 in β7). The binding of ATP positions the two lobes so that the catalytic residues align for catalysis.

1.5. Mitogen-activated protein kinase pathways

There are three clearly characterised families of the Mitogen-activated protein kinase (MAPK) pathway; the Ras-ERK pathway, c-Jun N-terminal kinase (JNK) and p38 kinase (Figure 1.5.1). These pathways act as signal transduction pathways which respond to a variety of external stimuli and evoke the appropriate response, such as proliferation, differentiation and apoptosis.[25]

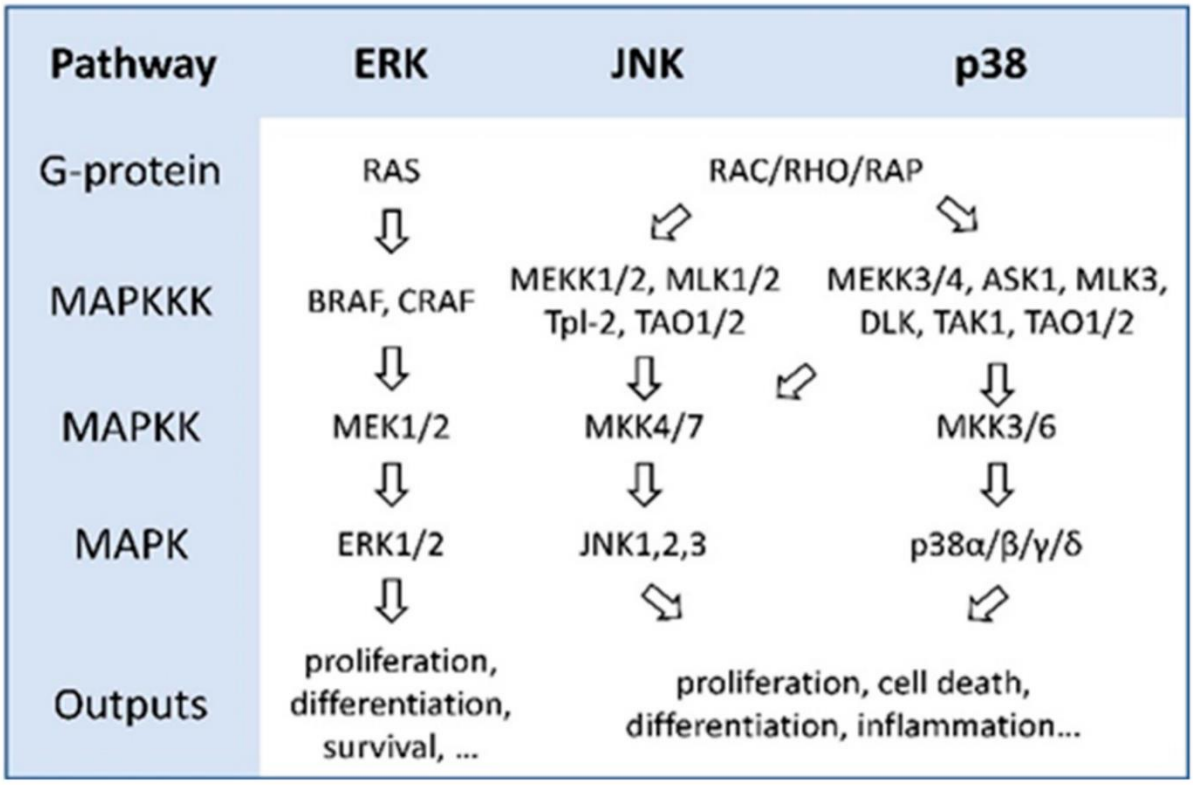

Figure 1.5.1. Summary of the different MAPK pathways[26]

1.5.1. The RAS/ERK pathway

This pathway is activated by the stimulation of the transmembrane receptors, RTKs or G protein coupled receptors.[27] To describe the activation of this pathway, EFG will be used as an example of a ligand and EGFR as its receptor.

For the activation of this RAS/ERK pathway, EGF binds to the extracellular portion of EGFR leading to the dimerization of two EGFR subunits at the inner side of the receptor. The tyrosine kinase domain of the kinase catalyses autophosphorylation and consequently phosphorylation of the other subunit. Following this, Grb2 (growth factor

receptor-bound protein 2, an adaptor protein) can bind and the Son of Sevenless (SOS) binds, guanine nucleotide exchange factors (GEFs), which is able to bind the membrane bound protein RAS, a small GTPase. Inactive RAS is bound to GDP and SOS catalyses the exchange of GDP to GTP, leading to RAS activation. There are three notable members of the RAS protein, N-RAS, K-RAS and H-RAS, which differ in their sites of action and have been shown to be somatically mutated in many cancers.[28] As the RAS protein acts as the start of the signal cascade of the RAS-ERK pathway, it serves as a key point and has been targeted for the treatment of cancers. Activated RAS is able to bind and phosphorylate effector proteins such as Raf, although this process is not well understood. There are three isoforms of RAF (i.e. A-Raf, B-Raf and C-Raf), and they phosphorylate MEK which subsequently phosphorylates ERK.

This cascade leads to the activation of transcription factors (TF) and, thus, the expression of many genes such as growth factors, cyclins, and cytokines. In normal mammalian cells the RAS-Raf complex dissociate shortly after its formation. This is done by GTP binding to RAS, thus reducing the GTPase activity of RAS. This leads to subsequent dissociation of the complex and turning off the MAPK pathway.

This pathway is particularly significant. Mutations in the MAPK pathway have been found in many cancers and it is thought that about 30% of all tumours have a mutated RAS oncogene. Considering that it is the start of the RAS/ERK signalling cascade, RAS mutations result in uncontrolled cell division, which enables cancer cells to evade cell death with characteristic immortality. Other kinases in this pathway are found with mutations in other cancer, for example B-Raf mutations are observed in melanoma.

1.5.2. The c-Jun N-terminal kinases

The c-Jun N-terminal kinase (JNK), also known as the stress-activated protein kinase (SAPK) family, consists of three proteins: JNK1, JNK2 and JNK3. Proteins JNK1 and JNK2 are expressed ubiquitously, and JNK3 is predominantly expressed in brain, heart and testes.[29] This pathway is primarily activated by cytokines (e.g. TNF and IL-1) and environmental stress including UV irradiation and DNA damage.[30] The activation of this pathway is very complex as there are 13 kinase kinases involved. Following its activation, JNK activates a number of proteins including transcription factors such as AP-

1 which is involved in controlling cellular processes such as apoptosis, differentiation, and proliferation.

1.5.3. P38 MAPK pathway

Much like the JNK pathway, the p38 pathway also plays a role in numerous biological functions including cellular development, cell cycle, senescence, tumorigenesis, and apoptosis. There are four splice variants of p38α, p38β, p38γ (ERK6, SAPK3), and p38δ (SAPK4).[31] This pathway is also activated by cytokines,[32] UV light, growth factors, heat and osmotic shock.[33]

P38 kinases are activated by MAP kinase kinases (MKKs) and two of them (MKK3 and MKK6) have been found to activate p38. Although the phosphorylation site is conserved in all p38 isoforms, it has been found that there is selectivity in the activation of the different isoforms. This can be seen in the activation of p38β for example; MKK3 is unable to activate this isoform, but MKK6 can activate it even though these two MKKs share 80% homology.[34] It has also been found that MKK4, which is upstream of JNK, can activate p38α and p38β in some cells, suggesting that the activation of this pathway is controlled based on the stimuli.[35] There are also MAPKK-independent mechanisms of activation which involve transforming growth factor-β-activated protein kinase 1 (TAB1). This activation is achieved by autophosphorylation of p38α after interaction with TBA1.[36].

Once p38 has been activated, it has many substrates including heat shock protein 27[37] and mitogen-and stress-activated protein kinase-1 (MSK1).[38] p38 also regulates the S phase of the cell cycle and activates the transcription factor of CHOP and p53 which are in turn activated during growth arrest and DNA damage.[39]

1.6. JAK2/STAT3 pathway

Communication between cells in a multicellular organism is crucial for the survival of the organism. Significant components that facilitate inter-cellular communication in the body are the cytokines. Cytokines are key players in the regulation of survival, growth,

differentiation, and effector functions of the cell. There are many cytokines which induce different biological responses, either pro- or anti-inflammatory. For the present work only IL-6 will be discussed with reference to how it activates the JAK2/STAT3 pathway (Figure 1.6.1).

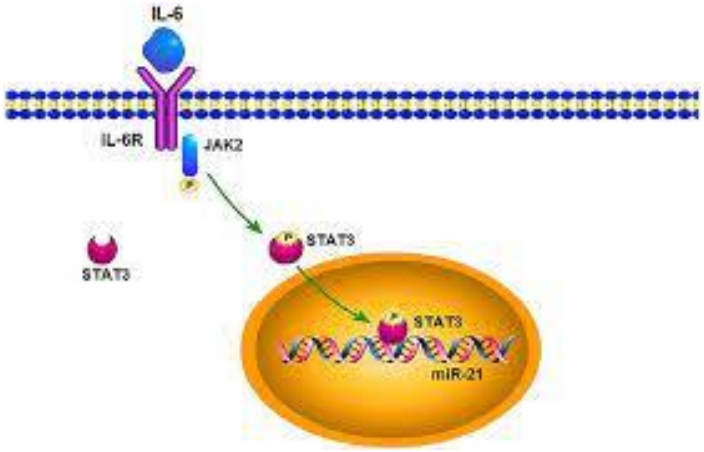

Figure 1.6.1. Scheme of the JAK2/STAT3 pathway.[40]

This pathway consists of cell surface receptors, JAK proteins (JAK1, JAK2, JAK3 and tyrosine kinase 2 or TYK2) and STAT proteins (STAT1, STAT2, STAT3, STAT4, STAT5 and STAT6). For the activation of the pathway, IL-6 binds to the IL-6 receptor-alpha (CD126) forming a complex which recruits the signalling receptor subunit, glycoprotein 130 (gp130) or the IL-6 receptor-beta. Once this complex has been formed, a second gp130 is recruited. Surprisingly it has been found that, although structurally similar, these gp130 proteins are two different epitopes which recognize the ligand, IL-6.[41] The ligand induced receptor dimerization brings the appropriate JAK to associate with the transmembrane receptor, leading to kinase activation through phosphorylation of the appropriate residue of the cytokine receptor. Then, these phosphorylated residues act as docking sites for the appropriate STAT proteins. Upon docking, STAT proteins are phosphorylated by JAK kinase and dissociate from the receptor to subsequently dimerize. The dimer then translocates to the nucleus where it modulates the expression of target genes.[42–44] In the tumour microenvironment, the IL-6/JAK/STAT3 pathway drives survival, proliferation, invasiveness and metastasis of the tumour cells while supressing the immune response.

Aberrant activation of the JAKs family has been found to play a key role in autoimmune diseases and haematological malignancies. Somatic activation of JAK1 has been found in about 20% of adult T-cell acute lymphoblastic leukaemia[45] while JAK2 over expression has been found in haematological disorders such as multiple myeloma and myeloproliferative neoplasms.[46]

1.7. Protein Kinase inhibitors

By 2019 more than 40 PKIs have been approved by the FDA, Table 1.7.1.1, and almost all of them for application in oncology. These inhibitors are also used for the treatment of infectious, neurological and metabolic diseases.[47] There is a number of reasons as to why protein kinases are chosen as targets. For example, the size of the human kinome gives a larger variety in targets,[47] the fact that kinases are activated through phosphotransfer cascade, their activation/deactivation leads to physiological changes or because inducing their activation can be used to interfere with the out of control cell growth.[47]

As described in Section 1.4.2, protein kinases control the communication within the cell. They are structurally similar, with many conserved sites. The ATP binding site has been widely studied. Many PKIs bind to this site, both to the active or inactive conformations. Other PKIs bind to allosteric sites of the kinases.

They are a number of factors that must be taken into consideration while designing new kinases inhibitors: (i) is the inhibitor targeting the active or inactive form of the kinases; and (ii) is the inhibitor going to be ATP-competitive or non-competitive. As described in section 1.4.2., there are significant structural changes in the kinase from the inactive to the active form, thus both forms can be targeted based on which one gives the most selectivity. In terms of structural diversity, there is more diversity in the inactive form of kinases when compared to active counterparts. Activated PKs are usually structurally homologous due to the conserved nature of protein activation.[48]

1.7.1. Types of kinase inhibitors

There are different types of PKIs which show different binding modes and they are schematically presented in Figure 1.4.1.

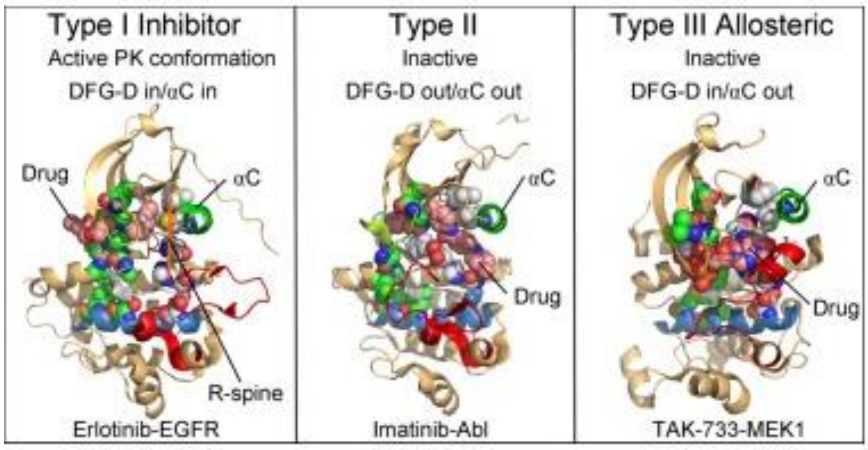

Figure 1.4.1. Types of kinase inhibitors.[49]

Type I inhibitors: This category constitutes most PKIs on the market. They are also known as ATP-competitive inhibitors. They bind competitively to the ATP binding site and recognize the active conformation of the kinase. Type I inhibitors typically consist of a heterocyclic ring system that occupies the space of the purine's ATP in its binding site, and it serves as a scaffold for side chains that occupy the adjacent hydrophobic region. Examples include vemurafenib or zelboraf. The key issue with this type of inhibitors is that the ATP binding site is highly conserved across most kinases, selectivity is impossible to achieve, thus leading to toxic side effects.

Type II inhibitors: These are also ATP competitive inhibitors, but they recognize the inactive conformation of the kinase instead of the active form. Movement of the activation loop to the DFG-out conformation exposes an additional hydrophobic binding site directly adjacent to the ATP binding site that is also occupied by this type of inhibitors. Examples include imatinib (i.e. gleevec) or sorafenib (i.e. nexavar). This type of inhibitor addresses the selectivity issue of type I, but due to cellular mutations, eventually type II inhibitors stop being effective.

Type III inhibitors: These compounds bind outside the ATP binding site in an allosteric site. They can bind to kinases even when ATP is bound and because of the allosteric binding the conformation of the kinase is disturbed. Such inhibitors are optimal as selectivity can be achieved where the inhibitor does not bind to the highly conserved ATP site. Examples include trametinib (i.e. mekinist).

Table 1.7.1.1. Current kinase inhibitors[50]

Name	Known Target	Inhibitor Class	Indications
	BRAF		
Dabrafenib	BRAF	I	Melanoma and NSCLC with BRAF mutations
Encorafenib	BRAFV600E/K	I	BRAFV600E/K mutant melanoma with binimetinib
Vemurafenib	A/B/C-Raf, BRAF (V600E), SRMS, ACK1, MAP4K5, FGR	I	Melanoma with BRAFV600E mutation and ECD
	Bruton tyrosine kinase		
Acalabrutinib	Bruton tyrosine kinase	Covalent (V)	MCL
Ibrutinib	Bruton tyrosine kinase	Covalent (V)	MCL, CLL, WM, graph vs host disease.
	Mitogen-activated protein kinase kinase (MEK)		
Binimetinib	MEK1/2	III	BRAF V600E/K melanoma with encorafenib
Cobimetinib	MEK1/2	III	Melanoma with BRAF V600E/K mutations with vemurafenib
Trametinib	MEK1/2	III	Melanoma (2013) and NSCLC (2017) with BRAF mutations
	Cyclin-dependent-kinase 4/6		
Abemaciclib	CDK4/6	I	HR+, HER- BC
Palbociclib	CDK4/6	I	ER+ and HER2- BC
Ribociclib	CDK4/6	I	HR+-EGFR- metastatic BC

Name	Known Target	Inhibitor Class	Indications
Anaplastic lymphoma kinase (ALK)			
Alectinib	ALK and RET	II	ALK+ NSCLC
Brigatinib	ALK, ROS1, IGF-1R, Flt3, EGFR	I	ALK+ NSCLC after crizotinib
Ceritinib	ALK, IGF-1R, InsR, ROS1	II	ALK+ NSCLC as first-line treatment or after crizotinib resistance
Crizotinib	ALK, c-Met (HGFR), ROS1, MST1R	II	ALK+, ROS1+ NSCLC
Entrectinib	TRKA/B/C, ROS1, ALK	I	ROS1+ NSCLC; solid tumors with NTRK fusion proteins
Lorlatinib	ALK	I	ALK+ NSCLC
Fusion of breakpoint cluster region and Abelson (BCR-ABL)			
Bosutinib	BCR-ABL, Src, Lyn, Hck		CML
Dasatinib	BCR-ABL, EGFR, Src, Lck, Yes, Fyn, Kit, EphA2, PDGFRβ	I	Ph+ chronic ML and ALL
Imatinib	BCR-ABL, Kit, PDGFR	II	Ph+ CML or ALL, CEL, DFSP, HES, GIST, MDS/MDP
Nilotinib	BCR-ABL, PDGFR, DDR1	II	Ph+ CLL
Ponatinib	BCR-ABL, BCR-ABL T315I, VEGFR, PDGFR, FGFR, EphR, Src family kinases, Kit, RET, Tie2, Flt3	II	Ph+ CML or ALL
Epidermal growth factor receptor (EGFR)			
Afatinib	EGFR, ErbB2, ErbB4	Covalent (V)	NSCLC
Dacomitinib	EGFR/ErbB2/ErbB4	I	EGFR- mutated NSCLC
Erlotinib	EGFR	I	SCLC and PaC
Gefitinib	EGFR	I	NCLC
Lapatinib	EGFR, ErbB2	II	BC
Neratinib	ErbB2/HER2	Covalent (V)	HER2+ breast cancer
Osimertinib	EGFR T970M	Covalent (V)	NSCLC
Vandetanib	EGFRs, VEGFRs, RET, Brk, Tie2, EphRs, Src family kinases	I	MTC
FMS-like tyrosine kinase 3 (FLT3)			
Gilteritinib	FLT3	I	AMLwith FLT3 mutation5
Midostaurin	FLT3	I	ALL Flt3 mutation+
Fibroblast growth factor receptors (FGFR)			
Erdafitinib	FGFR1/2/3/4	I	Urothelial carcinoma
Janus kinase (JAK)			
Ruxolitinib	JAK1 and 2	I	MF and PV
Neurotrophic Tyrosine Receptor Kinase (NTRK)			
Larotrectinib	NTRK	I	Solid tumors with NTRK gene fusion proteins
Vascular endothelial growth factor (VEGFR)			
Axitinib	VEGFR1/2/3, PDGFRβ	II	RCC
Carbozantinib	RET, Met, VEGFR1/2/3, Kit, TrkB, Flt3, Axl, Tie2, ROS1	I	Metastatic MTC, advanced RCC and HCC
Lenvatinib	VEGFRs, FGFRs, PDGFR, Kit, RET	II	DTC
Pazopanib	VEGFR1/2/3, PDGFRα/β, FGFR1/3, Kit, Lck, Fms, Itk	I	RCC, STS
Regorafenib	VEGFR1/2/3, BCR-ABL, BRAF, BRAF(V600E), Kit, PDGFRα/β, RET, FGFR1/2, Tie2, Eph2A	II	CRC, GIST
Sorafenib	B/C-Raf, BRAF (V600E), Kit, Flt3, RET, VEGFR1/2/3, PDGFRβ	II	RCC, DTC and HCC
Sunitinib	PDGFRα/β, VEGFR1/2/3, Kit, Flt3, CSF-1R, RET	II	RCC, GIST, PNET

1.7.2. Challenges and breakthroughs in the discovery of kinase inhibitors

Signalling pathways are involved in complex crosstalks, for instance the Pi3K/AKT and RAS/MAPK pathways interfere with each other at the ERK kinase, these two pathways can also be activated by molecules in the STAT pathway (Figure 1.7.2.1). It has been found that tumour cells are able to circumvent the effect of PKIs by activating parallel pathways which elicit the same effect as the inhibited kinase(s)[51]. This clearly represents a challenge in the design of kinase inhibitors, because when targeting one particular kinase in a pathway, another pathway can be affected or triggered.

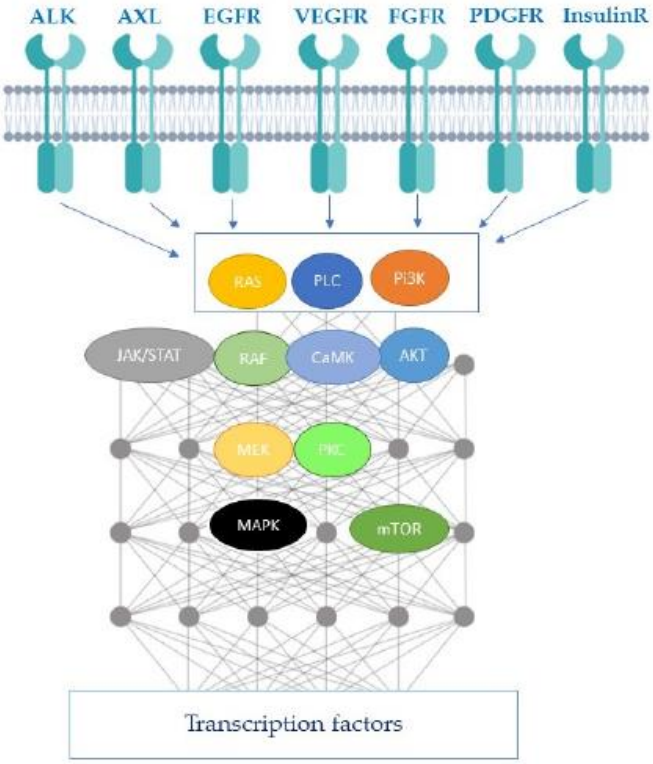

Figure 1.7.2.1. Schematic representation of kinase crosstalk.[50]

Other important challenges facing the design of kinases inhibitors are selectivity and resistance (intrinsic and acquired). Given that the ATP binding site is the best understood part of the kinase, almost 50% of the PKIs approved by the FDA by 2019 were type I PKIs, this poses an issue for selectivity. The ATP binding site is highly

conserved across kinase families; thus, many type I inhibitors are not very selective, oftentimes these inhibitors are used as multikinase inhibitors. Examples of this include dasatinib (targeting BCR-ABL, Src, or Kit, among others) and Sorafenib (B/C-Raf or VEGFR1/2/3, among others). Higher levels of selectivity are achieved with type II and allosteric inhibitors, because they use the additional hydrophobic pocket adjacent to the ATP binding site which is facilitated by the DFG-out conformation.[52]

Kinase selectivity can be difficult to achieve but once it has been achieved there are other issues which arise for the TKIs, the most notable is the development of resistance. In the case of anticancer PKIs, with *intrinsic* resistance the tumour does not respond to treatment; this could be because many issues but the most notable one is the differences in sensitivity of the inhibitor across the various mutations leading to the tumour. This has been notably seen in non-small cell lung cancer (NSCLC) with EGFR-mutant patients.[53] The most common type of resistance is *acquired* resistance, which has been seen with most TKIs. Studies have shown that there about 50 types of mutations which lead to imatinib resistance.[54]

1.8. Methods used to assess PKIs activity and mechanism of action

1.8.1. Flow cytometry

Flow cytometry is a technique used to measure a number of physical characteristics of a single cell. It is used in all stages of drug discovery and development. Some of the parameters that can be measured include optical and fluorescence characteristics (derived from antibodies or dyes). In principle, flow cytometry is related to the fluorescence emission and light scattering resulting from a laser beam which is the excitation source. When this laser strikes a moving particle, the data obtained gives information about the biochemical and molecular aspects of the cell.

The basic components of a flow cytometer are: (i) a fluidic arrangement that transports the cells through the system. This has two components; the sheath fluid and pressurized lines; (ii) an optical system, this consists of the optical bench which holds the excitation (lasers, lenses, and collection optics in fixed position) (iii) signal detection and processing, hence signals generated by cells passing through the cytometer are detected and converted into digital signal that can be displayed as dots or histograms.[55]

A number of methods have been developed and tailored for different applications. Whole cells can be analysed to afford information on the cell membrane, cytoplasm and the nucleus. Therefore, we can analyse specific organelles such as the mitochondria, DNA (cell cycle and apoptosis), RNA, cytokines, protein contents, or kinase phosphorylation.

As mentioned in section 1.2.2, apoptosis is a common type of cell death that can be observed in the morphological and biochemical changes of the cell. As discussed before some of the pathways that trigger apoptosis include caspase cleavage which can activate degradation enzymes that cleave DNA. Therefore, flow cytometry can be used to measure apoptosis and study the cycle of a cell using a stain of propidium iodide (PI) which is a DNA intercalating agent that fluoresces when bound to DNA (excitation 488 nm and emission 600 nm).

1.8.1.1. Cell cycle analysis

The cell cycle is analysed by quantifying DNA in the cells at different time points to observe changes in a population. In a growing population of cells there are three main subpopulations with different DNA content as seen in Figure 1.8.1.1.1; these populations can be identified by PI staining, as mentioned before.

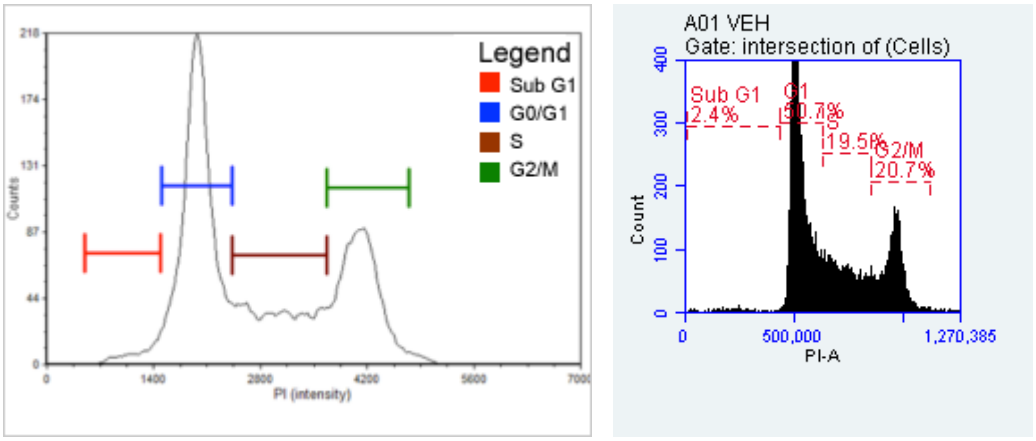

Figure 1.8.1.1.1. Scheme of the cell cycle profile[56]

The population in the G_0/G_1 subgroup consists of cells which are resting/preparing for DNA replication These cells have roughly the same amount of DNA (2N, where N is the haploid chromosome number). In the second population, S phase or synthesis phase, the cells are replicating the nuclear DNA. Cells in this population have higher amount of DNA than cells in the G_0/G_1 phase, but not double. In the third population, G_2/M phase, nuclear DNA has been replicated and the cell is preparing for cell division. The DNA content is double of that of G_0/G_1 because this phase also contains cells which are undergoing cell division. Once cell division is complete the cells will have the same amount of DNA as those in the G_0/G_1 phase. The sub-G_1 population of cells shows dead cells, either by apoptosis or some other type of cell death, which have lower DNA content.

In normal cellular proliferation, cells move from one to the next, but sometimes the cells get arrested in one phase before they undergo apoptosis. There are a number of circumstances that can lead to cell cycle arrest including drug treatment, UV, or changes in the microenvironment. These conditions cause the cell to stop the replication cycle and repair any damaged DNA. Once that is completed the cells come out of the arrest and continue replicating, but if the damage cannot be repaired apoptosis is initiated.

1.8.1.2. Detection of cell death with Annexin V/PI

While PI staining alone can tell us the DNA content of a given population, it does not tell us how the cells in that population died. In order to detect distinguish between apoptosis or necrosis, the annexin V/PI assay is used. Healthy cells have a distribution of plasma membrane phospholipids on the inner and outer sides of the cell membrane. Under normal conditions choline phospholipids can be found on the outer side, whereas aminophospholipids such phosphatidyl serine (PS) can be found on the inner side. During apoptosis this distribution changes. PS can be found on the outer leaflet of the membrane. This change occurs early on in apoptosis, before the mitochondrial membrane is compromised, to provide signalling for microphages to phagocytose apoptotic bodies. Detection of exposed PS can help to estimate the percentage of cells undergoing apoptosis in the population. Annexin V which reversibly bind to PS, allows for quantification of this process.

In this assay, fluorescein isothiocyanate (FITC) bound annexin V binds to the exposed PS on the outer leaflet of the membrane. It does not cross the cell membrane, and thus it will be able to indicate which population is in early or in late apoptosis. Additionally, PI binds to nucleic acids. It cannot cross then cell membrane, hence it cannot stain non-apoptotic cells or cells in early apoptosis.[57] Viable cells exclude both annexin V and PI (lower left quadrant), early apoptotic cells exclude PI (lower right quadrant) and late apoptotic/necrotic cells stain positive for both (upper right quadrant), Figure 1.8.1.2.1.

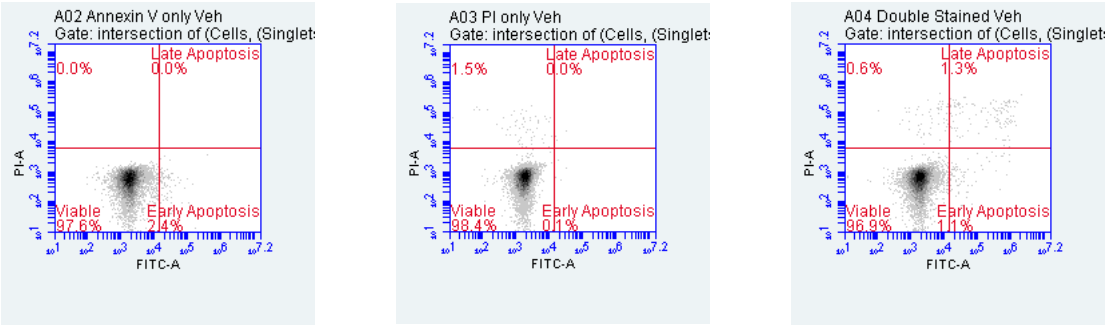

Figure 1.8.1.2.1 Representative images of gating strategy for annexin V-FITC and PI staining using BD Accuri flow cytometer.

1.8.2. Western blot

Western blot is a technique used to separate and identify specific proteins, based on molecular weight, from a complex mixture of proteins extracted from a whole cell. There are three elements to separate and visualize proteins by this technique: (i) separation by size, (ii) transfer to solid support and (iii) marking the protein of interest with the appropriate primary and secondary antibody.

First, sample preparation is required and considering that this technique is used to separate and visualise specific cell proteins, the cell must be lysed to obtain its protein content. This is done using RIPA buffer, which is an ionic detergent solution which disrupts the membranes and solubilises cytoplasmic proteins as well as protease and phosphatase inhibitors to prevent the denaturation of proteins. Once the protein has been collected, the protein concentration must be found to ensure that the samples can be compared on equivalent bases. The protein concentration is determined using the bovine serum albumin (BSA) assay, which uses standards to determine the concentration of other proteins. The absorbance of the known standard is measured using a spectrometer and is plotted against concentration to give a standard curve which is then used to determine the protein concentration of the unknown sample (Figure 1.8.2.1).

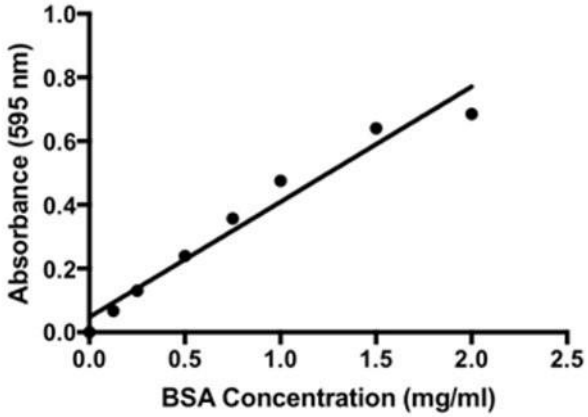

Figure 1.8.2.1. BSA standard curve.[58]

Once the protein concentration is known, the samples are prepared using the loading buffer, which consist of glycerol (to ensure that the sample sink easily into the wells during gel electrophoresis), bromophenol blue (acts as the tracking dye), sodium dodecyl sulphate (SDS, to denature proteins and give them an overall negative charge) and DL-dithiothreitol (DTT, reduces disulphide bonds in the proteins) (Figure 1.8.2.2).

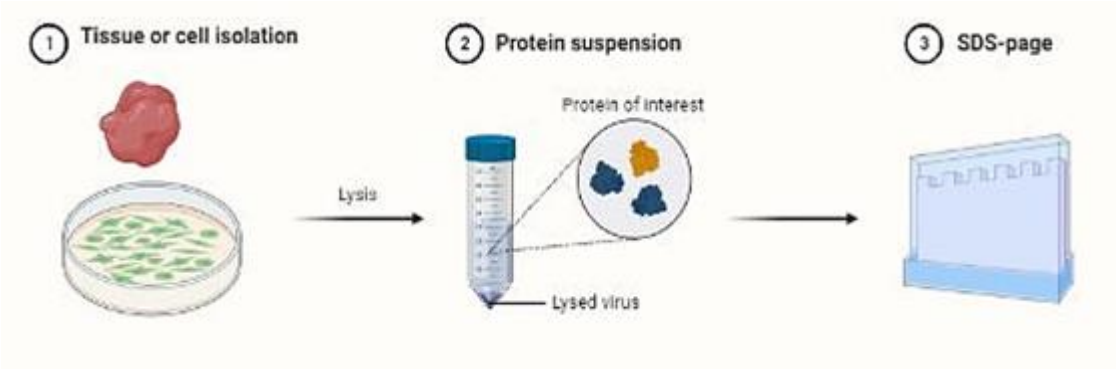

Figure 1.8.2.2. Preparation of samples and blotting process for Western Blotting.[59]

The second step is blotting and for this there are two types of gels used in western blots, the stacking and separating gel and the resolving gel. There is a range in pore size for the acrylamide gels, which allows for accurate separation of proteins based on their molecular weight. Smaller proteins pass through the pores faster and they require smaller pores. for Larger proteins require a lower percentage gel to allow them to pass through the gel. The stacking gel is slightly acidic compared to the resolving gel and also has lower acrylamide concentration. When separation is complete, the proteins are transferred to a membrane. There are two membrane types which can be used, poly-vinylidene fluoride (PVDF) and nitrocellulose membranes. The proteins stick to the membrane through hydrophobic interactions allowing for the probing and visualization of the proteins.

Next, the processes of blocking, antibody incubation and detection take place (Figure 1.8.2.3). High background due non-specific binding sites on the membrane can be an issue with western blotting. To avoid this the membrane is incubated with a blocking solution consisting of non-fat milk diluted in TBST or BSA in TBST. This prevents

antibodies from binding to nonspecific bands on the membrane. Following blocking the membrane is incubated with the antibody of interest, the primary antibody. This is carried out for the specific period of time that the respective antibody requires to bind and detect a specific protein, such as ERK. Antibodies bind to an epitope of the protein on the membrane. Following incubation, the membrane must be washed to minimize background and remove any unbound antibody. Once the membrane is washed, it is incubated with a secondary antibody, conjugated to horseradish peroxidase, which recognises a specific domain of the primary antibody. Electrochemiluminescence (ECL), containing luminol is next used to detect the protein, when the luminol is oxidised by Horseradish peroxidase (HRP) light is emitted which can then be detected by the Gel Doc.[60]

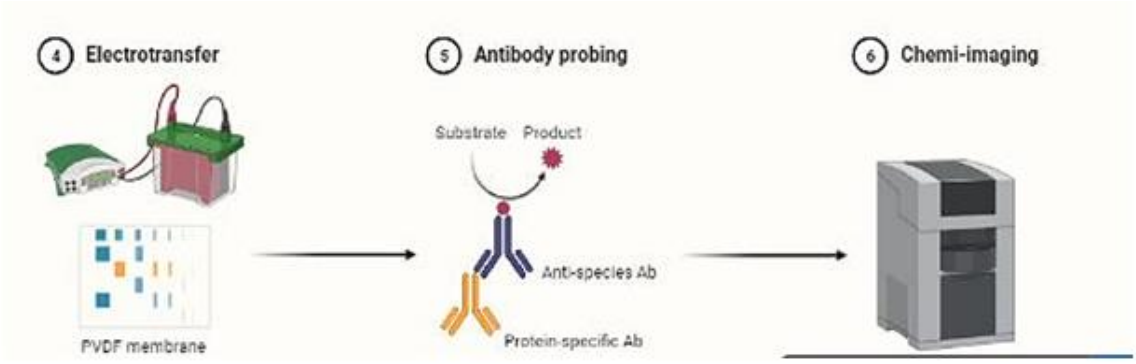

Figure 1.8.2.3. Transfer, blocking and incubation steps for Western Blotting.[59]

1.9. Previous work leading up to the present research

Previous research in the Rozas group focused on the design, synthesis, and biological evaluation of DNA minor groove binders, which were evaluated for their DNA affinity and effect on cancer cell viability. Some of these compounds were found to induce cell death at low concentrations.

Several biophysical studies such as isothermal calorimetry, UV titration methods and surface plasmon resonance, showed that some compounds inducing high levels of apoptosis did not bind to the minor groove.[61] These results led to the conclusion that, for these compounds, there must be a different apoptotic mechanism of action. Specifically, it was observed that these compounds exhibit structural similarities to the commercially available anticancer drug, sorafenib, an inhibitor of several protein

kinases, such as VEGFR, PDGFR and Raf family kinases, in terms of the diaryl system, and urea/guanidine functionalities (Figure 1.9.1).

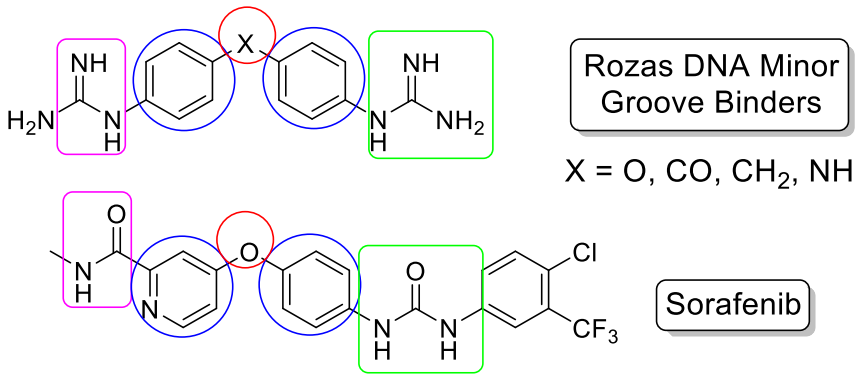

Figure 1.9.1. General structure of DNA minor groove binders prepared in the Rozas group and structure of sorafenib.

Based on these structural similarities, it was postulated that those compounds with a high antiapoptotic profile but were not found to be DNA minor groove binders could potentially act as PKIs, leading to the design, synthesis, and biological evaluation of novel 4,4'-bis-guanidium (N-substituted) and 3,4'-bis-guanidinium derivatives (Figure 1.9.2) as PKIs.[62]

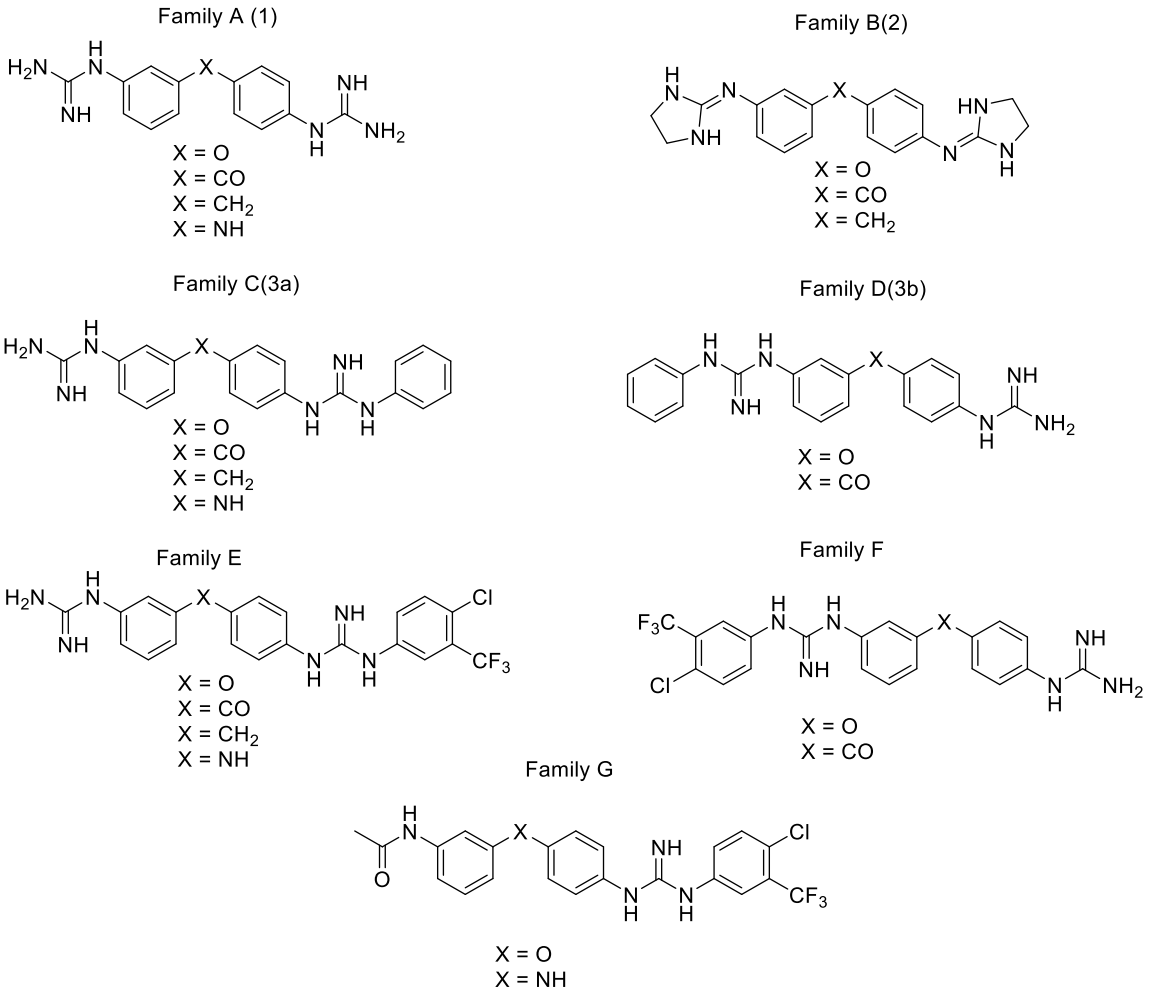

Figure 1.9.2. First generation of 4,4'-bis guanidine-like derivatives previously prepared in Rozas' lab as potential protein kinase inhibitors.

It was found that several of these compounds had good cell-growth inhibitory activity in selected cancer cell lines, namely HL-60 (human leukemia), HUH-7 (liver carcinoma), RKO (colorectal cancer) and MCF-7 (breast cancer). Assessment of the effect of these compounds in several kinases and kinases pathways, by means of a commercial panel, was carried out showing that lead compound **1** (Figure 1.9.3) displayed inhibition of the Raf-1/MEK-1 kinase pathway in >90% at 10 µM concentration.

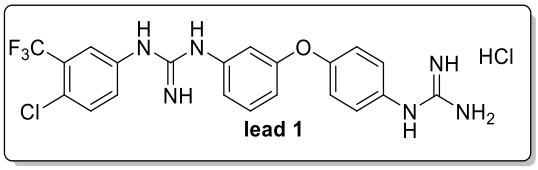

Figure 1.9.3. Structure of lead compound **1**.

A FRET experiment with B-Raf indicated that compound **1** did not displace ATP.[62] However, further protein expression studies with the RKO cell line displayed a reduction of phosphorylated ERK with **1**,[62] indicating the downregulation of the MAPK pathway, probably through allosteric type III binding. Further *in silico* docking studies in an in-house developed model of ATP-containing active B-Raf,[63] showed when ATP was present, there was an electrostatic interaction between the guanidium cation of **1** and one of the phosphate groups of ATP. Additionally, the 4-chloro-3-trifluoromethylphenyl group of **1** was oriented towards the hydrophobic pocket of the kinase.[62]

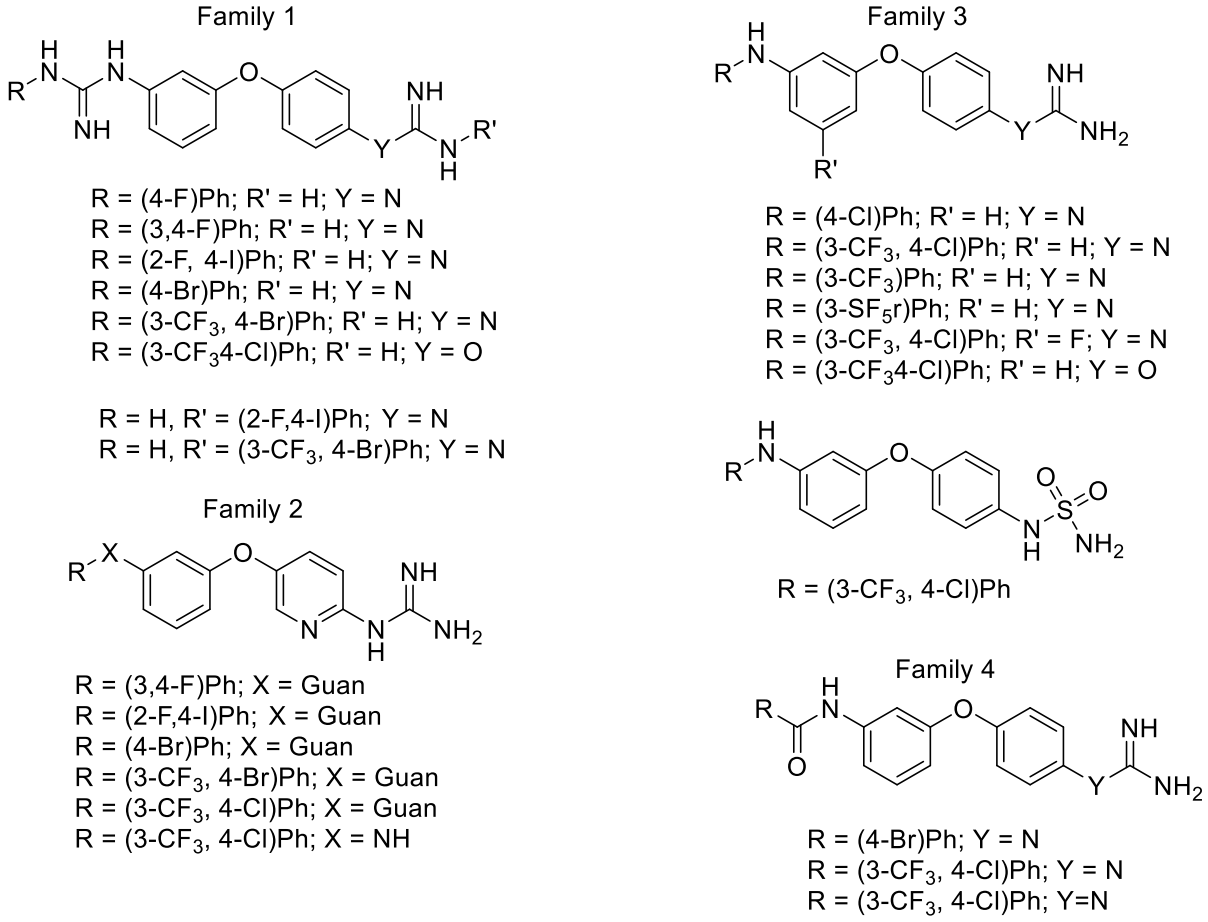

Figure 1.9.4. Second generation of 3,4'-bis-guanidine derivatives prepared in Rozas' lab.

To improve the activity of lead compound **1**, a second generation of derivatives were designed, synthesized, and biologically studied to elucidate the mode of action of these

modified compounds (Figure 1.9.4). Many of these new derivatives were found to inhibit cellular growth at low µM concentrations in different cancer cell lines (e.g. HL-60, MCF-7, HeLa –cervical cancer) and in particular lead compound **2** (Figure 1.9.5) was identified showing up to nine-fold increase in activity in HeLa cell line compared to **1**.[64]

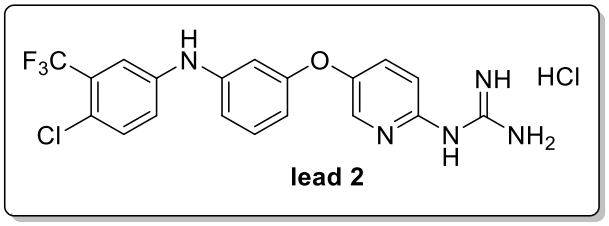

Figure 1.9.5. Structure of lead compound **2**

1.10. References

(1) Globocanhttps://gco.iarc.fr/today/online-analysis-pie?v=2020&mode=cancer&mode_population=continents&population=900&populations=900&key=total&sex=0&cancer=39&type=0&statistic=5&prevalence=0&population_group=0&ages_group%5B%5D=0&ages_group%5B%5D=17&nb_items=7&group_cancer=1&include_nmsc=1&include_nmsc_other=1&half_pie=0&donut=0.

(2) da Costa Vieira, R. A.; Biller, G.; Uemura, G.; Ruiz, C. A.; Curado, M. P. Breast Cancer Screening in Developing Countries. *Clinics (Sao Paulo).* **2017**, *72* (4), 244–253. https://doi.org/10.6061/clinics/2017(04)09.

(3) Hanahan, D.; Weinberg, R. A. Hallmarks of Cancer: The next Generation. *Cell* **2011**, *144* (5), 646–674. https://doi.org/10.1016/j.cell.2011.02.013.

(4) Fedi P. Tronick SR, A. S. Growth Factors. *Cancer Med.* **1997**, 41–64.

(5) Lukashev, M. E.; Werb, Z. ECM Signalling: Orchestrating Cell Behaviour and Misbehaviour. *Trends Cell Biol.* **1998**, *8* (11), 437–441. https://doi.org/10.1016/s0962-8924(98)01362-2.

(6) Giancotti, F. G.; Ruoslahti, E. Integrin Signaling. *Science* **1999**, *285* (5430), 1028–1032. https://doi.org/10.1126/science.285.5430.1028.

(7) Medema, R. H.; Bos, J. L. The Role of P21ras in Receptor Tyrosine Kinase Signaling. *Crit. Rev. Oncog.* **1993**, *4* (6), 615–661.

(8) Kerr, J. F.; Wyllie, A. H.; Currie, A. R. Apoptosis: A Basic Biological Phenomenon with Wide-Ranging Implications in Tissue Kinetics. *Br. J. Cancer* **1972**, *26* (4), 239–257. https://doi.org/10.1038/bjc.1972.33.

(9) Mohammad, R. M.; Muqbil, I.; Lowe, L.; Yedjou, C.; Hsu, H.-Y.; Lin, L.-T.; Siegelin, M. D.; Fimognari, C.; Kumar, N. B.; Dou, Q. P. Broad Targeting of Resistance to Apoptosis in Cancer. *Semin. Cancer Biol.* **2015**, *35 Suppl* (0), S78–S103.

https://doi.org/10.1016/j.semcancer.2015.03.001.

(10) Shalini, S.; Dorstyn, L.; Dawar, S.; Kumar, S. Old, New and Emerging Functions of Caspases. *Cell Death Differ.* **2015**, *22* (4), 526–539. https://doi.org/10.1038/cdd.2014.216.

(11) Fulda, S. Targeting Extrinsic Apoptosis in Cancer: Challenges and Opportunities. *Semin. Cell Dev. Biol.* **2015**, *39*, 20–25. https://doi.org/https://doi.org/10.1016/j.semcdb.2015.01.006.

(12) Huang, K.; Zhang, J.; O'Neill, K. L.; Gurumurthy, C. B.; Quadros, R. M.; Tu, Y.; Luo, X. Cleavage by Caspase 8 and Mitochondrial Membrane Association Activate the BH3-Only Protein Bid during TRAIL-Induced Apoptosis. *J. Biol. Chem.* **2016**, *291* (22), 11843–11851. https://doi.org/10.1074/jbc.M115.711051.

(13) Extrinsic Apoptosis Pathway https://www.creative-diagnostics.com/extrinsic-apoptosis-pathway.htm.

(14) Czabotar, P. E.; Lessene, G.; Strasser, A.; Adams, J. M. Control of Apoptosis by the BCL-2 Protein Family: Implications for Physiology and Therapy. *Nat. Rev. Mol. Cell Biol.* **2014**, *15* (1), 49–63. https://doi.org/10.1038/nrm3722.

(15) Xiong, S.; Mu, T.; Wang, G.; Jiang, X. Mitochondria-Mediated Apoptosis in Mammals. *Protein Cell* **2014**, *5* (10), 737–749. https://doi.org/10.1007/s13238-014-0089-1.

(16) Fulda, S.; Debatin, K.-M. Extrinsic versus Intrinsic Apoptosis Pathways in Anticancer Chemotherapy. *Oncogene* **2006**, *25* (34), 4798–4811. https://doi.org/10.1038/sj.onc.1209608.

(17) Pabo, C. O.; Sauer, R. T. PROTEIN-DNA RECOGNITION. *Annu. Rev. Biochem.* **1984**, *53* (1), 293–321. https://doi.org/10.1146/annurev.bi.53.070184.001453.

(18) Sirajuddin, M.; Ali, S.; Badshah, A. Drug–DNA Interactions and Their Study by UV–Visible, Fluorescence Spectroscopies and Cyclic Voltametry. *J. Photochem. Photobiol. B Biol.* **2013**, *124*, 1–19. https://doi.org/https://doi.org/10.1016/j.jphotobiol.2013.03.013.

(19) Walker, B. A.; Boyle, E. M.; Wardell, C. P.; Murison, A.; Begum, D. B.; Dahir, N. M.; Proszek, P. Z.; Johnson, D. C.; Kaiser, M. F.; Melchor, L. Mutational Spectrum, Copy Number Changes, and Outcome: Results of a Sequencing Study of Patients With Newly Diagnosed Myeloma. *J. Clin. Oncol. Off. J. Am. Soc. Clin. Oncol.* **2015**, *33* (33), 3911–3920. https://doi.org/10.1200/JCO.2014.59.1503.

(20) Cowan-Jacob, S. W.; Möbitz, H.; Fabbro, D. Structural Biology Contributions to Tyrosine Kinase Drug Discovery. *Curr. Opin. Cell Biol.* **2009**, *21* (2), 280–287. https://doi.org/https://doi.org/10.1016/j.ceb.2009.01.012.

(21) G. Manning, DB. Whyte, R. Martinez, T. Hunter, S. S. The Protein Kinase Complement of the Human Genome. *Science.* **2002**, *298* (5600), 1912–1934.

(22) Kornev, A. P.; Haste, N. M.; Taylor, S. S.; Ten Eyck, L. F. Surface Comparison of Active and Inactive Protein Kinases Identifies a Conserved Activation Mechanism. *Proc. Natl. Acad. Sci.* **2006**, *103* (47), 17783 LP-17788. https://doi.org/10.1073/pnas.0607656103.

(23) Knighton, D. R.; Zheng, J. H.; Ten Eyck, L. F.; Ashford, V. A.; Xuong, N. H.; Taylor, S. S.; Sowadski, J. M. Crystal Structure of the Catalytic Subunit of Cyclic Adenosine Monophosphate-Dependent Protein Kinase. *Science* **1991**, *253* (5018), 407–414. https://doi.org/10.1126/science.1862342.

(24) Yang, J.; Garrod, S. M.; Deal, M. S.; Anand, G. S.; Woods, V. L.; Taylor, S. Allosteric Network of CAMP-Dependent Protein Kinase Revealed by Mutation of Tyr204 in the P+1 Loop. *J. Mol. Biol.* **2005**, *346* (1), 191–201. https://doi.org/https://doi.org/10.1016/j.jmb.2004.11.030.

(25) Zhang, W.; Liu, H. T. MAPK Signal Pathways in the Regulation of Cell Proliferation in Mammalian Cells. *Cell Res.* **2002**, *12* (1), 9–18. https://doi.org/10.1038/sj.cr.7290105.

(26) Lee, S.; Rauch, J.; Kolch, W. Targeting MAPK Signaling in Cancer: Mechanisms of Drug Resistance and Sensitivity. *International Journal of Molecular Sciences* . 2020. https://doi.org/10.3390/ijms21031102.

(27) Huynh, H.; Nguyen, T. T. T.; Chow, K.-H. K.-P.; Tan, P. H.; Soo, K. C.; Tran, E. Over-

Expression of the Mitogen-Activated Protein Kinase (MAPK) Kinase (MEK)-MAPK in Hepatocellular Carcinoma: Its Role in Tumor Progression and Apoptosis. *BMC Gastroenterol.* **2003**, *3* (1), 19. https://doi.org/10.1186/1471-230X-3-19.

(28) Pratilas, C. A.; Solit, D. B. Targeting the MAPK Pathway: Physiological Feedback and Drug Response. *Clin. Cancer Res.* **2010**, clincanres.3064.subyr. https://doi.org/10.1158/1078-0432.CCR-09-3064.

(29) Davis, R. J. Signal Transduction by the JNK Group of MAP Kinases. *Cell* **2000**, *103* (2), 239–252. https://doi.org/https://doi.org/10.1016/S0092-8674(00)00116-1.

(30) Weston, C. R.; Davis, R. J. The JNK Signal Transduction Pathway. *Curr. Opin. Genet. Dev.* **2002**, *12* (1), 14–21. https://doi.org/https://doi.org/10.1016/S0959-437X(01)00258-1.

(31) Zarubin, T.; Han, J. Activation and Signaling of the P38 MAP Kinase Pathway. *Cell Res.* **2005**, *15* (1), 11–18. https://doi.org/10.1038/sj.cr.7290257.

(32) Freshney, N. W.; Rawlinson, L.; Guesdon, F.; Jones, E.; Cowley, S.; Hsuan, J.; Saklatvala, J. Interleukin-1 Activates a Novel Protein Kinase Cascade That Results in the Phosphorylation of Hsp27. *Cell* **1994**, *78* (6), 1039–1049. https://doi.org/10.1016/0092-8674(94)90278-x.

(33) Raingeaud, J.; Gupta, S.; Rogers, J. S.; Dickens, M.; Han, J.; Ulevitch, R. J.; Davis, R. J. Pro-Inflammatory Cytokines and Environmental Stress Cause P38 Mitogen-Activated Protein Kinase Activation by Dual Phosphorylation on Tyrosine and Threonine. *J. Biol. Chem.* **1995**, *270* (13), 7420–7426. https://doi.org/10.1074/jbc.270.13.7420.

(34) Parker, C. G.; Hunt, J.; Diener, K.; McGinley, M.; Soriano, B.; Keesler, G. A.; Bray, J.; Yao, Z.; Wang, X. S.; Kohno, T. Identification of Stathmin as a Novel Substrate for P38 Delta. *Biochem. Biophys. Res. Commun.* **1998**, *249* (3), 791–796. https://doi.org/10.1006/bbrc.1998.9250.

(35) Jiang, Y.; Gram, H.; Zhao, M.; New, L.; Gu, J.; Feng, L.; Di Padova, F.; Ulevitch, R. J.; Han, J. Characterization of the Structure and Function of the Fourth Member of P38 Group Mitogen-Activated Protein Kinases, P38delta. *J. Biol. Chem.* **1997**, *272*

(48), 30122–30128. https://doi.org/10.1074/jbc.272.48.30122.

(36) Ge, B.; Gram, H.; Di Padova, F.; Huang, B.; New, L.; Ulevitch, R. J.; Luo, Y.; Han, J. MAPKK-Independent Activation of P38alpha Mediated by TAB1-Dependent Autophosphorylation of P38alpha. *Science* **2002**, *295* (5558), 1291–1294. https://doi.org/10.1126/science.1067289.

(37) Stokoe, D.; Engel, K.; Campbell, D. G.; Cohen, P.; Gaestel, M. Identification of MAPKAP Kinase 2 as a Major Enzyme Responsible for the Phosphorylation of the Small Mammalian Heat Shock Proteins. *FEBS Lett.* **1992**, *313* (3), 307–313. https://doi.org/10.1016/0014-5793(92)81216-9.

(38) Deak, M.; Clifton, A. D.; Lucocq, L. M.; Alessi, D. R. Mitogen- and Stress-Activated Protein Kinase-1 (MSK1) Is Directly Activated by MAPK and SAPK2/P38, and May Mediate Activation of CREB. *EMBO J.* **1998**, *17* (15), 4426–4441. https://doi.org/10.1093/emboj/17.15.4426.

(39) Huang, C.; Ma, W. Y.; Maxiner, A.; Sun, Y.; Dong, Z. P38 Kinase Mediates UV-Induced Phosphorylation of P53 Protein at Serine 389. *J. Biol. Chem.* **1999**, *274* (18), 12229–12235. https://doi.org/10.1074/jbc.274.18.12229.

(40) Zhu, C.; Zhang, M.; Hu, J.; Li, H.; Liu, S.; Li, T.; Wu, L.; Han, B. Prognostic Effect of IL-6/JAK2/STAT3 Signal-Induced MicroRNA-21-5p Expression on Short Term Recurrence of Hepatocellular Carcinoma after Hepatectomy. *Int. J. Clin. Exp. Pathol.* **2018**, *11* (8), 4169–4178.

(41) Pflanz, S.; Kurth, I.; Grötzinger, J.; Heinrich, P. C.; Müller-Newen, G. Two Different Epitopes of the Signal Transducer Gp130 Sequentially Cooperate on IL-6-Induced Receptor Activation. *J. Immunol.* **2000**, *165* (12), 7042–7049. https://doi.org/10.4049/jimmunol.165.12.7042.

(42) Heinrich, P. C.; Behrmann, I.; Müller-Newen, G.; Schaper, F.; Graeve, L. Interleukin-6-Type Cytokine Signalling through the Gp130/Jak/STAT Pathway. *Biochem. J.* **1998**, *334 (Pt 2* (Pt 2), 297–314.

(43) Imada, K.; Leonard, W. J. The Jak-STAT Pathway. *Mol. Immunol.* **2000**, *37* (1), 1–11. https://doi.org/https://doi.org/10.1016/S0161-5890(00)00018-3.

(44) Camporeale, A.; Poli, V. IL-6, IL-17 and STAT3: A Holy Trinity in Auto-Immunity? *Front. Biosci. (Landmark Ed.* **2012**, *17*, 2306–2326. https://doi.org/10.2741/4054.

(45) Mullighan, C. G.; Zhang, J.; Harvey, R. C.; Collins-Underwood, J. R.; Schulman, B. A.; Phillips, L. A.; Tasian, S. K.; Loh, M. L.; Su, X.; Liu, W. JAK Mutations in High-Risk Childhood Acute Lymphoblastic Leukemia. *Proc. Natl. Acad. Sci. U. S. A.* **2009**, *106* (23), 9414–9418. https://doi.org/10.1073/pnas.0811761106.

(46) Badelita, S.; Dobrea, C.; Colita, A.; Dogaru, M.; Dragomir, M.; Jardan, C.; Coriu, D. The Simultaneous Occurrence of Multiple Myeloma and JAK2 Positive Myeloproliferative Neoplasms - Report on Two Cases. *J. Med. Life* **2015**, *8* (1), 55–61.

(47) Zhang, J.; Yang, P. L.; Gray, N. S. Targeting Cancer with Small Molecule Kinase Inhibitors. *Nat. Rev. Cancer* **2009**, *9*, 28.

(48) Kuhn, D. Targeting Protein Kinases for Cancer Therapy. By David J. Matthews and Mary E. Gerritsen. *ChemMedChem* **2010**, *5* (11), 1948–1949. https://doi.org/https://doi.org/10.1002/cmdc.201000398.

(49) Wu, P.; Nielsen, T. E.; Clausen, M. H. FDA-Approved Small-Molecule Kinase Inhibitors. *Trends Pharmacol. Sci.* **2015**, *36* (7), 422–439. https://doi.org/https://doi.org/10.1016/j.tips.2015.04.005.

(50) Pottier, C.; Fresnais, M.; Gilon, M.; Jérusalem, G.; Longuespée, R.; Sounni, N. E. Tyrosine Kinase Inhibitors in Cancer: Breakthrough and Challenges of Targeted Therapy. *Cancers* . 2020. https://doi.org/10.3390/cancers12030731.

(51) Alexander, P. B.; Wang, X.-F. Resistance to Receptor Tyrosine Kinase Inhibition in Cancer: Molecular Mechanisms and Therapeutic Strategies. *Front. Med.* **2015**, *9* (2), 134–138. https://doi.org/10.1007/s11684-015-0396-9.

(52) Garuti, L.; Roberti, M.; Bottegoni, G. Non-ATP Competitive Protein Kinase Inhibitors. *Curr. Med. Chem.* **2010**, *17* (25), 2804–2821. https://doi.org/10.2174/092986710791859333.

(53) Hsu, W.-H.; Yang, J. C.-H.; Mok, T. S.; Loong, H. H. Overview of Current Systemic

Management of EGFR-Mutant NSCLC. *Ann. Oncol.* **2018**, *29*, i3–i9. https://doi.org/10.1093/annonc/mdx702.

(54) Gramza, A. W.; Corless, C. L.; Heinrich, M. C. Resistance to Tyrosine Kinase Inhibitors in Gastrointestinal Stromal Tumors. *Clin. cancer Res. an Off. J. Am. Assoc. Cancer Res.* **2009**, *15* (24), 7510–7518. https://doi.org/10.1158/1078-0432.CCR-09-0190.

(55) Adan, A.; Alizada, G.; Kiraz, Y.; Baran, Y.; Nalbant, A. Flow Cytometry: Basic Principles and Applications. *Crit. Rev. Biotechnol.* **2017**, *37*, 163–176.

(56) cell cycle profile https://www.nexcelom.com/applications/cellometer/fluorescent-assays/cell-cycle-analysis/.

(57) Wlodkowic, D.; Telford, W.; Skommer, J.; Darzynkiewicz, Z. Apoptosis and beyond: Cytometry in Studies of Programmed Cell Death. *Methods Cell Biol.* **2011**, *103*, 55–98. https://doi.org/10.1016/B978-0-12-385493-3.00004-8.

(58) Brzica, H.; Abdullahi, W.; Reilly, B. G.; Ronaldson, P. T. A Simple and Reproducible Method to Prepare Membrane Samples from Freshly Isolated Rat Brain Microvessels. *J. Vis. Exp.* **2018**, No. 135. https://doi.org/10.3791/57698.

(59) Western Blotting https://noteshippo.com/western-blotting-introduction-principle-steps-results-applications/.

(60) Mahmood, T.; Yang, P.-C. Western Blot: Technique, Theory, and Trouble Shooting. *N. Am. J. Med. Sci.* **2012**, *4* (9), 429–434. https://doi.org/10.4103/1947-2714.100998.

(61) Diez-Cecilia, E.; Kelly, B.; Perez, C.; Zisterer, D. M.; Nevin, D. K.; Lloyd, D. G.; Rozas, I. Guanidinium-Based Derivatives: Searching for New Kinase Inhibitors. *Eur. J. Med. Chem.* **2014**, *81*, 427–441. https://doi.org/https://doi.org/10.1016/j.ejmech.2014.05.025.

(62) Diez-Cecilia, E.; Carson, R.; Kelly, B.; van Schaeybroeck, S.; Murray, J. T.; Rozas, I. Probing a 3,4′-Bis-Guanidinium Diaryl Derivative as an Allosteric Inhibitor of the

Ras Pathway. *Bioorg. Med. Chem. Lett.* **2015**, *25* (19), 4287–4292. https://doi.org/https://doi.org/10.1016/j.bmcl.2015.07.082.

(63) Previtali, V.; Trujillo, C.; Boisson, J.-C.; Khartabil, H.; Henon, E.; Rozas, I. Development of the First Model of a Phosphorylated, ATP/Mg2+-Containing B-Raf Monomer by Molecular Dynamics Simulations: A Tool for Structure-Based Design. *Phys. Chem. Chem. Phys.* **2017**, *19* (46), 31177–31185. https://doi.org/10.1039/C7CP05038K.

(64) Previtali, V.; Mihigo, H. B.; Amet, R.; McElligott, A. M.; Zisterer, D. M.; Rozas, I. Exploring the Anti-Cancer Mechanism of Novel 3,4'-Substituted Diaryl Guanidinium Derivatives. *Pharmaceuticals* . 2020. https://doi.org/10.3390/ph13120485.

Chapter 2- Objectives

Previous work in the Rozas' group found bis-guanidine compounds hypothesised to be inhibitors of the Ras/ERK pathway. Lead compound **1** (Figure 2.1.1) was postulated to be an allosteric inhibitor of B-Raf by combining the results obtained from a FRET experiment with B-Raf revealing no displacement of ATP upon binding and from an in vitro kinase assay against MEK-1 peptide substrate; this hypothesis was also supported by computational studies. Additionally, compound **1** was shown to downregulate other

substrates such as Akt, MEK and ERK by Western Blot assays.[1] Following these positive results, a new family of derivatives were designed and synthesised, including compounds with different hydrophobic heads, linkers, and polar moieties. These derivatives were screened against a variety of cancer cell lines and thus lead compound **2** (Figure 2.1) was identified.

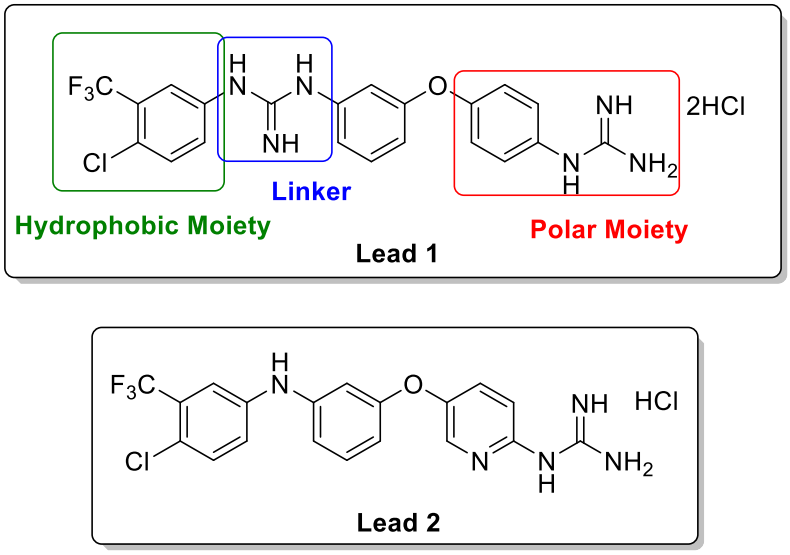

Figure 2.1. Chemical structure of lead compounds **1** and **2** and identification of the most relevant moieties.

Considering the promising results of these lead compounds as potential kinase inhibitors and anticancer agents, several objectives (computational, synthetic and biological objectives) are proposed to enhance the biological results obtained as well as to determine the mechanism of action of these compounds.

2.1. Computational objectives

Previously, the Rozas group in collaboration with Dr. Cristina Trujillo (School of Chemistry, TCD) and Prof. Eric Henon (University of Reims Champagne-Ardenne, Reims, France) developed a model of the active form of ATP-containing B-Raf protein kinase.[2] Based on this model, we propose to computationally study previous and newly design derivatives of lead compounds **1** and **2**, figure 2.1.1, by docking them allosterically in B-Raf.

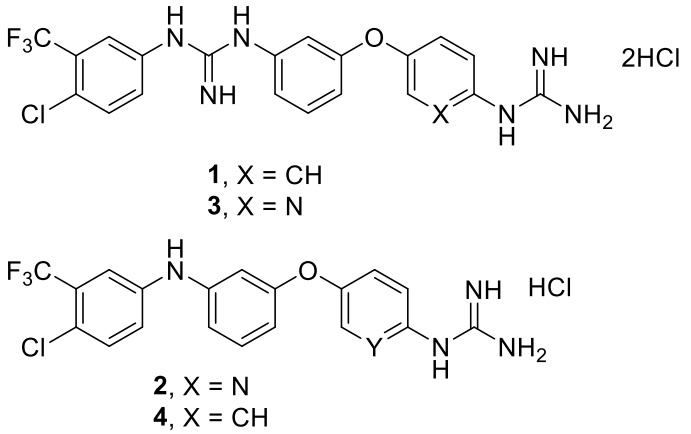

Figure 2.1.1. Compounds docked in B-Raf

In a parallel study within an on-going collaboration with the group of Prof. Daniela Zisterer (School of Biochemistry and Immunology, TCD), protein JAK2, of the JAK2/STAT3 pathway, was identified as a potential target for lead compound **2**. Thus, we propose to perform docking studies with derivatives of compound **2** in the JAK2 structure.

2.2. Synthetic objectives

Based on the already mentioned results, new derivatives of the lead compound **2** are proposed in order to improve its biological activity. Thus, we will introduce changes at the three different moieties identified in the lead compound, as well as changing the substitution pattern on the diaryl system or the nature of one of the aryl rings (Figure 2.2.1).

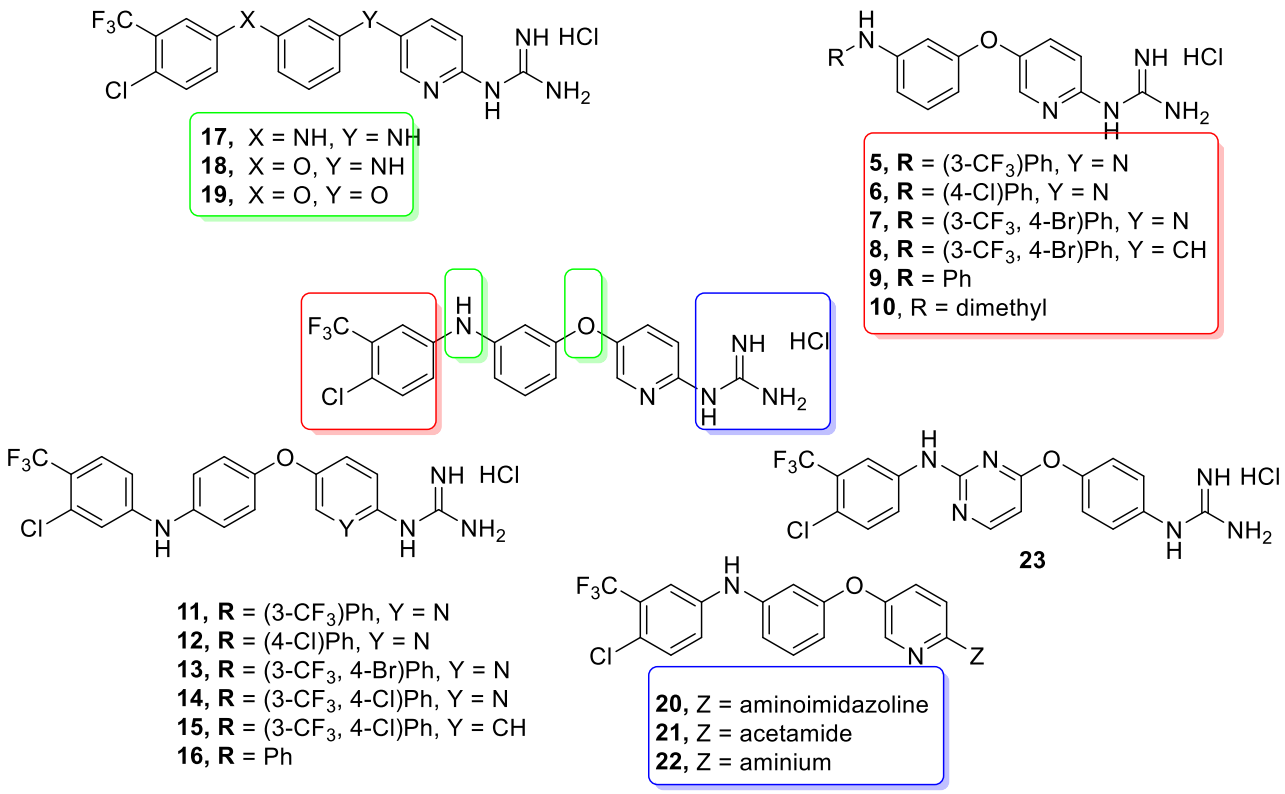

Figure 2.2.1. Proposed structural modifications on lead compound **2** to be investigated in this work.

Thus, changes in the hydrophobic moiety (red box in Figure 2.2.1) will be explored by introducing CF_3, Cl and Br in different positions of the phenyl ring, thus probing the hydrophobic pocket of the receptor. Following the previous docking studies of lead **1** and **2** in B-Raf, we will explore the effect of changing the substitution around the centre ring. This change will allow us to see the effect of the orientation that the cationic and lipophilic moieties take when binding to the target (black box in Figure 2.2.1).

Changes to the linker (green box in Figure 2.2.1) will allow us to understand the importance of hydrogen bond donors (HBDs) and acceptors (HBAs) in binding to the target. Figure 2.2.3 shows the proposed retrosynthetic Schemes for the preparation of the new compounds with different linkers.

In the blue box in Figure 2.2.1 the changes proposed for the polar moiety are shown, thus, we will explore the change of pyridino guanidines by phenyl or pyridyl 2-aminoimidazoline (i.e. loosing a HBD and increasing lipophilicity), acetamide (i.e. loosing two key interactions, the electrostatic interaction from the guanidinium as well as HBDs,

but gaining a HBA) or an amino group (i.e. removing completely the guanidino-like structure). Finally, the nature of the central phenyl group will be changed by a pyrimidine (purple box in Figure 2.2.1), thus introducing new potential interactions.

All these compounds will be prepared following methodologies already developed in the Rozas' group and some new synthetic approaches. The derivatives will be synthesised through nucleophilic aromatic substitution, S_NAr, Buchwald-Hartwig chemistry and Ullmann type coupling. Guanidylation will be carried using mercury (II) chloride and a Boc protected guanidine source. All final Boc-protected derivatives will be deprotected using different organic and inorganic solutions and the purity (>95%) of all final hydrochloride salts will be assessed by HPLC before biological assays.

2.3. Biological Objectives

The ability of the new derivatives proposed to inhibit growth or kill tumor cells will be evaluated commissioning a general screening with several types of cancer cells from the NCI-60 Human Tumor Cell Lines Screen. This screening is carried out using a sulforhodamine B (SRB) assay, with the effect of a 10 μM single dose measured in a first step, followed by measuring the effect of five different doses. This will help to determine which compounds cause cell death and which compounds cause cell growth inhibition and will provide a very broad profile of the potential of these compounds as anticancer agents.

Additionally, the mechanism of cell death caused by lead compound **1** and some of its analogues will be assessed by flow cytometry and Western blotting.

Finally, the mechanism of action of lead compound **2** and its derivatives will be studied by evaluating their effect on oncogenic signalling pathways, including RAS/ERK, PI3K/Akt and JAK2/STAT3 pathways by means of Western Blott assays.

2.4. Refences

(1) Diez-Cecilia, E.; Carson, R.; Kelly, B.; van Schaeybroeck, S.; Murray, J. T.; Rozas, I. Probing a 3,4'-Bis-Guanidinium Diaryl Derivative as an Allosteric Inhibitor of the Ras Pathway. *Bioorg. Med. Chem. Lett.* **2015**, *25* (19), 4287–4292. https://doi.org/https://doi.org/10.1016/j.bmcl.2015.07.082.

(2) Previtali, V.; Trujillo, C.; Boisson, J.-C.; Khartabil, H.; Henon, E.; Rozas, I. Development of the First Model of a Phosphorylated, ATP/Mg2+-Containing B-Raf Monomer by Molecular Dynamics Simulations: A Tool for Structure-Based Design. *Phys. Chem. Chem. Phys.* **2017**, *19* (46), 31177–31185. https://doi.org/10.1039/C7CP05038K.

Chapter 3 – Computational studies

As mentioned in Chapter 1, cancer remains a global and serious public health challenge and is considered one of the significant causes of death in our lifetime. While we have advanced in the understanding of the disease through biology, the development of small molecules for the treatment of cancer is still time consuming and expensive. This is where computational methods become an asset for drug discovery as it makes the whole process more focused, cheaper, and faster (Figure 3.1).

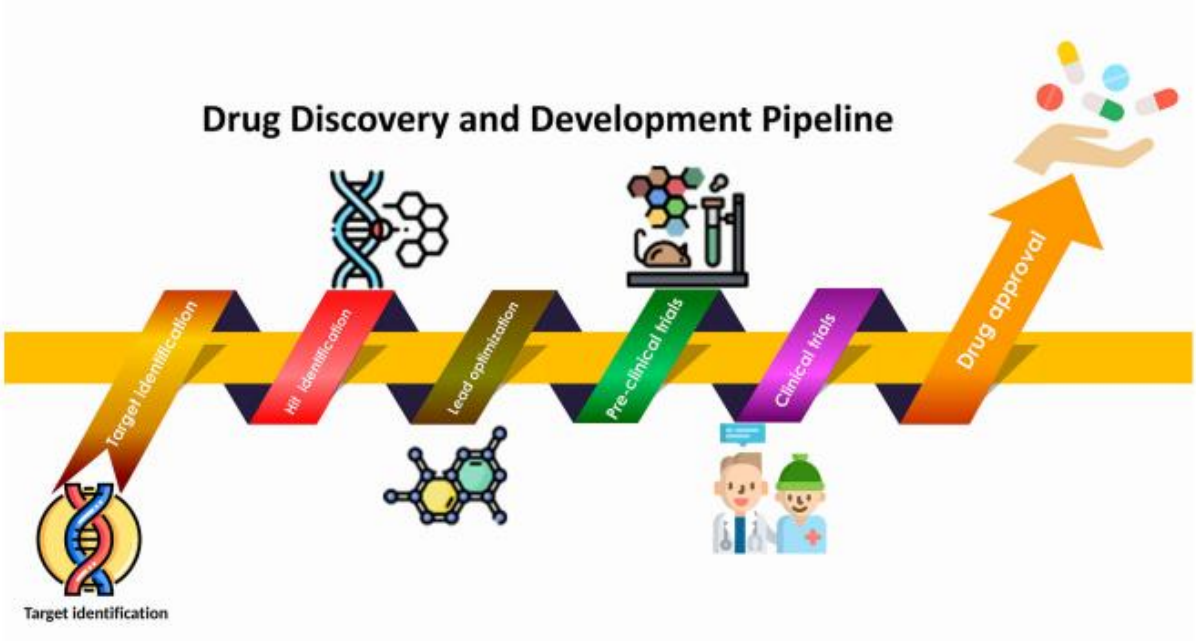

Figure 3.1. A workflow for drug discovery: from target identification to drug approval.[1]

Traditionally in drug discovery, a molecule is designed to aim to one specific target. While this can mirror the in-vitro tests where the specific target is isolated, it is less likely to be an effective model for the in-vivo process where the target does not exist in isolation and involves a rather complex set of factors contributing to the disease. One-molecule one-target approach is ineffective where multiple stages of the disease pathway need to be manipulated and considering that many drug molecules are considered as poly-pharmacological. Furthermore, as mentioned in Chapter 1, a family of proteins such as kinases can have conserved amino acid sequence, which can make

the design of a molecule that is selective for only one target, a difficult process. Thus, drug discovery requires us to understand interactions between the drugs and the many targets they can have and this can be achieved by using computational techniques.

Computational methods are frequently employed in the drug discovery process; different computational tools can be used for ligand discovery based on the information available. Therefore, there are two key approaches: structure-based drug design (SBDD) and ligand-based drug design (LBDD).

Structure-based drug design (SBDD, Figure 3.2) consists of the design and optimization of a potential drug by means of identifying the interacting elements of the target and the ligand which are responsible of the corresponding biological activity. Therefore, it requires the 3-dimensional structure of the target to be known. The completion of the human genome project has fuelled the development of structure-based drug design, while X-ray crystallography and NMR have greatly impacted the further identification of new targets. Knowing the 3-D structures of the targets, new specific/selective ligands can be designed. Hence, SBDD is a great tool for designing and developing new ligands by looking at their affinity to the target through molecular docking.

Molecular docking investigates the binding pattern and interactions between the ligand and the target.[2] It is assumed that ligands bind to the target through the classical "lock and key" paradigm or through the induced fit mechanism. In the "lock and key" approach, only the static geometrical, physical and chemical complementary between the ligand and the receptor are considered, and for that reason it is also known as rigid-rigid docking method.[3] On the contrary, in the induced fit/flexible docking methodology, flexible ligands are docked into a pocket or active site of the target with flexible residues. When a docking experiment has been performed, various binding poses are obtained which are ranked by the Gscore. The Gscore is an empirical scoring function that represents the binding affinity (kcal mol^{-1}) where the best poses are those with lower Gscore values.

In the ligand-based drug design (LBDD, Figure 3.2) the 3D structure of the target is not known, instead new ligands and derivatives are designed based on molecular similarities

of known ligands as molecules tend to similarly exert their biological activity due to similarities in their interaction with the targets.[1]

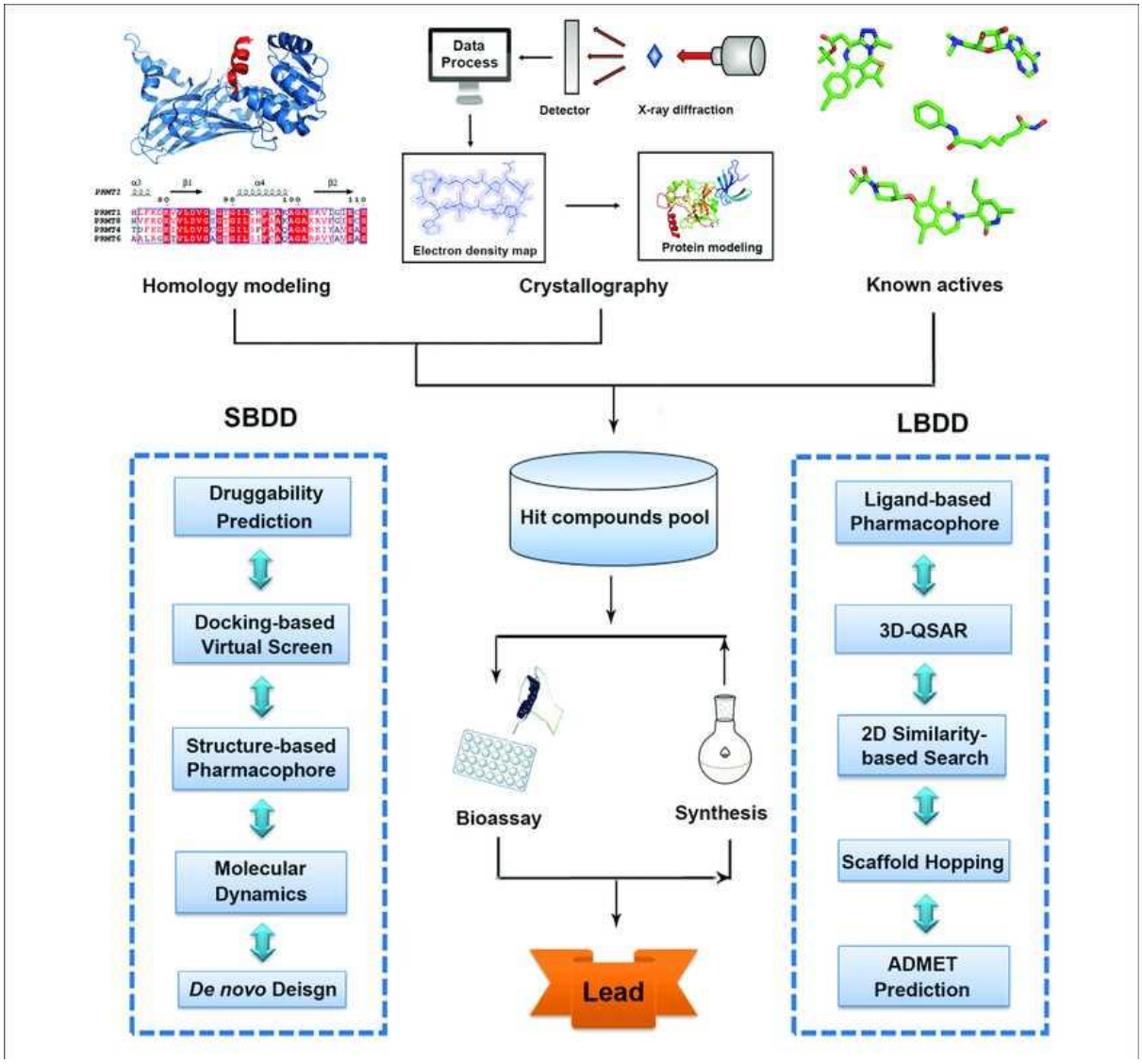

Figure 3.2. Traditional workflow of structure-based drug design (SBDD) and ligand-based drug design (LBDD)[4]

3.1. Docking studies of derivatives of lead compounds 1 and 2 in the in-house ATP-containing model of B-Raf

Previous computational studies showed that compound **1** interacts with the B-Raf model through an allosteric region found behind the ATP binding site as well as with a phosphate group of the ATP molecule itself (Figure 3.1.1).[5]

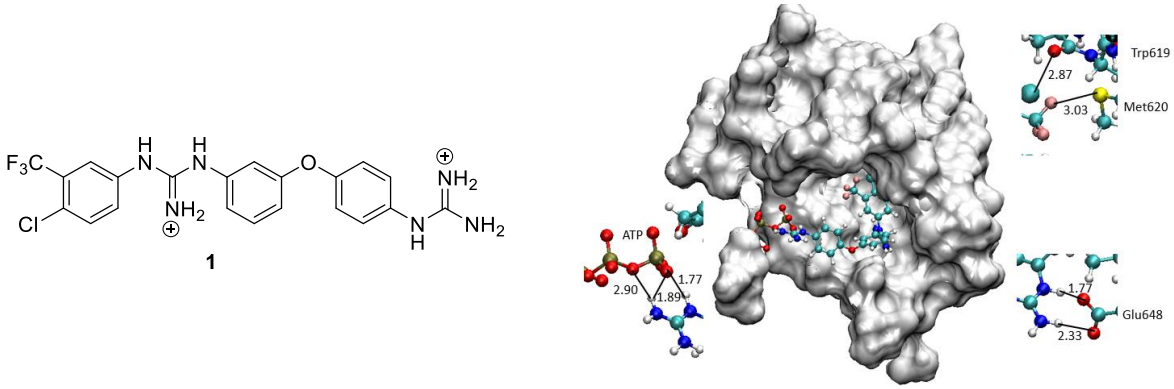

Figure 3.1.1. Structure of lead compound **1** and best pose obtained in the docking of **1** within the in-house developed ATP-containing B-Raf model using Autodock Vina.

The main interactions established between lead compound **1** and B-Raf comprise bifurcated HBs between the mono-substituted guanidinium cation and two negatively charged ATP phosphate groups (at 1.77, 2.9 and 1.89 Å, Figure 3.1.1) and a parallel HB interaction between the di-substituted guanidinium group and Glu648 (at 1.77 and 2.33 Å, Figure 3.1.1). Both sets of HBs are reinforced by ionic interactions due to the charged nature of guanidinium, phosphate and carboxylate groups.

However, lead compound **2** does not properly 'fit' into this binding site (Figure 3.1.2), because even though the hydrophobic pocket is also filled with the hydrophobic moiety of the molecule, instead of parallel HBs there is only one HB between the bridging secondary amine and the carboxylate of Glu648. Substitution of the di-substituted guanidino group in lead compound **1** by a secondary amino group in lead compound **2** results in shortening of the molecule, and this is reflected in elongating the HBs formed between the mono-substituted guanidium moiety, and the ATP's phosphates. The

pyridine introduces Intramolecular HB within lead compound **2**, which has contacts with Asn137.

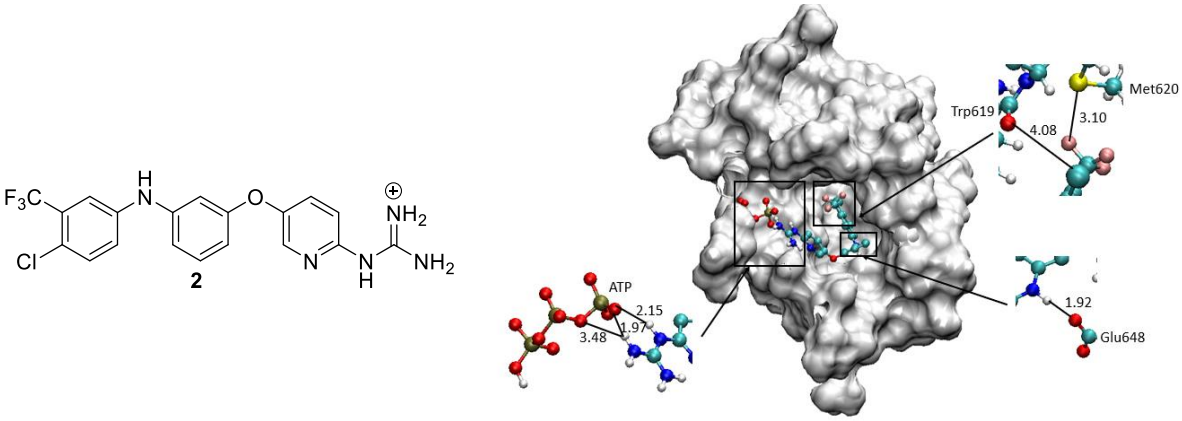

Figure 3.1.2. Structure of lead compound **2** and best pose obtained in the docking of **2** within our ATP-containing B-Raf model using Autodock Vina.

There are two main structural differences between lead compounds **1** and **2**, the disubstituted guanidino group vs. the secondary amino linker and the phenyl guanidinium vs. a pyridyl guanidinium system. To fully understand which of these differences lead to the drastic change in the binding to the target, two compounds with these features interchanged (compounds **3** and **4**, see structures in Figures 3.1.3 and 3.1.4) were also docked into the mentioned ATP-containing B-Raf model. These two compounds had been previously prepared by Dr. Viola Previtali in Rozas' group. From her previous biochemical studies with lead compound **1** and **3** in a variety of cell lines (see Table 3.1.1), it was concluded that the introduction of the pyridyl group leads to improved activity probably because the intramolecular hydrogen bond (IMHB) interaction formed between the guanidinium, and the pyridine ring may conformationally restrict the guanidinium group.

Table 3.1.1. Previous biochemical studies with compound **1** and its derivatives in a variety of cancer cell lines.[6]

cell line[a]	**1 (μM)**	**3 (μM)**	**4 (μM)**
HL-60	9.72	2.36	4.33

MCF-7	11.8	4.91	2.02
H929	4.85	6.35	3.72
U266	20.5	11.74	5.18

[a]Cell lines: HL-60, leukaemia;[7] MCF-7, breast cancer;[8] NCI-H929 & U266B1, multiple myeloma.[9,10]

When docked, compound **3** shows similar interactions with the target as the lead compound **1**, i.e. the bifurcated HBs between the mono-substituted guanidinium with two negatively charged ATP phosphate groups and a parallel HB interaction between the di-substituted guanidinium system and Glu64 (Figure 3.1.3). Both sets of HBs are reinforced by ionic interactions due to the charged nature of guanidinium, phosphate and carboxylate groups. Additionally, the pyridine ring introduces an IMHB which conformationally locks the mono-substituted guanidinium system. This may explain the increased specificity observed in the docking of this compound.

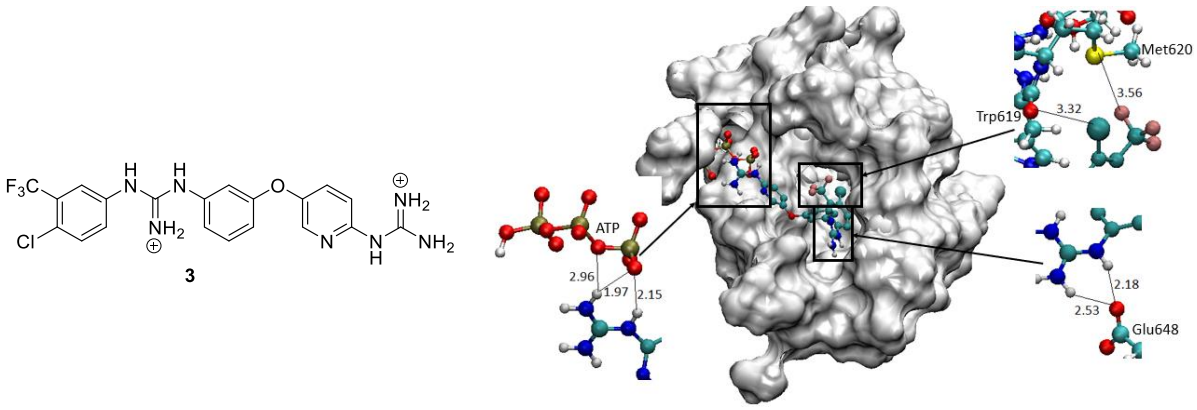

Figure 3.1.3. Structure of compound **3** and best pose obtained in the docking of **3** within our ATP-containing B-Raf model using Autodock Vina.

Similar to lead compound **2**, compound **4** has a significantly shorter structure due to the replacement of the disubstituted guanidine by a secondary amine (Figure 3.1.4). Although this molecule fits well into the hydrophobic pocked, it does not reach the ATP phosphoryl groups to form the expected bifurcated HBs, even though the ATP molecule in the model was allowed to move closer to the allosteric site to interact with the ligand. Accordingly, the parallel HBs previously observed with the disubstituted guanidine are now lost.

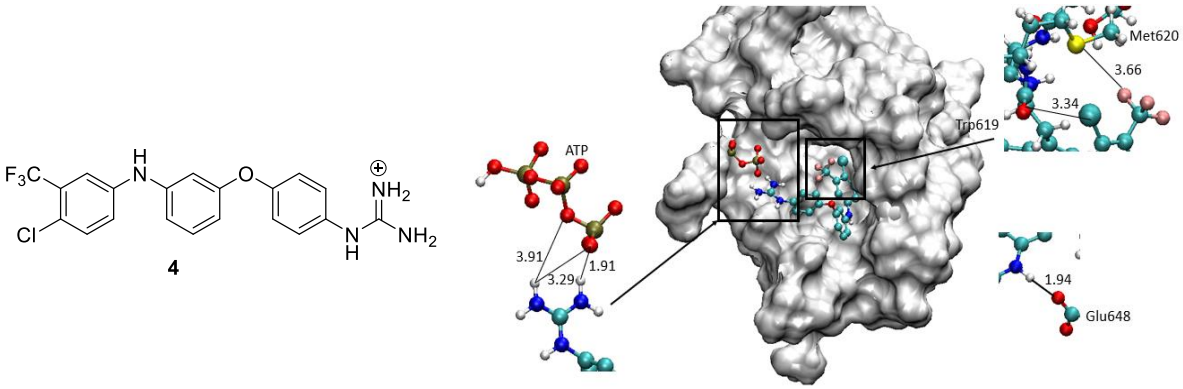

Figure 3.1.4. Structure of compound **4** and best pose obtained in the docking of **4** within our ATP-containing B-Raf model using Autodock Vina.

3.2. Docking studies of lead compound 1 and its derivative 3 as ATP competitive inhibitors of B-Raf

Following the observation of how compound **1** and its derivatives docked into the ATP-containing B-Raf model, other possible mechanisms of action for compound **1** and its derivatives were explored. Thus, considering that **1** optimally binds to the hydrophobic pocket and the ATP molecule, we explored the possibility of lead compound **1** competitively binding to the ATP binding site. Accordingly, compounds **1** and **3** were docked into a crystal structure of B-Raf with the DFG out and the αC-helix in (PDB: 6N0P), which is co-crystalized with LXH254, a known type 2 inhibitor (Figure 3.2.1).[11]

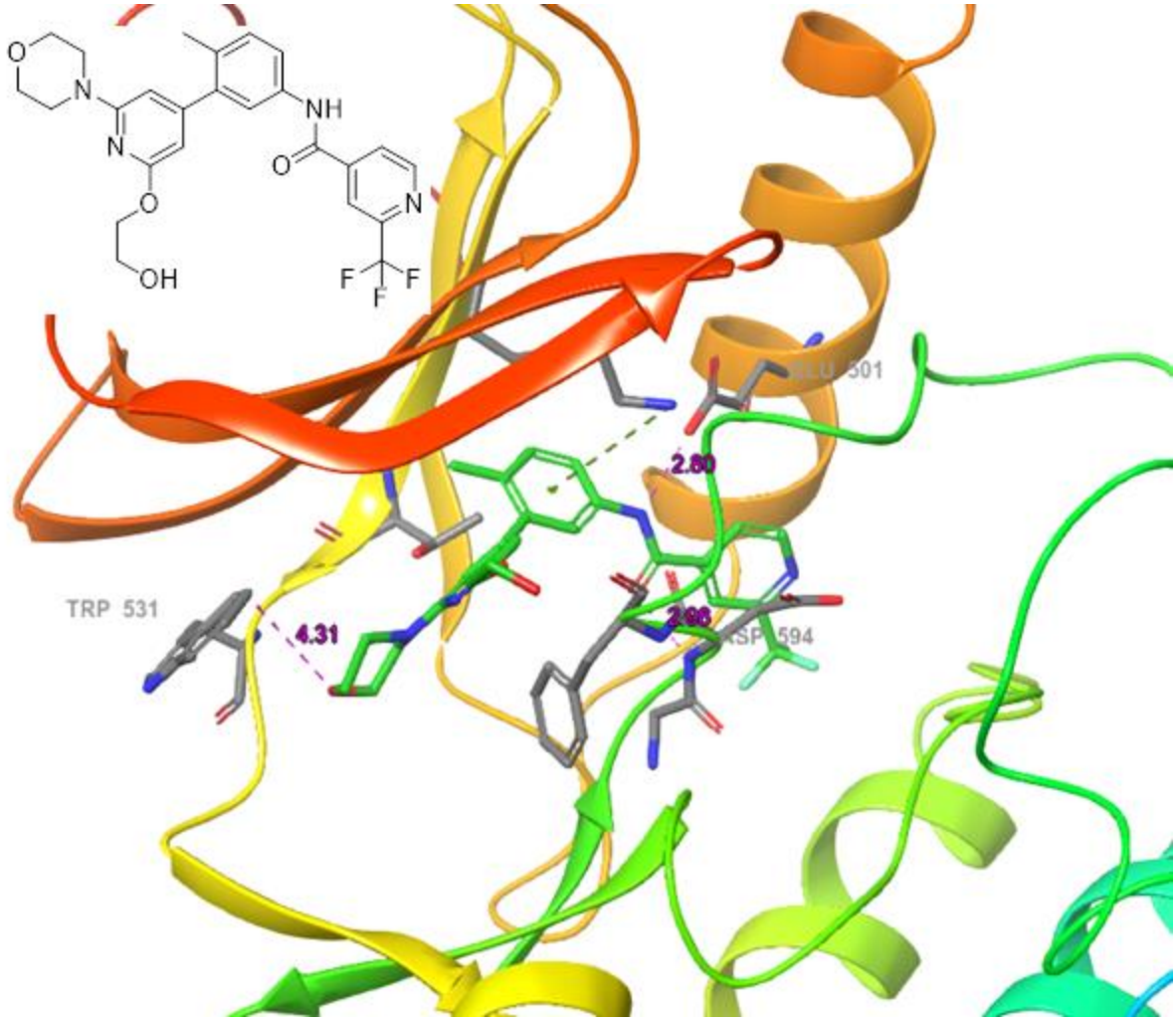

Figure 3.2.1. Structure of ATP competitive inhibitor LXH254, and structure of B-Raf co-crystalized with LXH254.

In the actual co-crystalized structure there are many key interactions between ligand and target; for example, the CF_3 pyridyl moiety fits well into the hydrophobic pocket, like other type II inhibitors, there is a HB interaction between Phe595 and the hydroxyl group, and also there is a π-cation interaction between the middle aromatic ring and Lys483.

The best pose obtained by docking compound **1** to the mentioned B-Raf crystal structure using Glide,[12] shows that **1** can bind to the ATP binding site with ease. The 2D ligand interaction representation (Figure 3.2.2, left) shows that the compound forms strong and stable interactions with the receptor. Like LXH254, compound **1** forms a π-cation interaction with Lys483, and also establishes additional strong interactions

including electrostatic interaction with Glu501 and further π-cation interactions with Trp531, Phe583 and Phe595.

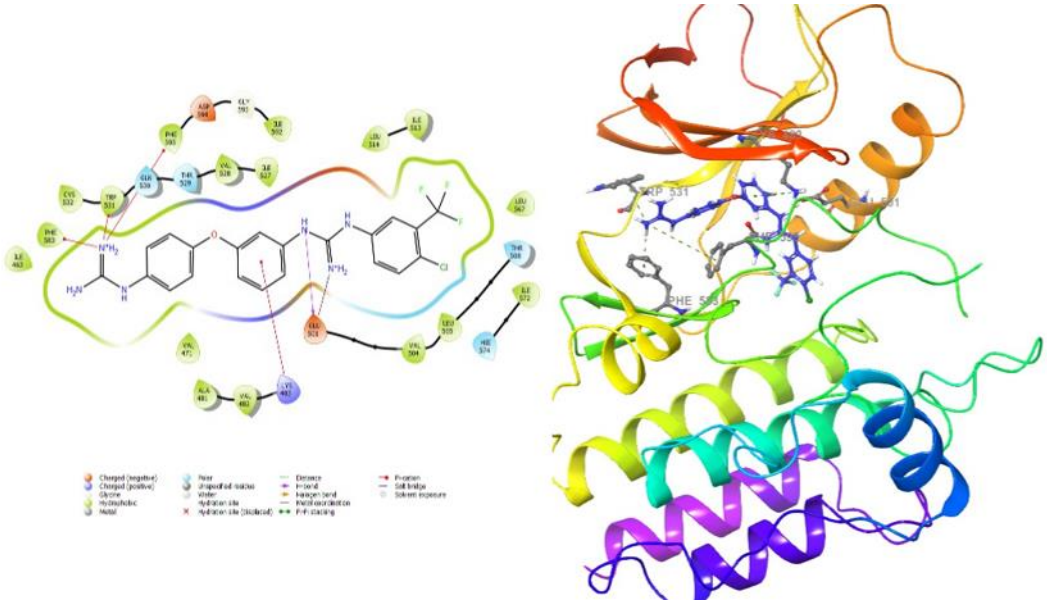

Figure 3.2.2. Best pose of **1** (Glide G-score of -7.51 kcal mol^{-1}) docked in the B-Raf crystal structure 6N0P using Glide Docking in the Schrodinger Suite.

Similar to its analogue **1**, the best pose of compound **3** docked into the B-Raf active structure shows that this derivative can also nicely bind to the ATP binding site with an even better G-score (Figure 3.2.3). The 2D ligand interaction representation (Figure 3.2.3, left) shows that the compound forms strong and stable interactions with the receptor. The mono-substituted guanidinium interacts with the hinge region of the kinase by forming a HB interaction with Cys532 (O···HN distance 1.8 Å), as well as π-cation interactions with Trp531. The pyridine is situated in a hydrophobic region near the hinge, which is approximately 4.79 Å away from Phe595, forming π-π stacking interactions. The di-substituted guanidine forms bifurcated HBs with Glu501 (1.41 and 2.42 Å) as well as ionic interactions with this same residue. The central phenyl system is out of the plane of the molecule allowing the di-substituted guanidine to form the mentioned bifurcated HB. Finally, the hydrophobic moiety occupies the hydrophobic region/type 2 pocket.

Both compounds **1** and **3** establish the same type of interactions, and are similarly oriented, but the pyridine ring of compound **3** provides an extra interaction that explains the better G-score obtained.

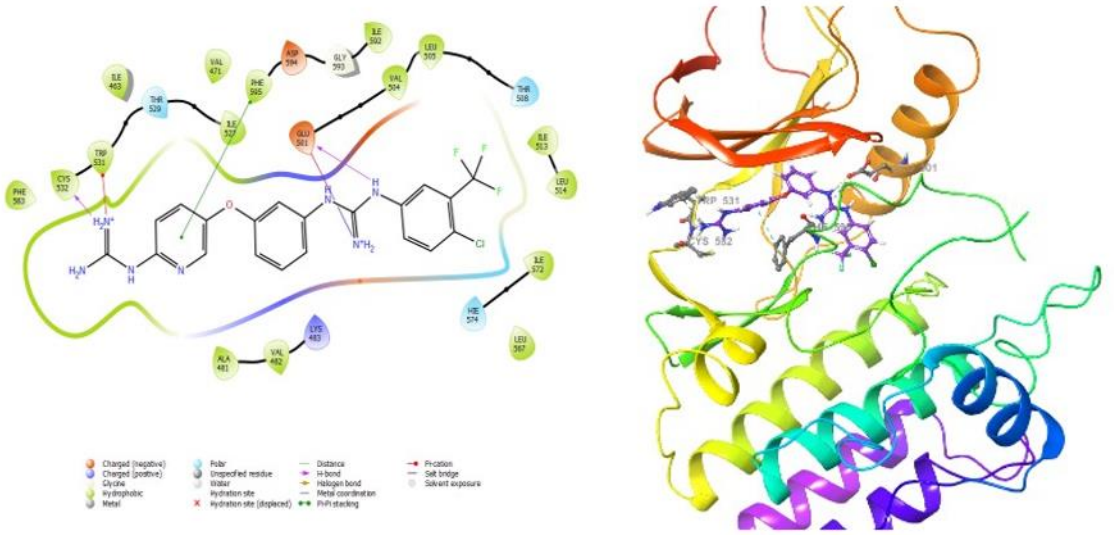

Figure 3.2.3. Best pose of **3** (Glide G-score of -10.01 kcal mol^{-1}) docked in the B-Raf crystal structure 6N0P, using Glide Docking in the Schrodinger Suite.

When looking at the overlayed structures (Figure 3.2.4) we can see that **1**, **3** and LXH254 are similar in size and occupy the same amount of space. All three compounds occupy the same hydrophobic pocket with the corresponding hydrophobic moieties. Regarding the linker between the diaryl system and the hydrophobic head, which in the case of compounds **1** and **3** is a guanidine, HB and electrostatic interactions with Glu501 are formed, However, compound LXH254, which shows an amido linker unable to form electrostatic interactions, HBs are established with Glu501 and Asp594. The inhibitor LXH254 and compound **1** form π-cation interactions between the central aromatic ring and Lys483; however, **3** forms instead π-π interactions with Phe595. Additionally, LXH254 forms a HB between an oxygen of the protein backbone and the OH; compound **1** forms π-cation interactions between the mono-substituted guanidine and Trp531,

Phe583 and Phe595; and finally, compound **3** forms a HB with Cys532 and a π-cation interaction with Trp531 at the mono substituted guanidine.

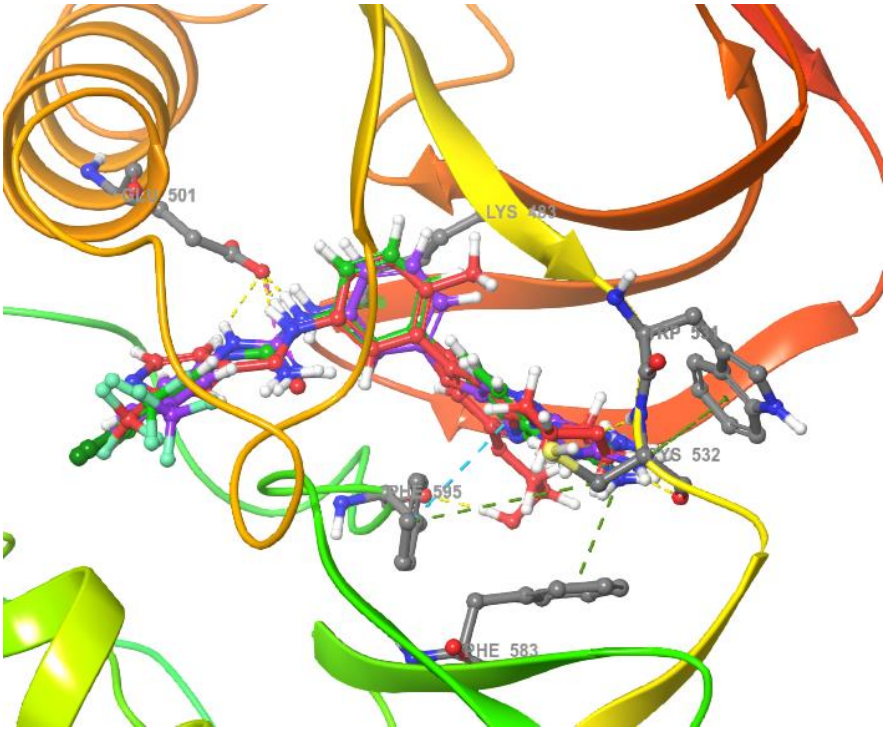

Figure 3.2.4. Overlaying of the best poses of **3** (purple) and compound **1** (green) docked in the ATP site of the B-Raf structure 6N0P also showing the native ligand, LXH254 (red),[13] image generated by Maestro.

3.3. Docking studies of derivatives of lead compound 1 as allosteric inhibitors with a B-Raf crystal structure without ATP

Ponatinib (Figure 3.3.1) is a BCR-ABL inhibitor commercially available for the treatment of chronic myeloid leukaemia, and, like many kinase inhibitors, it is also a B-Raf inhibitor. Unlike other Raf inhibitors, ponatinib binds B-Raf by forming interactions with an allosteric site as well as with the ATP binding site (Figure 3.3.1). Therefore, the structure of B-Raf co-crystallised with ponatinib (PDB: 6P3D[14]) provides a wonderful

template to study whether lead compound **1** and its derivative **3** could bind allosterically.

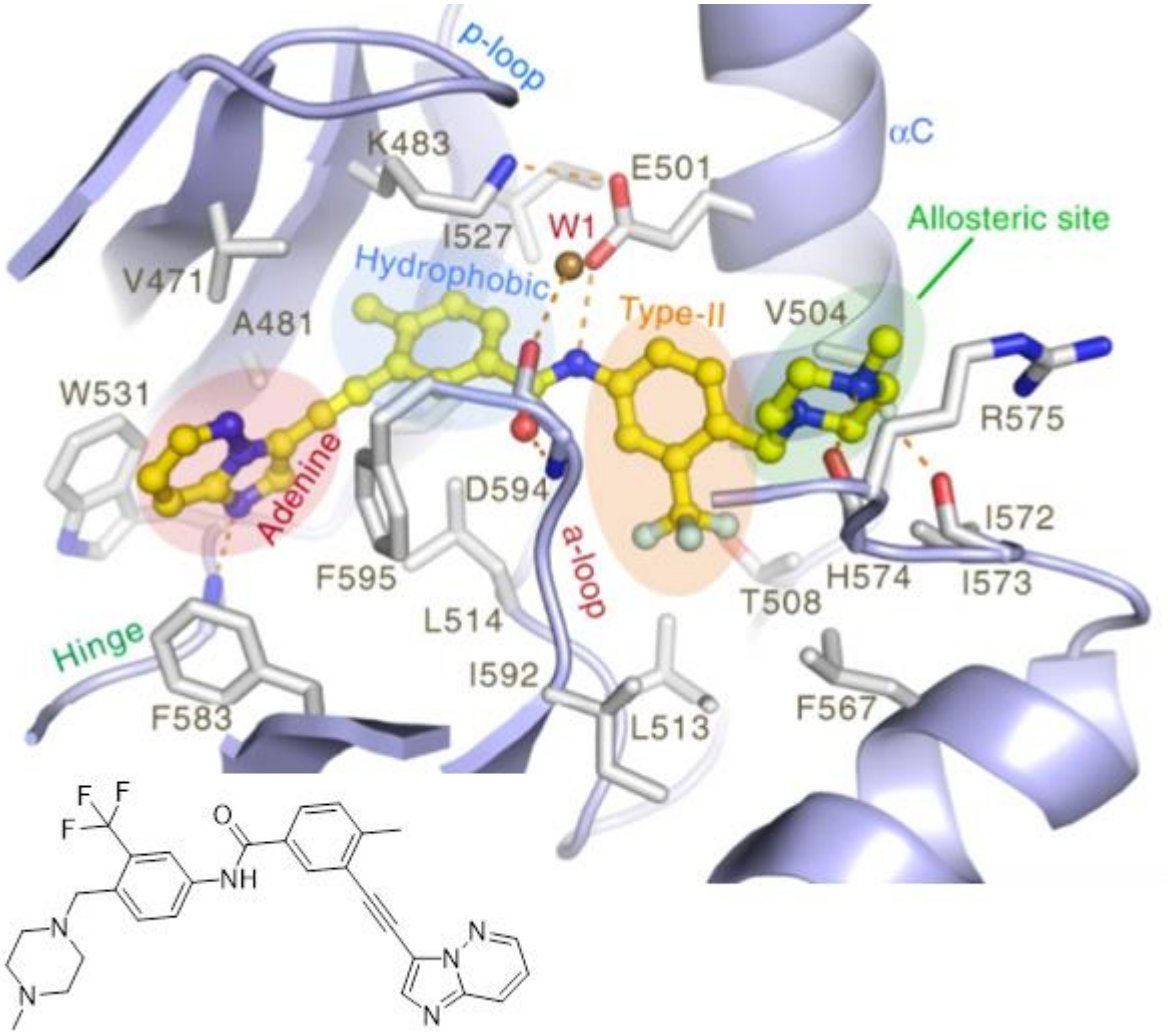

Figure 3.3.1. Structure of the allosteric inhibitor ponatinib and structure of B-Raf co-crystalized with ponatinib (PDB: 6P3D).[14]

Both compounds **1** and **3** dock well in the allosteric site of this B-Raf structure similarly to type 2 inhibitor ponatinib. In the best poses of the docking of these derivatives (Figures 3.3.2 and 3.3.3) it is observed that the di-substituted guanidine forms electrostatic as well as HB interactions with Glu501. Moreover, the pyridine ring in **3** and the corresponding phenyl ring in **1** form π-π stacking interactions with Phe595.

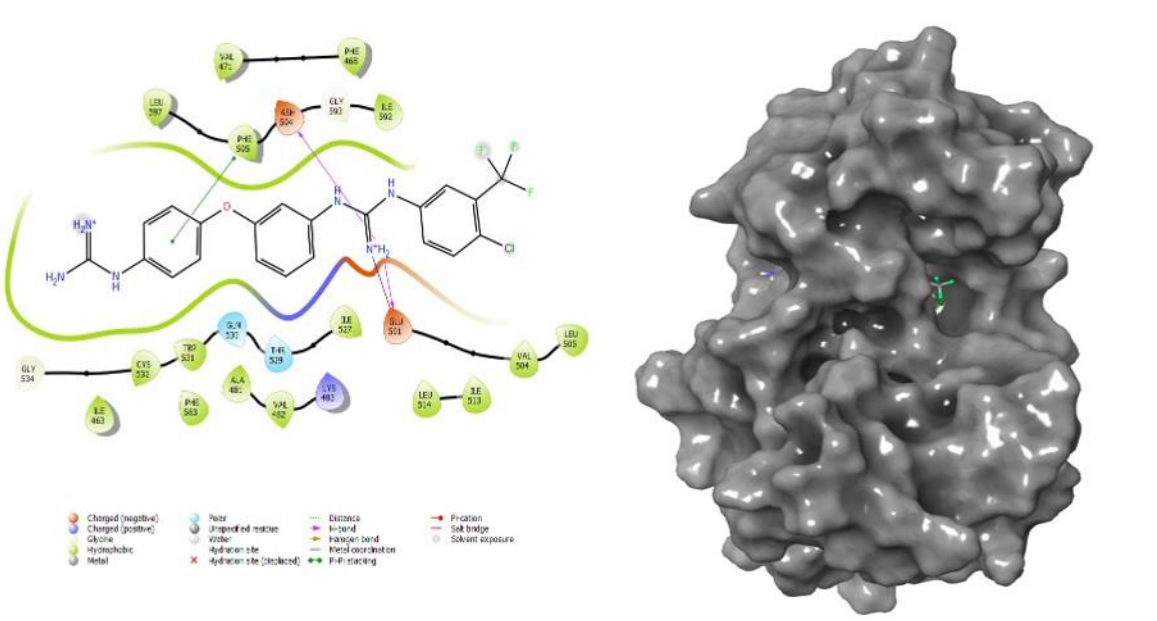

Figure 3.3.2. Best pose of **1** (Glide G-score of -6.24 kcal mol^{-1}) docked in the B-Raf crystal structure 6P3D using Glide Docking in the Schrodinger Suite.

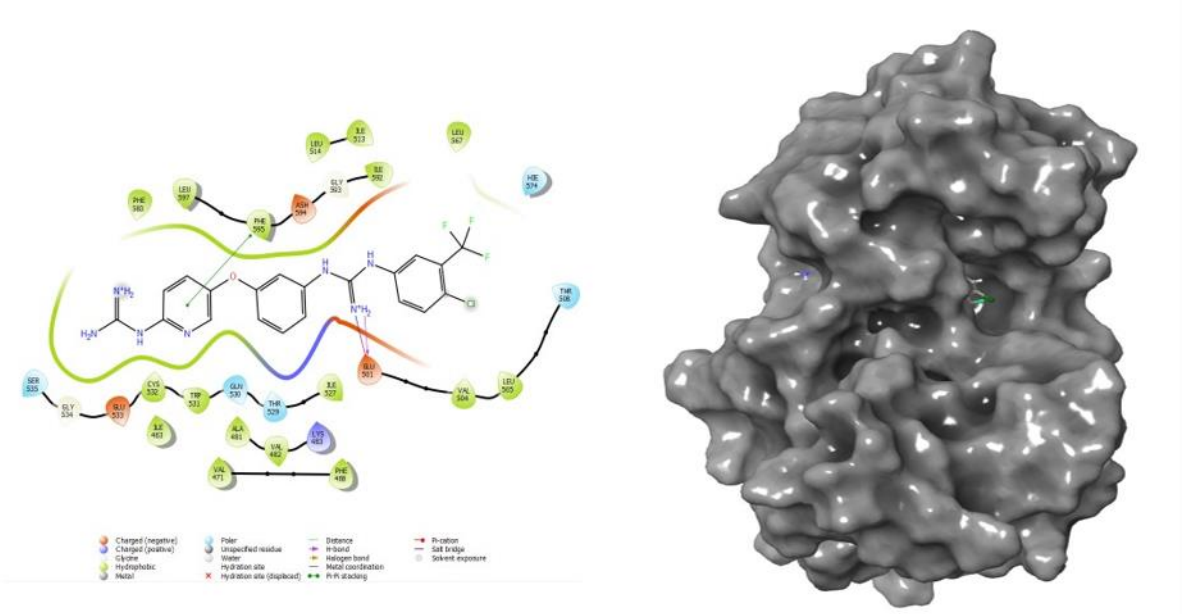

Figure 3.3.3. Best pose of **3** (Glide G-score of -7.58 kcal mol^{-1}) docked in the B-Raf crystal structure 6P3D using Glide Docking in the Schrodinger Suite.

These compounds do not form the same number of interactions with the target as ponatinib and this can be explained by their different structure as seen when overlapping them (Figure 3.3.4).

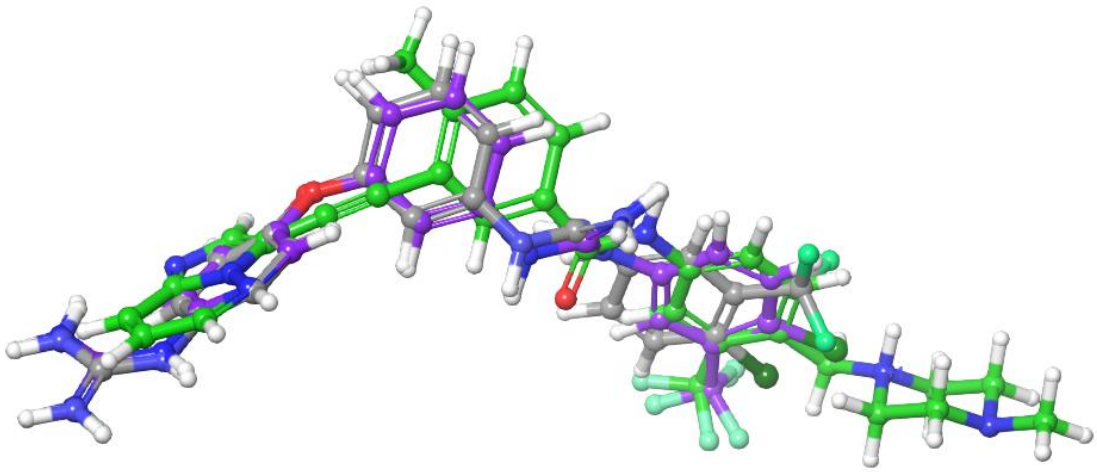

Figure 3.3.4. Overlaying the conformations found in the best pose of the docking of compounds **3** (purple) and **1** (grey) to the B-Raf structure 6P3D and that of the co-crystallised ligand ponatinib (green), image generated by Maestro.

3.4. Docking studies of lead compound 2 and its derivatives into a crystal structure of JAK2

While compound **2** had shown cytotoxic activity against cancer cell lines, there was no concrete evidence suggesting whether it exerted such cytotoxicity by inhibiting a particular kinase. In collaboration with Prof. Zisterer (School of Biochemistry and Immunology, TCD), the mechanism of action of compound **2** was studied finding that this compound inhibits a variety of kinases including JAK2 of the JAK/STAT pathway. Thus, we explored the possible binding interactions between compound **2** and JAK2 by performing docking studies.

In the last years, several JAK2 kinase inhibitors have been reported and approved by the FDA as anticancer agents including ruxolitinib, fedratinib and baricitinib; furthermore, other inhibitors such as gandotinib, pacritinib and XL 019 are undergoing clinical trials (Figure 3.4.1).

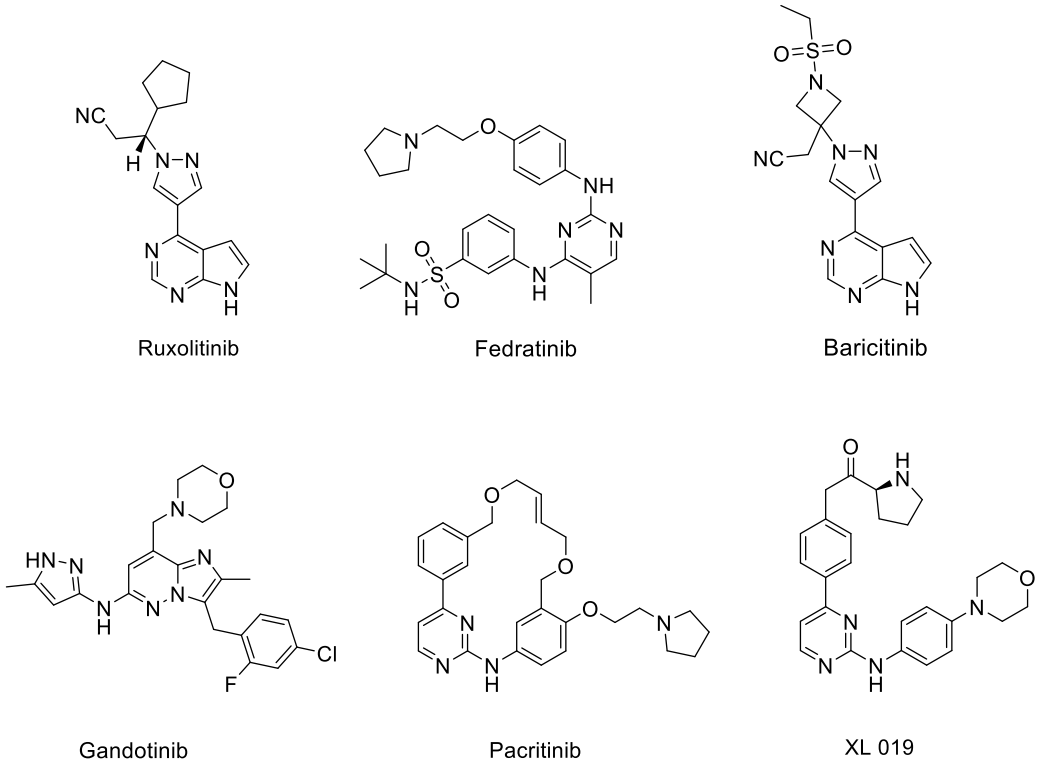

Figure 3.4.1. Structures of the JAK2 inhibitors ruxolitinib, fedratinib, baricitinib, gandotinib, pacritinib and XL 019.

Understanding ligand receptor interactions is of at most importance in structure-based drug design, thus, we used this method to rank our compounds based on their docking scores and potential pharmacological interactions with JAK2. As characteristic to all kinases, the structure of JAK2 contains both the N and the C lobes linked by a hinge region and the most important residues in the JAK2's hinge region are Glu930 and Leu932, as well as Asp994 and Phe995 in the A-loop.[15] Lin and co-workers recently identified the most important interactions established between known JAK2 ATP competitive inhibitors and JAK2 binding site (Figure 3.4.2) and the key contacts were HB and hydrophobic interactions.

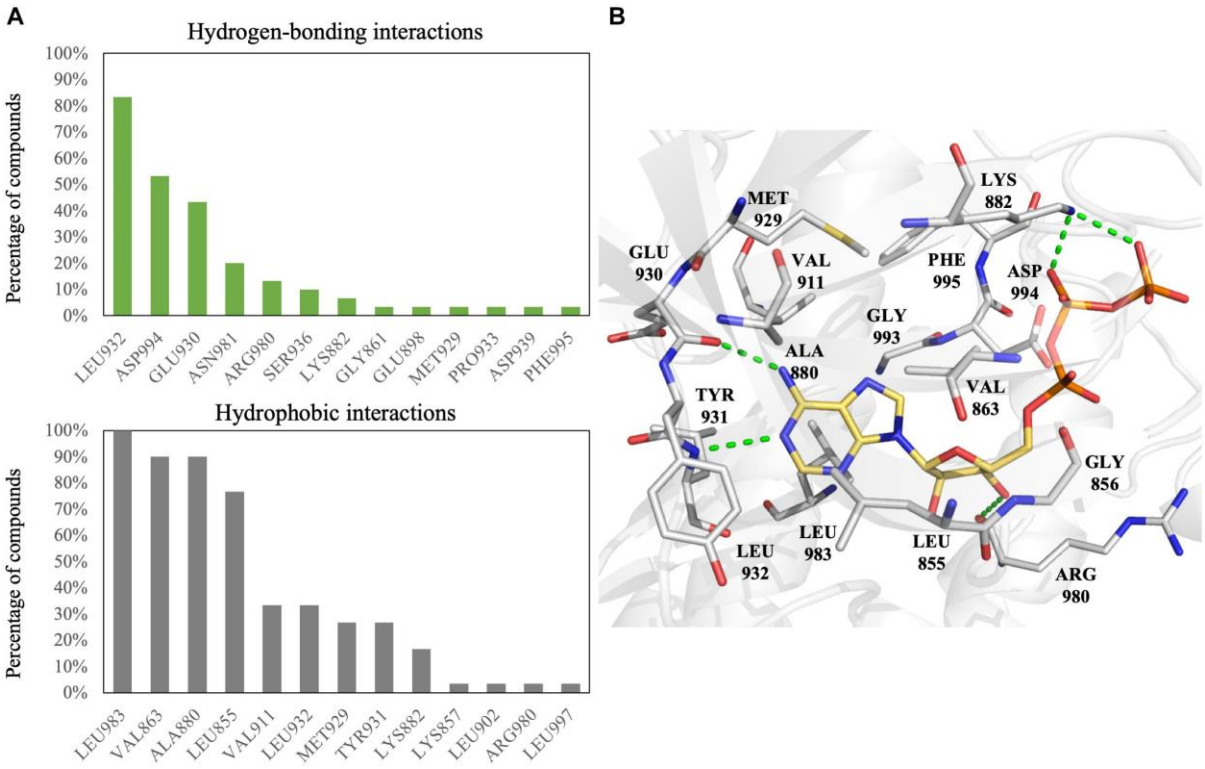

Figure 3.4.2. Interaction analysis for JAK2 inhibitors and JAK2 kinase. (A) Interactions of JAK2 binding site residues identified from known JAK2 inhibitors: HB (green) and hydrophobic (grey) Interactions. (B) Binding pose of ATP (yellow) in JAK2 (grey) as shown with Pymol. Green dashed lines denote HBs.[15]

When designing competitive kinase inhibitors, interactions with hinge residues are considered to be critical. In Lin's study,[15] it was found that 90% of known JAK2 inhibitors form HBs with the Leu-932 of the hinge region, and over 50% form HBs with the Asp994 in the DFG motif. Many of the JAK2 inhibitors also form HBs with the Glu930 residue; however, the number of contacts found was below the 50% cut-off point to be considered as a key interaction. A HB interaction between the Asp994 residue and JAK2 inhibitors is also common. When ATP binds to the JAK2 binding site, it does not interact with Asp994, but forms HBs between its phosphate group and the Lys882 residue; additionally, the adenosine ring forms HBs with the Leu932 and Glu930 residues.

The hydrophobic interactions identified by Lin et al. involved residues Leu983, Ala880, Val863 and Leu855 which form a hydrophobic pocket near the ATP molecule. This

pocket can be exploited when designing JAK2 inhibitors by including lipophilic groups in the structure. Considering that biochemical studies had been carried out with cells that did not have any JAK2 mutation, a crystal structure without mutations was used for the docking studies. A crystal structure of JAK2 with low resolution (i.e. 2.5 Å) co-crystallised with JZH which is a potent inhibitor was chosen (PDB: 3JY9) (Figure 3.4.3).

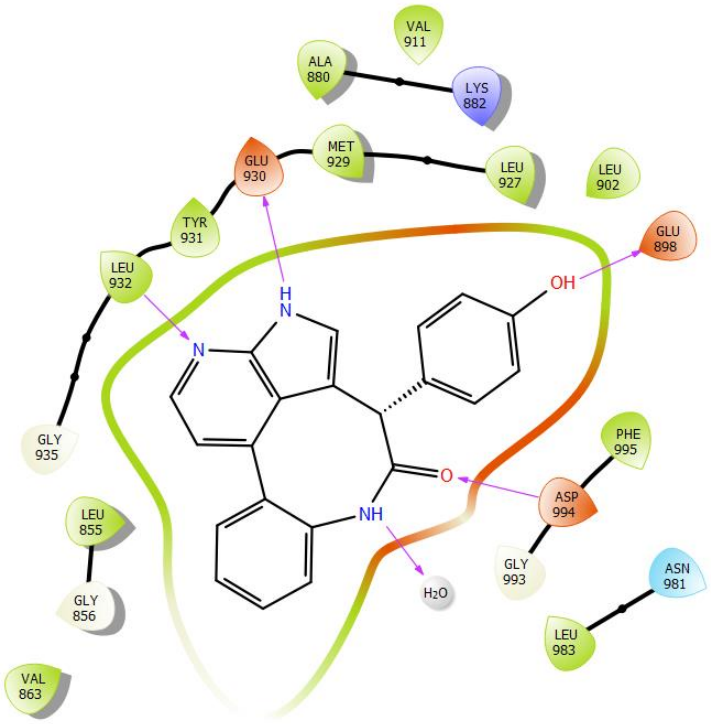

Figure 3.4.3. Ligand JZH co-crystallised with JAK2 (PDB: 3JY9). From the 2-D interaction diagram, JZH is seen to form HBs with many of the residues including Glu930 and Asp994, image generated by Maestro.

Docking of compound **2** to this JAK2 crystal structure (Figure 3.4.4) shows that the guanidinium group forms a bifurcated HB (2.66 and 1.75 Å) and a salt bridge with Asp 994 in the hinge region. Additionally, this guanidinium forms another HB with Lys 857 (2.07 Å) also in the hinge region of JAK2. The secondary amino group forms another HB with Glu930 further increasing the interaction of **2** with the hinge region. Interestingly, compound **2** also forms a halogen bond with Phe995 through the Cl substituent in the hydrophobic moiety.

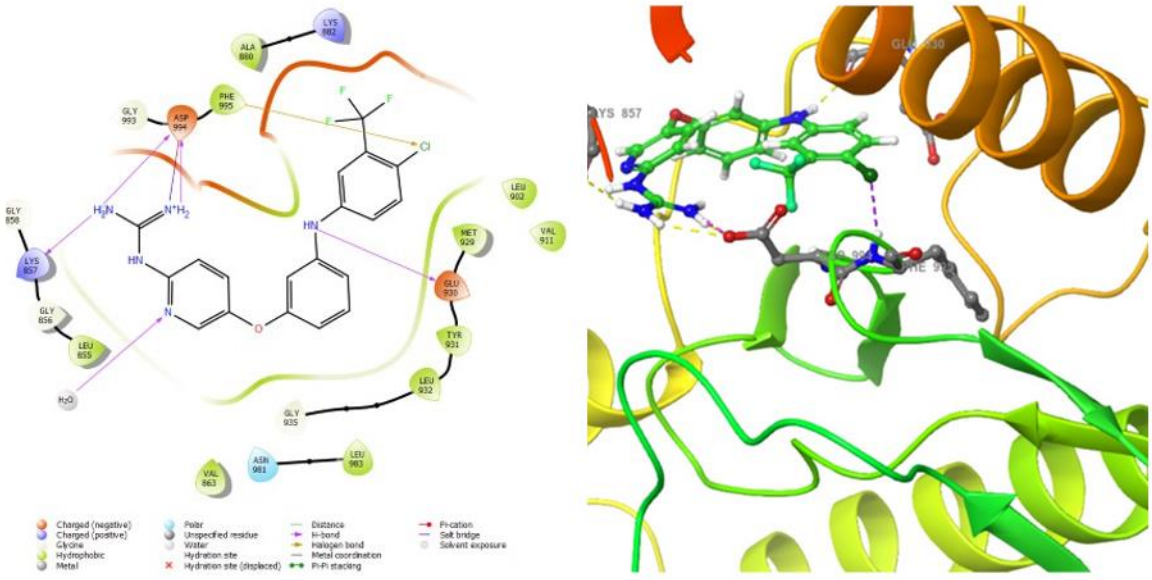

Figure 3.4.4. Best pose of compound **2** (Glide G-score of -11.19 kcal mol^{-1}) docked in the PDB:3JY9 crystal structure of JAK2, using Induced Fit Docking Protocol Glide in the Schrodinger Suite.

Following these results, we next analysed the binding of several derivatives of lead compound **2** by docking them to the same JAK2 crystal structure. First, we studied the effect of introducing changes in the hydrophobic moiety. Thus, docking of compounds **5-10** to the JAK2 template was carried out and the structures and G-scores obtained are shown in Figure 3.4.5.

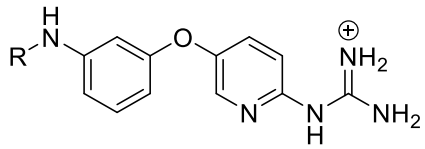

5, R = (3-CF_3)Ph
6, R = (4-Cl)Ph
7, R = (3-CF_3, 4-Br)Ph
9, R = Ph
10, R = dimethyl

Compound	G-score (kcal mol^{-1})
2	-11.19
7	-11.96
5	-8.86
6	-8.74
9	-7.51
10	-7.82

Figure 3.4.5. Structures of derivatives of lead compound **2** with modified hydrophobic head and G-scores obtained in their docking to JAK2 structure 3JY9.

Docking of compound **7** showed similar interactions as those formed by compound **2** (Figure 3.4.6), that is, the halogen bond with Phe995 formed now by the Br substituent, the HB between the secondary amine and Glu930 as well as the HB and salt bridge between the guanidinium group and Asp94. Additionally, there is a newly introduced π-π stacking interaction with the middle Ph ring and Tyr931.

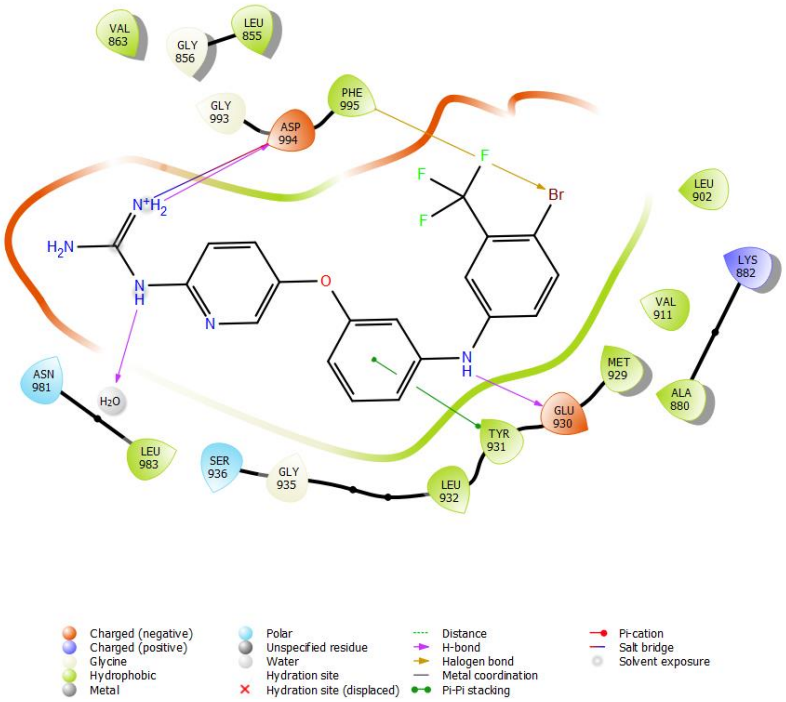

Figure 3.4.6. Best pose found for **7** docked in the JAK2 crystal structure 3JY9, using Induced Fit Docking Protocol Glide in the Schrodinger Suite.

When one or both of the substituents on the Ph ring of the hydrophobic moiety are removed, as in compounds **5, 6, 9 and 10**, a significant decrease in the G-score value is observed. Thus, in the case of compound **5** in which there is no substitution in the 4 position of the Ph ring, the contribution to binding of the halogen bond with Phe995 disappears (Figure 3.4.7, left). In compound **6** which does not have the CF_3 group in the Ph ring, even though the same interactions as in compound **2** occur (Figure 3.4.7, right), the G-score value is smaller (less negative), suggesting that two substituents are needed in the Ph ring of the hydrophobic moiety for the optimal binding to JAK2.

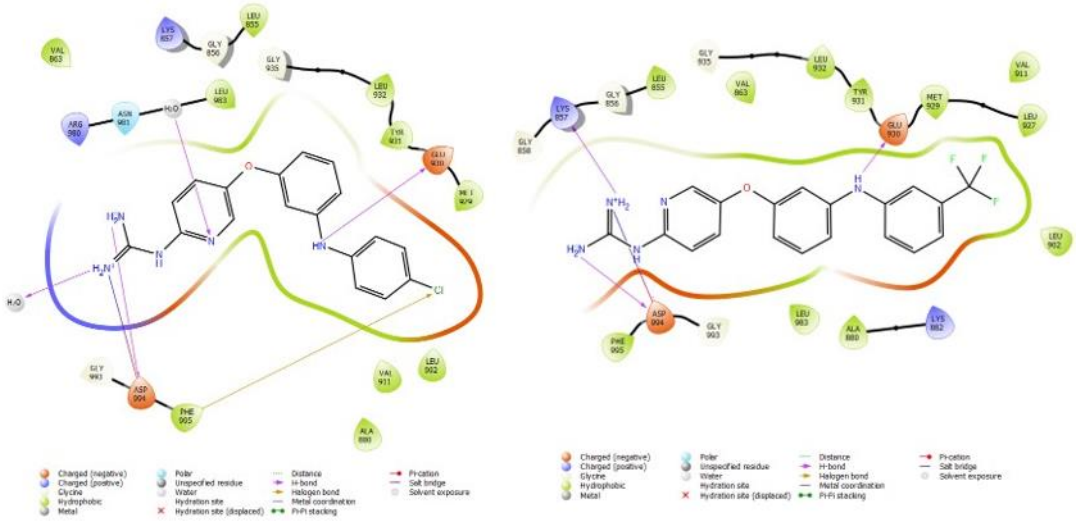

Figure 3.4.7. Best pose found for compounds **5** and **6** docked in the JAK2 crystal structure 3JY9, using Induced Fit Docking Protocol Glide in the Schrodinger Suite.

Much like compounds **5** and **6**, docking of compounds **9** and **10** (Figure 3.4.8) shows worse G-score values (i.e. less negative), again suggesting that a hydrophobic moiety with a Ph ring substituted with a halogen and a CF_3 groups is needed for optimal binding to JAK2.

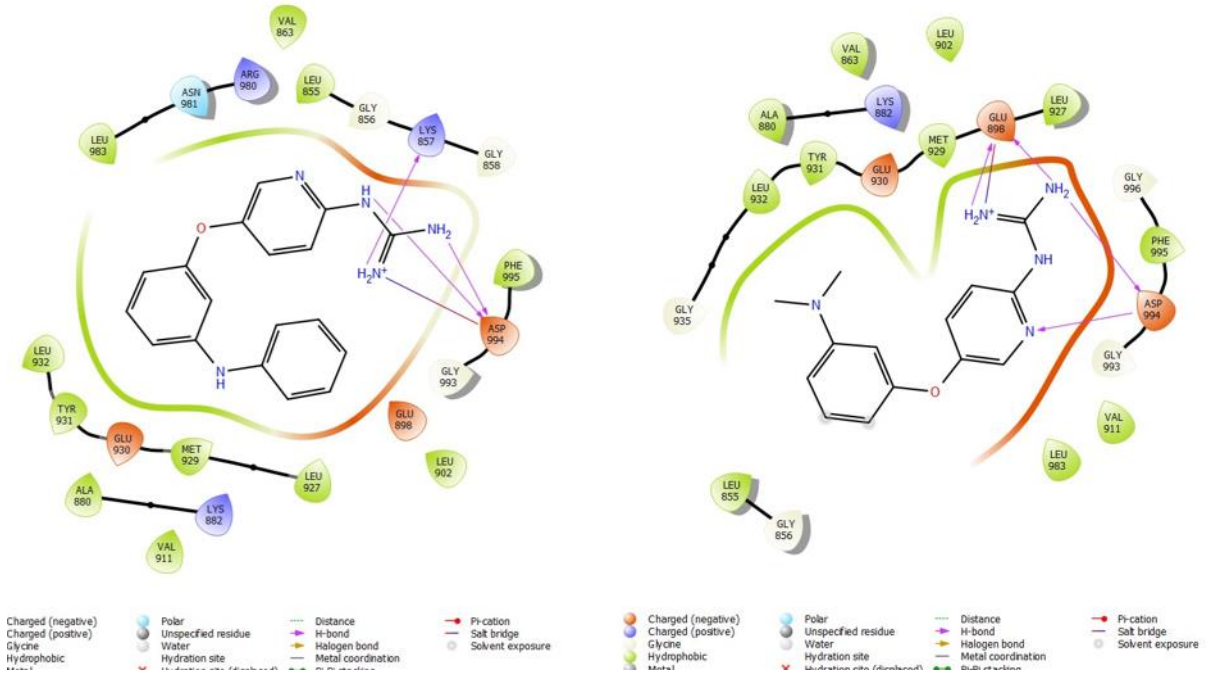

Figure 3.4.8. Best pose found for compounds **9** and **10** docked in the JAK2 crystal structure 3JY9, using Induced Fit Docking Protocol Glide in the Schrodinger Suite.

Next, we explore the effect that a change of linkers (X and Y in Figure 3.4.9) may have in the binding to JAK2 by docking compounds **17-19** into the crystallographic structure 3JY9.

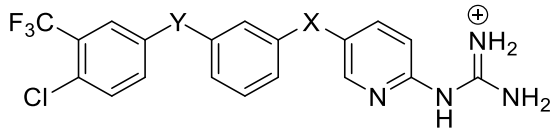

17, X = NH, Y = NH
18, X = O, Y = NH
19, X = O, Y = O

Compound	G-score (kcal mol^{-1})
2	-11.19
17	-11.59
19	-9.49
18	-9.69

Figure 3.4.9. Structures of derivatives of lead compound **2** with modified linkers and G-scores obtained in their docking to JAK2 structure 3JY9.

Thus, docking of compound **17** (Y = NH and X = NH, Figure 3.4.10, up left) shows the same interactions as those established by compound **2**, but the overall G-score values are better (more negative) indicating that **17** has a more efficient binding to JAK2. When both X and Y linkers are changed to -O-, docking of compound **19** (Figure 3.4.10, down left) results in a much worse G-score (less negative). This can be explained by the loss of two key interactions: the HB with Glu930 and the halogen bond with Phe995, even though a π-π stacking interaction between the middle Ph ring of the ligand and Tyr931 is newly formed. In the case of compound **18** docking (Figure 3.4.10, up right), similar interactions as **19** are lost without gaining any new interaction.

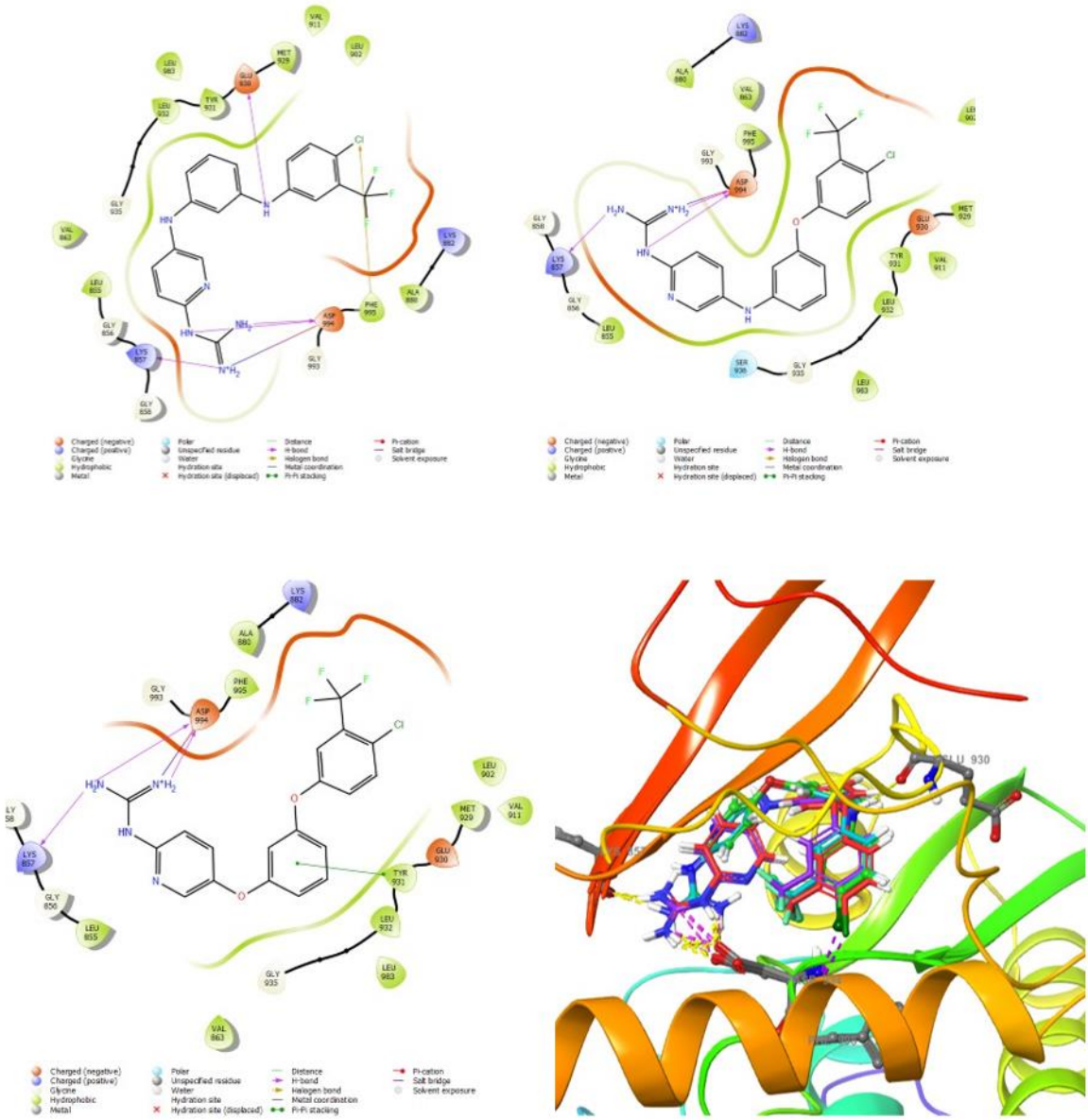

Figure 3.4.10. Best pose found for compounds **17** (up left) and **19** (up right) and **18** (down left) docked in the JAK2 crystal structure 3JY9 and the overlying of the three ligands in the JAK2 binding site (down right), using Induced Fit Docking Protocol Glide in the Schrodinger Suite.

We then explored the effect that modifying the polar moiety of compound **2** would have in binding to JAK2 (Figure 3.4.11). When the guanidinium cation attached to the pyridine ring in **2** is replaced by a 2-aminoimidazolinium group (compound **20**), upon

docking to JAK2 the same interactions as those observed in the docking of **2** were observed except for the halogen bond with Phe995 (Figure 3.4.12, up).

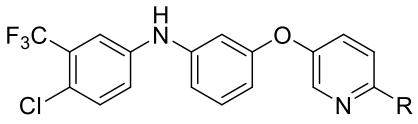

20, Z = aminoimidazoline
21, Z = acetamide
22, Z = aminium

Compound	G-score (kcal mol^{-1})
2	-11.189
20	-10.389
21	-12.944
22	-11.93

Figure 3.4.11. Structures of derivatives of lead compound **2** with modified polar moiety and G-scores obtained in their docking to JAK2 structure 3JY9.

Moreover, when we switched the guanidinium group of **2** by an acetamide (compound **21**), upon docking, the structure loses the horse-shoe shape observed in the docked compound **2** and the salt bridge between the guanidinium and Asp994 is lost, even though all the other interactions are retained (Figure 3.4.12, down left). Additionally, as the acetamide group contains an HB acceptor (HBA), a new HB with Lys857 is formed, inverting the situation observed in the binding of compound **2** where Lys857 was the HBA.

When there is no substitution and the amine is free, compound **22** (Figure 3.4.12, down right), the HB between the Glu930 and the secondary amine is retained, which is interacting with the hinge region. The primary amine forms hydrogen bond with Asp994 but does not form the significant electrostatic interactions formed by the guanidine, the HB with Lys857 is also lost.

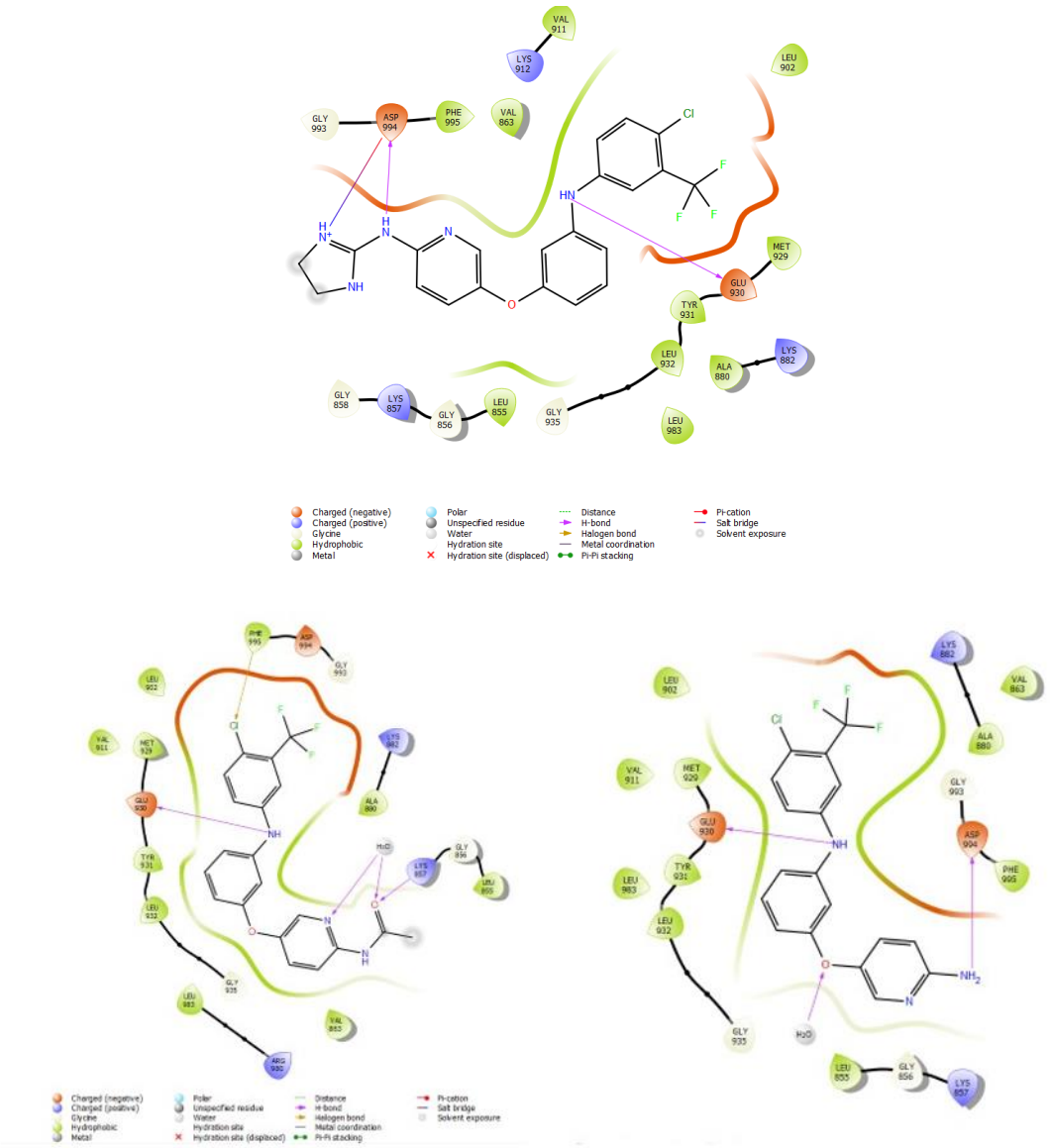

Figure 3.4.12. Best pose found for compounds **20** (up), **21** (down left) and **22** (down right) docked in the JAK2 crystal structure 3JY9, using Induced Fit Docking Protocol Glide in the Schrodinger Suit.

Finally, when we change the substitution pattern on the diaromatic system from 3,4'- to 4,4'-substitution (Figure 3.4.13) upon docking to JAK2 the values of the G-score are worse than those of lead compound **2**, also showing different interactions with the target.

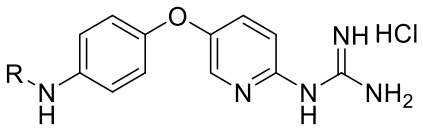

11, R = (3-CF_3)Ph
12, R = (4-Cl)Ph
13, R = (3-CF_3, 4-Br)Ph
14, R = (3-CF_3, 4-Cl)Ph
16, R = Ph

Compound	Gscore (kcal mol^{-1})
2	-11.189
13	-8.019
14	-7.832
11	-8.791
12	-7.398
16	-5.943

Figure 3.4.13. Structures of derivatives of lead compound **2** with modified substitution arrangement and G-scores obtained in their docking to JAK2 structure 3JY9.

Docking of compound **13** to JAK2 does not result in such strong binding as that of lead **2**. Upon binding to the JAK2 structure, compound **13** loses the mentioned horse-shoe shape due to the substitution pattern leading to the loss of the HB between Glu930, in the hinge region and the secondary amine. In its docked conformation, the guanidinium group of **13** forms electrostatic and HB interactions with Asp994, Glu1015 and Asp976 (Figure 3.4.14).

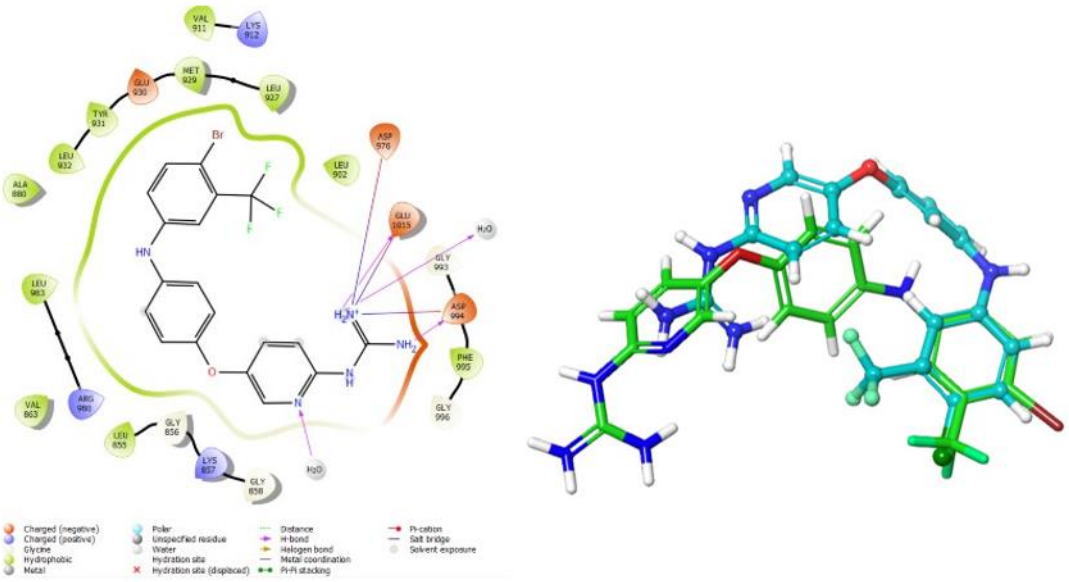

Figure 3.4.14. Best pose found for compound **13** docked in the JAK2 crystal structure 3JY9 (left) and overlayed structures of compounds **13** (green) and **2** (blue) (right), using Induced Fit Docking Protocol Glide in the Schrodinger Suite.

In the case of the docking of compound **14** to the JAK2 structure, electrostatic interactions with Asp939 as well as HBs are observed between Asp939 and the guanidine (Figure 3.4.15). Furthermore, when the structures of **14** and **2** were overlayed, differences are observed. Thus, the overall length of compound **14** increases, what can explain why no interactions with the same residues as lead **2** are observed. The horse-shoe shaped structure of lead compound **2** orientates the hydrophobic moiety and the guanidinium moieties into the corresponding pockets to achieve the mentioned interactions, and this is not possible in **14**.

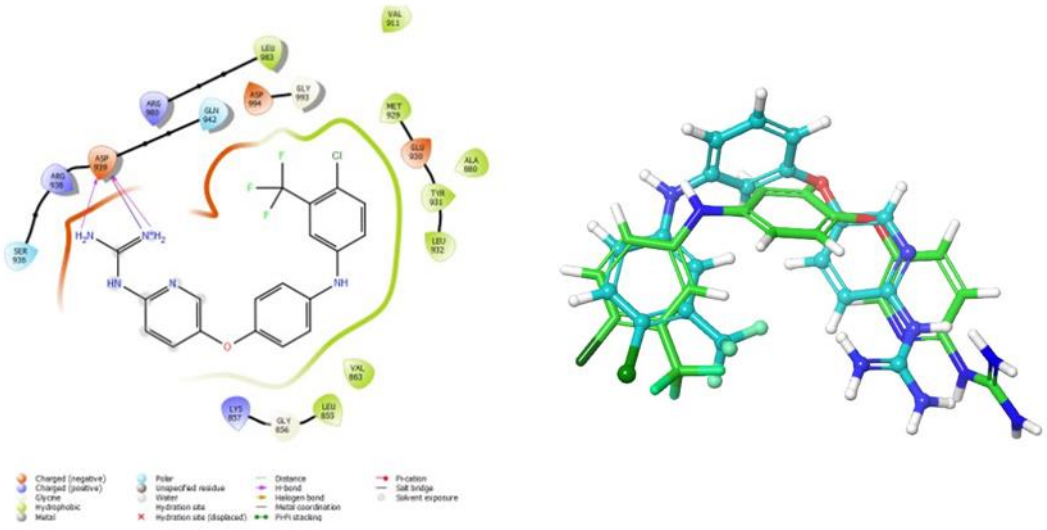

Figure 3.4.15. Molecular docking of **14** docked in the crystal structure 3JY9 and overlayed structures of compounds **2** (blue) and **14** (green), using Induced Fit Docking Protocol Glide in the Schrodinger Suite.

When the substituents are removed from compound **13** in compound **16** (Figure 3.4.16, left), the only interaction maintained is the one with Asp939, the electrostatic and HB interactions are maintained, and the loss of other interactions are reflected in the less negative Gscore obtained. In compound **12** where only the 4-Cl is present (Figure 3.4.16, up right) there are the same interactions as those in **16** and the decrease in the Gscore could be attributed to the introduction of the large Cl group. In compound **11** where CF_3

is present (Figure 3.4.16, down right) the same interactions are achieved and the Gscore is lower. From this we can postulate that the CF_3 group represents a better fit into the hydrophobic pocket, which is also seen in the 3,4'-substituted compounds.

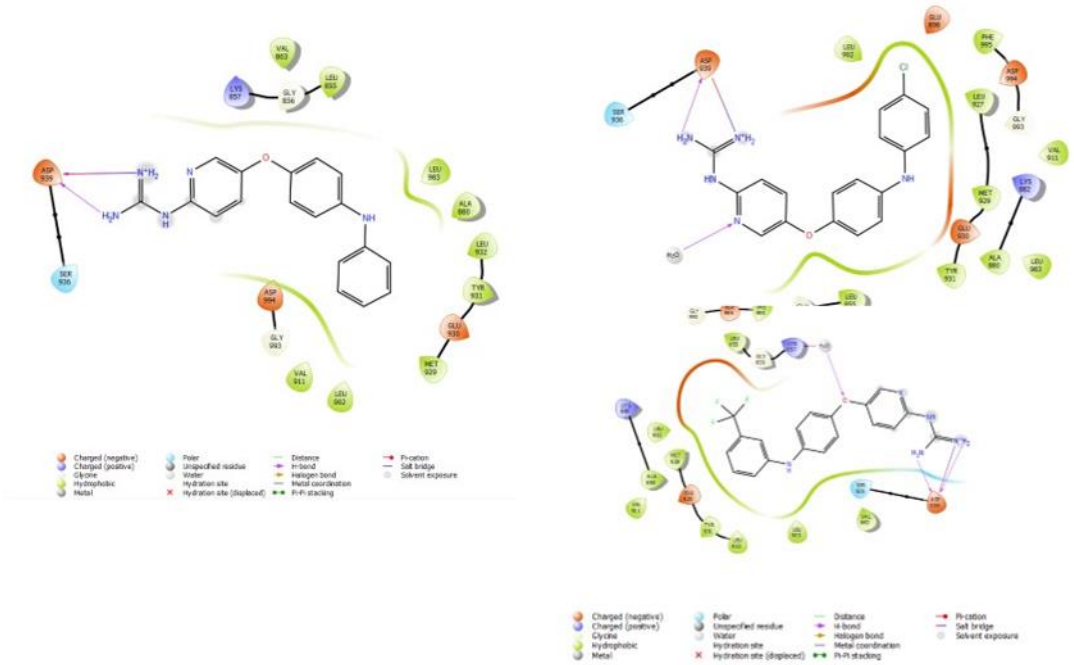

Figure 3.4.16. Best pose found for compounds **16** (left), **12** (up right) and **11** (down right) docked in the JAK2 crystal structure 3JY9, using Induced Fit Docking Protocol Glide in the Schrodinger Suite.

3.5. Conclusions and future perspectives

Lead compounds **1** and **2** as well as their derivatives were docked in an in-house developed model of B-Raf containing ATP, which allowed to observe a number of key contacts such as the strong electrostatic interactions with the target by means of the di-substituted guanidine (compounds **1** and **3**), interactions between the guanidinium cation and ATP phosphates and loss of these interactions with ATP in the shorter derivatives (compounds **2** and **4**). Thus, these theoretical outcomes are in agreement with the biochemical results previously obtained.

Lead compound **1** and its derivatives were also docked into a B-Raf crystallographic structure (6N0P) as ATP competitive inhibitors. This permitted us to have a different perspective on the potential binding of lead compound **1**. When docked in 6N0P, both compounds **3** and **1** were found to form strong interactions with the receptor, which were comparable to the native ligand (LXH254) found in the crystallographic structure mentioned. These compounds were also docked in 6P3D, which is the crystal structure of B-Raf with ponatinib, a type 2 Raf inhibitor, bound to an allosteric site.

Lead compound **2** and its derivatives were docked in the crystallographic structure of JAK2 (PDB: 3JY9) as biochemical studies suggest targeting this kinase as the cytotoxic mode of action of these compounds. Upon docking of compound **2**, this compound adopt a horse-shoe shaped conformation, allowing it to form key interactions with the binding site, including the hinge region of the kinase. Different derivatives of the ligand varying the hydrophobic moiety, linker, polar system, and substituent orientation pattern were also docked in this target showing the effect these modifications have on binding to the JAK2 structure.

The biochemical studies carried out showed that lead 1 caused cell cycle arrest at concentrations lower than 10 µM, this suggest that the compound could potentially have other targets in the cells. Therefore, considering all the derivatives that have been prepared so far, ligand-based pharmacophore screening deserves to be carried out and thus the achieved pharmacophore can be screened against a database of FDA approved anti-cancer drugs in order to analyse other potential targets.

Compound 2 gave very good results in the docking studies with the 3JY9 crystal structure that corresponds to the JAK2 kinase; thus, it would be interesting to carry out molecular dynamic simulations to assess the stability of the compound bound to the active site of the target and a more accurate assessment of the corresponding binding energy.

3.6. References

(1) Cui, W.; Aouidate, A.; Wang, S.; Yu, Q.; Li, Y.; Yuan, S. Discovering Anti-Cancer Drugs via Computational Methods. *Front. Pharmacol.* **2020**, *11*, 733. https://doi.org/10.3389/fphar.2020.00733.

(2) Ferreira, L. G.; Dos Santos, R. N.; Oliva, G.; Andricopulo, A. D. Molecular Docking and Structure-Based Drug Design Strategies. *Molecules* . 2015. https://doi.org/10.3390/molecules200713384.

(3) Salmaso, V.; Moro, S. Bridging Molecular Docking to Molecular Dynamics in Exploring Ligand-Protein Recognition Process: An Overview. *Front. Pharmacol.* **2018**, *9*, 923. https://doi.org/10.3389/fphar.2018.00923.

(4) SBDD and LBDD https://www.creative-biolabs.com/drug-discovery/therapeutics/structure-based-screening.htm.

(5) Previtali, V.; Trujillo, C.; Boisson, J.-C.; Khartabil, H.; Henon, E.; Rozas, I. Development of the First Model of a Phosphorylated, ATP/Mg2+-Containing B-Raf Monomer by Molecular Dynamics Simulations: A Tool for Structure-Based Design. *Phys. Chem. Chem. Phys.* **2017**, *19* (46), 31177–31185. https://doi.org/10.1039/C7CP05038K.

(6) Previtali, V.; Mihigo, H. B.; Amet, R.; McElligott, A. M.; Zisterer, D. M.; Rozas, I. Exploring the Anti-Cancer Mechanism of Novel 3,4'-Substituted Diaryl Guanidinium Derivatives. *Pharmaceuticals* . 2020. https://doi.org/10.3390/ph13120485.

(7) HL-60 Cell Line https://www.atcc.org/products/ccl-240

(8) MCF-7 Cell Line https://www.atcc.org/products/ccl-240

(9) H929 Cell Line https://www.atcc.org/products/crl-9068

(10) U266 Cell Line https://www.atcc.org/products/tib-196

(11) Ramurthy, S.; Taft, B. R.; Aversa, R. J.; Barsanti, P. A.; Burger, M. T.; Lou, Y.; Nishiguchi, G. A.; Rico, A.; Setti, L.; Smith, A. Design and Discovery of N-(3-(2-(2-Hydroxyethoxy)-6-Morpholinopyridin-4-Yl)-4-Methylphenyl)-2-(Trifluoromethyl)Isonicotinamide, a Selective, Efficacious, and Well-Tolerated RAF Inhibitor Targeting RAS Mutant Cancers: The Path to the Clinic. *J. Med. Chem.* **2020**, *63* (5), 2013–2027. https://doi.org/10.1021/acs.jmedchem.9b00161.

(12) Sherman, W.; Day, T.; Jacobson, M. P.; Friesner, R. A.; Farid, R. Novel Procedure for Modeling Ligand/Receptor Induced Fit Effects. *J. Med. Chem.* **2006**, *49* (2), 534–553. https://doi.org/10.1021/jm050540c.

(13) Nishiguchi, G. A.; Rico, A.; Tanner, H.; Aversa, R. J.; Taft, B. R.; Subramanian, S.; Setti, L.; Burger, M. T.; Wan, L.; Tamez, V. Design and Discovery of N-(2-Methyl-5'-Morpholino-6'-((Tetrahydro-2H-Pyran-4-Yl)Oxy)-[3,3'-Bipyridin]-5-Yl)-3-(Trifluoromethyl)Benzamide (RAF709): A Potent, Selective, and Efficacious RAF Inhibitor Targeting RAS Mutant Cancers. *J. Med. Chem.* **2017**, *60* (12), 4869–4881. https://doi.org/10.1021/acs.jmedchem.6b01862.

(14) Cotto-Rios, X. M.; Agianian, B.; Gitego, N.; Zacharioudakis, E.; Giricz, O.; Wu, Y.; Zou, Y.; Verma, A.; Poulikakos, P. I.; Gavathiotis, E. Inhibitors of BRAF Dimers Using an Allosteric Site. *Nat. Commun.* **2020**, *11* (1), 4370. https://doi.org/10.1038/s41467-020-18123-2.

(15) Lin, T. E.; HuangFu, W.-C.; Chao, M.-W.; Sung, T.-Y.; Chang, C.-D.; Chen, Y.-Y.; Hsieh, J.-H.; Tu, H.-J.; Huang, H.-L.; Pan, S.-L. A Novel Selective JAK2 Inhibitor Identified Using Pharmacological Interactions. *Front. Pharmacol.* **2018**, *9*, 1379. https://doi.org/10.3389/fphar.2018.01379.

Chapter 4 – Synthesis of derivatives of lead compound 2

Guanidines are found in nature in abundance in the amino acid arginine or the nitrogenous backbone of guanine in DNA and RNA.[1,2] Guanines are considered as organic superbases with the pK_a of the conjugate acid being ~13,[3] thus at physiological pH is found in its protonated guanidinium form. Guanidine derivatives are interesting from chemical and biological points of view due to their ability to form hydrogen bonds (HBs) that allows them to be good catalysts,[4] and interact with different biological targets providing guanidine derivatives with a wide variety of biological activities. Besides forming HBs, the guanidinium cation can form other interactions (i.e. ionic or π-cation) with amino acids or DNA and RNA bases. Given its versatility, the guanidine moiety is found in many commercially available drugs (Figure 4.1) including antidiabetic agents (e.g. metformin), anti-influenza (e.g. zanamivir), or chemotherapeutic agents (e.g. cilengitide).[5]

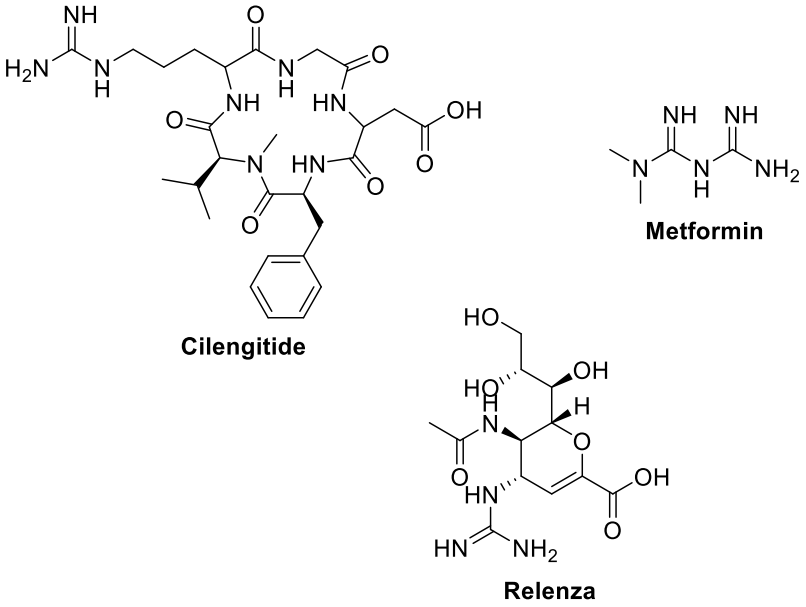

Figure 4.1. Commercial drugs containing guanidine moieties.

In the present work we are aiming to prepare derivatives of a guanidine containing lead compound (compound **2**) that had shown interesting biological activity as kinase inhibitor and anticancer agent.

4.1. Synthesis of derivatives of compound 2 exploring the lipophilic moiety and diaromatic substitution pattern

4.1.1. Preparation of precursor amino derivatives

The ATP binding site of kinases is very well studied as previously mentioned; however, we have additionally focused in the hydrophobic pocket which is also well known, and thus we have prepared derivatives of the lead compound **2** with various hydrophobic moieties ranging in sizes (compounds **3-7**). As mentioned in the Introduction, previous work with lead compound **2** showed that when the (3-CF_3, 4-Cl)Ph was used as the lipophilic moiety, low IC_{50} values were achieved against a variety of cancer cells. Now, we will further explore which substituents in this phenyl ring may improve this activity. Additionally, considering that many 4,4'-substituted diaryl bis-guanidine derivatives have been prepared in the Rozas group as DNA minor groove binders, but only the 3,4'-

substituted derivatives have been studied as protein kinase inhibitors, we will also explore if the substitution pattern on the diaromatic system (compounds **8-12**) has an effect on the kinase inhibition activity (Figure 4.1.1.1).

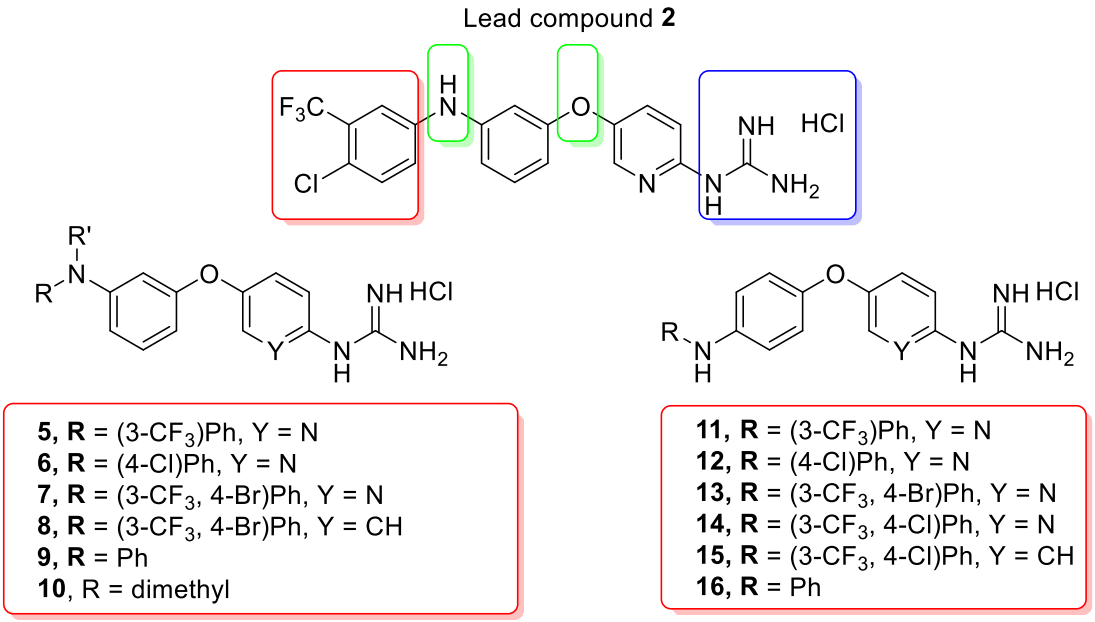

Figure 4.1.1.1. Proposed derivatives of the lead compound **2** with changes at the hydrophobic moiety and in the diaryl substitution pattern.

The retrosynthetic approach for the compounds proposed (Figure 4.1.1.2) requires the preparation of key diaryl amines which synthesis involves first reacting 5-bromo-2-ntropyridine and an aminophenol (acetylated or deacetylated) in a nucleophilic aromatic substitution (S_NA) to produce the corresponding anilino nitropyridine system. Next, the hydrophobic moiety (R in Figure 4.1.1.2) will be attached to the anilino nitropyridine system by forming a C-N bond in a Buchwald-Hartwig reaction with the desired arylbromo derivative. The nitro group will be then reduced to form the key diaryl amine, which will next be guanidylated using *N,N'*-bis-(*tert*-butoxycarbonyl)-*S*-methylisothiourea. The final step will involve Boc deprotection to give the desired final salt.

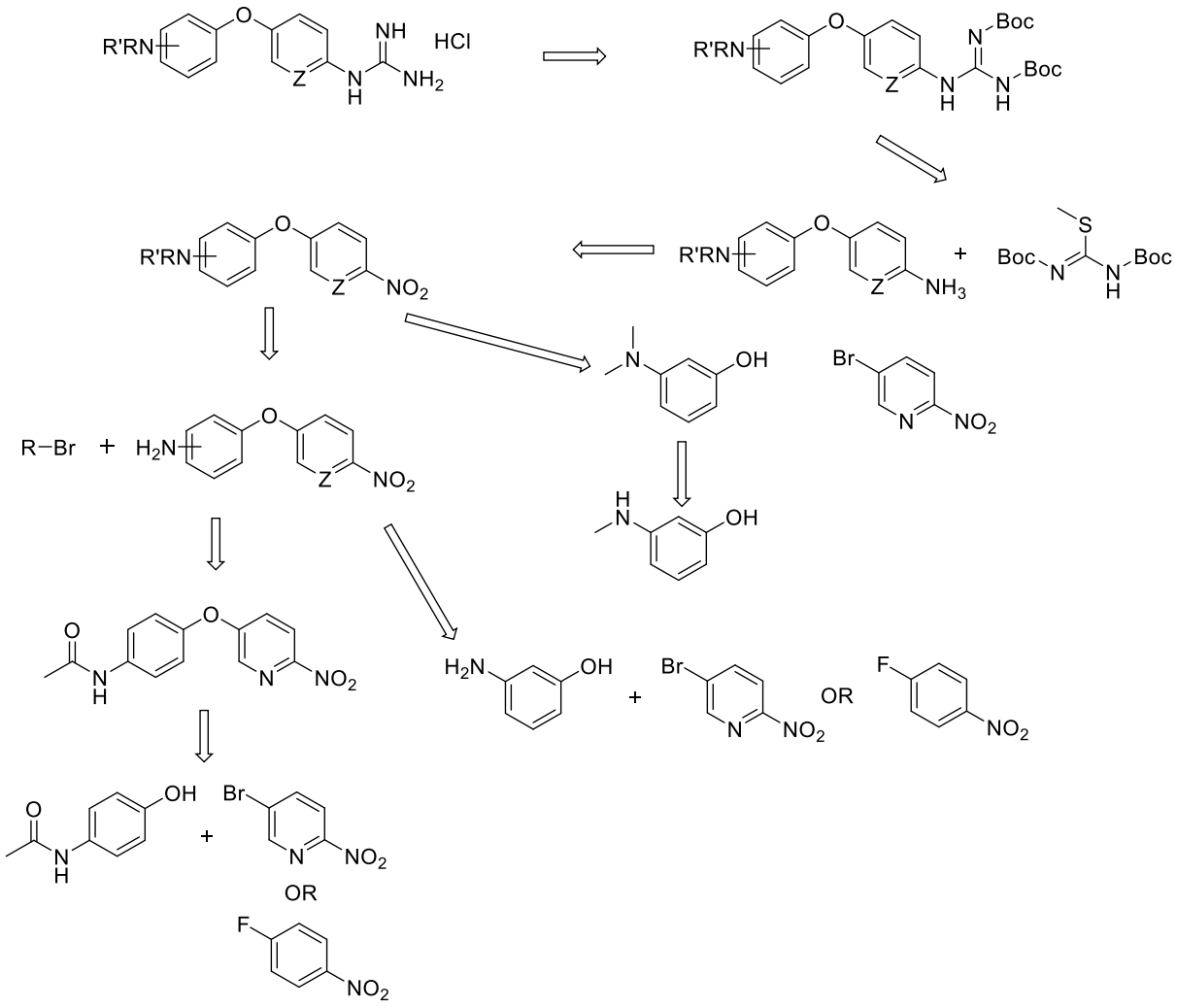

Figure 4.1.1.2. Schematic for the preparation of 3-amino-4'-guanidino phenyloxypyridines and 4-amino-4'-guanidino phenyloxypyridines.

Following the proposed retrosynthesis and with the aim to synthesise different 4,4'- or 3,4'-diaryl guanidines we started to prepare the corresponding synthetic blocks conveniently functionalised. Thus, diaryl amine **25** was prepared by reacting 5-bromo-2-nitropyridine (**23**) and 3-aminophenol (**24**) through a nucleophilic aromatic substitution, S_NAr, reaction (Scheme 4.1.1.1).[6]

Scheme 4.1.1.1. Synthesis of a functionalised amine **15** through a SNAr.

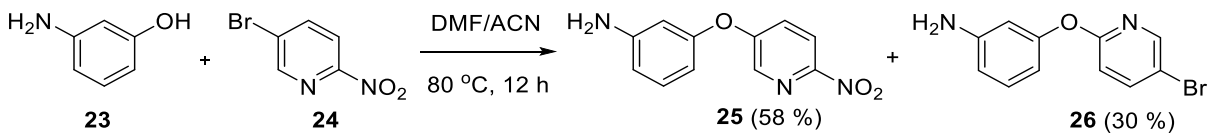

The aromatic system is activated towards S_NAr due to the presence of the electron withdrawing group (i.e. NO_2), which stabilises the intermediate to give the desired product (Figure 4.1.1.3). Halogens are good leaving groups (F>>>Br = Cl >I) as they have stable conjugate acids. In this reaction 5-bromo-2-nitropyridine was chosen due to the affordable price.

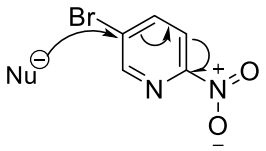

Figure 4.1.1.3. Nucleophilic Aromatic substitution

The side product **26** was produced due to the proximity of the nitro group to the pyridine N atom, which influences the chemical properties of the heterocycle. Pyridine has a low electron density at position 2 and 4 of its ring, as seen from its resonance forms (Figure 4.1.1.4); thus, if these electrophilic positions are substituted with a potential leaving group, S_NAr can occur at these points.

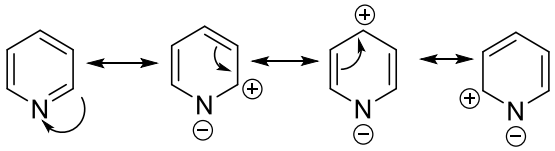

Figure 4.1.1.4. Resonance structures of pyridine

Next, anilino nitropyridine **29** was prepared in good yield (65%) by reacting **24** and 4-acetaminophenol at room temperature with caesium carbonate as the base.[7] The deprotected amino derivative **29** was achieved by reflux of **28** in HCl/MeOH overnight (Scheme 4.1.1.2).

Scheme 4.1.1.2. Synthesis of a functionalised amine **29** through a S_NAr.

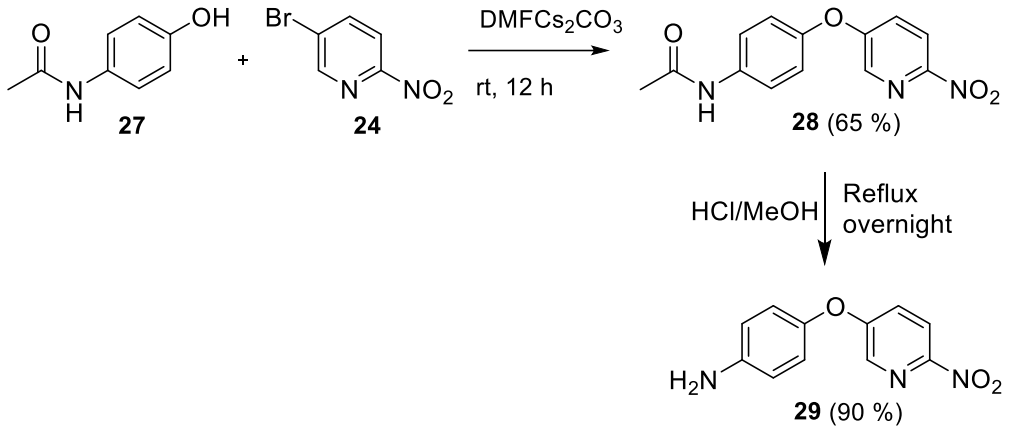

Both **31** and **32**, phenyl diaryl amines, were also synthesised with S_NAr (Scheme 4.1.1.3) the products were achieved following purification of crudes.

Scheme 4.1.1.3. Synthesis of a functionalised amine **31** and **32** through a S_NAr.

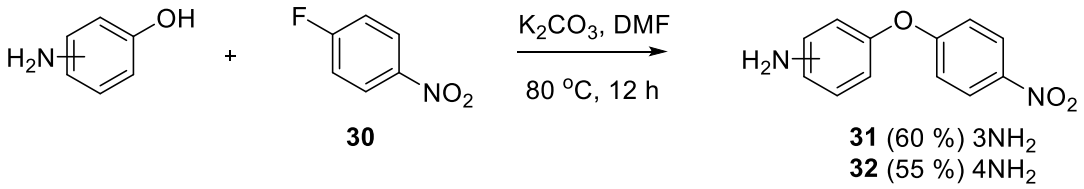

Once the key aniline derivative **25, 29, 31** and **32** were prepared, the next step consisted of the introduction of an aromatic system to the anilino NH_2 forming an aryl amine. Aryl amines are found in a variety of biologically active compounds and therefore their synthesis has been thoroughly studied. The corresponding C-N bond formation has been investigated extensively over the last few decades. Initially Ullmann and Goldberg reported the introduction of aromatic amines with cupper as the catalyst; however, this method was too inefficient due to the cupper by-products formed.[8] Over the last

decade Buchwald and Hartwig developed palladium and cupper-based catalysts which facilitate C-C coupling, and they extended this newly developed strategy, which uses mild and inexpensive conditions, to C-N coupling (Figure 4.1.1.5).

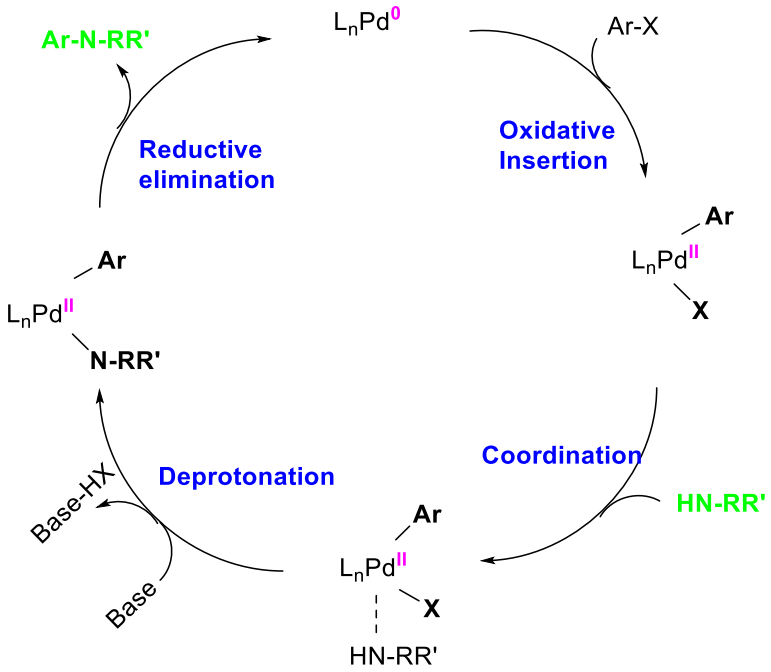

Figure 4.1.1.5. Scheme of the catalytic cycle in the Buchwald-Hartwig amination

The C-N bond is formed by a palladium catalysed reaction between an aryl halide and an aromatic amine in the presence of a stochiometric amount of base.[9] There are four steps in the catalytic cycle leading to the desired product. The first step involves the oxidative insertion of Pd(0) into the aryl-halogen bond, forming a Pd(II) complex. The second step consists of the coordination of the amine to the complex, with both the halogen and the amine now connected to the same palladium atom. In the third step the halogen is removed by the base, and finally a reductive elimination results in the formation of the C-N bond and recovery of the Pd(0) catalyst that can be reused (Figure 4.1.1.5). There are many factors that can affect the success of the reaction, such as the ligand, the base, the solvent, the Pd source and the substrate itself.[10] Based on previous

work by Drs. Elena Diez-Cecilia and Viola Previtali in the Rozas group, suitable conditions were found for different substrates (Scheme 4.1.1.4).[11–13]

Scheme 4.1.1.4. Buchwald-Hartwig coupling reaction

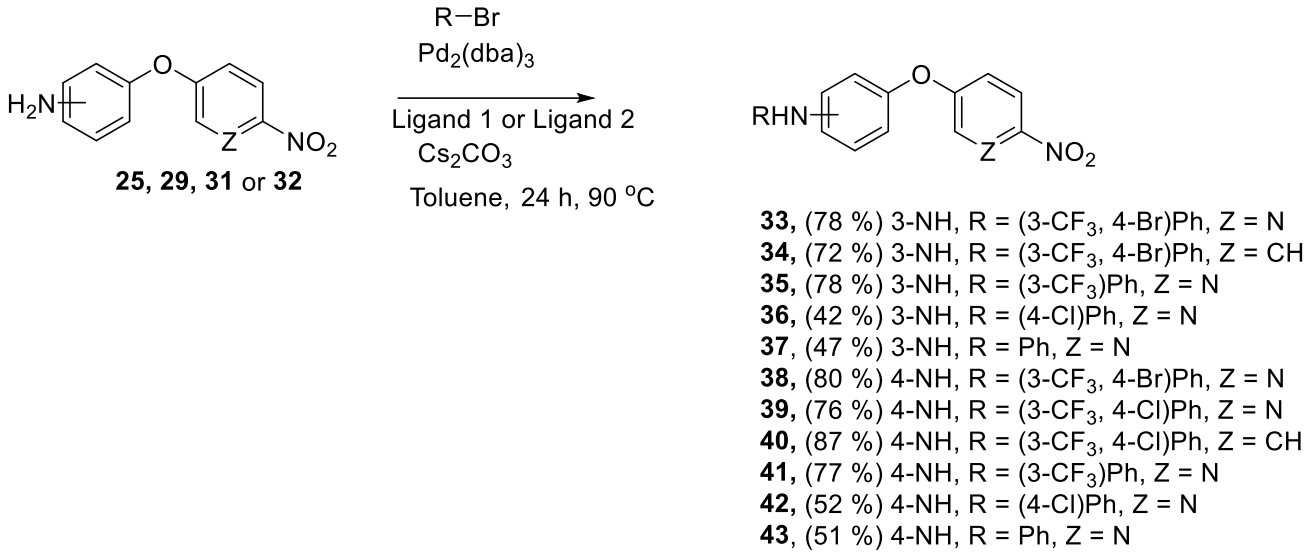

As mentioned above the success of this reaction often depends on different variables and parameters such as ligand (Figure 4.1.1.6), Pd source, base, and solvent.

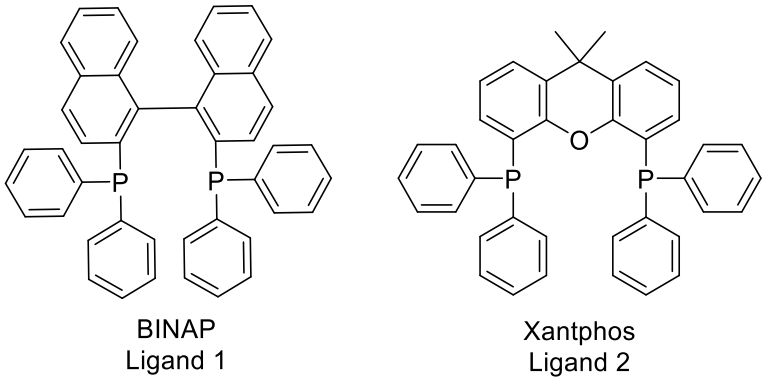

Figure 4.1.1.6. Diphosphine ligands BINAP and Xantphos

Fortunately, in the case of the phenyl compounds the chosen starting conditions [i.e. tris-(dibenzylideneacetone)-di-palladium(0) [$Pd_2(dba)_3$] (3 mol%), 2,2'-bis-(di-phenylphosphino)-1,1'-(bi-naphthyl) (BINAP (3 mol%)), sodium *tert*-butoxide (NaO^tBu) (1.4 eq.) in dry toluene (2 mL $mmol^{-1}$) at 90 °C] afforded aimed compounds **34** and **40** in high yields (72% and 87%, respectively) (Scheme 4.1.1.4). The yield was much lower when BINAP was used for the pyridyl compounds, thus to improve yields a bulky ligand, 4,5-bis-(diphenylphosphino)-9,9-dimethylxanthene (Xantphos) was used. This is probably due to the ability of the N atom of the pyridine ring to interact with the catalyst metal centre.[14, 15] The use of Xantphos has the ability to increase the electron density on the metal centre (Pd) due to its electron rich phosphine substituents and by its ability to align the appropriate molecular orbitals of Pd for the oxidative step insertion into the aryl halide.

In order to synthesise the derivative with a dimethylamine substituent in the 3 position of the diaryl system (**45**) a different approach was used. Thus, 3-aminophenol was treated with methyl iodide first and then in a S_NAr with 5-bromo-2-nitropyridine in the presence of caesium carbonate overnight, to yield the corresponding quaternary amine which was washed with 5% $NaHCO_3$, to yield compound **44** (Scheme 4.1.1.5, top). Compound **45** was achieved through S_NAr (Scheme 4.1.1.5, bottom).

Scheme 4.1.1.5. Methylation of **13** with methyl iodide (top), synthesis of a functionalised amine **45** through a S_NAr (bottom)

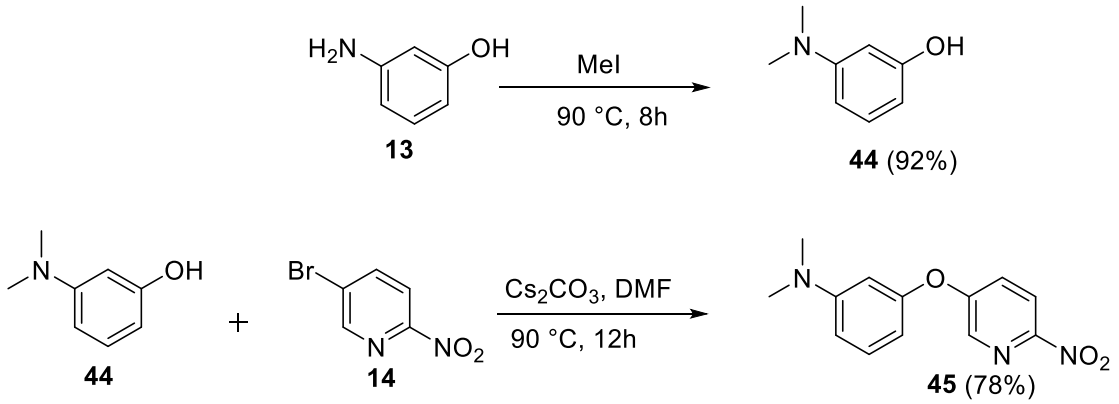

In order to introduce the corresponding guanidine system, reduction of the nitro group was next required. There are many reactions available for the reduction of a nitro group to an amine, but Pd catalysed reductions are favoured as they give high yields.[16] Accordingly, compounds **46-50** were obtained in very good yields by the hydrogenation of **35, 37, 41, 43** and **45** using 10% Pd/C (Scheme 4.1.1.6).

Scheme 4.1.1.6. Reduction of the nitro group with 10% Pd/C.

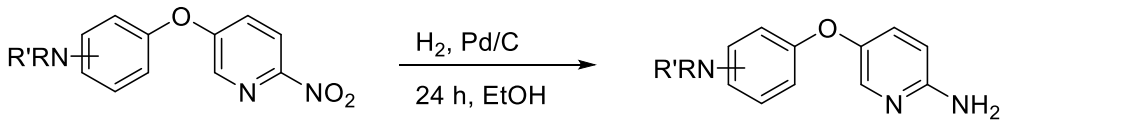

35, 37, 41, 43 and 45

46, (80 %) 3-NH, R = (3-CF_3)Ph, R' = H
47, (97%) 3-NH, R = Ph, R' = H
48, (85 %) 3-NH, R = CH_3, R' = CH_3
49, (88 %) 4-NH, R = (3-CF_3)Ph, R' = H
50, (95 %) 4-NH, R = Ph, R' = H

Despite the very high yields achieved by palladium catalysed reductions, they have been found to lead to hydrodehalogenation[17] occurring at different rates depending on the halogen (I > Br > Cl >> F) due to the dissociation energy of carbon-halogen bonds.[18] In the case of compounds **35** and **41** the C-F bond is very strong and hence it is less likely to break. Hence, for the selective reduction of the nitro group of sensitive halogen containing compounds (**33, 34, 36, 38-40,** and **42**), tin(II) chloride dihydrate was used rendering compounds **51-57**[19] with lower yields (Scheme 4.1.1.7).[20]

Scheme 4.1.1.7. Selective nitro reduction with tin(II) chloride dihydrate

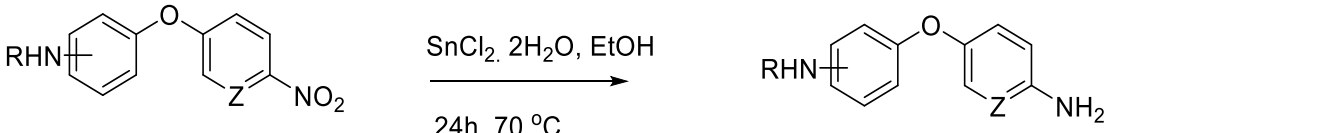

33, 34, 36, 38-40, and 42),

51, (69 %) 3-NH, R = (3-CF_3, 4-Br)Ph, Z = N
52, (64 %) 3-NH, R = (3-CF_3, 4-Br)Ph, Z = CH
53, (69 %) 3-NH, R = (4-Cl)Ph, Z = N
54, (80 %) 4-NH, R = (3-CF_3, 4-Br)Ph, Z = N
55, (83 %) 4-NH, R = (3-CF_3, 4-Cl)Ph, Z = N
56, (77 %) 4-NH, R = (3-CF_3, 4-Cl)Ph, Z = CH
57, (64 %) 4-NH, R = (4-Cl)Ph, Z = N

4.1.2. Guanidylation reactions

The Rozas group has worked for more than 25 years in the preparation of diverse guanidines and 2-aminoimidazolines and, thus, a number of synthetic methods have been developed to introduce the corresponding guanidine-like moiety onto a molecule.

One of the most classical approaches to the introduction of a guanidine system involves first the reaction between a primary or secondary amine with a protected guandinylating reagent such as thioureas, *S*-methyl-pseudothioureas, and chloroformamidines, followed by a deprotection step (Scheme 4.1.2.1).[21]

Scheme 4.1.2.1. Reaction route for the preparation of guanidinium salts

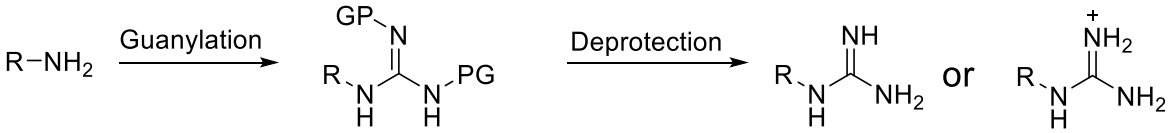

One of the most straightforward methods was reported by Kim and Qian[22] using mercury(II) chloride and a thiourea derivative. In this reaction a nucleophilic aryl/alkyl amine reacts with the thiourea derivative (electrophile), which is substituted by an

electron withdrawing group to increase its electrophilicity (Figure 4.1.2.1), using activating agents such as thiophilic metal salts ($HgCl_2$ or $CuCl_2$) or the Mukaiyama reagent (2-chloro-1-methylpyridinium iodide) as well as a base (e.g. Et_3N) to deprotonate the amine following nucleophilic attack (Scheme 4.1.2.2).[22].

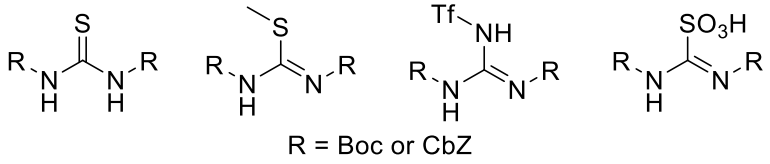

Figure 4.1.2.1. Examples of protected guanidylating agents

Scheme 4.1.2.2. General guanidylation reaction Scheme

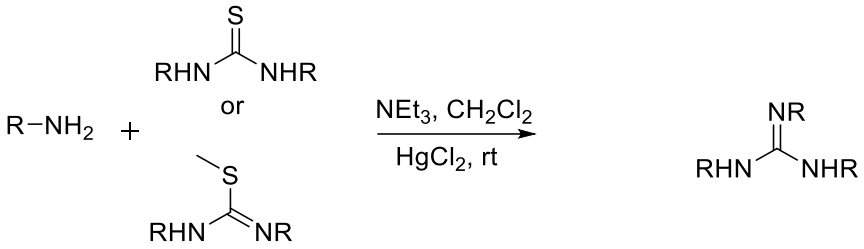

The first step in the guanidylation reaction (Scheme 4.1.2.3) is the nucleophilic attack of the 1,3-bis-(*tert*-butoxycarbonyl)-2-methyl-2-thiopseudourea. Trimethylamine, the base, then deprotonates the amine. Next, sulphur coordinates to the mercury in mercury chloride and the methylated sulphur makes it a better leaving group as Me-S-Hg adduct as well as triethylammonium hydrochloride and the desired Boc protected is achieved.

Scheme 4.1.2.3. Mechanism of $HgCl_2$ mediated guanidylation

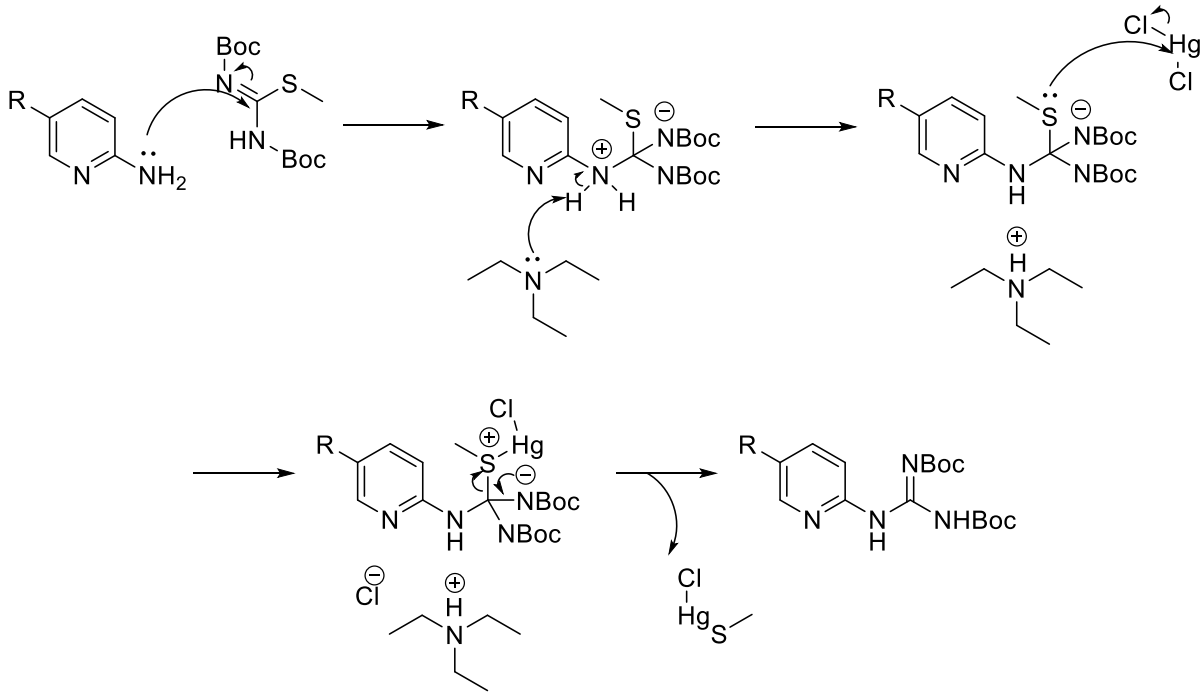

While di-Boc protected thioureas are most commonly used, ethoxycarbonyl substituted thioureas can also be useful and they can be prepared using the corresponding isothiocyanate.[21] This substituted thiourea then can be reacted with an amine to form the corresponding guanidine by displacement of sulphur in the presence of ethyl-3-aminopropyl carbodiimide hydrochloride (EDCI) (Scheme 4.1.2.4) without major side products.[23] The formation of the thiourea is facilitated by the increased reactivity of the isothiocynate by the carbamate.[24]

Scheme 4.1.2.4. General Scheme of substituted thiourea preparation and amine addition

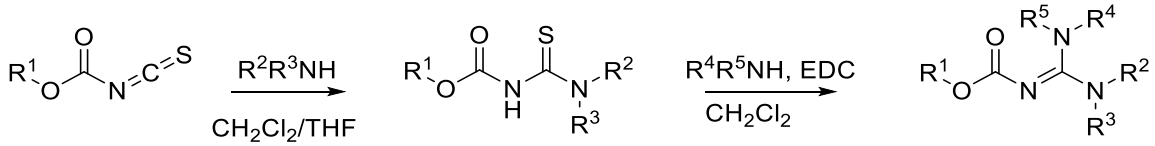

In the present case, the preparation of the Boc protected guanidines was carried out by using *N,N'*-bis-(*tert*-butoxycarbonyl)-*S*-methylisothiourea, mercury(II) chloride and triethylamine resulting in good to excellent yields (Scheme 4.1.2.5).

Scheme 4.1.2.5. $HgCl_2$ mediated guanidylation

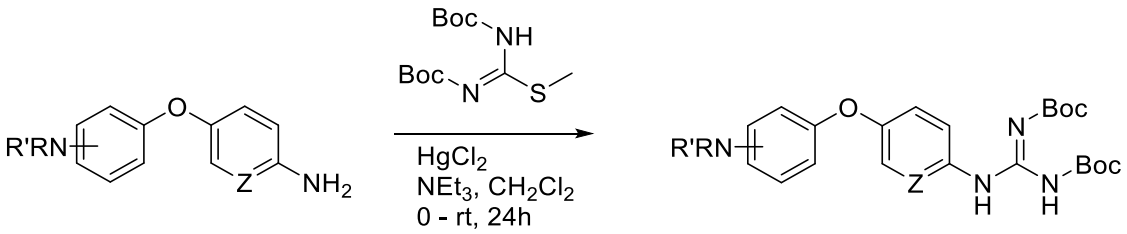

46-57

58, (88 %) 3-NH, R = (3-CF_3, 4-Br)Ph, R' = H, Z = N
59, (88 %) 3-NH, R = (3-CF_3, 4-Br)Ph, R' = H, Z = CH
60, (83 %) 3-NH, R = (3-CF_3)Ph, R' = H, Z = N
61, (78 %) 3-NH, R = (4-Cl)Ph, R' = H, Z = N
62, (77 %) 3-NH, R = Ph, R' = H, Z = N
63, (78 %) 3-NH, R = CH_3, R' = CH_3, Z = N
64, (80 %) 4-NH, R = (3-CF_3, 4-Br)Ph, R' = H, Z = N
65, (76 %) 4-NH, R = (3-CF_3, 4-Cl)Ph, R' = H, Z = N
66, (76 %) 4-NH, R = (3-CF_3, 4-Cl)Ph, R' = H, Z = CH
67, (81 %) 4-NH, R = (3-CF_3)Ph, R' = H, Z = N
68, (82 %) 4-NH, R = (4-Cl)Ph, R' = H, Z = N
69, (81 %) 4-NH, R = Ph, R' = H, Z = N

Considering that these derivatives need to be Boc-deprotected and that water/ethanol soluble salts are needed for the biological evaluation of the compounds, the corresponding hydrochloride salts were prepared following established procedures in the Rozas group.[11] These procedures involve treatment of the Boc-protected guanidines with HCl 4M solutions in 1,4-dioxane, which were further diluted in a 1,4-dioxane until reaching a final concentration of 0.2M (Scheme 4.1.2.6).

Scheme 4.1.2.6. Guanidine deprotection with 4M HCl/dioxane

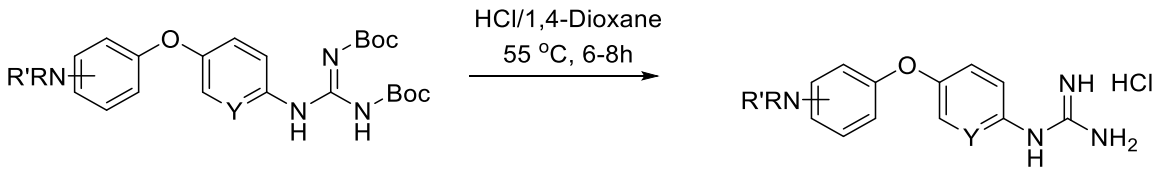

58-69

5, **R** = (3-CF_3)Ph, Y = N
6, **R** = (4-Cl)Ph, Y = N
7, **R** = (3-CF_3, 4-Br)Ph, Y = N
8, **R** = (3-CF_3, 4-Br)Ph, Y = CH
9, **R** = Ph
10, R = dimethyl
11, **R** = (3-CF_3)Ph, Y = N
12, **R** = (4-Cl)Ph, Y = N
13, **R** = (3-CF_3, 4-Br)Ph, Y = N
14, **R** = (3-CF_3, 4-Cl)Ph, Y = N
15, **R** = (3-CF_3, 4-Cl)Ph, Y = CH
16, **R** = Ph

4.2. Synthesis of derivatives of lead compound 2 modifying the linkers

Given the results obtained from the computational studies (see Chapter 3, section 3.4) where the linker NH forms HB interactions with Glu930, we decided to explore the effect of switching the positions of the linker as in compound **18** (Figure 4.2.1), using linkers without a HB donor as seen in compound **19** (Figure 4.2.1) or using HB donors in both linkers as seen in compound **17** (Figure 4.2.1).

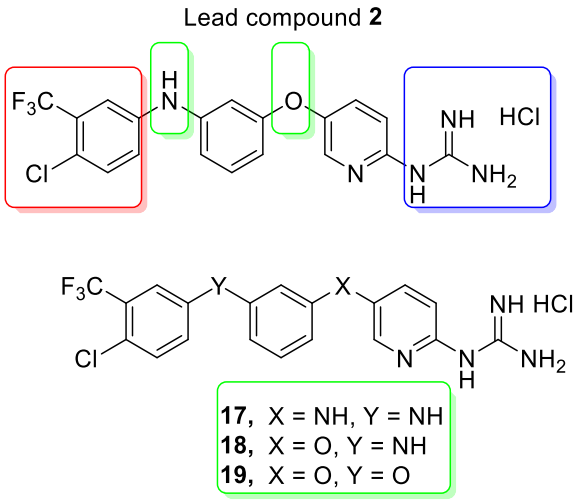

Figure 4.2.1. Structure of the derivatives of lead compound **2** exploring the linker moiety.

The retrosynthetic approach considered for these derivatives (Figure 4.2.2) shows that in order to make the connected aryl systems with different linkers, a different combination of Buckwald-Hartwig amination and Ullman type of coupling may be used. Thus, the achieved nitro derivatives can then be reduced to give the amine. The amines will be then guanidylated using *N,N'*-bis-(*tert*-butoxycarbonyl)-*S*-methylisothiourea and will be followed by Boc deprotection to give the desired final salts.

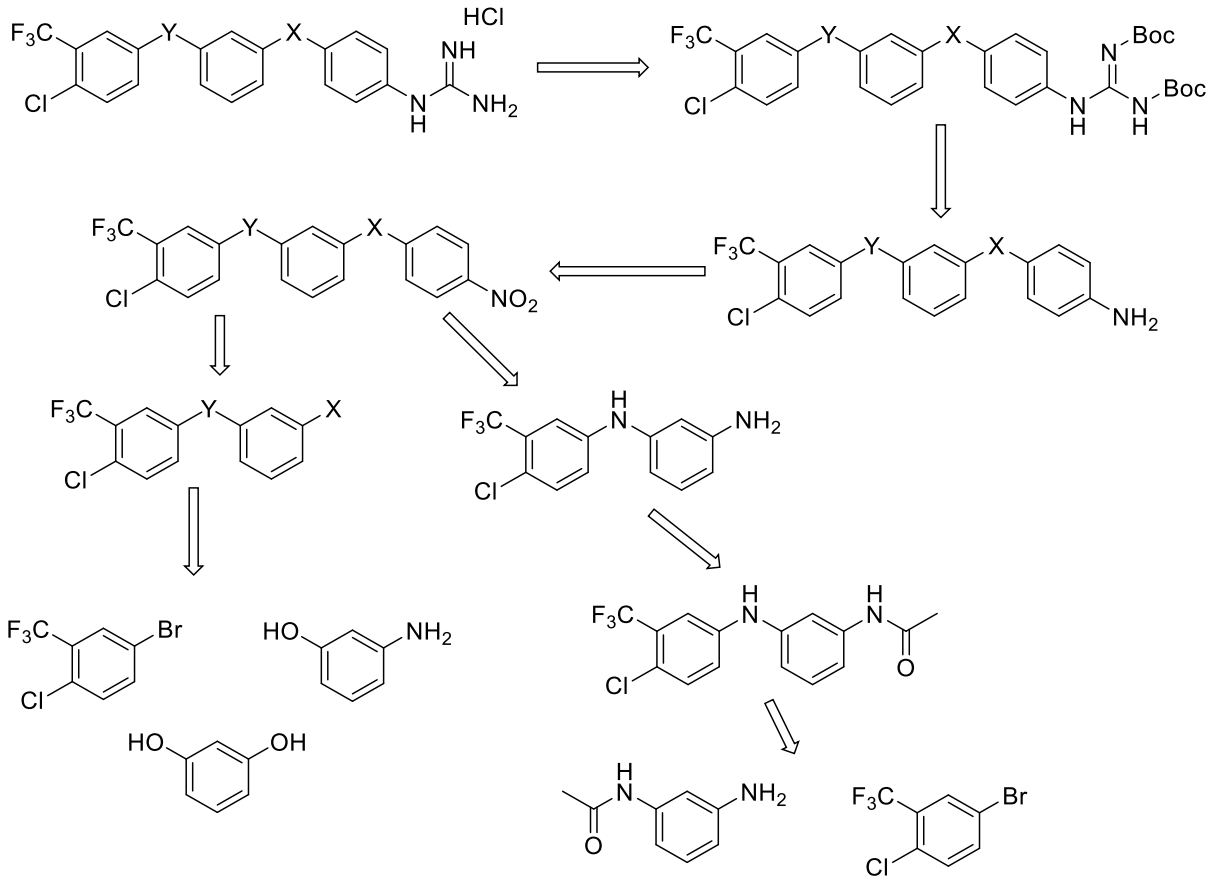

Figure 4.2.2. Schematic for the preparation of the compounds proposed to explore the linker moiety

The preparation of the compounds discussed in the previous section involved first a nucleophilic aromatic substitution between the appropriate aminophenol and an aromatic moiety carrying a nitro group that will be converted in the substrate for the guanidylation. It is known that the selectivity in this reaction is based on the differences in $pK_{a(H)}$ values between the aromatic amino ($pK_{aH} \approx 4.4$) and hydroxy ($pK_{aH} \approx 9.8$) groups; hence, when a base such as a carbonate ($pK_a \approx 10$) is used in the reaction, the hydroxy group gets deprotonated and acts as the nucleophile. Thus, the conditions we were using in those previous reactions were not suitable for the preparation of the

amino linked derivatives, and accordingly we approach the preparation of the new derivatives by first preparing the corresponding nitro and/or amino precursors via an Ullmann coupling.

Hence, in order to prepare the intermediate **73** (Scheme 4.2.1), a S_NAr reaction was first explored but gave mostly the unwanted symmetric compound **71** (Scheme 4.2.1); for that reason, we also used Ullmann type coupling (Scheme 4.2.1). For the synthesis of nitro precursor **72**, the diphenyl amine was prepared by the reaction between 3-aminophenol and 5-bromo-2-chlorobenzotrifluoride, while for compound **73** resorcinol was used instead of 3-aminophenol (Scheme 4.2.1).

Scheme 4.2.1. Synthesis of a functionalised hydroxyl **71** through a S_NAr (top) and synthesis of a functionalised amines **72** and **73** through Ullmann type coupling (bottom)

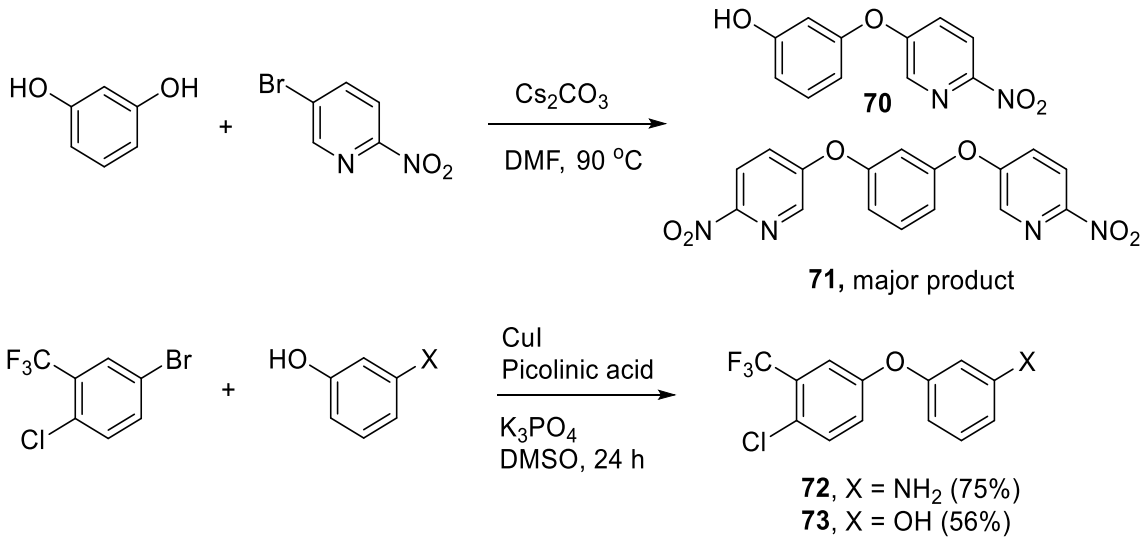

The general mechanism proposed for this type of Ullmann coupling (Figure 4.2.3) involves the use of monodentate or bidentate ligands and the reactivity of the X group changes in the order I > Br > Cl.[25]

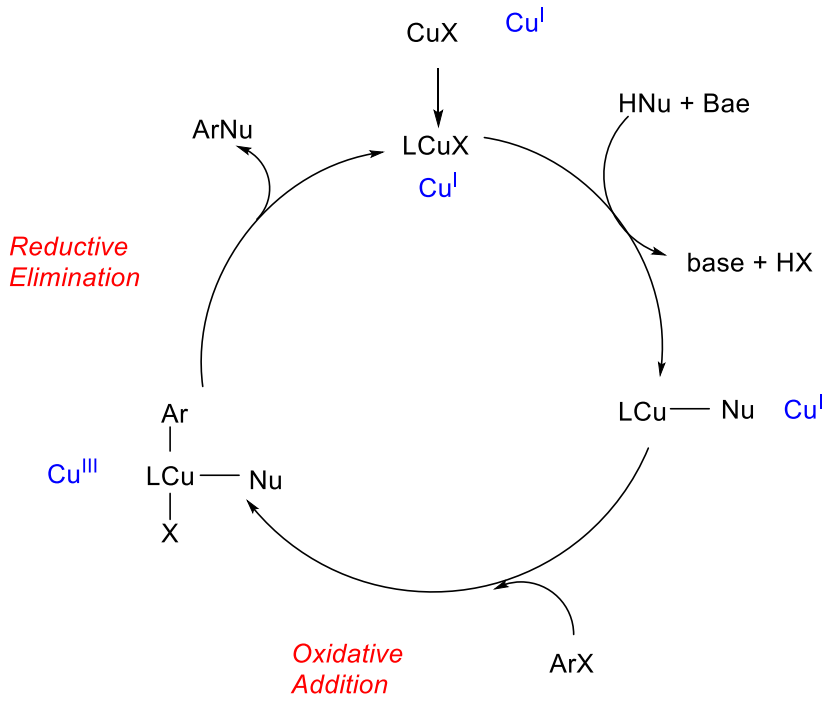

Figure 4.2.3. General mechanism for Ullmann coupling

The reported work of Maiti and Buchwald involved the use of copper catalysts and various conditions to increase selectivity between the *N*-arylation and the *O*-arylation products when using 3-aminophenols.[26] Electron-rich, -deficient and -neutral aryl halides were used, and conditions set for aryl bromides and aryl iodides to favour one product over the other. The competition between these two arylations is summarised in Figure 4.2.4.[25] The deprotonation step is the most important in this reaction. The amino group is more nucleophilic than the hydroxyl one and therefore, binds before deprotonation occurs. The more acidic phenolic group binds, in its ionic form, after the deprotonation occurs faster than the amino group. Therefore, the selectivity of O- over N-arylation depends on the nucleophilicity of the amine and on the rate of deprotonation. This approach was utilised in the synthesis of the amino intermediate **72**, which was achieved in good yields (75%).

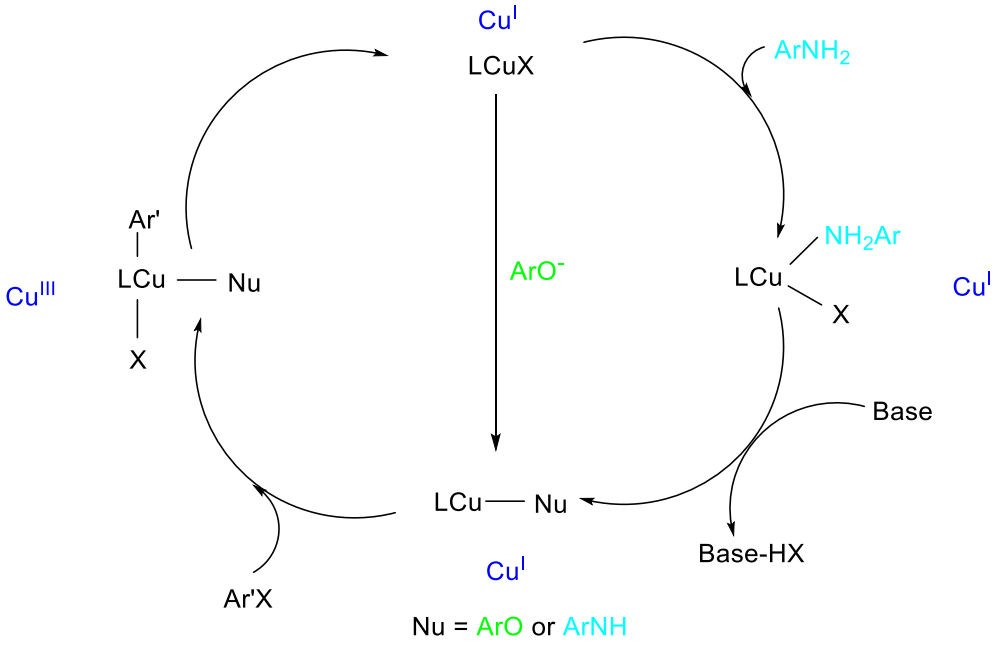

Figure 4.2.4. Mechanism of selectivity between the amino and phenyl[25]

For the preparation of intermediate **73** there was no issue of selectivity; however, there was a by-product in which the trifluoro phenol was added to both OH groups and thus the yield was modest (55%).

For the synthesis of the amino precursor **74** (Scheme 4.2.2), Buckwald-Hartwig amination was used initially using 3-aminoaniline as starting material; however, the unwanted compound **75** was found to be the main product. Accordingly, the commercially available acetylated 3-aminoaniline in 1,4-dioxane were used instead, and thus intermediate **76** was achieved with a yield of 57%. To obtain the corresponding free amine, **76** was refluxed in HCl/MeOH yielding **74** in good yields (74%).

Scheme 4.2.2. Buchwald-Hartwig coupling reactions

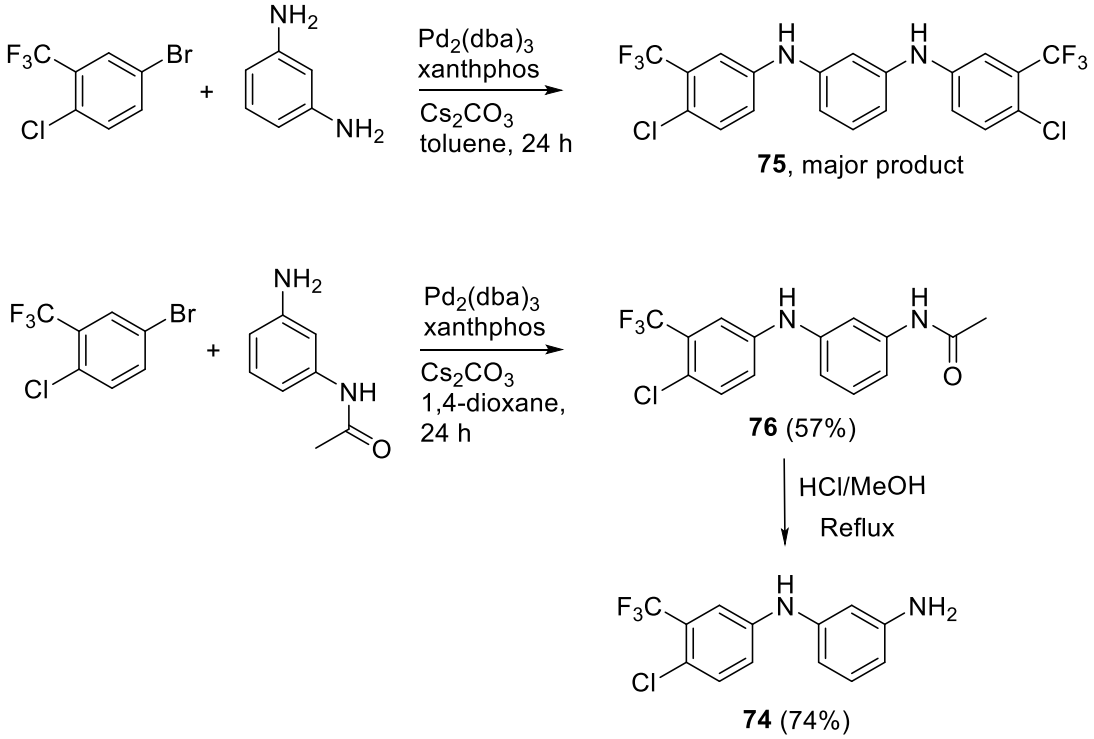

In order to prepare intermediate **77** (Scheme 4.2.3), nucleophilic aromatic substitution was used with the same conditions as mentioned before with 5-bromo-2-nitropyridine. The product was achieved in 40% yields and the expected by-product **78** was also obtained in low yield (23%).

Scheme 4.2.3. Nucleophilic aromatic substitution

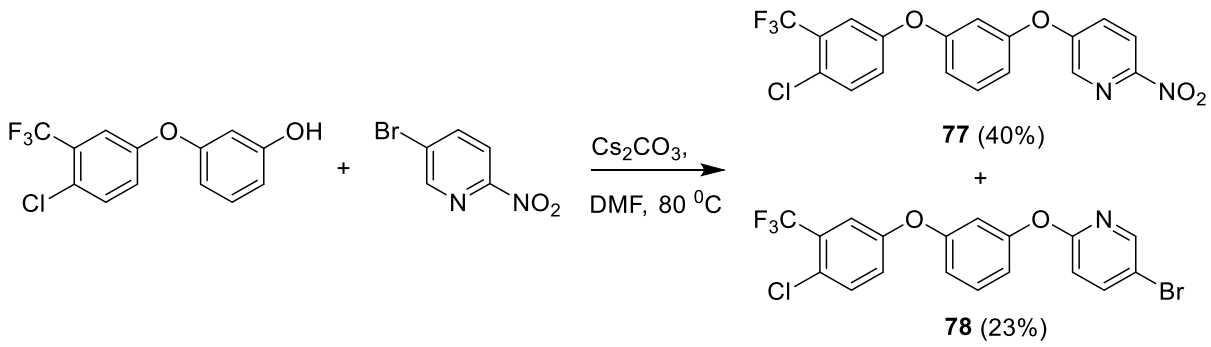

Precursors **79** and **80** (Scheme 4.2.4) were synthesised through Buchwald amination reactions, these were carried out as previously described and yields of 78% and 80%, were respectively obtained.

Scheme 4.2.4. Buchwald-Hartwig coupling

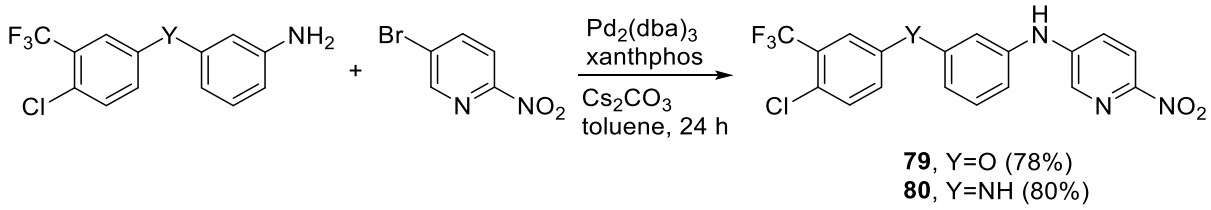

Nitro intermediates **77**, **79** and **80** were next reduced to the corresponding amino systems (**81-83**) by using the previously described $SnCl_2 \cdot 2H_2O$ conditions (Scheme 4.2.5). These aromatic amino systems were then subjected to guanidylation using *N,N'*-bis-(*tert*-butoxycarbonyl)-*S*-methylisothiourea to obtain Boc-protected compounds **84-86** that were finally deprotected under usual conditions to give final HCl salts **17-19** (Scheme 4.2.5, bottom).

Scheme 4.2.5. Selective nitro reduction with tin(II) chloride dihydrate (top); guanidylation and Boc deprotection with 4M HCl/dioxane (bottom).

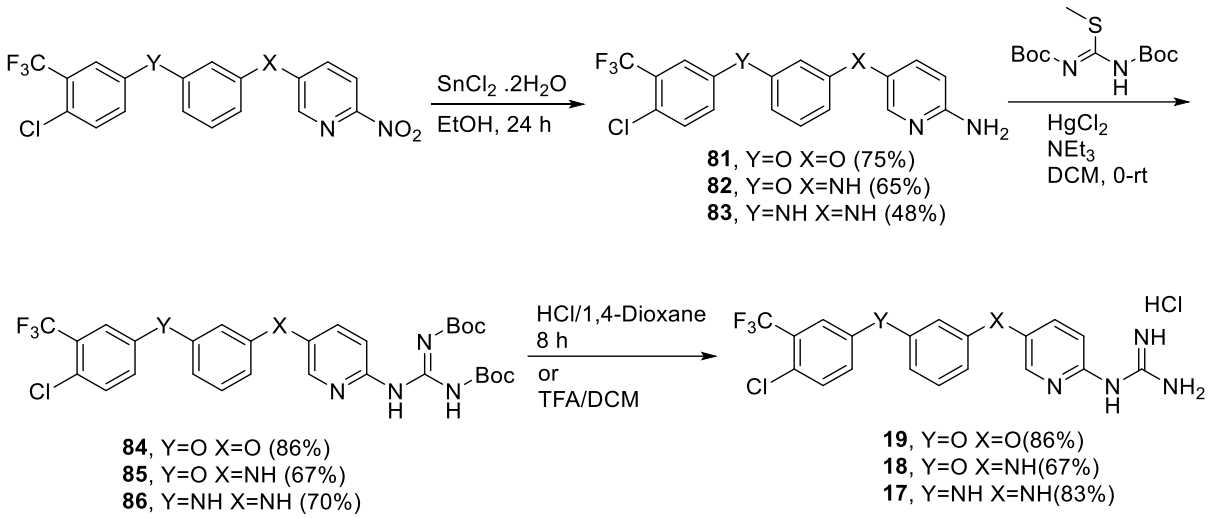

NMR was used to characterise the compounds post purification, in order to show how it was used compound **19** will be used as example. There are many techniques which allow us to look at relationships between protons which then allows us to identify each proton. In compound **19** we can see that we have 3 aromatic systems, on the H^1 spectrum we would expect to find these protons in to be found the aromatic region, 6-9 ppm.

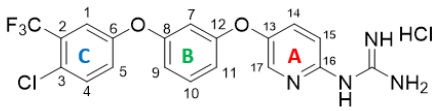

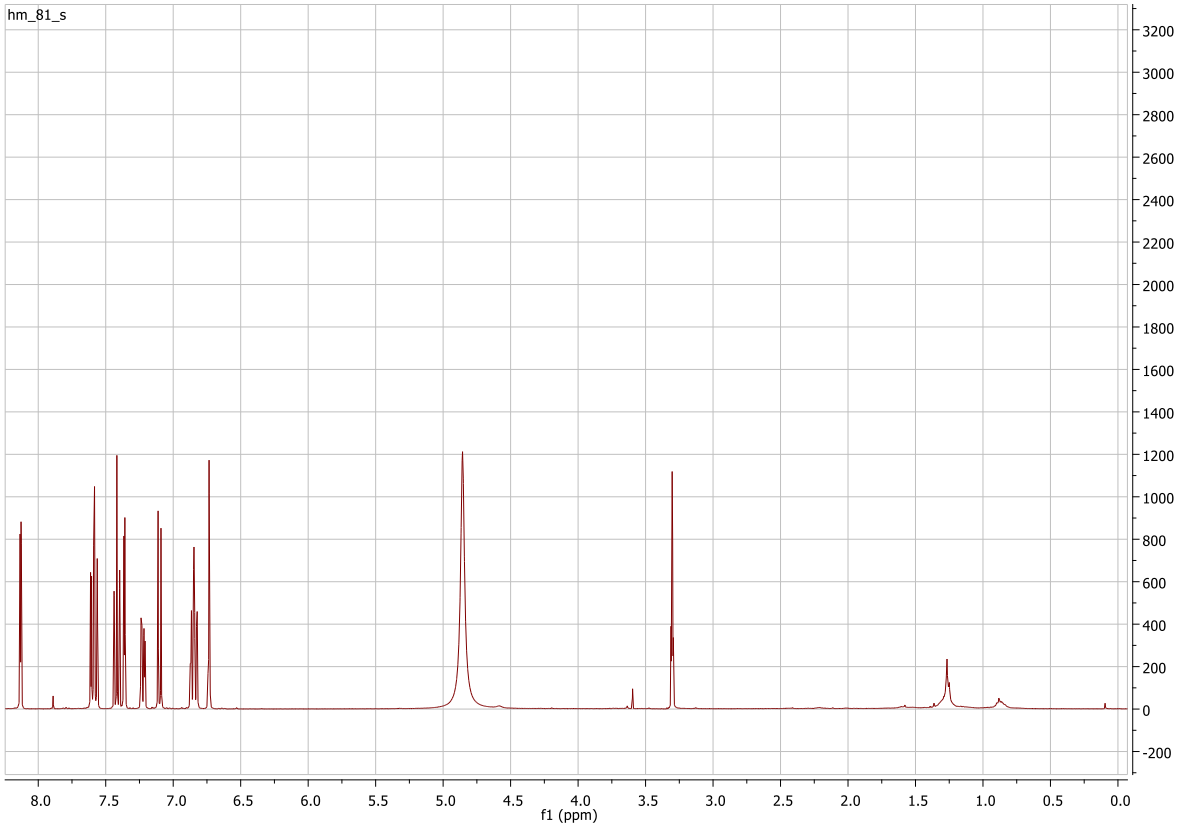

Figure 4.2.5. Structure and ^{1}H NMR spectrum of compound **19.**

Techniques like selective TOCSY can then be used to find the different proton systems to distinguish between the 3 systems. Once these have been identified we can then use the splitting pattern to identify the different protons. In the case of compound **19**. We have system A, B and C. In A (red on the spectrum) and C (blue on the spectrum) we can see that there are 3 protons thus we use the there position to distinguish between the two systems, with the red protons we can see that we have one proton that's extremely downstream, this is caused by have an electron withdrawing group near it, i.e. the guanidinium, thus we can postulate that the system in red is A. following this we can use their splitting pattern to identify the protons, as discussed in Figure 4.1.1.4. the pyridyl system is electron deficient, at positions 2, 4 and 6, therefore we can expect protons in these positions to have a downstream shift, with this we can deduce that the protons at 8.51 (d) and 7.6 (dd) ppm are in this positions, using the splitting pattern we can which proton is which, in this can the proton at position 2 which is next to the EW nitrogen in pyridine and has long range J value is the proton at 8.52 ppm

.

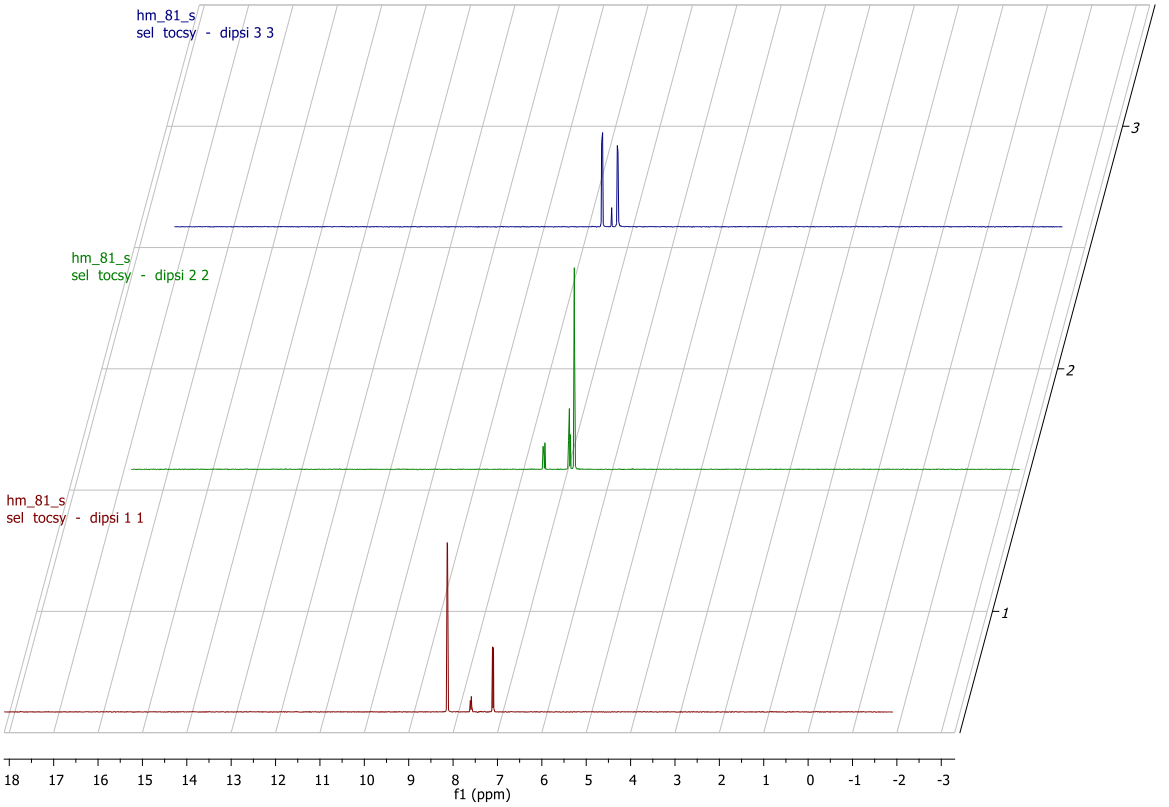
hm_81_s
sel tocsy - dipsi 3 3
hm_81_s
sel tocsy - dipsi 2 2
hm_81_s
sel tocsy - dipsi 1 1
3
2
1
18 17 16 15 14 13 12 11 10 9 8 7 6 5 4 3 2 1 0 -1 -2 -3
f1 (ppm)

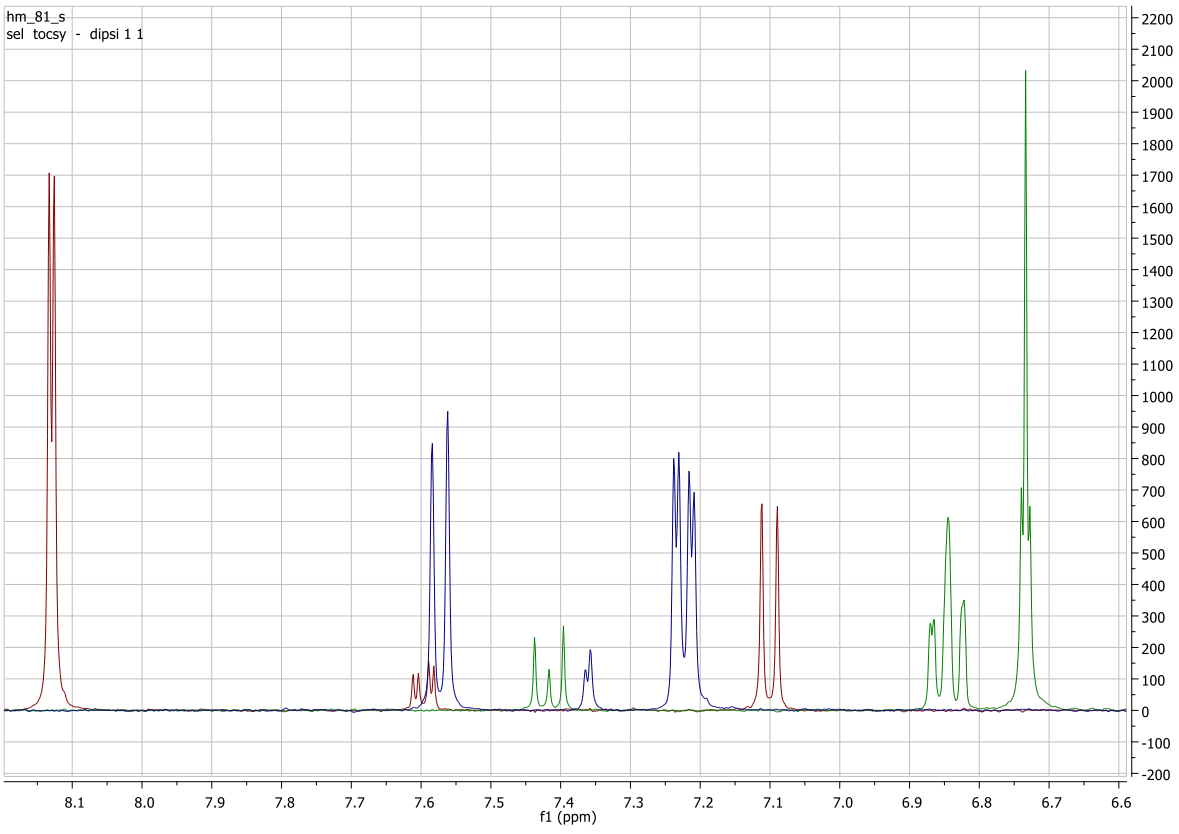
hm_81_s
sel tocsy - dipsi 1 1
2200 2100 2000 1900 1800 1700 1600 1500 1400 1300 1200 1100 1000 900 800 700 600 500 400 300 200 100 0 -100 -200
8.1 8.0 7.9 7.8 7.7 7.6 7.5 7.4 7.3 7.2 7.1 7.0 6.9 6.8 6.7 6.6
f1 (ppm)

Figure 4.2.6. Stack ^{1}H NMR spectra of compound **19.**

HSQC was used alongside C^{13} spectrum to assign the carbons, these 2D studies shows the correlation between the carbons and protons and the distinguishing between substituted carbons and quaternary carbons. Figure xx shows the 2D spectra shows the relationship between the carbons and protons. In the C^{13} we can also the C-F coupling, which further helps us assign the carbons.

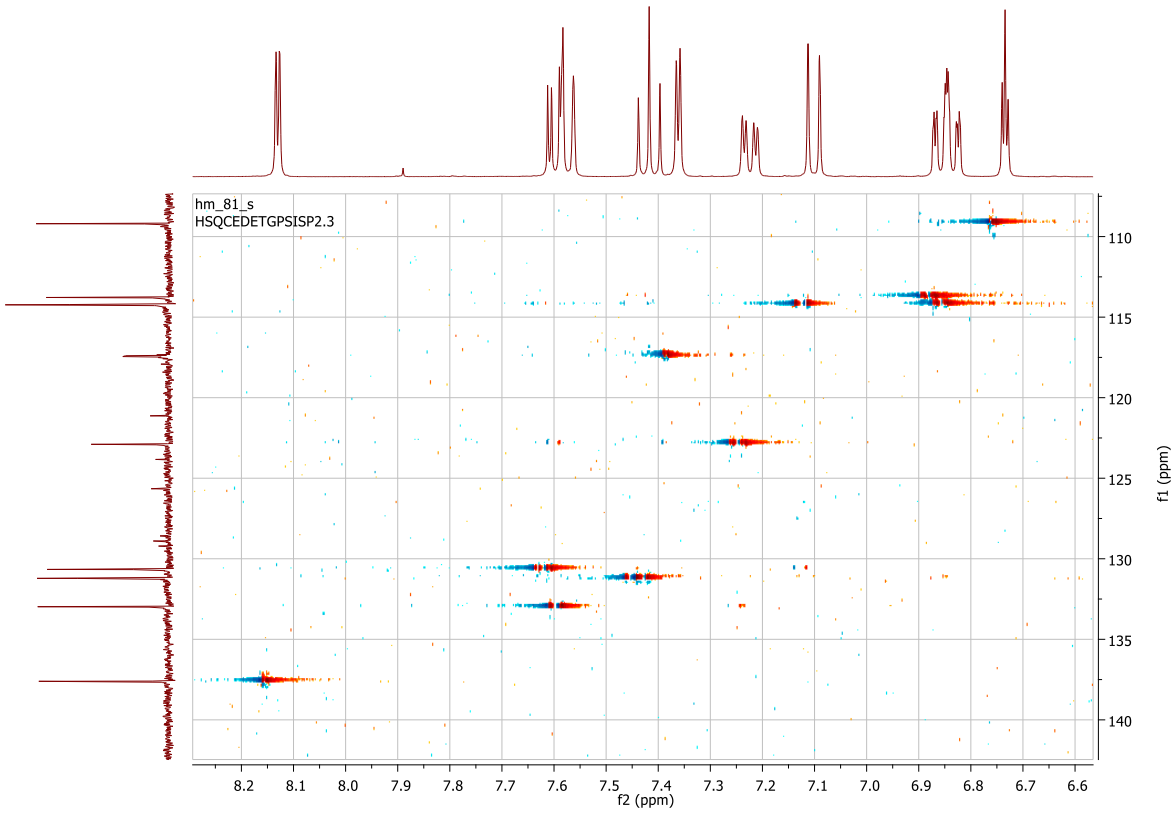

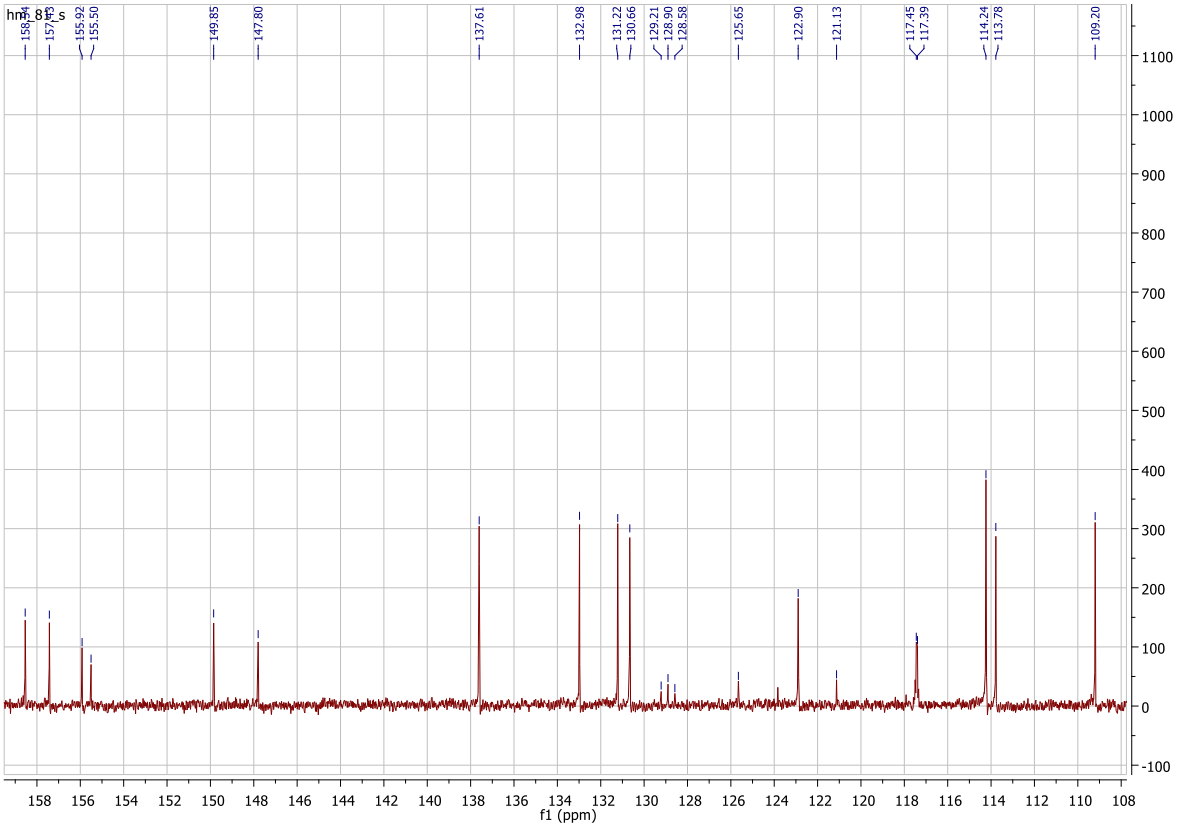

Figure 4.2.7. HSQC and ^{13}C NMR spectra of compound **19.**

4.3. Synthesis of derivatives of lead compound 2 exploring the polar moiety

According to the results obtained in the computational study (Chapter 3), the polar moiety of lead compound **2** forms strong interactions with the target, therefore we proposed to evaluate the importance of this moiety by replacing the guanidine with a 2-aminoimidazoline or an acetamide group as well as by removing the guanidine entirely (Figure 4.3.1).

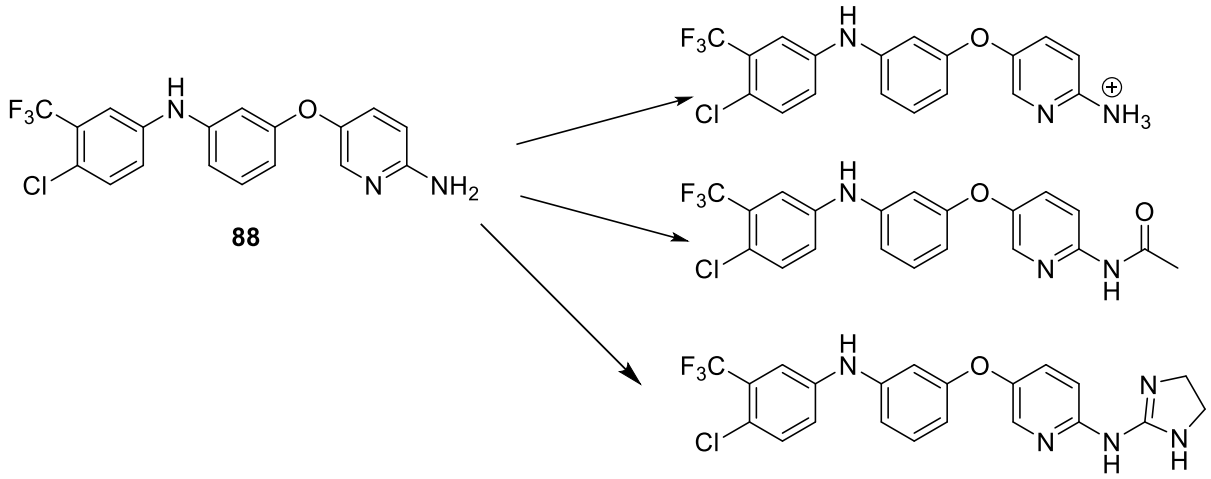

Figure 4.3.1. Proposed structures introducing new polar moieties

In order to introduce these new systems, an appropriate 2-aminopyridyl intermediate is needed (**88** in Figure 4.3.1), which was prepared by adding the third aryl system to the previously synthesised amine **25** using Buckwald-Hartwig amination with Xantphos as the ligand (Scheme 4.3.1), the nitro intermediate obtained (**87**) was next reduced with $SnCl_2 \cdot 2H_2O$ to give compound **88**.[13]

Scheme 4.3.1. Buchwald-Hartwig coupling and Selective nitro reduction with tin(II) chloride dihydrate

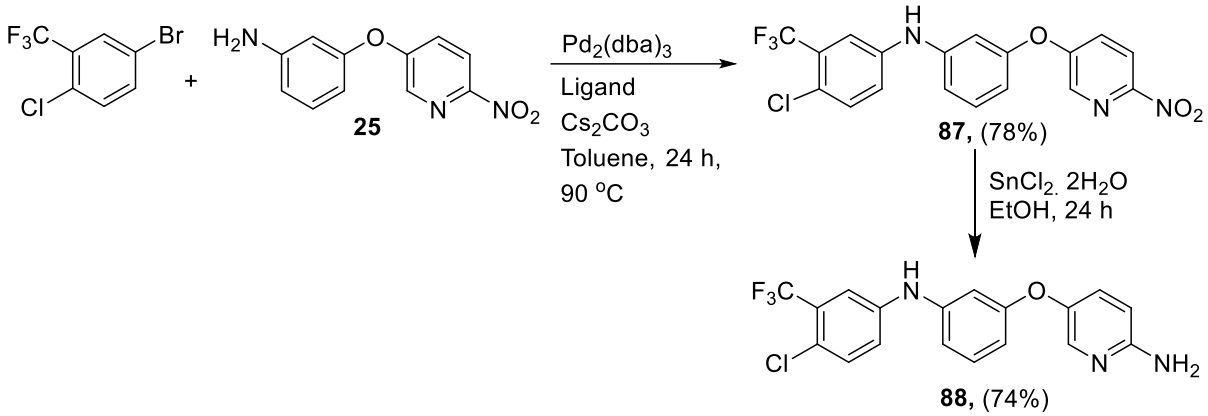

For the introduction of the 2-aminoimidazoline system, the Rozas group had developed a method involving the use of *N,N'*–bis-(*tert*-butoxycarbonyl)imidazolidine-2-thione (**89**).[27] Thus, compound **89** can be synthesised by the Boc protection of 2-imidazolinethione using di-*tert*-butyl dicarbonate in the presence of an excess of sodium hydride suspended in anhydrous THF (Scheme 4.3.2), which gives **89** in a high yield after recrystallization.

Scheme 4.3.2. Synthesis of *N,N'*–bis-(*tert*-butoxycarbonyl)imidazolidine-2-thione (**89**) from 2-imidazolinethione.

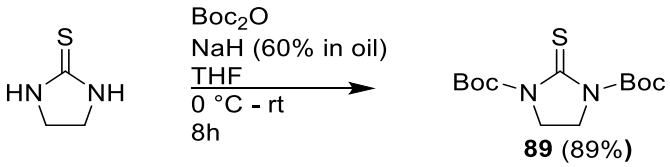

This procedure uses the same mild conditions as the Kim and Qian guanidylation method ($HgCl_2$ and NEt_3)[27] and accordingly tolerates a range of functional groups. The main advantage of this method is that it is compatible with poorly nucleophilic or labile amines such as anilines and aminopyridines allowing for the preparation of the

corresponding aryl-2-iminoimidazolidine derivatives, as their bis-Boc protected precursors, in good yields after purification.

Scheme 4.3.3. Proposed addition/elimination guanidylation mechanism *via* $HgCl_2$ mediated desulfurization of 1,3-bis-(*tert*-butoxycarbonyl)-2-methyl-2-thiopseudourea yielding *N*-aryl-*N',N''*-di-Boc protected guanidine.

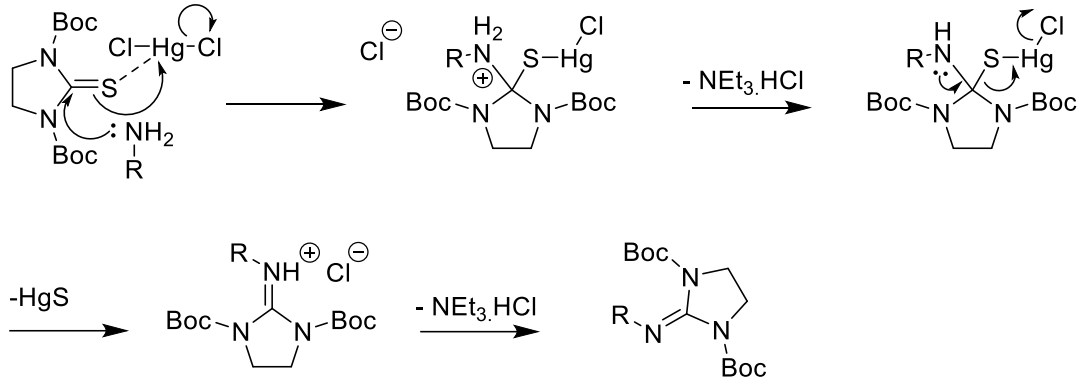

Coordination between the S atom and Hg enhances the electrophilic nature of the C=S quaternary carbon facilitating the concerted nucleophilic attack of the amine at that C atom (addition). The resulting tetrahedral intermediate is deprotonated at the NH group and the desired Boc protected 2-aryliminoimidazolidine derivatives formed upon loss of HgS (elimination) as shown in Scheme 4.3.3. Following this reaction, compound **90** (Scheme 4.3.4) was prepared in very good yield and was deprotected with 1:1 TFA:DCM to give the final salt.[27]

Scheme 4.3.4. 2-Aminoimidazolylation of **88** and Boc deprotection with TFA/CH_2Cl_2

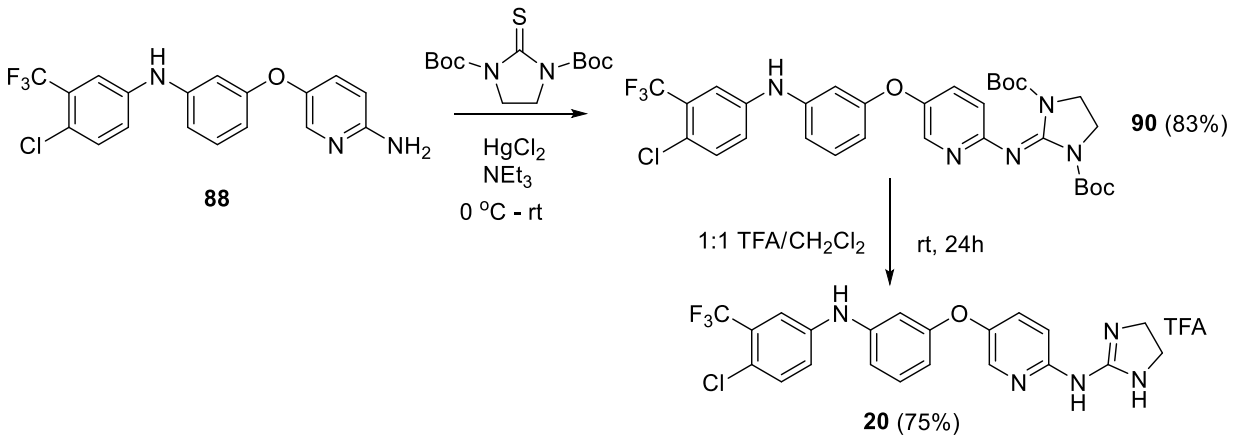

Preparation of the *N*-acetyl derivative (**21**) was carried out by reacting the primary amine precursor (**88**) with acetic anhydride, and triethylamine in dichloromethane for 6 hours, giving the final product in 85% yield (Scheme 4.3.5).

Scheme 4.3.5. Acetylation of **88**

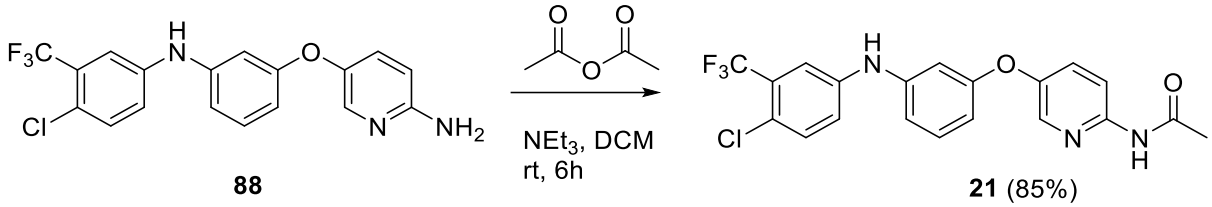

Finally, to prepare the derivative with an unsubstituted ammonium group (**22**), the neutral amino precursor **88** was stirred at 55 °C for 6 hours and was achieved in 92% yield, Scheme 4.3.6.

Scheme 4.3.6. Protonation of **88**

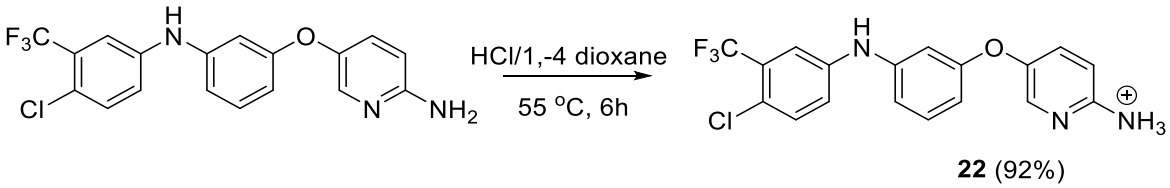

22 (92%)

4.4. Preparation of a 2-aminopyrimidine derivative

As mentioned before, there is a number of biologically active molecules incorporating the guanidine moiety and there are some compounds which can be considered to carry a hidden guanidine in the form of a 2-aminopyrimidine. One of these molecules is imatinib (Figure 4.4.1), which is an inhibitor of the Bcr-Abl kinase, and it has been shown that this 'hidden' guanidine, forms an interaction with the Thr-315 residue in the binding site of Bcr-Abl.[28]

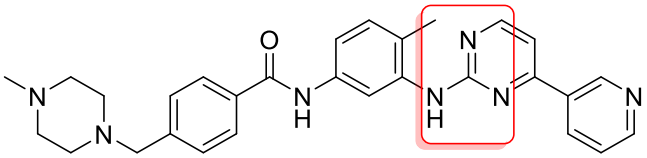

imatinib

Figure 4.4.1. Structure of imatinib, with the 'hidden' guanidine in the red box

There are other kinase inhibitors including JAK2 kinase inhibitors as seen in chapter 3 (Figure 3.4.1) that incorporate this type of 2-aminopyrimidine system these include fedratinib, pacritinib and XL019. This system in fedratinib has been shown to form interactions with key amino acids in the binding site of the target (i.e. Tyr931 and Leu932). Accordingly, preparation of compound **23** was proposed and the retrosynthetic Scheme is shown in Figure 4.4.2.

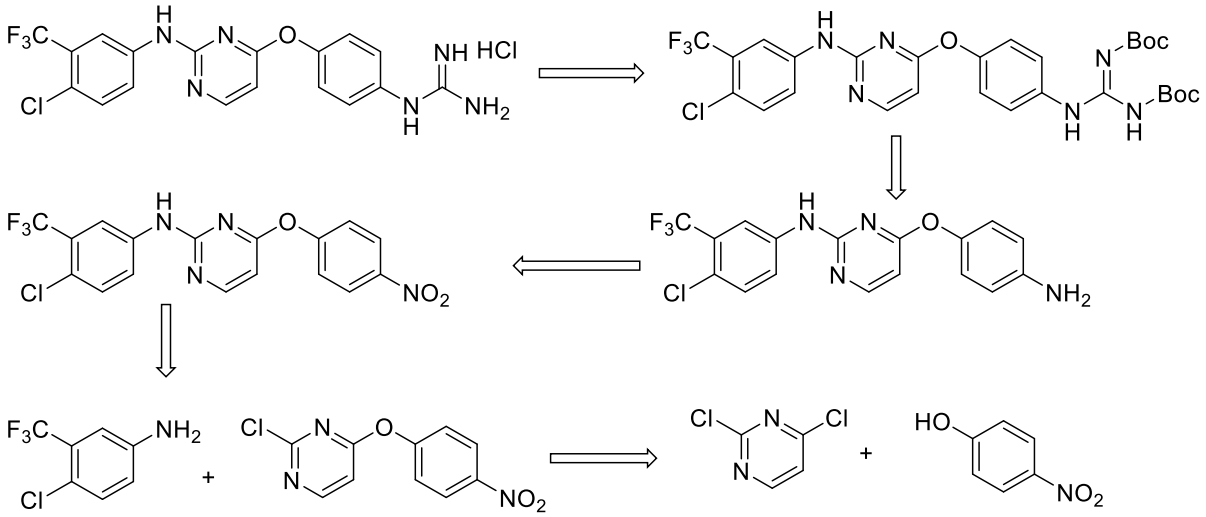

Figure 4.4.2. Schematic for the preparation of compound **23**.

Thus, diaryl **93** was synthesised by using the mentioned S_NAr type of reactions in which **92** is the nucleophile and **91** the electrophile. In compound **91** there are two substitution positions (i.e. 2 and 4 positions) and this may result in two products, **93** and **94**, compound **93** being the major product, thus showing that position 4 is more reactive (Scheme 4.4.1).

Scheme 4.4.1. Synthesis of **95** through a S_NAr

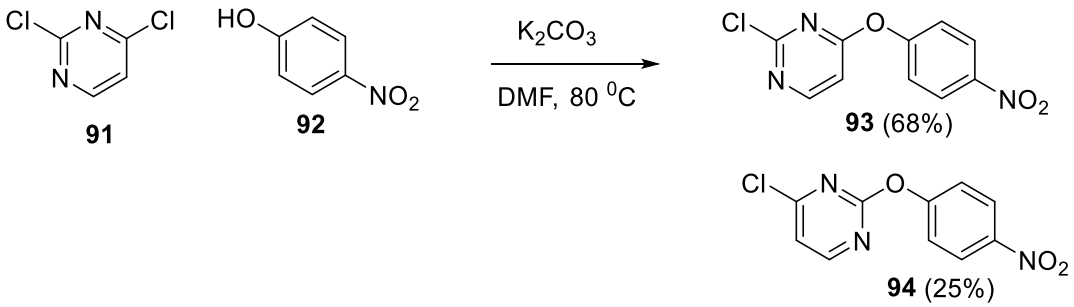

Next, the synthesis of **96** was approached and a Buchwald-Hartwig amination was used resulting in a very good yield of 82%. The nitro substituent of compound **96** was then reduced using tin (II) chloride dihydrate to yield **97** (62%) (Scheme 4.4.2). The

introduction of the corresponding guanidine moiety was pursued with the synthesis of the Boc protected derivative by reaction of **97** with *N,N'*-bis-(*tert*-butoxycarbonyl)-*S*-methylisothiourea, mercury (II) chloride and trimethylamine to yield **98** (86%). This Boc protected guanidino derivative was then deprotected using HCl 4M solutions in 1,4-dioxane, which was further diluted in a 1,4-dioxane until reaching a final concentration of 0.2M, to give **92** (86%) (Scheme 4.4.2).

Scheme 4.4.2. Synthetic Scheme of compound **92**.

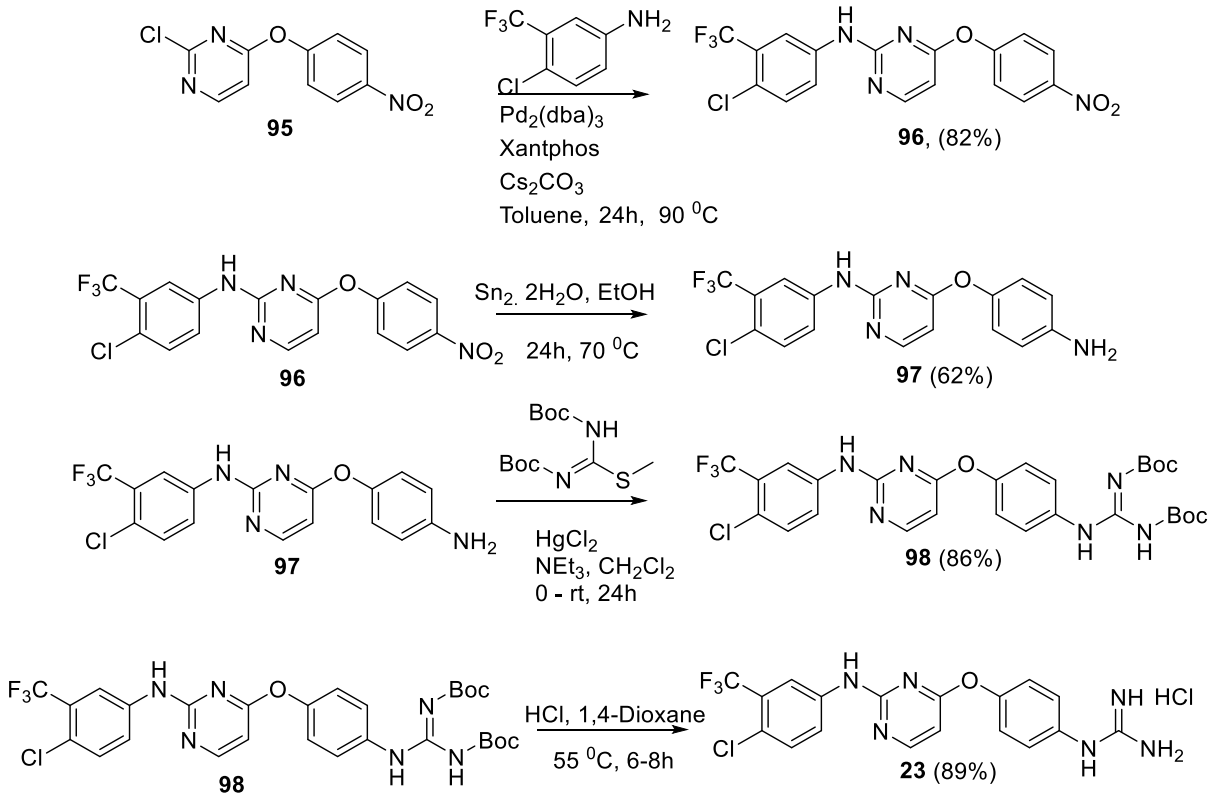

4.5. Conclusions

In this chapter we have presented the synthetic strategies used in the preparation of novel derivatives of lead compound **2** aiming to improve its biological activity. Based on our computational studies and previous biochemical results, we designed new compounds by changing different moieties to probe the different regions of the proposed target binding site.

In order to prepare compounds with different lipophilic moieties, the required precursors **25, 29, 31** and **32** were first synthesised using S_NAr reactions. Thus, for compounds **5-10**, 5-bromo-2-nitropyridine was reacted with 3-aminophenol with caesium carbonate at 80 °C overnight and for structures **11-16**, 4-acetaminophenol and 5-bromo-2-nitropyridine were reacted at room temperature overnight. The C–N bond was formed through Buchwald-Hartwig reactions between the di-aryl amino precursors and the desired bromine sources. The achieved nitro derivatives (**33-43**) were then reduced to give the amino structures through reduction with H_2 with Pd/C, in ethanol for derivatives without sensitive groups such as Cl or Br atoms (i.e. **35, 37, 41, 43** and **45**), whereas tin(II) chloride dihydrate was used as reducing reagent for derivatives with sensitive halogen groups such Cl or Br atoms (i.e. **33, 34, 36, 38-40,** and **42**). The amino intermediates were then guanidylated using *N,N'*-bis-(*tert*-butoxycarbonyl)-*S*-methylisothiourea to yield Boc-protected guanidino systems **58-69** and, next, Boc deprotection was carried out using 0.2M HCl to give the desired final HCl salts **5-16**.

The nature of the linkers of lead compound **2** was also explored by preparing derivatives **17-19.** These compounds were synthesised using methods such as S_NAr, Ullmann coupling and Buchwald amination. Ullmann coupling was used to prepare intermediates **72** and **73**. Compound **74** was then synthesised by Buchwald-Hartwig amination

between 5-bromo-2-chlorobenzotrifluoride and *m*-acetamidoaniline, yielding an acetamide Boc-protected intermediate that was deprotected using HCl/MeOH. Intermediate **77** was synthesised using S_NAr reactions, whereas precursors **79** and **80** were prepared using Buchwald amination. Following this, tin(II) chloride dihydrate reduction conditions were utilised to yield intermediates **81-83** that were then subjected to guanidylation reactions using *N,N'*-bis-(*tert*-butoxycarbonyl)-*S*-methylisothiourea to produce Boc derivatives **84-86** that were Boc-deprotected to give the final HCl salts **17-19**.

In order to explore the polar moiety of lead compound **2**, compound **88** was synthesised through Buchwald-Hartwig amination by using **25** as the amine source and 4-bromo-1-chloro-2-(trifluoromethyl)benzene as the halogen source.

The polar moiety was modified by substituting the guanidinium cation by 2-aminoimidazolinium, acetamide and an ammonium system (compounds **20-22**). The introduction of the 2-aminoimidazolinium cation was performed using the method developed by Dardonville and Rozas using Boc- protected thioimidazolinone to yield Boc-protected compound **90** that was deprotected using TFA/DCM to avoid the ring opening of the imidazoline ring to give **20**. The acetylation of precursor **88** was carried out using acetic anhydride to give the final product (**21**) in very good yields. Finally, to obtain the corresponding ammonium derivative **22**, the neutral precursor **88** was stirred with 0.2M HCl for 6 hours.

Finally, a 2-aminopyrimidine derivative (**23**) was prepared to explore how the introduction of this heterocycle can affect the biological activity. Thus, compound **23** was synthesised through the aforementioned reaction of S_NAr, Buchwald-Hartwig amination, tin(II) chloride dihydrate reduction conditions and the standard guanidylation conditions to yield **23** after Boc deprotection.

All compounds were fully characterised by means of ^{1}H and ^{13}C NMR spectroscopies and HRMS spectrometry, and their purity was determined by HPLC, where a minimum purity of 95% was required before proceeding to biological testing.

4.6. References

(1) Berlinck, R. G. S.; Burtoloso, A. C. B.; Trindade-Silva, A. E.; Romminger, S.; Morais, R. P.; Bandeira, K.; Mizuno, C. M. The Chemistry and Biology of Organic Guanidine Derivatives. *Nat. Prod. Rep.* **2010**, *27* (12), 1871–1907. https://doi.org/10.1039/C0NP00016G.

(2) Shaw J.W., Grayson D.H., R. I. Synthesis of Guanidines and Some of Their Biological Applications. In: Selig P. (Eds) Guanidines as Reagents and Catalysts I. https://doi.org/doi.org/10.1007/7081_2015_174.

(3) Tsutomu Ishikawa. *Superbases for Organic Synthesis: Guanidines, Amidines, Phosphazenes and Related Organocatalysts*; 2009.

(4) Cui, X.-Y.; Tan, C.-H.; Leow, D. Metal-Catalysed Reactions Enabled by Guanidine-Type Ligands. *Org. Biomol. Chem.* **2019**, *17* (19), 4689–4699. https://doi.org/10.1039/C8OB02240B.

(5) Saczewski, F.; Balewski, Ł. Biological Activities of Guanidine Compounds. *Expert Opin. Ther. Pat.* **2009**, *19* (10), 1417–1448. https://doi.org/10.1517/13543770903216675.

(6) Ishimoto, K.; Fukuda, N.; Nagata, T.; Sawai, Y.; Ikemoto, T. Development of a Scalable Synthesis of a Vascular Endothelial Growth Factor Receptor-2 Kinase

Inhibitor: Efficient Construction of a 6-Etherified [1,2,4]Triazolo[1,5-a]Pyridine-2-Amine Core. *Org. Process Res. Dev.* **2014**, *18* (1), 122–134. https://doi.org/10.1021/op4002824.

(7) Hasegawa, M.; Nishigaki, N.; Washio, Y.; Kano, K.; Harris, P. A.; Sato, H.; Mori, I.; West, R. I.; Shibahara, M.; Toyoda, H. Discovery of Novel Benzimidazoles as Potent Inhibitors of TIE-2 and VEGFR-2 Tyrosine Kinase Receptors. *J. Med. Chem.* **2007**, *50* (18), 4453–4470. https://doi.org/10.1021/jm0611051.

(8) Sherborne, G. J.; Adomeit, S.; Menzel, R.; Rabeah, J.; Brückner, A.; Fielding, M. R.; Willans, C. E.; Nguyen, B. N. Origins of High Catalyst Loading in Copper(i)-Catalysed Ullmann–Goldberg C–N Coupling Reactions. *Chem. Sci.* **2017**, *8* (10), 7203–7210. https://doi.org/10.1039/C7SC02859H.

(9) Laszlo Kurti Barbara Czako. *Strategic Applications of Named Reactions in Organic Synthesis*; 2005.

(10) Surry, D. S.; Buchwald, S. L. Dialkylbiaryl Phosphines in Pd-Catalyzed Amination: A User's Guide. *Chem. Sci.* **2011**, *2* (1), 27–50. https://doi.org/10.1039/C0SC00331J.

(11) Diez-Cecilia, E.; Kelly, B.; Perez, C.; Zisterer, D. M.; Nevin, D. K.; Lloyd, D. G.; Rozas, I. Guanidinium-Based Derivatives: Searching for New Kinase Inhibitors. *Eur. J. Med. Chem.* **2014**, *81*, 427–441. https://doi.org/https://doi.org/10.1016/j.ejmech.2014.05.025.

(12) Diez-Cecilia, E.; Carson, R.; Kelly, B.; van Schaeybroeck, S.; Murray, J. T.; Rozas, I. Probing a 3,4'-Bis-Guanidinium Diaryl Derivative as an Allosteric Inhibitor of the Ras Pathway. *Bioorg. Med. Chem. Lett.* **2015**, *25* (19), 4287–4292. https://doi.org/https://doi.org/10.1016/j.bmcl.2015.07.082.

(13) Previtali, V.; Mihigo, H. B.; Amet, R.; McElligott, A. M.; Zisterer, D. M.; Rozas, I. Exploring the Anti-Cancer Mechanism of Novel 3,4'-Substituted Diaryl Guanidinium Derivatives. *Pharmaceuticals* . 2020. https://doi.org/10.3390/ph13120485.

(14) Flapper, J.; Kooijman, H.; Lutz, M.; Spek, A.L.; van Leeuwen, P.W.N.M.; Elsevier, C.J.; Kamer, P. C. J. Nickel and Palladium Complexes of Pyridine−phosphine

Ligands and Their Use in Ethene Oligomerization. *Organometallics* **2009**, *28* (11), 3272–3281.

(15) Hartwig, J. F. Transition Metal Catalyzed Synthesis of Arylamines and Aryl Ethers from Aryl Halides and Triflates: Scope and Mechanism. *Angew. Chemie Int. Ed.* **1998**, *37* (15), 2046–2067. https://doi.org/10.1002/(SICI)1521-3773(19980817)37:15<2046::AID-ANIE2046>3.0.CO;2-L.

(16) Orlandi, M.; Brenna, D.; Harms, R.; Jost, S.; Benaglia, M. Recent Developments in the Reduction of Aromatic and Aliphatic Nitro Compounds to Amines. *Org. Process Res. Dev.* **2018**, *22* (4), 430–445. https://doi.org/10.1021/acs.oprd.6b00205.

(17) Chen, J.; Zhang, Y.; Yang, L.; Zhang, X.; Liu, J.; Li, L.; Zhang, H. A Practical Palladium Catalyzed Dehalogenation of Aryl Halides and α-Haloketones. *Tetrahedron* **2007**, *63* (20), 4266–4270. https://doi.org/https://doi.org/10.1016/j.tet.2007.03.061.

(18) Gellner, O. H.; Skinner, H. A. 244. Dissociation Energies of Carbon–halogen Bonds. The Bond Strengths Allyl–X and Benzyl–X. *J. Chem. Soc.* **1949**, No. 0, 1145–1148. https://doi.org/10.1039/JR9490001145.

(19) Bellamy, F. D.; Ou, K. Selective Reduction of Aromatic Nitro Compounds with Stannous Chloride in Non Acidic and Non Aqueous Medium. *Tetrahedron Lett.* **1984**, *25* (8), 839–842. https://doi.org/https://doi.org/10.1016/S0040-4039(01)80041-1.

(20) Yamabe, S.; Yamazaki, S. A DFT Study of Reduction of Nitrobenzene to Aniline with SnCl2 and Hydrochloric Acid. *J. Phys. Org. Chem.* **2016**, *29* (7), 361–367. https://doi.org/https://doi.org/10.1002/poc.3543.

(21) Alan R. Katritzky and Boris V. Rogovoy. Recent Developments in Guanylating Agents. *ARKIVOC* **2005**, 49–87.

(22) Kim, K. S.; Qian, L. Improved Method for the Preparation of Guanidines. *Tetrahedron Lett.* **1993**, *34* (48), 7677–7680. https://doi.org/https://doi.org/10.1016/S0040-4039(00)61537-X.

(23) Linton, B. R.; Carr, A. J.; Orner, B. P.; Hamilton, A. D. A Versatile One-Pot Synthesis of 1,3-Substituted Guanidines from Carbamoyl Isothiocyanates. *J. Org. Chem.* **2000**, *65* (5), 1566–1568. https://doi.org/10.1021/jo991458q.

(24) Poss, M. A.; Iwanowicz, E.; Reid, J. A.; Lin, J.; Gu, Z. A Mild and Efficient Method for the Preparation of Guanidines. *Tetrahedron Lett.* **1992**, *33* (40), 5933–5936. https://doi.org/https://doi.org/10.1016/S0040-4039(00)61092-4.

(25) Sambiagio, C.; Marsden, S. P.; Blacker, A. J.; McGowan, P. C. Copper Catalysed Ullmann Type Chemistry: From Mechanistic Aspects to Modern Development. *Chem. Soc. Rev.* **2014**, *43* (10), 3525–3550. https://doi.org/10.1039/C3CS60289C.

(26) Maiti, D.; Buchwald, S. L. Orthogonal Cu- and Pd-Based Catalyst Systems for the O- and N-Arylation of Aminophenols. *J. Am. Chem. Soc.* **2009**, *131* (47), 17423–17429. https://doi.org/10.1021/ja9081815.

(27) Dardonville, C.; Goya, P.; Rozas, I.; Alsasua, A.; Martín, M. I.; Borrego, M. J. New Aromatic Iminoimidazolidine Derivatives as A1-Adrenoceptor Antagonists: A Novel Synthetic Approach and Pharmacological Activity. *Bioorg. Med. Chem.* **2000**, *8* (7), 1567–1577. https://doi.org/https://doi.org/10.1016/S0968-0896(00)00089-4.

(28) Burgess, M. R.; Skaggs, B. J.; Shah, N. P.; Lee, F. Y.; Sawyers, C. L. Comparative Analysis of Two Clinically Active BCR-ABL Kinase Inhibitors Reveals the Role of Conformation-Specific Binding in Resistance. *Proc. Natl. Acad. Sci. U. S. A.* **2005**, *102* (9), 3395 LP-3400.

Chapter 5 – Biological evaluation of derivatives of lead compound 1

Previous research in the Rozas group found that lead compound **1** was a multi target inhibitor, aiming at kinases in the MAPK pathways; in particular, it was found to downregulate kinases downstream of B-Raf.[1,2] Immunoprecipitation and LanthaScreen assays suggested that lead **1** was targeting an allosteric site of B-Raf and this was also studied computationally.[3] Since compound **1** was showing promising results in cell

viability assays with different cancer cell lines, derivatives were prepared to find a more active compound.

In this chapter, some of the new derivatives of lead compound **1** prepared were screened in 59 different cell lines from nine different cancer groups including leukemia and colon cancer with the help of the National Cancer Institute, Developmental Therapeutics Program (NCI-DTP) panel service to determine their anticancer potential. Additionally, the mechanism by which lead **1** exerted cell death was elucidated by looking at its effects on the cell cycle and its ability to induce apoptosis in the leukemia cell line HL-60.

5.1. Cell viability studies

AlamarBlue and sulforhodamine B (SRB) cell viability assays were utilised to determine the cytotoxic effects of the chosen derivatives of lead compound **1** (Figure 5.1.1).

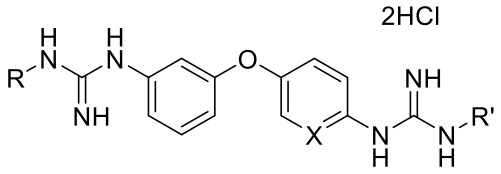

1, R = (3-CF_3,4-Cl)Ph, X = CH, R' = H
99, R = (3-CF_3,4-Br)Ph, X = CH, R' = H
100, R = (2-F,4-I)Ph, X = CH, R' = H
101, R = (2-F,4-I)Ph, X = NH, R' = H
102, R = (4-Br)Ph, X = NH, R' = H
103, R' = (3-CF_3,4-Br)Ph, X = CH, R = H
3, R = (3-CF_3,4-Cl)Ph, X = NH, R' = H

Figure 5.1.1. Bis-guanidine compounds related to lead compound **1** tested against different cancer cell lines

The AlamarBlue assay allows to quantitatively measure the proliferation of cells after treatment with different concentrations of a particular drug. The active component of the AlamarBlue® reagent is resazurin, which is a cell permeable, non-toxic compound that in its oxidised form is blue and non-fluorescent. When the cells are alive, they maintain a reducing environment within the cytosol and, therefore, when entering cells, resazurin is reduced to resorufin, a red and highly fluorescent compound. Thus, viable cells convert resazurin to resorufin, increasing the overall fluorescence that is then read

on a spectrophotometer.[4] The limitation of this assay is that it relies on the activity of the mitochondria, so if the cells are not metabolically viable the cells will be seen as "dead".

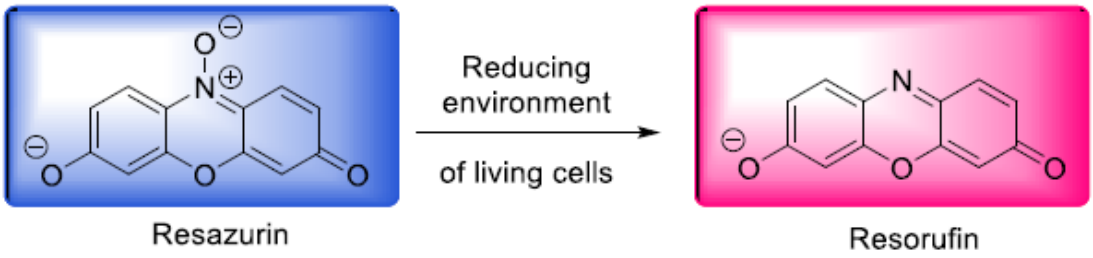

Figure 5.1. Resazurin, the active component of AlamarBlue® reagent is reduced to the highly fluorescent resorufin.

Even though the AlamarBlue assay shows the cytotoxicity of a drug, it does not distinguish between cytostatic and cytocidal drugs; in order to distinguish between the two types of cytotoxicity the SRB assay is used.[5] The SRB assay relies on the uptake of the negatively charged aminoxanthine dye by binding to proteins under mild basic conditions which are extracted under basic conditions; the amount of aminoxanthine dye bound can then be measured and cell proliferation can be extrapolated[6] (i.e. we can determine if the cells have proliferated, died or no change to growth of the cells has taken place).

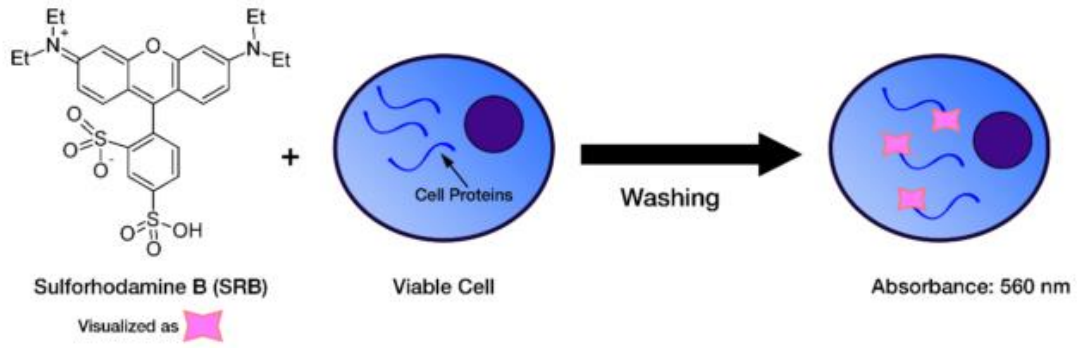

Figure 5.2. Aminoxanthine reacts with aldehyde groups to form linkages.[7]

The SRB assay is used for cell density determination, based on the measurement of cellular protein content. The method was optimized for the toxicity screening of compounds to adherent and suspension cells in a 96-well format, cells are inoculated into 96 well microtiter plates in 100 µL at plating densities ranging from 5,000 to 40,000 cells/well depending on the doubling time of individual cell lines. After 24 h, two plates of each cell line are fixed in situ with trichloroacetic acid (TCA), which fixes the cells onto the plate, to represent a measurement of the cell population for each cell line at the time of addition of the compound studied (Tz). The cells are incubated with the compound for 48 h and after this incubation period, cell monolayers are fixed with 10% (wt/vol) TCA and incubated for 60 min at 4 °C. Then, a SRB solution (100 µL) at 0.4% (w/v) in 1% acetic acid is added to each well, and plates are incubated for 10 min at room temperature. Next, excess dye was removed by washing the cells repeatedly with 1% (vol/vol) acetic acid. The protein-bound dye is dissolved in 10 mM Tris base solution for optical density (OD) determination at 515 nm using a microplate reader.

Using the absorbance measurements [time zero, (Tz), control growth, (C), and test growth in the presence of the compound studied at five concentration levels (Ti)], the percentage growth is calculated at each of the compound concentrations level. Finally, percentage growth inhibition is calculated as:

$[(Ti-Tz)/(C-Tz)] \times 100$ for concentrations for which $Ti \geq Tz$

$[(Ti-Tz)/Tz] \times 100$ for concentrations for which $Ti < Tz$.

Three dose response parameters are calculated for each experimental agent. Inhibition of 50% of the cell growth (GI_{50}) is calculated from the equation $(Ti-Tz)/(C-Tz)] \times 100 = 50$, which corresponds to the compound concentration resulting in a 50% reduction in the net protein increase (as measured by SRB staining) in control cells during the drug incubation. The compound concentration resulting in total growth inhibition (TGI) is calculated from Ti = Tz. The LC_{50} (concentration of the compound resulting in a 50% reduction in the measured protein at the end of the treatment as compared to that at the beginning), which indicates a net loss of cells following treatment and is calculated

from the equation (Ti-Tz)/Tz] x 100 = -50. Exact values for each of these three parameters are calculated if the level of activity is reached; however, if the effect is not reached or is exceeded, the value for that parameter is expressed as greater or less than the maximum or minimum concentration tested.[8,9]

The number reported for the one-dose assay is growth relative to the no-drug control, and relative to the time zero number of cells. This allows detection of both growth inhibition (values between 0 and 100) and lethality (values less than 0). This is the same as for the 5-dose assay, described below. For example, a value of 100 means no growth inhibition. A value of 40 would mean 60% growth inhibition. A value of 0 means no net growth over the course of the experiment. A value of -40 would mean 40% lethality. A value of -100 means all cells are dead.[8]

Compounds submitted to the NCI screening (Figure 5.1.1) were selected based on their activity in previous in-house AlamarBlue assays in the HL-60 cell line.[10]

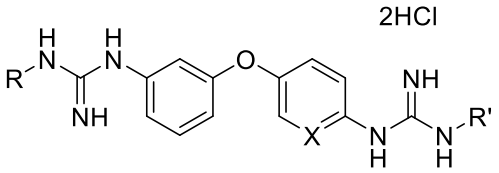

1,	R = (3-CF_3,4-Cl)Ph, X = CH, R' = H
99,	R = (3-CF_3,4-Br)Ph, X = CH, R' = H
100,	R = (2-F,4-I)Ph, X = CH, R' = H
101,	R = (2-F,4-I)Ph, X = NH, R' = H
102,	R = (4-Br)Ph, X = NH, R' = H
103,	R' = (3-CF_3,4-Br)Ph, X = CH, R = H
3,	R = (3-CF_3,4-Cl)Ph, X = NH, R' = H

Figure 5.1.1. Bis-guanidine compounds related to lead compound **1** tested against different cancer cell lines.

5.1.1. Cell viability studies in leukemia cell lines

Leukemia is a cancer of the blood and bone marrow, according to the WHO in 2020 there was an estimated 474,519 new cases of leukemia in both male and females of all ages, as this cancer affects everyone in society including children, there is a great amount of effort to find therapeutics that target it. The NCI screening panel uses six cell

lines derived from patients with leukemia from a variety of age, descriptions found in appendix.

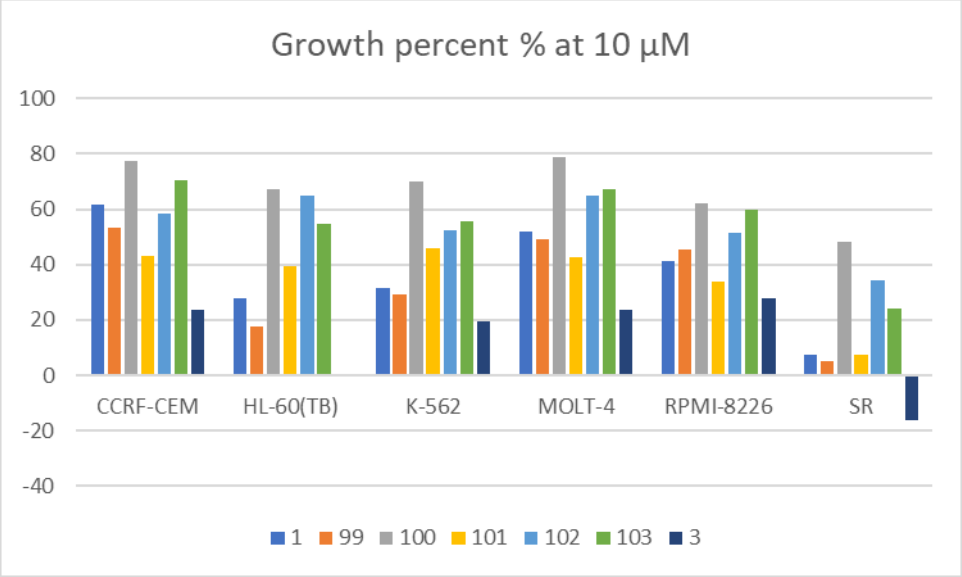

Figure 5.1.1.1. The effect of derivatives of lead compound **1** on leukemia cell lines.

Many of the compounds screened in leukemia cancer cell lines (Figure 5.1.1.1) lead to increased cell growth compared to lead **1**. In compound **1** the highest cell growth is observed in the CCRF-CEM cell line, while in the rest of the cell lines the inhibition of the cell growth is low to moderate. In **3** where the polar moiety was changed, the cell growth activity observed was even lower than **1**, suggesting that **3** is more active than **1** as a cell growth inhibitor. Furthermore, compound **3** even causes cell death in the SR cell line. In **99**, where the hydrophobic head was modified, there is no change in the inhibitory effect over all the cell lines compared to **1**; therefore, making the hydrophobic moiety bigger does not change the activity of **1** in the leukemia cell lines tested. Regarding the rest of the derivatives tested, no increase in growth inhibition is observed; thus, the changes introduced in those compounds compared to the structure of **1** were not favourable for anticancer activity.

5.1.2. Cell viability studies in Non-Small Cell Lung Cancer cell lines

According to the American Cancer Society 80-85% of lung cancers are Non-Small Cell Lung Cancers (NSCLC)[11] and according to the WHO over 2 million new cases of lung cancer were reported in 2020 in both sexes and all ages. Nine NSCLC cell lines were used in the NCI screening, which are described in the appendix.

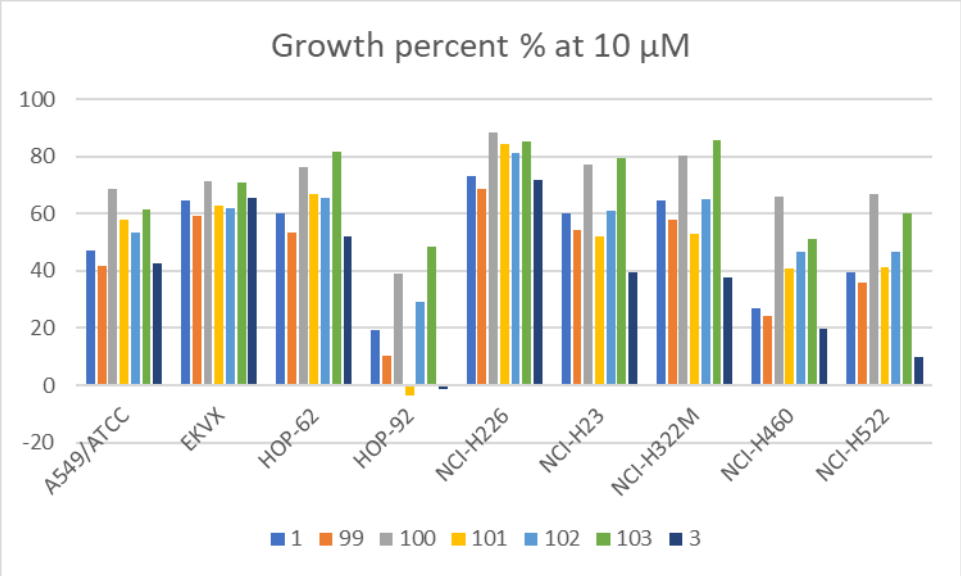

Figure 5.1.2.1. The effect of derivatives of lead compound **1** on NSCLC cell lines.

When the NSCLC cell lines (Figure 5.1.2.1) were treated with the compounds studied there was no major cell growth inhibition in most of them. In A549, EKVX, HOP-62, NCI-H226, NCI-H23 and NCI-H322M cell lines the growth percentage was over 40%, suggesting that our compounds did not have major effect on the viability of the cells. In the NCI-H460 cell line compounds **1**, **99** and **3** had a percentage growth of less than 30%, suggesting that these compounds are leading to growth inhibition. In the case of compound **103** there is a doubling in the growth percentage suggesting that the relative

position of the guanidine and the hydrophobic head has an effect on the activity of lead **1**. In the cell line HOP-92 the most notable effect on growth activity is observed, with some compounds leading to cell death. Thus, in this cell line, compound **1** drives to only a 19% in the cell growth, and this changes favourably with compounds **99**, **101** and **3**. In **99** cell growth decreases up to 9%, and in compounds **101** and **3** cell death starts being observed, with **101** having a slightly higher % cell death, suggesting that the bigger 4-iodo substitution is favourable.

5.1.3. Cell viability studies in colon cancer cell lines

Colorectal cancer, also known as colon or rectal cancer depending on where it starts, is a cancer of the large intestine. There was almost 2 million cases of colorectal cancer in 2020 of both sexes and all ages. In our case, seven cell lines were screened by the NCI, these are described in the appendix.

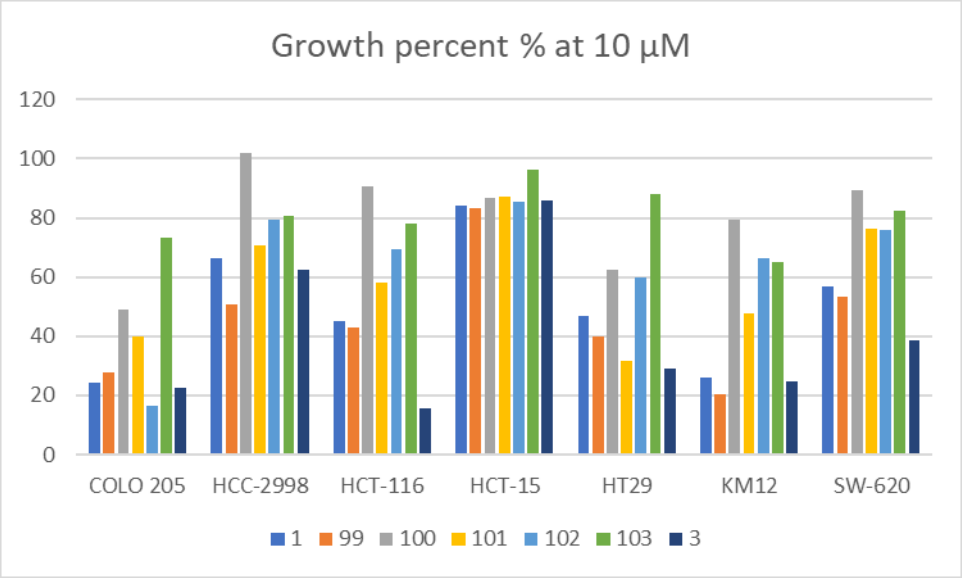

Figure 5.1.3.1. The effect of derivatives of lead compound **1** on colon cancer cell lines.

In the colon cancer cell lines, all of the compounds screened had no major effect on cell growth. The most majorly effected cell line is COLO 205 where all cell growth remains under 50%, except with **103**. With compounds **1**, **99**, **101** and **3** cell growth in HT29 and KM12 remains under 50%, in the other cell lines growth is significant, above 50%. This

suggest that in most of the cell lines screened our compounds are ineffective in causing cell growth inhibition or cell death.

5.1.4. Cell viability studies in CNS cancer cell lines

Brain and CNS cancers are found in the brain and spinal cord. The brain is protected by the blood-brain barrier which prevents many cancer treatments from reaching the cancer cells, thus new treatments are always being researched. The NCI utilised six cell lines derived from patients with CNS cancer with our compounds.

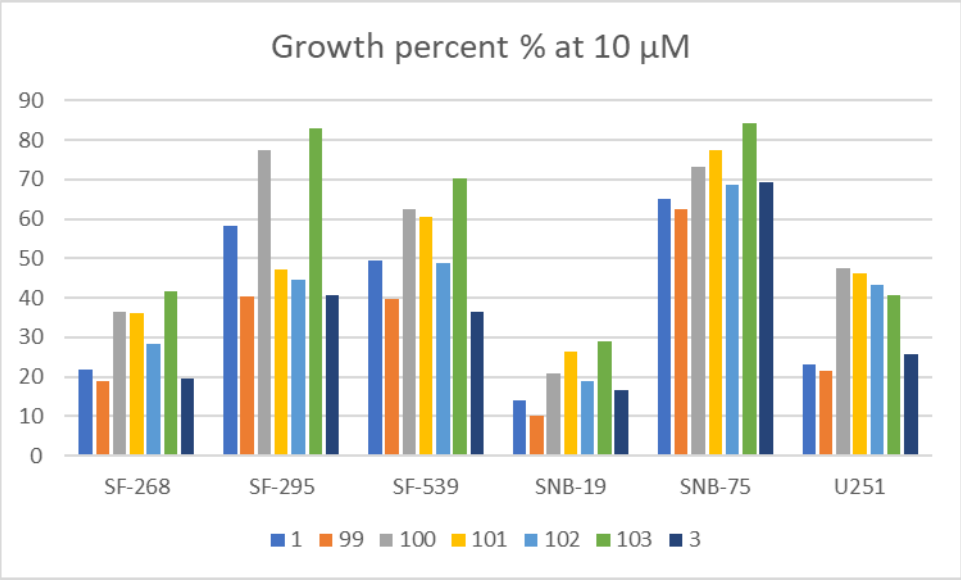

Figure 5.1.4.1. The effect of derivatives of lead compound **1** on CNS cancer cell lines.

None of the compounds studied exerts cell death in these CNS cell lines (Figure 5.1.4.1). All of the compounds performed relatively poorly in CNS cell lines much like what we observed for the colon cancer cell lines. Thus, the cell lines studied did not experience significant growth inhibition, with the exception of SNB-19 that when treated with **99** showed less than 30% cell growth. This compound is the only one seen to perform better than lead **1** in these cell lines.

5.1.5. Cell viability studies in melanoma cancer cell lines

Melanoma is a type of skin cancer with an estimated number of cases over 300,000 reported in 2020. The NCI utilised nine cell lines derived from patients with melanoma cancer in the screening of our compounds.

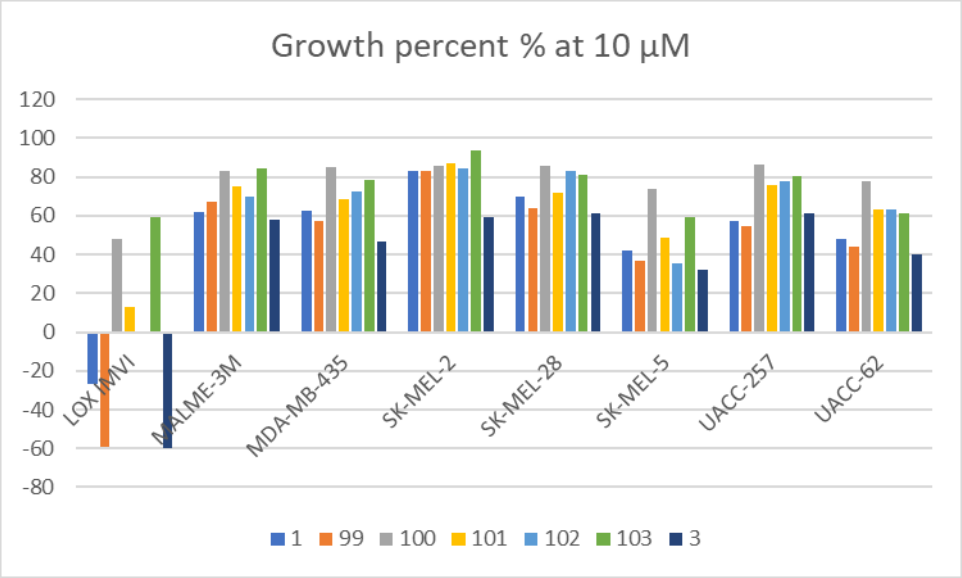

Figure 5.1.5.1. The effect of derivatives of lead compound **1** on melanoma cell lines

Most of the melanoma cancer cell lines (Figure 5.1.4.1) were not sensitive to the compounds screened. Thus, upon treatment with the compounds all of the cell lines saw moderate to high cell growth except for LOX IMVI. In the particular case of the LOX IMVI line, cell death is recorded with compounds **1**, **99** and **3**, and an increase in activity with respect to **1** is seen when both the hydrophobic head and the polar moiety were modified.

5.1.6. Cell viability studies in ovarian cancer cell lines

Ovarian cancer is one of the most common types of cancer in women, with over 300,000 cases reported in 2020. In the screening performed by the NCI, seven cell lines derived from patients with ovarian cancer were used.

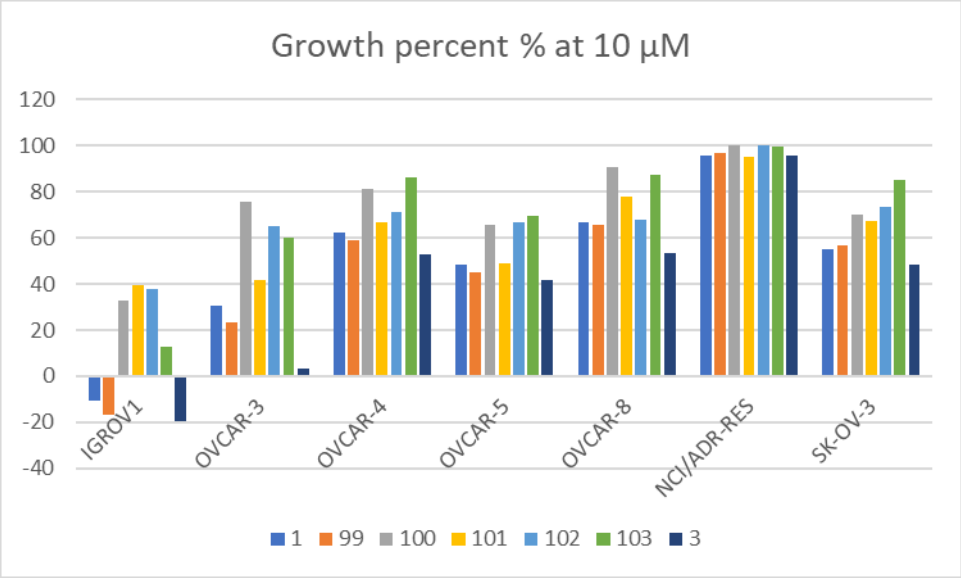

Figure 5.1.6.1. The effect of derivatives of lead compound **1** on ovarian cancer cell lines

Most of the ovarian cancer cell lines studied (Figure 5.1.6.1) were not sensitive to the compounds screened. Most of the cell lines saw moderate to high cell growth except for IGROV1, which show to undergo cell death with three of the compounds, **1, 99** and **3**. Looking at the changes in cell death percentage among these three compounds it can be suggested that the changes introduced in **99** and **3** were favourable in increasing the activity of lead **1**.

5.1.7. Cell viability studies in renal cancer cell lines

Renal cancer is cancer of the kidneys, according to the National Health Services in the United Kingdom,[12] it usually effects adults in there 60 and is rare in people under 50.

The NCI uses seven cell lines derived from patients with renal cancer from different age groups.

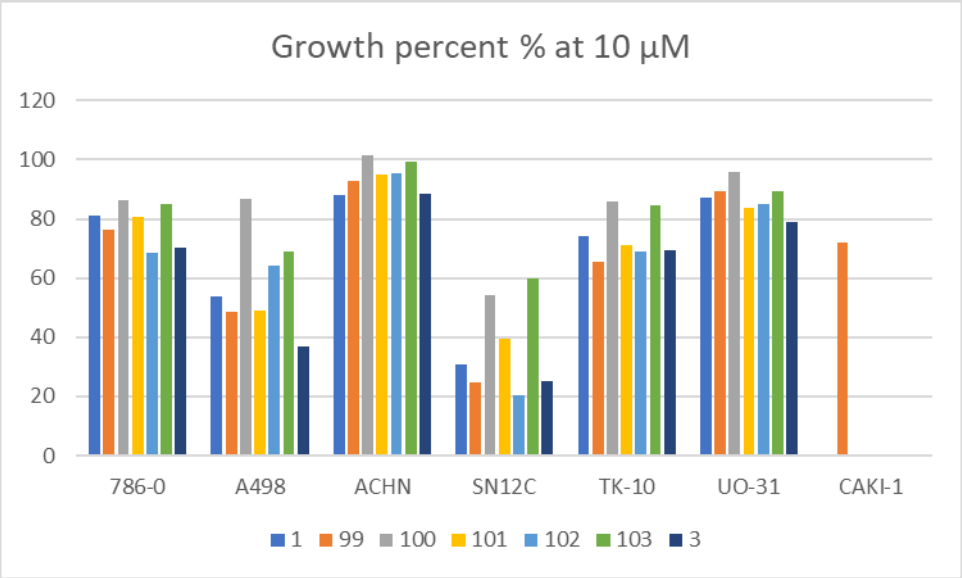

Figure 5.1.7.1. The effect of derivatives of lead compound **1** on renal cancer cell lines

Treatment with our compounds of many of the renal cancer cell lines (Figure 5.1.7.1) lead to increased cell growth compared to lead **1**. Treatment with this compound results in relatively high percentage growth across all of the cell lines, with the exception of SN12C at 30% growth, suggesting that this compound is not active in the renal cell lines screened. Compound **3** drives to similar high percentage growth as **1**, except in the A498 line where growth goes down from 53% to 36%. In the case of compound **99** no change in the inhibitory effect of the cell growth is observed, and therefore it can be concluded that enlarging the hydrophobic head does not result in a change in the activity of **1** in renal cancer cell lines. This same effect is seen in all of the cell lines screened, thus suggesting that these bis-guanidine compounds are not very effective against renal cancer.

5.1.8. Cell viability studies in breast cancer cell lines

Breast cancer is one of the most common and aggressive types of cancer in women, with an estimated over 2 million cases reported in 2020 in which this was the most

occurring cancer worldwide amongst both sexes and all age groups. In their screening, the NCI uses seven cell lines derived from patients with breast cancer.

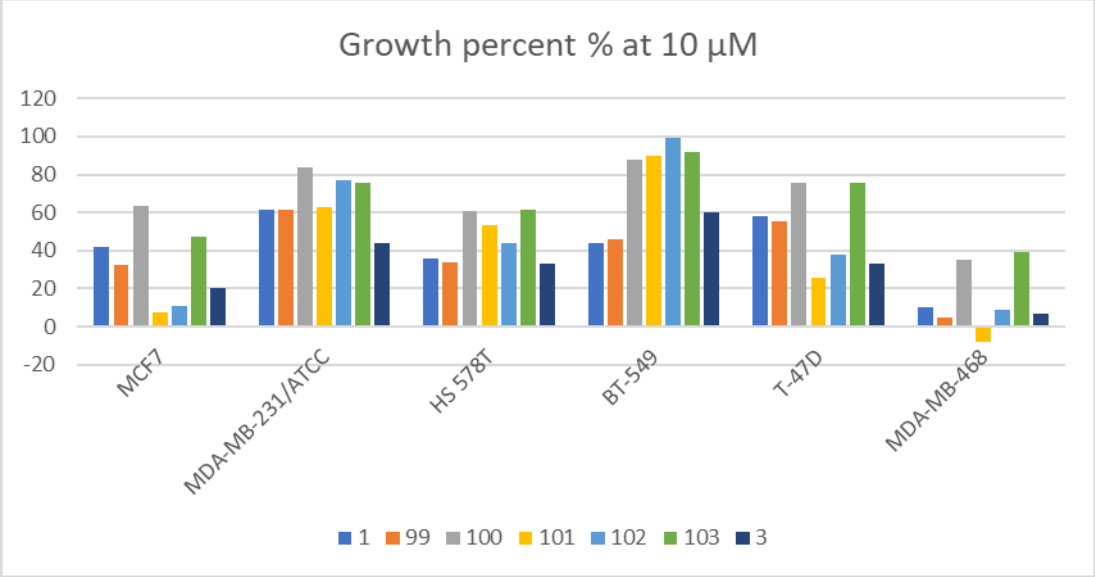

Figure 5.1.7.1. The effect of derivatives of lead compound **1** on breast cancer cell lines

Many of the compounds studied lead to increased cell growth in the breast cancer cell lines screened (Figure 5.1.7.1) compared to lead **1**, and, in fact upon treatment some of the cell lines experienced minor to no cell death. After treatment with compound **1** the highest cell growth is seen in the MDA-MB-231/ATCC and T-47D cell lines, while in the other cell lines the growth is low to moderate. With compound **3** the cell growth is even lower than with **1** in all of the cell lines, suggesting that **3** is more active in causing growth inhibition. Compound **99** does not change the growth inhibitory effect of any cell line; thus, it seems that enlarging the hydrophobic moiety does not change the activity of **1** in breast cancer cell lines. Both compounds **103** and **102** do not lead to cell growth inhibition, and compound **99** results in an increase of growth compared to lead **1** in all of the cell lines screened. Assays with **101** show a decrease in cell growth compared to **100** in some of the cell lines such as MCF-7, suggesting that the substitution of a phenyl ring by a pyridine increases the activity. We also start to see cell death in the MDA-MB-

468 cell line, which has had low percentage growth across all of the compounds screened.

5.2. Evaluation of the cytotoxic potential of compound 3

Compound **3** was found to be the most active compound from the NCI screening, as it was found to inhibit cell growth most frequently and in some cases cause cell death. Therefore, to assess its full cytotoxic potential, five doses were used (i.e. 0.01, 0.1,1, 10, 100 μM) to determine its corresponding GI_{50}, LC_{50} and TGI values (Table 5.2.1).

Table 5.2.1. Evaluation of the cytotoxicity compound **3** in different cancer cell lines.

Cell line	GI_{50} μM	LC_{50} μM	TGI μM	Cell line	GI_{50} μM	LC_{50} μM	TGI μM
	Leukemia				**Melanoma**		
CCRF-CEM	2.29	100	10.23	**LOX IMVI**	1.41	5.37	2.75
HL-60(TB)	1.32		3.47	**MALME-3M**	2.29	75.86	7.94
K-562	1.51	100	10.47	**M14**	3.24	100	19.50
MOLT-4	2.14	100	8.13	**MDA-MB-435**	1.66	8.13	3.63
RPMI-8226	1.55	100	3.98	**SK-MEL-2**	1.78	6.46	3.39
SR	1.41	100	3.80	**SK-MEL-28**	2.04	33.11	5.89
	NSCL			**SK-MEL-5**	2.51	67.61	6.92
A549/ATCC	1.91	95.50	17.38	**UACC-257**	2.88	83.18	12.88
EKVX	2.75	61.66	13.49	**UACC-62**	2.40	69.18	12.88
HOP-62	2.04	100	5.75		**Ovarian Cancer**		
HOP-92	1.15	11.48	3.47	**IGROV1**	1.07	5.89	2.51
NCI-H226	2.19	100	6.31	**OVCAR-3**	2.00	60.26	5.37
NCI-H23	1.74	10	4.17	**OVCAR-4**	2.51	69.18	9.33
NCI-H322M	1.70	8.71	3.89	**OVCAR-5**	1.91	30.20	5.75
NCI-H460	1.48	8.71	3.63	**OVCAR-8**	3.31	100	18.62
NCI-H522	2.19	74.13	5.75	**NCI/ADR-RES**	40.74	100	100
	Colon			**SK-OV-3**	2.69	61.66	10.47
COLO 205	1.41	6.61	3.09		**Renal Cancer**		
HCC-2998	1.66	6.76	3.39	**786-0**	4.79	100	24.55
HCT-116	1.74	100	4.90	**A498**	1.70	42.66	6.31
HCT-15	19.50	100	67.61	**ACHN**	13.18	64.57	29.51
HT29	1.91	38.02	5.62	**CAKI-1**	3.31	57.54	17.38
KM12	1.48	5.75	2.88	**RXF 393**	1.82	45.71	4.79
SW-620	1.95	100	4.79	**SN12C**	2.19	43.65	8.91
	CNS			**TK-10**	4.37	69.18	21.88
SF-268	1.10	5.89	2.57	**UO-31**	12.88	67.61	29.51
SF-295	2.09	46.77	7.94		**Breast Cancer**		
SF-539	1.55	5.89	3.02	**MCF7**	1.23	7.24	3.02
SNB-19	1.29	5.62	2.69	**MDA-MB-231/ATCC**	2.00	31.62	5.25
SNB-75	0.51	10.72	2.95	**HS 578T**	1.78	100	4.68
U251	1.26	6.31	2.82	**BT-549**	1.70		3.39

	Prostate Cancer			**T-47D**	2.09	100	
PC-3	1.07	6.46	2.63	**MDA-MB-468**	1.38	7.08	3.16
DU-145	2.24	19.50	5.25				

Compound **3** inhibits cell growth in the HL-60 cell line at low concentration (TGI = 3.47 μM) and performed less well than in the CCRF-CEM cell line, where the TGI = 10.23 μM. Considering that in many of the leukemia cell lines screened the TGI was found to be around 8-10 μM and the LC_{50} to be >100 μM, we can conclude that at all of the concentrations tested **3** is cytostatic rather than cytocidal.

In most of the NSCL cell lines compound **3** induced cell death (i.e. had a measurable LC_{50}) the most notable being NCI-H322M and NCI-H460 cell lines, with both of them having an LC_{50} of 8.71 μM. In these cell lines the GI_{50} values were found to be <5 μM, with the HOP-92 cell line experiencing total growth inhibition at a low concentration of 3.47 μM. The same trend is seen with the colon cancer cell lines, with LC_{50} values lower that those obtained in the leukemia cell lines. The lowest LC_{50} value obtained for **3** in the colon cancer cell lines was 5.75 μM in KM12 cells while for the HCT cell lines the LC_{50} obtained was >100 μM.

Compound **3** performs even better with the CNS cancer cell lines, being SNB-75 cancer cells the ones where **3** was most efficient (i.e. lowest GI_{50} value of all the cell lines tested). All of the calculated TGI values obtained for this group of cancer cells are <10 μM with LC_{50} values of <100 μM. In the melanoma cell lines all the GI_{50} values measured for **3** are <5 μM and the TGI values <20 μM, being the LC_{50} for LOX IMVI (5.37 μM) the lowest of all the cells screened and the corresponding GI_{50}, TGI and LC_{50} with the M14 line the highest values in all the melanoma cells.

The GI_{50} values obtained with ovarian cancer cell lines are relatively low, with the exception of the NCI/ADR-RES cell line, which is 40.74 μM being the corresponding LC_{50} and TGI values above 100 μM. The LC_{50} values calculated in all the cells are high with the exception of the IGROV1 line. Compound **3** performs in the same way with renal, prostate and breast cancer cell lines as with the ovarian cancer cell lines.

5.3. Study of the effect of lead 1 on the cell cycle of HL-60 cells

5.3.1. AlamarBlue assays

Given that **1** was the lead compound in which many biochemical and biophysical studies were based,[1,2] we studied whether this compound leads to cell death or cell cycle arrest in the HL-60 cell line. AlamarBlue assays were used to find the IC_{50} value, which was found to be 8.59 µM at 48 hours and 3.7 µM at 72 hours (Figure 5.3.1.1).

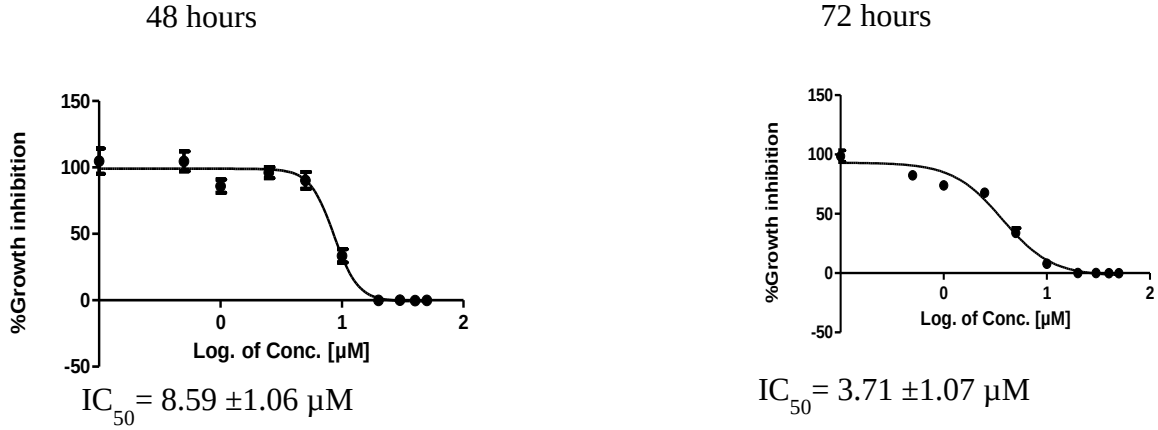

Figure 5.3.1.1. Effect of **1** on the viability of leukemia cell line HL-60. HL-60 cells were seeded at 5 x10^4 cells/well in 96 well plates. Cells were treated with vehicle [0.1% EtOH (v/v)] or a range of concentrations of 1 (1 – 20 µM). After 48/72 hours 10% AlamarBlue (v/v) was added to each well. Plates were incubated in the dark for up to 5 hours until a colour change was observed in the vehicle. Fluorescence was measured using a SpectraMax Gemini plate reader at excitation wavelength 544 nm and emission wavelength 590. Values represent the mean ± S.E.M of three independent experiments.

5.3.2. Flow cytometric analysis

Results from the AlamarBlue assays showed a decrease in cell viability following treatment of HL-60 cells with compound **1**; thus, it was necessary to determine whether the observed decrease in cellular viability was due to cell cycle arrest, cell death or a

combination of both. Flow cytometric analysis of PI stained cells was therefore employed because the cell cycle can be analysed by quantifying DNA in the cells at different time points to observe changes in a population. In a growing population of cells there are three main sub-populations with different DNA content as seen in the introduction Figure 1.8.2.1; these populations can be identified by PI staining. The population in the G_0/G_1 subgroup consists of cells which are resting/preparing for DNA replication These cells have roughly the same amount of DNA (2N, where N is the haploid chromosome number). In the second population, S phase or synthesis phase, the cells are replicating the nuclear DNA. Cells in this population have higher amount of DNA than cells in the G_0/G_1 phase, but not double. In the third population, G_2/M phase, nuclear DNA has been replicated and the cell is preparing for cell division. The DNA content is double of that of G_0/G_1 because this phase also contains cells which are undergoing cell division. Once cell division is complete the cells will have the same amount of DNA as those in the G_0/G_1 phase. The sub-G_1 population of cells shows dead cells, either by apoptosis or some other type of cell death, which have lower DNA content.

At 48 hours cell death starts being observed at 20 µM and below there is no notable difference in the sub G_0/G_1 compared to the vehicle, thus there is no increase in cell death; at higher concentrations there is a significant increase in the DNA content in the sun G_0/G_1 phase, suggesting that cells are dying at these concentrations. In the G_1 phase an increase in the number of cells is noticed at a compound concentration of 20 µM and below compared to the vehicle; this suggests that the cells might be in cell arrest. There is a decrease in DNA content in the S and G_2/M phases compared to the vehicle when using concentrations beyond 10 µM (Figure 5.3.2.2 and Table 5.3.2.1).

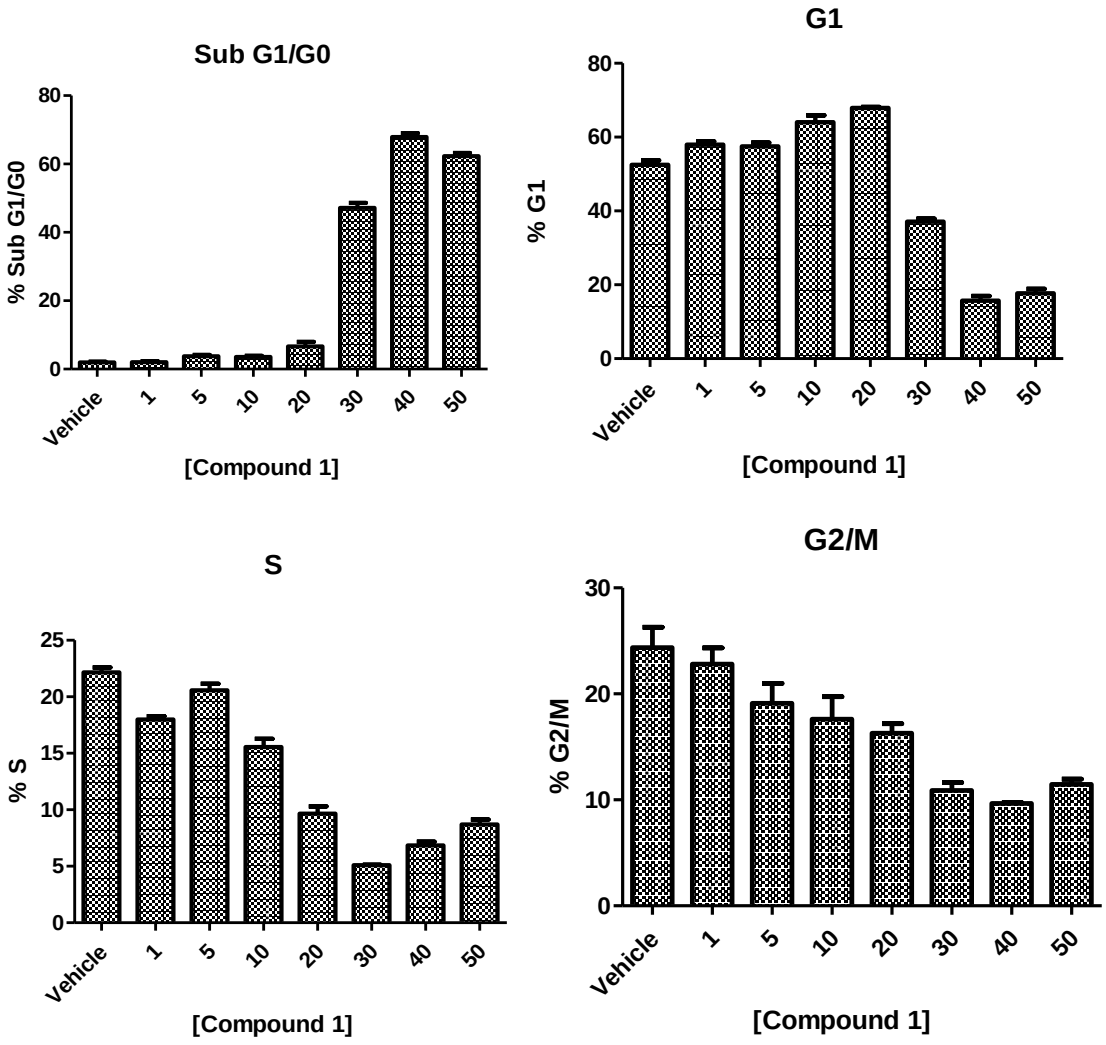

Figure 5.3.2.2. HL-60 cells were seeded at 40 x10^4 cells/mL in 12 well plates. Cells were treated with a vehicle [0.5% EtOH (v/v)] or 1, 5, 10 - 50 µM of compound **1** for 48 hours. Following the incubation time cells were harvested and fixed with 70% ethanol and stained with propidium iodide. Cells were analysed by flow cytometry using BD FACs Accuri software. 10,000 single cells were gated on control and vehicle treated cells and the percentage of cells in sub G_0/G_1 peak was determined by quantification of DNA content. Values represent the mean ± S.E.M of three independent experiments.

After 72 hours, cells in the sub G_0/G_1 phase have increased for higher concentrations (20, 30, 40 and 50 µM), but at concentrations 10 µM and below, population of cells in sub G_0/G_1 are comparable to that of the vehicle and the two previous time points. The same trend is observed in the other phases (Figure 5.3.2.3 and Table 5.3.2.1).

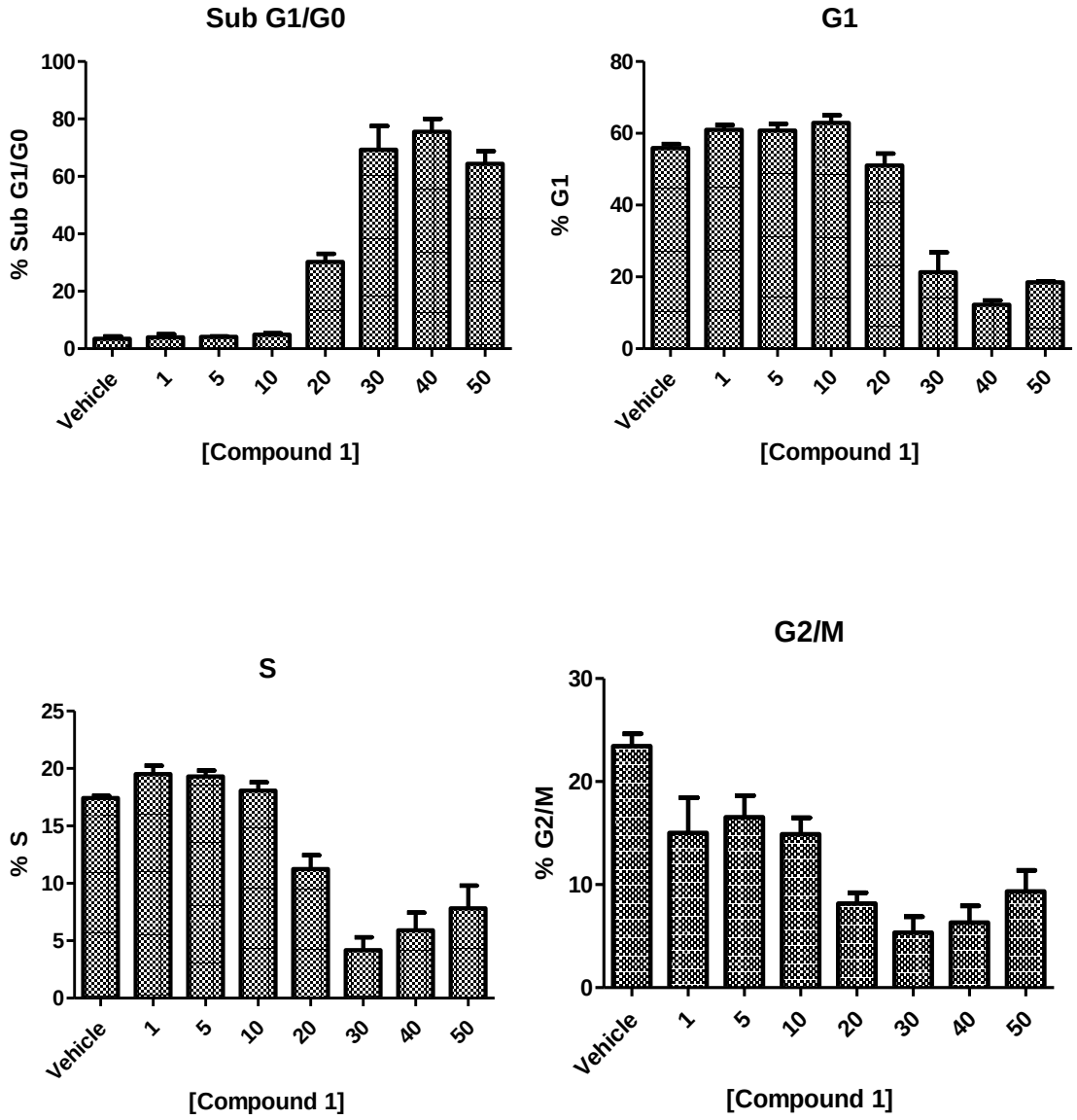

Figure 5.3.2.3. HL-60 cells were seeded at 40 x10^4 cells/mL in 12 well plates. Cells were treated with a vehicle [0.5% EtOH (v/v)] or 1, 5, 10 - 50 µM of **1** for 72 hours. Following the incubation time cells were harvested and fixed with 70% ethanol and stained with propidium iodide. Cells were analysed by flow cytometry using BD FACs Accuri software. 10,000 single cells were gated on control and vehicle treated cells and the percentage of cells in sub G_0/G_1 peak was determined by quantification of DNA content. Values represent the mean ± S.E.M of three
independent experiments.

Table 5.3.2.1. Analysis of cell cycle profile of HL-60 cells treated with **1**: percentage of cells in sub G_0/G_1, G_1, S and G_2/M peaks. Values represent the mean ±S.E.M of three independent experiments.

48 Hours	Sub G0/G1	G1	S	G2/M
Vehicle	1.96 ± 0.20	52.49 ± 1.19	22.15 ± 0.45	24.36 ± 1.93
1	2.06 ± 0.29	57.94 ± 0.88	17.98 ± 0.30	22.82 ± 1.50
5	3.78 ± 0.36	57.50 ± 0.99	20.58 ± 0.58	19.10 ± 1.88
10	3.57 ± 0.34	64.05 ± 1.87	15.55 ± 0.73	17.61 ± 2.12
20	6.66 ± 1.29	67.87 ± 0.30	9.66 ± 0.63	16.28 ± 0.92
30	47.14 ± 1.51	37.09 ± 0.82	5.10 ± 0.03	10.89 ± 0.76
40	67.91 ± 1.11	15.70 ± 1.26	6.83 ± 0.35	9.67 ± 0.09
50	62.33 ± 0.92	17.71 ± 1.19	8.70 ± 0.44	11.47 ± 0.50

72 Hours	Sub G0/G1	G1	S	G2/M
Vehicle	3.49 ± 0.78	55.91 ± 1.13	17.42 ± 0.20	23.43 ± 1.20
1	3.92 ± 1.09	60.99 ± 1.29	19.51 ± 0.74	15.00 ± 3.43
5	4.17 ± 0.14	60.79 ± 1.85	19.29 ± 0.53	16.53 ± 2.12
10	4.87 ± 0.48	62.91 ± 2.15	18.06 ± 0.73	14.88 ± 1.61
20	30.18 ± 2.85	51.04 ± 3.33	11.24 ± 1.21	8.17 ± 1.05
30	69.29 ± 8.25	21.29 ± 5.52	4.18 ± 1.12	5.33 ± 1.57
40	75.53 ± 4.47	12.21 ± 1.25	5.90 ± 1.54	6.31 ± 1.63
50	64.41 ± 4.40	18.47 ± 0.30	7.83 ± 1.98	9.34 ± 2.04

5.3.3. Study of the cell death induced by lead 1

Cell death was further analysed by flow cytometric analysis of annexin V/PI stained cells, which is a method that allows for the identification of apoptosis. Viable cells exclude both annexin V and PI (lower left quadrant, Figure 5.3.3.1), early apoptotic cells exclude PI (lower right quadrant, Figure 5.3.3.1) and late apoptotic/necrotic cells stain positive for both (upper right quadrant, Figure 5.3.3.1). For this study the HL-60 cell line was used.

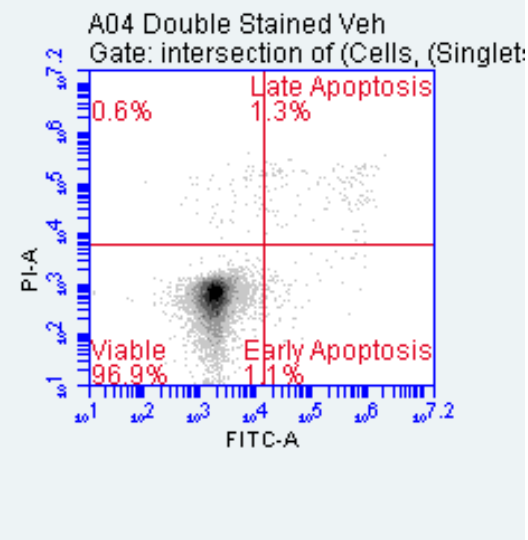

Figure 5.3.3.1. Representative images of gating strategy for annexin V-FITC and PI staining using BD Accuri flow cytometer.

After 48 hours, no cell death is noticed at lower concentrations and only at 20 µM a small amount of cell death is started to be seen which increases with higher concentrations. Again, this does not align with the AlamarBlue HL-60 results, but it does align with the outcomes of the NCI screening discussed in section 5.1.1. That data shows that based on the SRB assay with the HL-60 cell line, compound **1** causes cell growth inhibition but not cell death, suggesting that **1** might be cytostatic rather that cytocidal at these low concentrations, as we start to see cell death only at high concentrations (Figure 5.3.3.2).

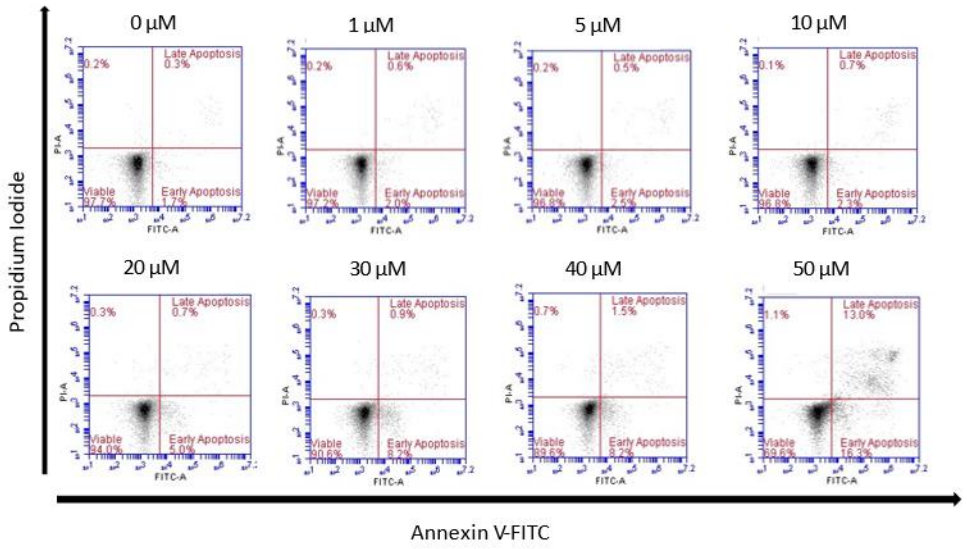

Figure 5.3.3.2. HL-60 cells were seeded at a density of 40 x10^4 cells/mL and were treated with either vehicle control [0.5% EtOH (v/v)] or various concentrations of **1** (1-50 µM) for 48 hours. After incubation cells were harvested and stained with annexin V/propidium iodide (PI) and were analysed by flow cytometry using BD FACs Accuri software. 10,000 cells were gated on vehicle treated cells.

At 72 hours again there was no notable cell death at 10 µM and lower concentrations, whereas at 20 µM and above the cells were dying at a significant rate. At 40 and 50 µM most of the cells had gone into apoptosis (Figure 5.3.3.3).

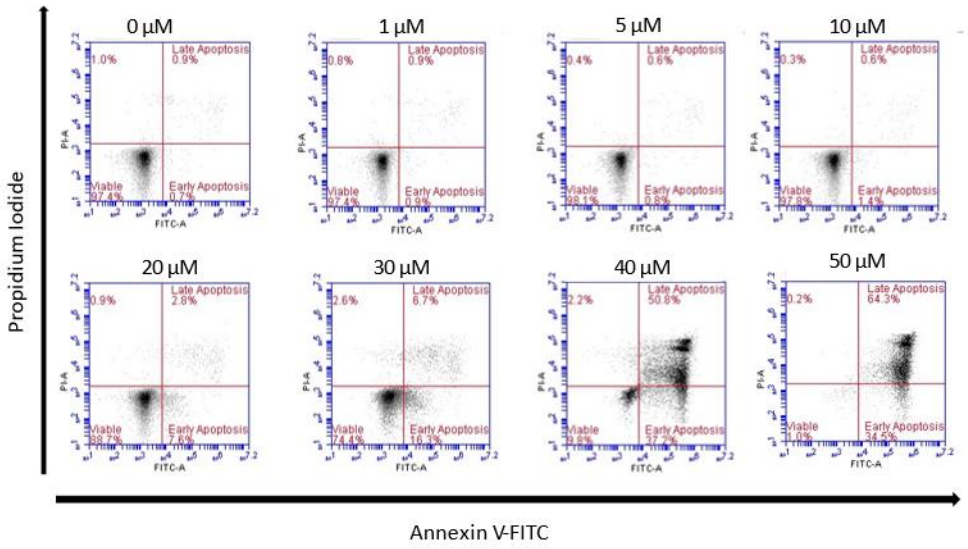

Figure 5.3.3.3. HL-60 cells were seeded at a density of 30 x10^4 cells/mL and were treated with either vehicle control [0.5% EtOH (v/v)] or various concentrations of **1** (1-50 µM) for 72 hours. After incubation cells were harvested and stained with annexin V/propidium iodide (PI) and were analysed by flow cytometry using BD FACs Accuri software. 10,000 cells were gated on vehicle treated cells.

5.3.4. Study of the initiators/effectors in the apoptosis induced by lead 1.

Apoptotic cell death is mediated through the cleavage and thus activation of initiator (e.g. caspase 8 and 9) and effector (e.g. caspase 3) caspases. A series of experiments was undertaken to determine the involvement of caspases in the observed induced apoptosis of 1. Therefore, HL-60 cells were treated with either vehicle (0.5% EtOH) or 1 (1, 5, 10, 20, 30, 40 µM) for 48 hours. Lysates were prepared and run on a 15% SDS-PAGE gel before being probed for full length pro-form caspase 3 and cleaved active fragments of caspase 3. Treatment with 1 at 30 µM resulted in an observable decrease in full length caspase 3 and the presence of the active cleaved fragments of caspase 3 (Figure 5.3.4.1).

In order to determine the involvement of the extrinsic and/or intrinsic apoptotic pathway in the cell death induced by **1**, the reduction of full-length initiator caspases 8 and 9 was also examined. As before, HL-60 cells were treated with either vehicle (0.5% EtOH) or **1** (1, 5, 10, 20, 30, 40 μM) for 48 hours. A visible decrease in the pro-form of caspase 8 was observed following treatment with **1** (Figure 5.3.4.2) suggesting that this compound induces apoptosis through this extrinsic pathway.

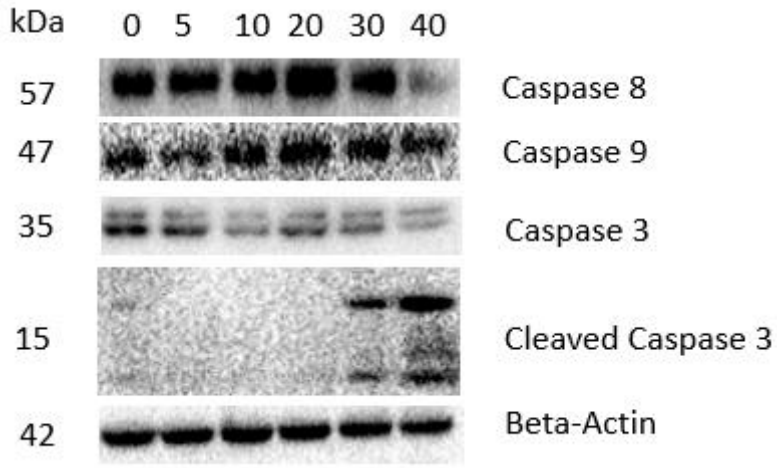

Figure 5.3.4.1. HL-60 cells were seeded at a density of 40 x10^4 cells/mL and were treated with either vehicle [0.5% EtOH (v/v)] and **1** (5 – 50 μM). After incubation for 48 hours cells were harvested, lysed and 20 μg of protein was loaded and separated on 15% SDS-page gel, transferred to PVDF membrane, and probed with the appropriate antibody. Anti-beta-actin was used as a loading control.

5.3.5. Study of the potential synergism between lead compound 1 and sorafenib in inducing cell death in HL-60 cells

Once we found that at 10 μM concentration **1** did not lead to apoptosis, we aimed to study if at 10 μM compound **1** could increase the activity of the known kinase inhibitor sorafenib (Section 1.9) synergistically. Thus, for this experiment the HL-60 cells were treated as before for control with 10 μM of **1**; then, the cells were treated with sorafenib (2.5, 5, 7.5 and 10 μM), and additionally, cells were treated with a combination of **1** at 10 μM and sorafenib at 2.5, 5, 7.5 and 10 μM for 48 and 72 hours.

At 10 µm of **1** after 48 h, there was no notable cell death, comparable to the vehicle. At 2.5 µm sorafenib did not induce notable cell death (4.5%), but in combination with **1**, cell death was increased to 19.9%. At 5 µm, sorafenib alone induced 13.1% cell death; however, when **1** was added cell death increased to 38.9%. At 7.5 µm, sorafenib alone induced 41.1% apoptosis, but when combined with **1** this increased to 74.5%. This synergistic increment was observed again at 10 µm, when apoptosis increased from 74.6% to 97.6% (Figure 5.3.5.1). At 72 hours this synergistic increase in activity was even stronger.

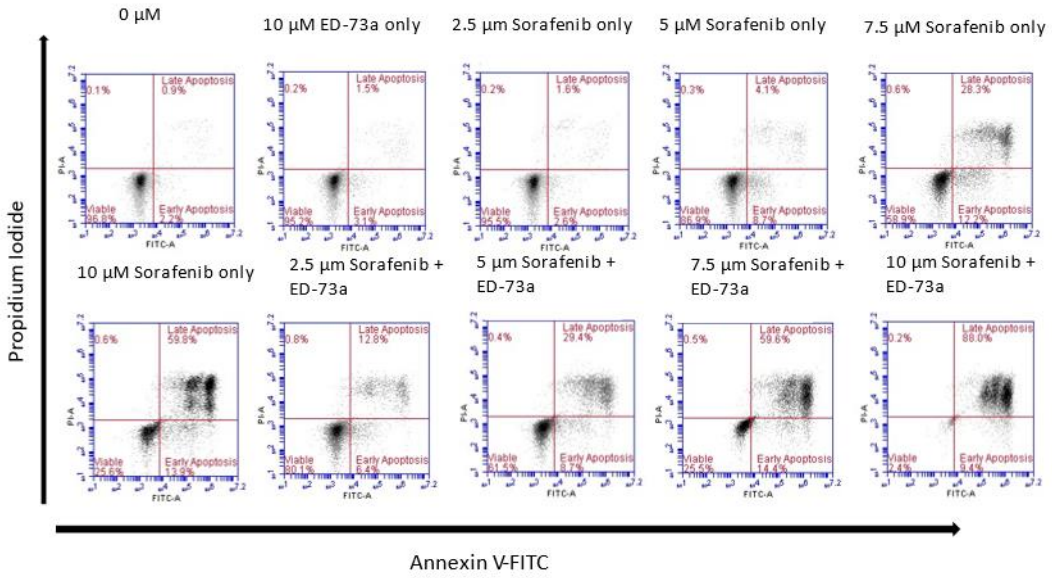

Figure 5.3.5.1. HL-60 cells were seeded at a density of 40 x10^4 cells/mL and were treated with either vehicle control [0.5% EtOH (v/v)] or **1** (10 µM), various concentrations of sorafenib (2.5-10 µM) or a combination of 1 at 10 µM and sorafenib at the mentioned concentrations for 48 hours. After incubation cells were harvested and stained with annexin V/propidium iodide (PI) and were analysed by flow cytometry using BD FACs Accuri software. 10,000 cells were gated on vehicle treated cells.

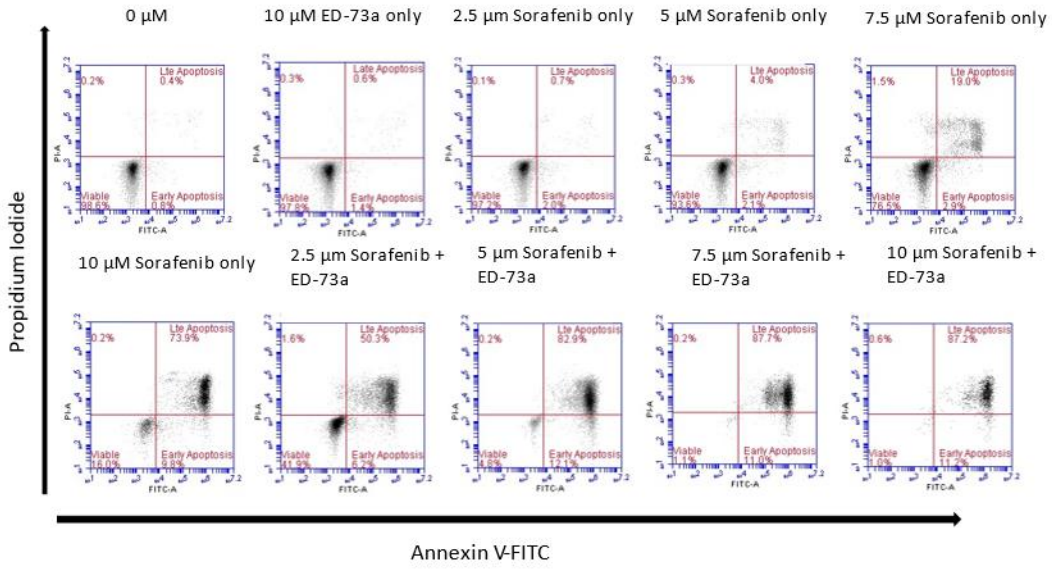

Figure 5.3.5.2. HL-60 cells were seeded at a density of 40 x10^4 cells/mL and were treated with either vehicle control [0.5% EtOH (v/v)] or **1** (10 µM), various concentrations of sorafenib (2.5-10 µM) or a combination of 1 at 10 µM and sorafenib at the mentioned concentrations for 48 hours. After incubation cells were harvested and stained with annexin V/propidium iodide (PI) and were analysed by flow cytometry using BD FACs Accuri software. 10,000 cells were gated on vehicle treated cells.

5.4. Conclusions and future perspectives

In this chapter we have described the biochemical evaluation of lead compound **1** and its derivatives which were previously synthesised as potential anti-cancer agents. This evaluation involved (i) the study of their effects on cell viability with the SRB assay at a concentration of 10 µM utilising a broad panel of cancer cell lines (carried out by the NCI) and with the AlamarBlue assay in the HL-60 leukemia cell line, (ii) deducing the mode of cell death and apoptotic pathway followed and (iii) a co-treatment with a known kinase inhibitor, Sorafenib, in HL-60 to assess potential synergic effects.

In the different cancer categories screened in the NCI panel it was found that most of the compounds did not lead to growth inhibition. It was found that the structural modifications that made the largest difference in activity were the size of the

hydrophobic moiety, as seen in **99**, and the nature of polar moiety as seen in **3**. When these changes were made, we saw decrease in cell growth compared to lead **1** and cell death in some cases. Compound **3** was selected for further screening where the LC_{50}, GI_{50} and TGI values were calculated using five doses (i.e., 0.01, 0.1,1, 10, 100 μM). In the leukemia cell lines the LC_{50} values were found to be above 100 μM, while the lowest LC_{50} value was 5.37 μM in the LOX IMVI melanoma cell line, suggesting that this compound could have a cytotoxic effect on the melanoma cell line.

Giving that **1** was the original lead compound and many biochemical and biophysical studies had been carried out with it, we studied whether this compound leads to cell death or cell cycle arrest, and thus the HL-60 cell line was used for this study. AlamarBlue assays were used to find the IC_{50} was found to be 8.59 μM at 48 hours but the activity increased dramatically, between 48 hours and 72 hours when the IC_{50} was found to be 3.7 μM.

Utilising flow cytometry it was found that at concentration of 10 μM and below HL-60 cells went into G_1 cell cycle arrest and that no cell death was observed even after 72 hours. This was further confirmed with Annexin V/PI assays, which only showed significant apoptosis after 48 hours at 30 μM. We then studied the caspase cascade at 30 μM and above by means of Western blots finding that cell death starts at 30 μM after 48 hours. From this we can postulate that this compound is cytostatic at low concentrations and cytotoxic at higher concentrations.

Finally, we studied the synergistic effect of compound **1** with a known kinase inhibitor, sorafenib. It was found that **1** at a 10 μM concentration improved the activity of sorafenib at the low concentration of 2.5 μM increasing apoptosis from 2.7% to 56.5% at 72 hours. This is a positive initial result and further studies would be able to show the full synergetic effect of compound **1**, such as looking at key pathways in the HL-60 cell line using western blothing.

By means of flow cytometry it was possible to determine that the lead compound **1** caused apoptosis in the HL-60 cell line and Western Blot experiments allowed us to identify that this apoptosis was exerted through the caspase cascade. Taking this into consideration, other proteins could be studied to ensure that apoptosis is occurring;

these include proapoptotic proteins BIM, PUMA, BAD, BID, BIK, BAX, BAK and NOXA, and antiapoptotic proteins such as Bcl-2, Bcl-XL, Bcl-W and Mcl-1. These experiments will also confirm whether extrinsic or intrinsic pathways of apoptosis are occurring.

5.5. References

(1) Diez-Cecilia, E.; Kelly, B.; Perez, C.; Zisterer, D. M.; Nevin, D. K.; Lloyd, D. G.; Rozas, I. Guanidinium-Based Derivatives: Searching for New Kinase Inhibitors. *Eur. J. Med. Chem.* **2014**, *81*, 427–441. https://doi.org/https://doi.org/10.1016/j.ejmech.2014.05.025.

(2) Diez-Cecilia, E.; Carson, R.; Kelly, B.; van Schaeybroeck, S.; Murray, J. T.; Rozas, I. Probing a 3,4'-Bis-Guanidinium Diaryl Derivative as an Allosteric Inhibitor of the Ras Pathway. *Bioorg. Med. Chem. Lett.* **2015**, *25* (19), 4287–4292. https://doi.org/https://doi.org/10.1016/j.bmcl.2015.07.082.

(3) Previtali, V.; Trujillo, C.; Boisson, J.-C.; Khartabil, H.; Henon, E.; Rozas, I. Development of the First Model of a Phosphorylated, ATP/Mg2+-Containing B-Raf Monomer by Molecular Dynamics Simulations: A Tool for Structure-Based Design. *Phys. Chem. Chem. Phys.* **2017**, *19* (46), 31177–31185. https://doi.org/10.1039/C7CP05038K.

(4) Nakayama, G. R.; Caton, M. C.; Nova, M. P.; Parandoosh, Z. Assessment of the Alamar Blue Assay for Cellular Growth and Viability in Vitro. *J. Immunol. Methods* **1997**, *204* (2), 205–208. https://doi.org/https://doi.org/10.1016/S0022-1759(97)00043-4.

(5) Skehan, P.; Storeng, R.; Scudiero, D.; Monks, A.; McMahon, J.; Vistica, D.; Warren, J. T.; Bokesch, H.; Kenney, S.; Boyd, M. R. New Colorimetric Cytotoxicity Assay for Anticancer-Drug Screening. *JNCI J. Natl. Cancer Inst.* **1990**, *82* (13), 1107–1112.

https://doi.org/10.1093/jnci/82.13.1107.

(6) Orellana, E. A.; Kasinski, A. L. Sulforhodamine B (SRB) Assay in Cell Culture to Investigate Cell Proliferation. *Bio-protocol* **2016**, *6* (21), e1984. https://doi.org/10.21769/BioProtoc.1984.

(7) SRB assay https://www.cephamls.com/srb-cytotoxicity-assay-kit-colorimetric/.

(8) NCI-60 Screening Methodology https://dtp.cancer.gov/discovery_development/nci-60/methodology.htm.

(9) Vajrabhaya, L.; Korsuwannawong, S. Cytotoxicity Evaluation of a Thai Herb Using Tetrazolium (MTT) and Sulforhodamine B (SRB) Assays. *J. Anal. Sci. Technol.* **2018**, *9* (1), 15. https://doi.org/10.1186/s40543-018-0146-0.

(10) Previtali, V.; Mihigo, H. B.; Amet, R.; McElligott, A. M.; Zisterer, D. M.; Rozas, I. Exploring the Anti-Cancer Mechanism of Novel 3,4'-Substituted Diaryl Guanidinium Derivatives. *Pharmaceuticals* . 2020. https://doi.org/10.3390/ph13120485.

(11) NSCLC https://www.cancer.org/cancer/lung-cancer/about/what-is.html.

(12) Renal cancer https://www.nhs.uk/conditions/kidney-cancer/.

Chapter 6 – Biological evaluation of derivatives of lead compound 2

Following the computational studies presented in Chapter 3, we aimed to study the effect of lead compounds **1** and **2** and their derivatives on the MAPK/ERK pathway. Using Western immunoblot analysis in the HL-60 cell line, we looked at the expression and phosphorylation of ERK, which is found downstream of Ras (i.e. the initial protein in the MAPK signalling pathway). The results of this analysis showed that the derivatives of lead compound **1** led to the downregulation of pERK as compound **1** had been previously shown to do (see Chapter 5).[1,2] However, lead compound **2** and its derivative **4**, did not lead to the downregulation of p-ERK; in fact, compound **2** was found to upregulate p-ERK in the HL-60 cell line, suggesting that these compounds have a different mechanism of action (Figure 6.1).[3]

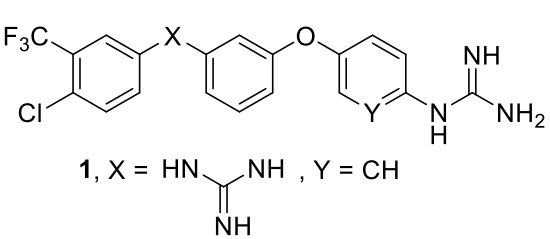

1, X = HN(C(=NH)NH) , Y = CH

2, X = NH, Y = N

4, X= NH, Y = CH

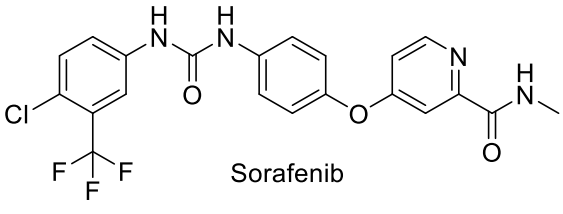

Sorafenib

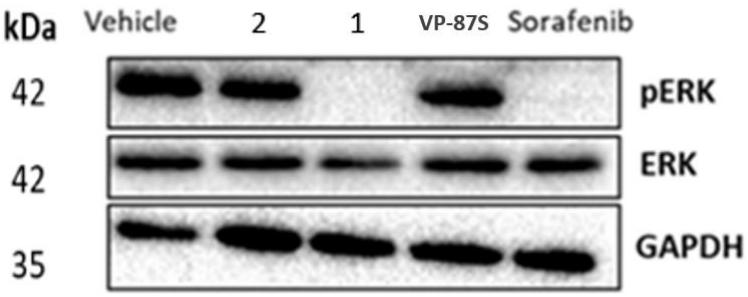

Figure 6.1. Effect of compounds **1**, **2**, **4** and sorafenib (as a control) on the level of expression of phosphorylated (activated) and total ERK. HL-60 cells were treated with either vehicle (0.1% EtOH), sorafenib (10 μM), compound **1** (10 μM), compound **2** (10 μM) or compound **4** (10 μM) for 16 hours. Cells were lysed and 20 μg protein was loaded, separated on 12% SDS-page gel and transferred to PVDF membrane. The membrane was then blocked and probed with anti-ERK and anti-pERK [1:1000] and anti-rabbit secondary antibodies. Anti-GAPDH [1:2500] was used as a loading control and probed with anti-mouse secondary.

6.1. Effect of lead compound 2 in the viability of Multiple Myeloma cell lines

Multiple myeloma (MM) is a cancer that affects white blood cells, produced in the bone marrow, with approximately 361 people being diagnosed every year in Ireland.[4] MM is currently treated with alkylating agents, which are very aggressive and unspecific chemotherapeutic agents. Therefore, more specific and effective therapies are needed.

In the Introduction we have discussed how kinases are implicated in the constitutive upregulation of many signalling pathways involved in the pathogenesis of several cancers and, in the specific case of MM, the RAS/Raf, JAK/STAT and PI3K/Akt pathways are particularly important.[5,6,7] The frequency and influence of dysregulated kinase activation in disease and cancer development has led to the design and synthesis of protein kinase inhibitors as novel therapeutic agents,[8] being this one of the most dynamic areas in modern drug discovery.[9] The Rozas group has previously designed several compounds which caused kinase inhibition in different cancer cell lines, and now, we aim to evaluate the mechanism of action of lead compound **2** and some of its derivatives specifically in the MM cell lines U266B1 and NCI-H929.

Following the Western blot analysis mentioned at the beginning of this Chapter, and within the on-going collaboration with Professor Daniela Zisterer (School of Biochemistry and Immunology, Trinity College Dublin), we studied the potential alternative mechanism of action of compound **2** in MM. These experiments were carried out by Dr. Rebecca Amet as part of her PhD. First, AlamarBlue assays were carried out on lead compounds **1** and **2** in the mentioned cell lines (drug-sensitive NCI-H929 and drug-resistant U266B1 cell lines) finding that both compounds decreased the viability of the MM cells in a dose dependent manner (Figure 6.1.1). The IC_{50} values calculated for compound **2** were of 3.3 ±0.2 μM and 3.9 ±0.4 μM and for compound **1** were 4.4 ± 0.5 μM and 17.5 ± 2.1 μM in NCI-H929 and U266B1 cells, respectively, indicating that the U266B1 cell line appears to be more resistant to compound **1** than to compound **2**. For that reason, further studies searching for MM therapies were pursued with compound **2**.

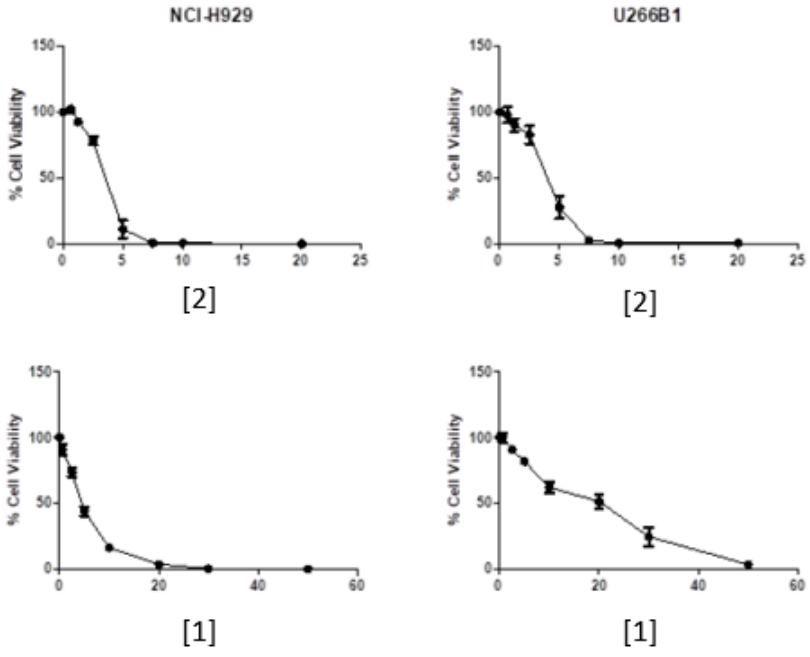

Figure 6.1.1. Multiple myeloma cell lines NCI-H929 and U266B1 were seeded at 5 x10^4 cells/well in 96 well plates. Cells were treated with a vehicle (0.5% (v/v) ethanol) or a range of concentrations of compounds **2** (0.625 – 20 μM) or **1** (0.625 – 50 μM). After 72 hours 10% Alamar blue (v/v) was added to each well. Plates were incubated in the dark for up to 5 hours until a colour change was observed in the vehicle. Fluorescence was measured using a SpectraMax Gemini plate reader at excitation wavelength 544 nm and

emission wavelength 590. Values represent the mean ±S.E.M of four independent experiments for **2** and three independent experiments for **1**.

6.2. Study of the effect of compound 2 in the cell cycle of NCI-H929 and U266B1 multiple myeloma cell lines

Results from the Alamar blue assays showed a decrease in cell viability following treatment of MM cells with lead compound **2**. Following this it was necessary to determine if the reduction in cellular viability was due to cell cycle arrest or cell death; thus, flow cytometric analysis of PI stained cells was carried out similar to the study performed with compound **1** (Chapter 5). Hence, the ability of compound **2** to induce cell cycle arrest was studied by analysing G_1, S, G_2/M, and sub G_1/G_0 sub-populations of PI stained cell population in the mentioned MM cell lines (i.e. NCI-H929 and U266B1) and the results are presented in Figure 6.2.1 and Table 6.2.1.

In the G_1, S or G_2/M sub-populations no increase in the percentage of cells was observed indicating that **2** does not induce cell cycle arrest. However, there was an increase in the percentage of cells present in the sub G_1/G_0 subpopulation indicative of cell death from as early as 8 hours even though this increment was not statistically significant until 24 hours post treatment in both cell lines. For example, in the NCI-H929 cells at the 24 hours timepoint from treatment with compound **2**, approximately 33.1% of cells were found in the sub G_1/G_0 subpopulation in comparison to vehicle treated cells where only 4.3% of them were found in that sub-population. Following compound **2** treatment, the percentage of cells in the sub G_1/G_0 sub-population increased with time reaching a maximum of 58.3% in NCI-H929 cells and 53.4% in U266B1 cells at 72 hours. The increase in the percentage of cells present in the sub G_1/G_0 sub-population was concomitant with a statistically significant decrease in cells presence in the G_1 and G_2/M subpopulations, most notably in G_1.

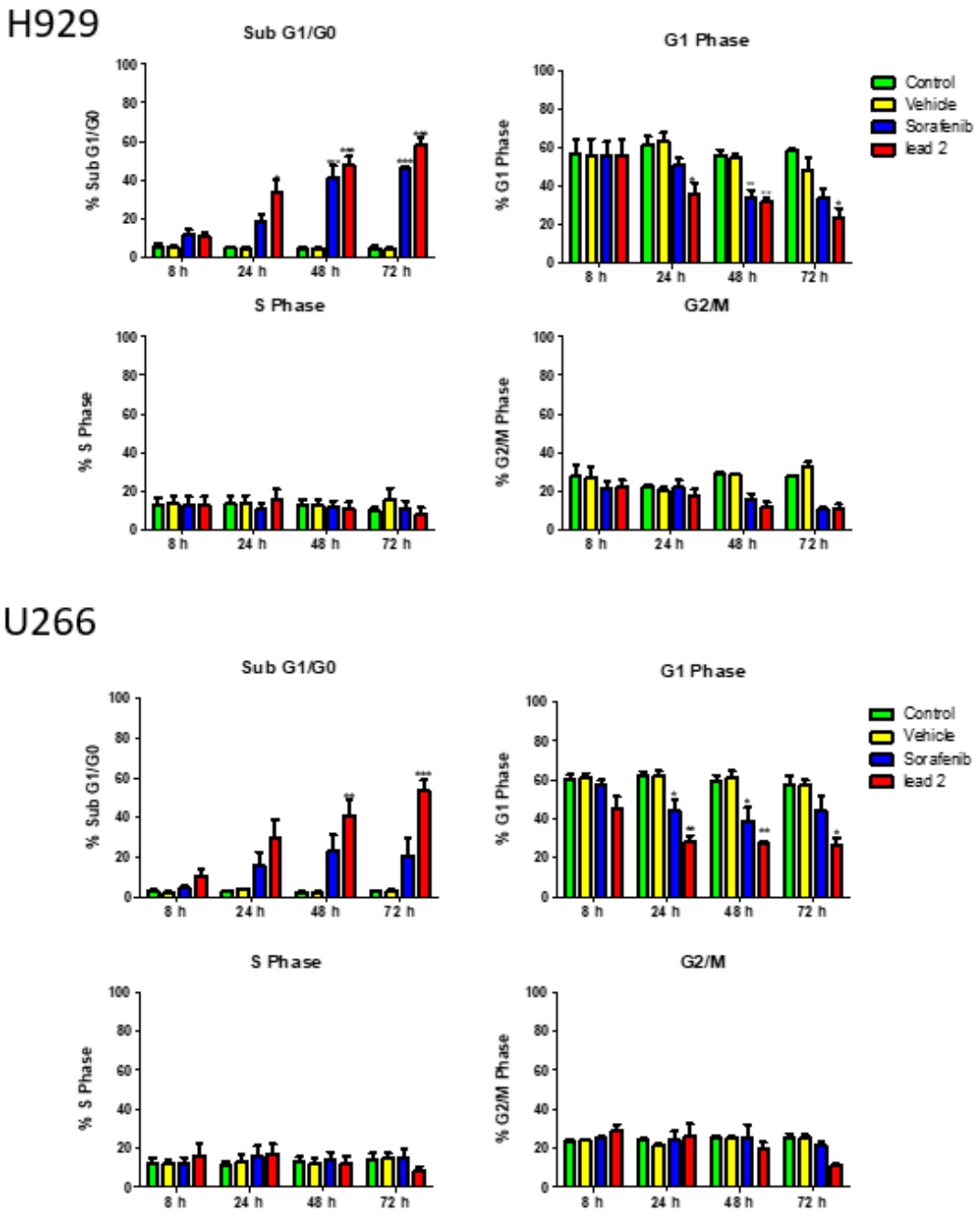

Figure 6.2.1. H929 and U266B1 cells were seeded at 30 x10^4 cells/mL in 12 well plates. Cells were treated with a vehicle (0.5% (v/v) ethanol), 10 µM sorafenib or 10 µM compound **2** for 8, 24, 48 and 72 hours. Following the appropriate incubation time cells were harvested and fixed with 70% ethanol and stained with propidium iodide. Cells were analyzed by flow cytometry using BD FACs Accuri software. 10,000 single cells were gated on control and vehicle treated cells and the percentage of cells in sub G_1/G_0 subpopulation was determined by quantification of DNA content. Values represent the mean ±S.E.M of three independent experiments.

Table 6.2.1. Effect of **2** and sorafenib on the cell population of the cell cycle subpopulations for NCI-H929 and U266B1 MM cell lines.

	NCI-H929				U266B1			
8 hours								
	Sub G_1/G_0	**G_1**	**S**	**G_2/M**	**Sub G_1/G_0**	**G_1**	**S**	**G_2/M**
Control	5.0 ± 1.8	56.3 ±7.5	12.8 ± 4	27.5 ± 5.8	2.8 ± 0.6	60.2 ±2.3	12.5 ±2.6	23.6 ± 0.6
Vehicle	4.8 ± 0.8	55.3 ±9.1	13.5 ±4.4	27 ± 5.4	2.4 ± 0.3	60.9 ±2.3	12 ± 1.9	24 ± 0.4
Sorafenib	11.8 ± 2.5	55.5 ±7.4	4.3 ± 4.6	20.9 ± 3.9	4.5 ± 0.7	57.6 ±2.2	12.3 ± 3	25.3 ± 0.8
2	10.5 ± 2.3	55.8 ±8.3	3.9 ± 4.7	22.2 ± 3.4	10.5 ± 3.8	44.9 ±6.5	16.2 ± 6	29.1 ± 2.9
24 hours								
	Sub G_1/G_0	**G_1**	**S**	**G_2/M**	**Sub G_1/G_0**	**G_1**	**S**	**G_2/M**
Control	4.7 ± 0.9	60.9 ±4.8	13.3 ±4.2	21.9 ± 1.5	2.6 ± 0.4	62.1 ±2.1	11.2 ±1.8	24 ± 0.8
Vehicle	4.3 ± 1.1	63 ± 4.7	13.3 ±4.6	20.2 ± 1.8	4 ± 0.1	61.7 ±2.7	13.1 ±3.6	21.3 ± 1.3
Sorafenib	18.1 ± 4	51 ± 3.4	10.4 ±3.1	21.8 ± 3.8	15.9 ± 6.8	44.2 ±5.8	15.8 ±5.4	24.3 ± 4.1
2	33.1 ± 7	35.4 ± 6	15.7 ±5.3	17.5 ± 3.7	29.2 ± 9.4	27.8 ±3.5	17.3 ± 5	26.2 ± 6
48 hours								
	Sub G_1/G_0	**G_1**	**S**	**G_2/M**	**Sub G_1/G_0**	**G_1**	**S**	**G_2/M**
Control	4.1 ± 1.3	55.7 ± 3	12.6 ±2.9	28.4 ± 1.7	2.2 ± 0.4	59.1 ±3.1	13.1 ±2.3	25.4 ± 1.2
Vehicle	4.6 ± 1	54.9 ±1.6	12.9 ±2.9	28.4 ± 0.8	2.2 ± 0.6	60.5 ±3.8	12.2 ±2.7	24.9 ± 1.5
Sorafenib	41 ± 6.5	33.5 ±4.5	12 ± 2.9	15.5 ± 3.2	22.9 ± 8.2	38.9 ±6.9	14 ± 4.2	25.1 ± 7
2	48 ± 4.25	31.8 ±2.1	10.9 ±3.4	11.8 ± 2.5	41.2 ± 7.8	27.4 ±1.1	12.5 ±3.4	19.4 ± 3.6
72 hours								
	Sub G_1/G_0	**G_1**	**S**	**G_2/M**	**Sub G_1/G_0**	**G_1**	**S**	**G_2/M**
Control	4.5 ± 1.2	58.7 ±0.8	9.7 ± 1.9	27.7 ± 0.5	2.7 ± 0.6	57.7 ±4.4	14.3 ±3.1	25.5 ± 2
Vehicle	4.4 ± 0.6	47.7 ± 7	15.7 ±5.9	32.9 ± 2	3 ± 0.6	56.8 ±3.2	14.8 ±2.6	25.6 ± 1.1
Sorafenib	46 ± 1.1	33.6 ±4.9	11 ± 4.1	10.5 ± 1.5	20.7 ± 8.4	43.8 ± 8	14.5 ±4.2	21 ± 2.5
2	58.3 ±	23.7	8 ± 3.4	10.6 ±	53.4 ±	26.2	8.6 ±	10.9 ±

	3.3	±4.8		2.6	5.4	±3.8	1.8	0.9

Cell death was further analysed by flow cytometry of annexin V/PI stained cells. As explained before, this technique allows identifying whether cells are undergoing apoptosis or necrosis, viable cells exclude both annexin V and PI (lower left quadrant of a four quadrants diagram), early apoptotic cells exclude PI (lower right quadrant) and late apoptotic/necrotic cells stain positive for both (upper right quadrant).

An observable increase in early and late apoptosis was detected in both MM cell lines (Figures 6.2.2A and 6.2.3A), from 5 µM concentrations of compound **2**; however, cell death was not significant until 7.5 µM, when the cells started to go into early and late apoptosis. When NCI-H929 cells were treated with a range of concentrations from 1.25 to 10 µM of compound **2**, they underwent apoptosis in a dose-dependent manner with significant apoptosis observed at the two highest concentrations tested. A concentration of 7.5 µM resulted in over 50% of NCI-H929 cells undergoing apoptosis while at 10 µM over 80% of cells had succumbed (Figure 6.2.2).

Similarly, compound **2** induced apoptotic cell death in the U266B1 cell line in a dose-dependent manner (Figure 6.2.3). Again, significant apoptosis was observed at 7.5 µM and 10 µM concentrations of compound **2** with 36.8% and 49.8% apoptosis induced, respectively. The overall percentage of cells undergoing apoptosis was somewhat reduced when compared to the results obtained for the NCI-H929 cell line.

In general, more apoptosis was detected by using the annexin V/PI staining than using PI staining alone. This may be due to the PI staining only detecting late apoptotic or necrotic cells, whilst annexin V/PI staining detects early phosphatidylserine exposure and is considered to be more sensitive.

(A)

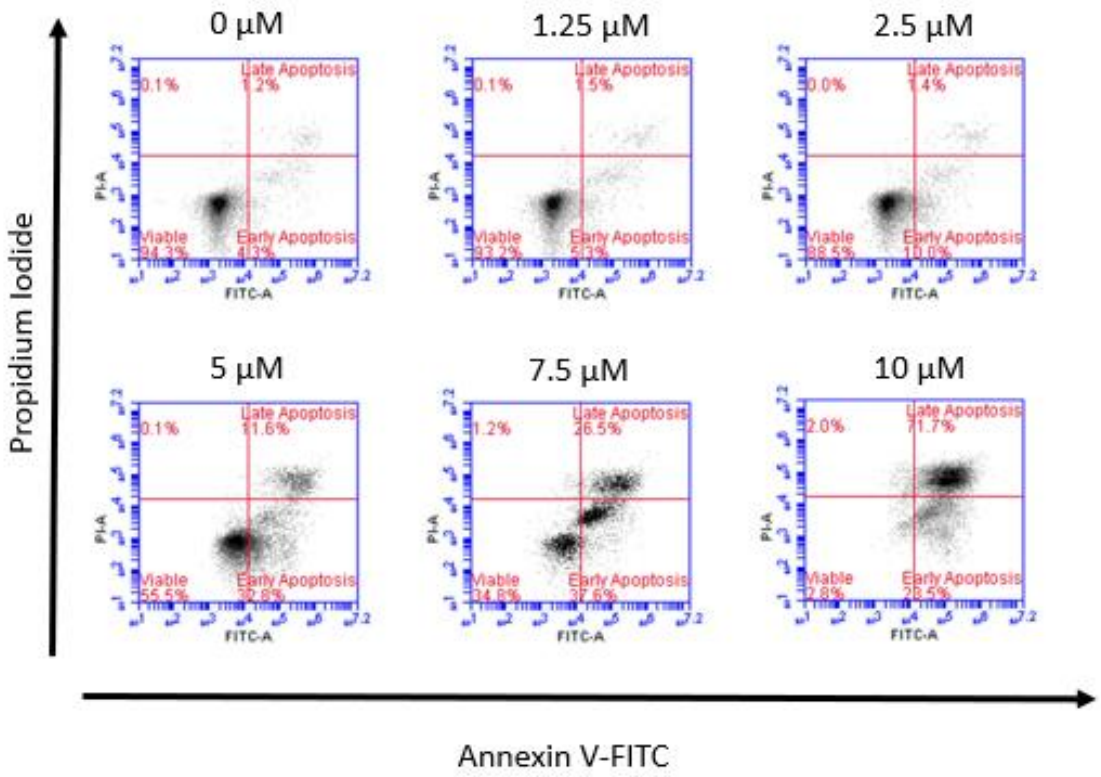

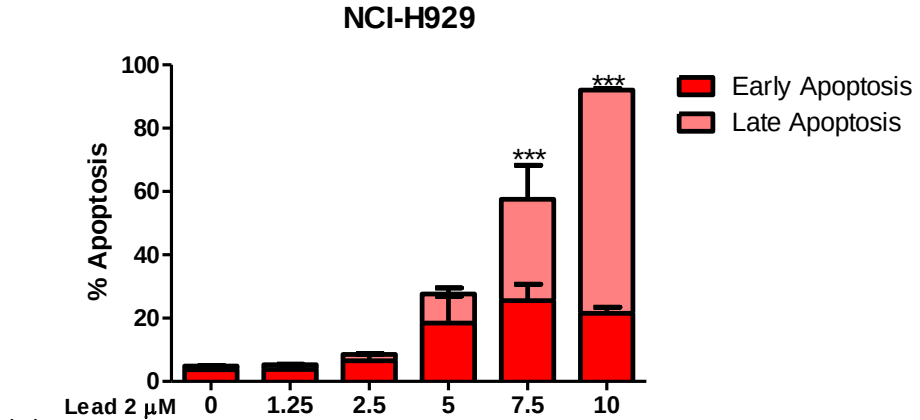

(B)

Figure 6.2.2. NCI-H929 cells were seeded at a density of 30 x10^4 cells/mL and were treated with either vehicle control (0.5% EtOH (v/v)) or various concentrations of **2** (1.25-10 µM) for 24 hours. After incubation cells were harvested and stained with Annexin V/Propidium Iodide (PI) and were analysed by flow cytometry using BD FACs Accuri software. 10,000 cells were gated on vehicle treated cells. (A) Representative dot plot of treated samples. (B) Values represent the mean ± S.E.M. of three independent experiments. Statistical analysis was performed using one-way ANOVA with Dunnett's multiple comparisons test comparing vehicle to treatments. *** $p < 0.001$.

(A)

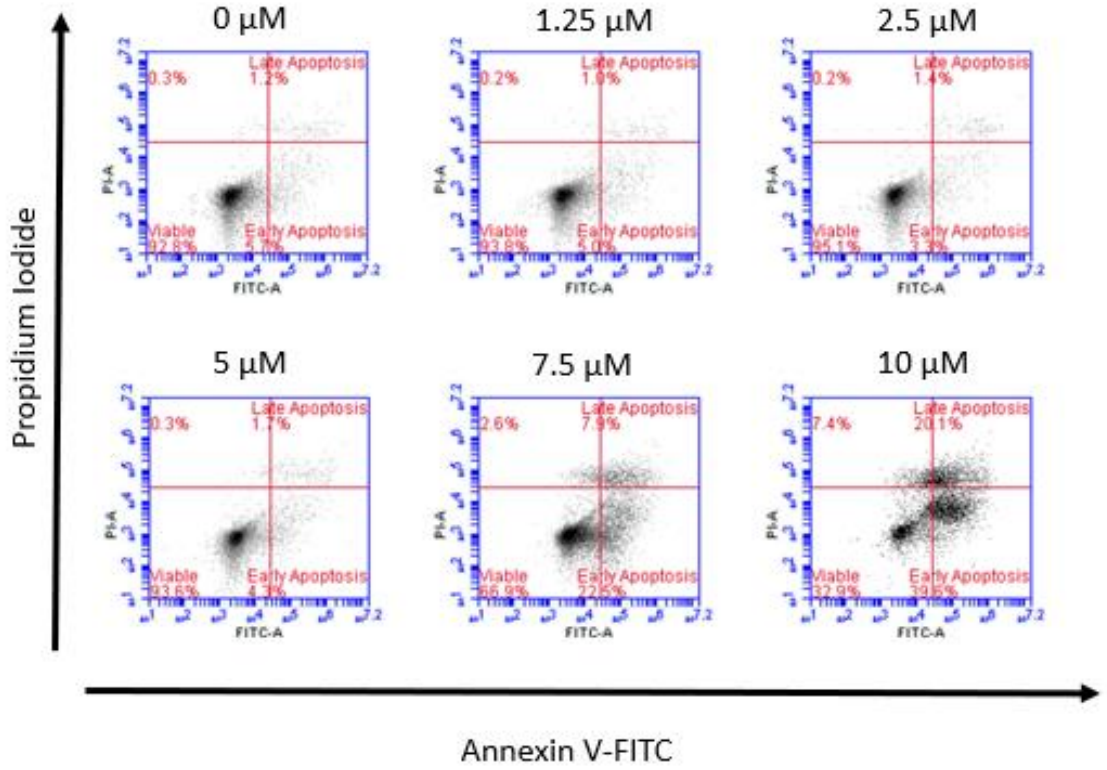

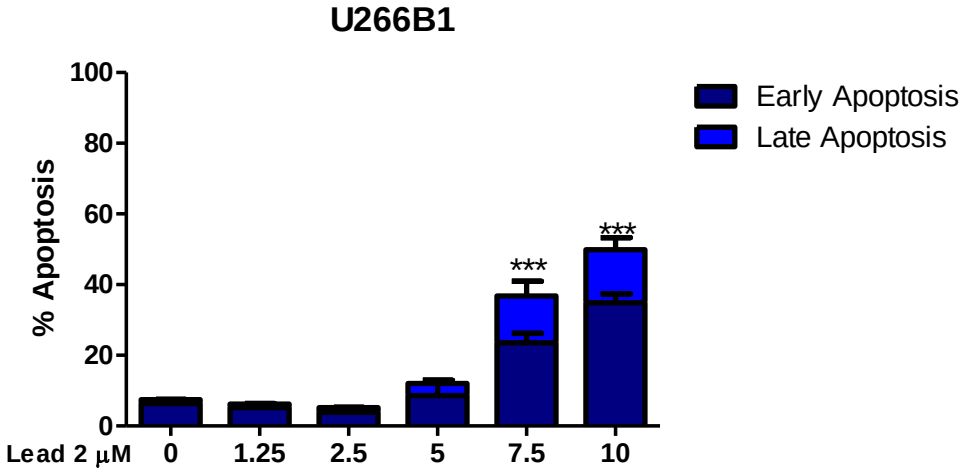

(B)

Figure 6.2.3. U266B1 cells were seeded at a density of 30 x10^4 cells/mL and were treated with either vehicle control (0.5% EtOH (v/v)) or various concentrations of lead **2** (1.25-10 µM) for 24 hours. After incubation cells were harvested and stained with Annexin V/Propidium Iodide (PI) and were analyzed by flow cytometry using BD FACs Accuri software. 10,000 cells were gated on vehicle treated cells. (A) Representative dot

plot of treated samples. (B) Values represent the mean ± S.E.M. of three independent experiments. Statistical analysis was performed using one-way ANOVA with Dunnett's multiple comparisons test comparing vehicle to treatments.*** p< 0.001.

6.3. Study of the mediators in the apoptosis induced by lead compound 2 in multiple myeloma cell lines

As discussed in the Introduction, apoptotic cell death is mediated through the cleavage and activation of initiator (e.g. caspase 8 and 9) and effector (e.g. caspase 3) caspases. Accordingly, and considering the apoptosis induced by compound **2**, a series of experiments were undertaken to determine which caspases were involved in the apoptotic process. Thus, using Western blots it was possible to observe that treatment of NCI-H929 cells with compound **2** resulted in an observable decrease in full length caspase 3 at 10 µM and the presence of the active cleaved fragments of caspase 3 at 10 µM (Figure 6.3.1). Similar results were observed in the U266B1 cell line with an noticeable increase in cleaved caspase 3 at 5 and 10 µM (Figure 6.3.2).

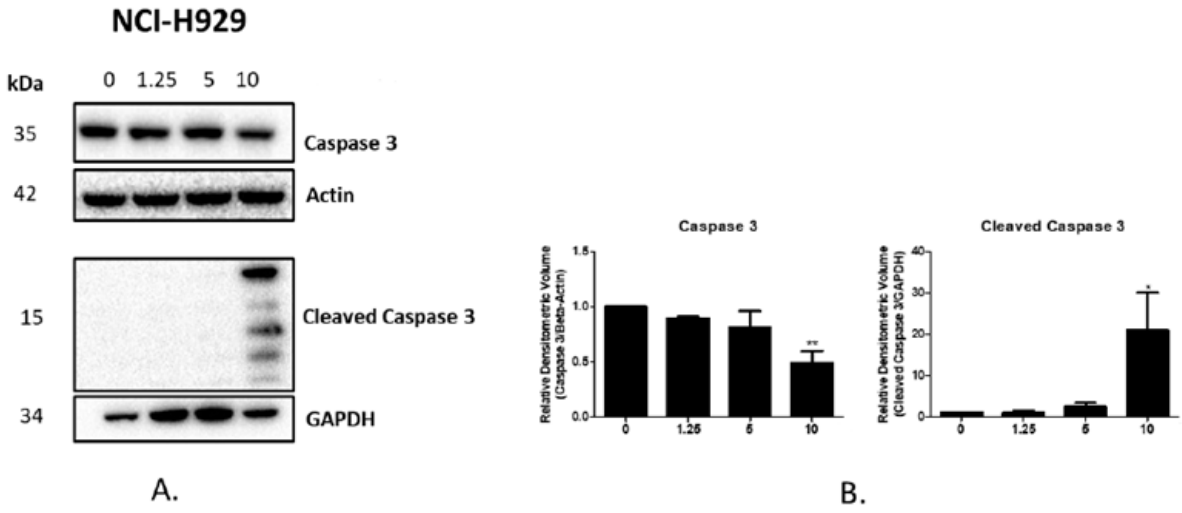

Figure 6.3.1. NCI-H929 cells were seeded at a density of 30 x10^4 cells/mL. Cells were treated with either vehicle [0.5% EtOH (v/v)] or Lead 2 (1.25, 5 and 10 µM) for 16 hours. (A). Cells were lysed and 20 µg of protein was loaded and separated on 15% SDS-page gels, transferred to PVDF membrane and probed with the appropriate antibody. Anti-GAPDH and anti-beta-actin were used as loading controls. Results are representative of 3 independent experiments. Western blots were normalised to GAPDH or beta-actin as a loading control. (B). Densitometric analysis of bands was carried out using image lab

software. Statistical analysis was performed using one-way ANOVA with Dunnett's post hoc test. *p<0.05, **p<0.01.

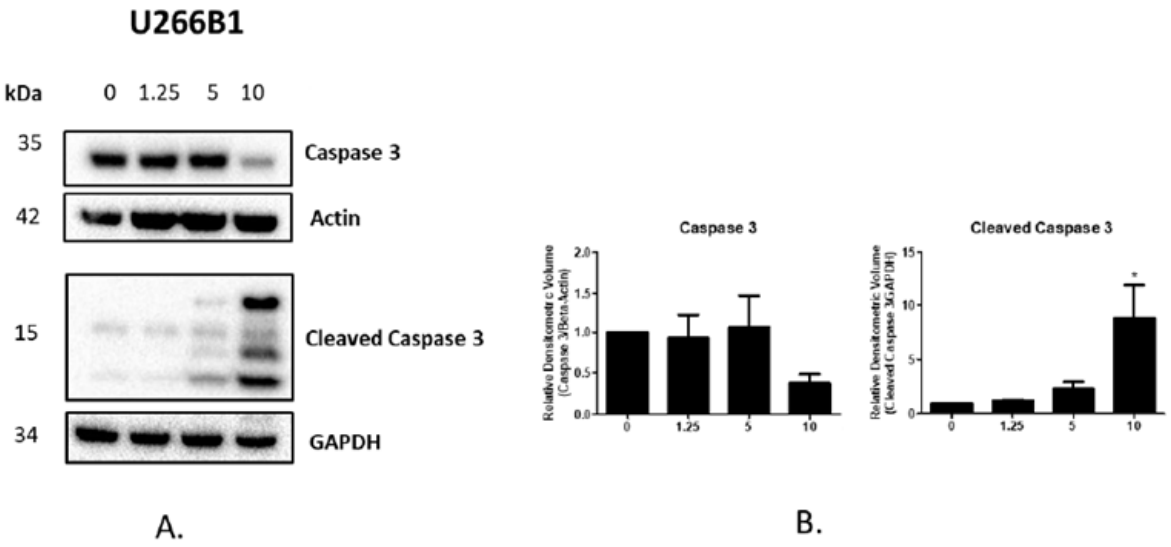

Figure 6.3.2. U266B1 cells were seeded at a density of 30 x10^4 cells/mL. Cells were treated with either vehicle [0.5% EtOH (v/v)] or Lead 2 (1.25, 5 and 10 µM) for 16 hours. (A). Cells were lysed and 20 µg of protein was loaded and separated on 15% SDS-page gels, transferred to PVDF membrane and probed with the appropriate antibody. Anti-GAPDH and anti-beta-actin were used as loading controls. Results are representative of 3 independent experiments. Western blots were normalised to GAPDH or beta-actin as a loading control. (B). Densitometric analysis of bands was carried out using image lab software. Statistical analysis was performed using one-way ANOVA with Dunnett's post hoc test. *p<0.05.

In order to determine the involvement of the extrinsic and/or intrinsic apoptotic pathway in the cell death induced by lead compound **2**, the reduction of full-length initiator caspases 8 and 9, respectively was also examined. A visible decrease of both pro-caspase 8 and 9 was observed in both MM cell lines following treatment with 10 µM of compound **2** (Figure 6.3.3). This would suggest that **2** induces apoptosis through both the intrinsic and extrinsic pathways.

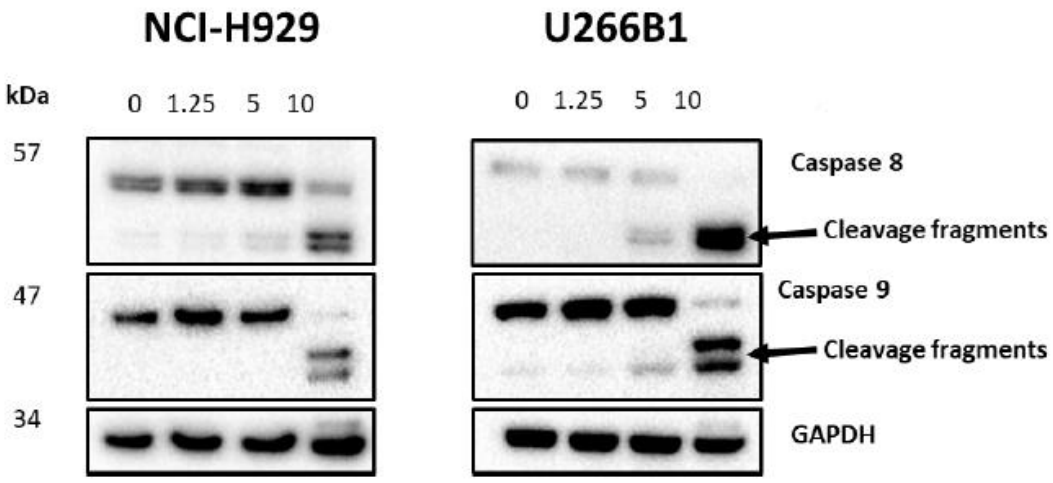

Figure 6.3.3. Compound **2** induces caspase 8 and 9 cleavage in NCI-H929 and U266B1 cells.

6.4. Study of the effect of compound 2 in the PI3K/Akt signalling pathway with multiple myeloma cell lines

In the previous section, lead compound **2** was shown to induce apoptosis in the MM cell lines U266B1 and NCI-H929. Given these promising results, the effects of compound **2** on oncogenic signalling pathways known to play a role in the pathogenesis and survival of MM cells were examined.[10] One of this pathways is the PI3K/Akt signalling pathway which is relevant in MM because this has been shown to multiple genes mutated in MM,[11,6] this pathway is also activated IL-6, which when deregulated, it has been shown to activate signalling pathways leading to survival, migration and proliferation.[12, 13]

Thus, NCI-H929 and U266B1 cells were treated with 10 µM of lead compound **2** for 30 minutes, 2, 4 or 8 hours. Cells were then collected, lysed, and ran on 12% SDS-PAGE gel before being transferred to PVDF membrane and probed for total Akt and phosphorylated-Akt (at Ser473). Anti-GAPDH was used as a loading control and the results are shown in Figure 6.4.1.

Compound **2** was shown to transiently increase the phosphorylation of Akt on Ser473 in both NCI-H929 and U266B1 cells. An initial increase was observed at 30 minutes with phosphorylation returning to basal levels at around 8 hours in the NCI-H929 cells and at the earlier timepoint of 2 hours in the U266B1 cells. No significant decrease in total or phosphorylated Akt was observed in the NCI-H929 cells at any of the time points examined.

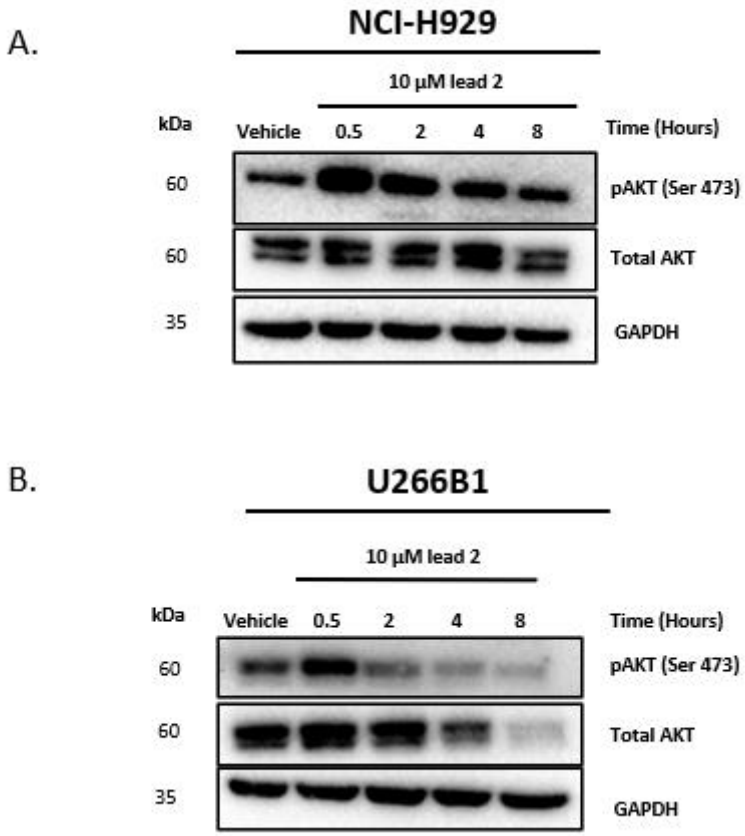

Figure 6.4.1. U266B1 and NCI-H929 cells were seeded at a density of 30 x10^4 cells/mL. Cells were also treated with either vehicle [0.5% EtOH (v/v)] or 10 µM 2 for 30 minutes, 2, 4 or 8 hours. Cells were lysed and equal amounts of protein were loaded and separated on 12% SDS -page gels, transferred to PVDF membrane and probed with the appropriate antibody. Anti-GAPDH was used as a loading control. Results are representative of 3 independent experiments. Western blots were normalised to total GAPDH as a loading control.

6.5. Study of the effect of compound 2 on the JAK/STAT pathway in multiple myeloma cell lines

The JAK/STAT signalling pathway has been found to be involved in oncogenesis and constitutive activation of STAT3, which has been associated with tumorigenesis in various types of human cancers including MM. The U266B1 cell line has a mutation leading to the constitutive activation, and therefore, phosphorylation of STAT3 on the residues Tyr705 and Ser727 via an IL-6 dependent autocrine loop.[5] Phosphorylation of STAT3 on Tyr705 is the first cited event for its activation and has been convincingly demonstrated to correlate with STAT3 DNA binding and transcriptional activity.[14] Therefore, the effect of compound **2** on STAT3 signalling was initially studied in the U266B1 cell line by western blot analysis to look at the levels of phosphorylated STAT3 prior to and post treatment with lead compound **2**. Thus, U266B1 cells were treated with 10 µM of compound **2** for 30 minutes, 2, 4 or 8 hours. Cells were then collected, lysates were prepared, and proteins were separated out on a 12% SDS-PAGE gel. Gels were probed with anti-phospho-STAT3 (Tyr705), anti-phospho-STAT3 (Ser727) and anti-total STAT3 antibodies. Anti-GAPDH was used as a loading control. Lead compound **2** was found to inhibit STAT3 phosphorylation on Tyr705 in a time-dependent manner (Figure 6.5.1). A decrease in STAT3 phosphorylated on Tyr705 was observed from 30 minutes and this band was no longer visible after 2 hours.

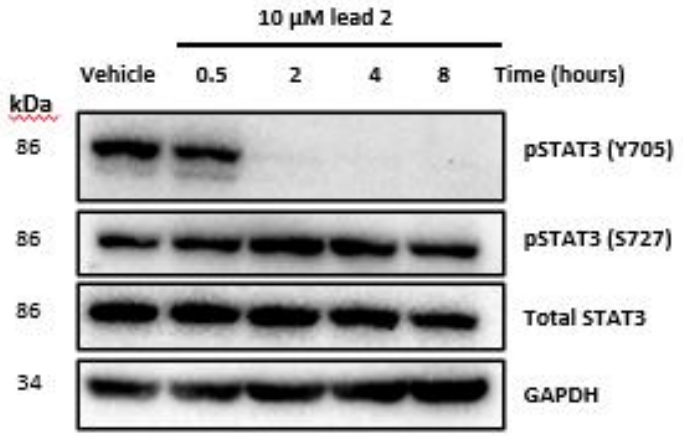

Figure 6.5.1. Compound **2** inhibits constitutively active STAT3 signaling in U266B1 cells.

The effect of lead **2** on STAT3 phosphorylation in the NCI-H929 cell line was next examined. This cell line does not possess constitutively active phosphorylation on Tyr705; however, it is phosphorylated on Ser727. Similar to the U266B1 cell line, lead compound **2** showed no visible effects on the expression levels of Ser727 phosphorylated or total STAT3 (Figure 6.5.2).

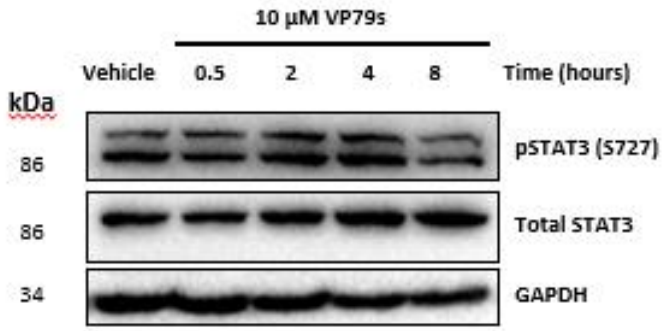

Figure 6.5.2. Lead compound **2** has no effect on phospho-STAT3 (Ser727) in NCI-H929 cells.

Given that the tumour microenvironment protects myeloma cells against the cytotoxic effects of drugs, the ability of lead **2** to overcome this resistance was next examined. As previously discussed, MM cells rely heavily on pro-survival factors from the bone marrow microenvironment (BMM) in order to facilitate their survival and proliferation. One key survival factor which is known to play a role in MM cell survival through the activation of the JAK/STAT pathway, in particular JAK2/STAT3, is IL-6.[15] As aforementioned, the NCI-H929 cell line does not possess constitutively active phosphorylation on Tyr705. Therefore, in order to induce STAT3 phosphorylation on Tyr705 the NCI-H929 cells were pre-treated with 1 ng/mL of human recombinant IL-6 for 30 minutes prior to treatment with lead compound **2** for 30 minutes, 4 or 16 hours. Cells were collected and prepared for western blotting for the indicated timepoints. Additionally, cells were collected at 16 hours for flow cytometric analysis of cell death with annexin V/PI staining.

Western blot analysis illustrated that lead **2** was capable of inhibiting IL-6-induced STAT3 phosphorylation from as early as 4 hours and sustained this inhibition until 16 hours (Figure 6.5.3). Moreover, flow cytometric analysis by annexin V/PI staining of IL-6 treated cells and lead **2** alone treated cells demonstrated that lead **2** could induce significant apoptotic cell death even in the presence of the cell survival cytokine IL-6 (Figure 6.5.4). Of note, IL-6 did appear to elicit some survival advantage to the NCI-H929 cells demonstrating the importance of the activation of this pathway has on MM cell survival; however, the difference between the apoptotic NCI -H929 cell treated with IL-6 was not significant compared to that of U266B1.

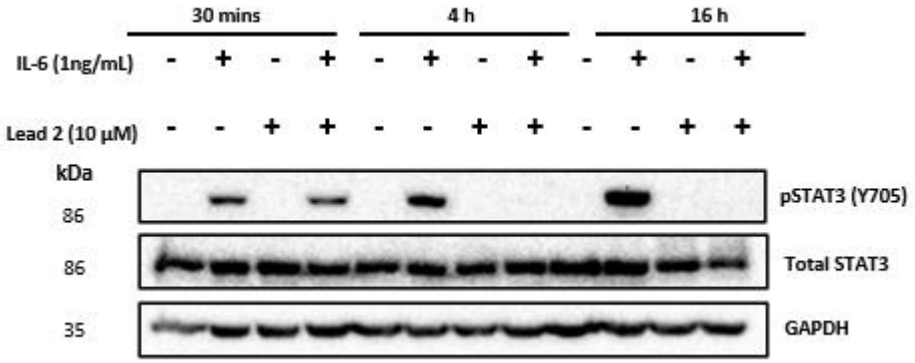

Figure 6.5.3. Lead **2** can inhibit IL-6 induced STAT3 signaling and induce cell death in NCI-H929 cells.

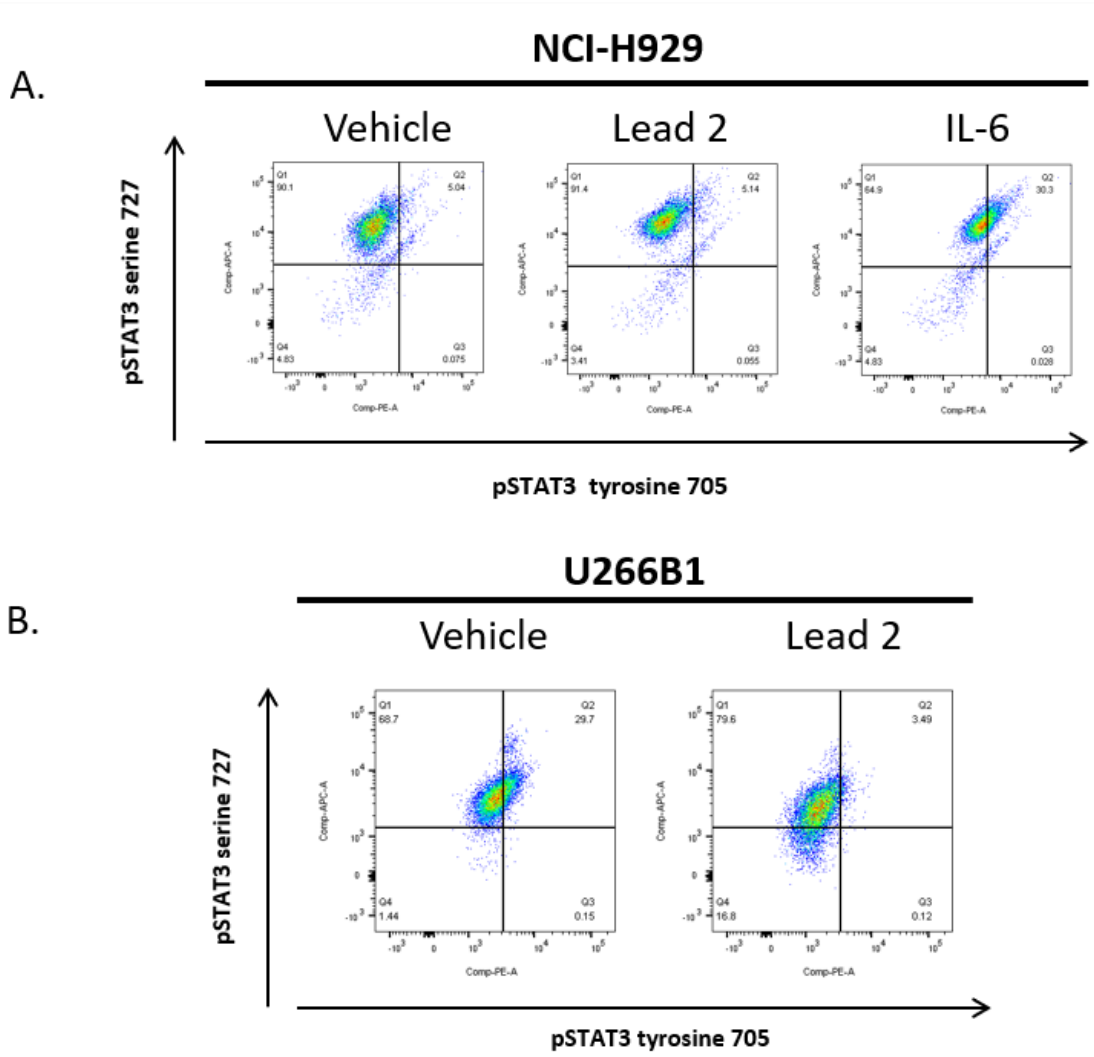

Figure 6.5.4. Lead **2** inhibits STAT3 Tyr705 phosphorylation both in NCI-H929 and U266B1 cell lines as evidenced by flow cytometry.

Aberrant STAT3 activation in cancer is not fully understood. However, in most instances, hyperphosphorylation of STAT3 is mediated by unchecked intrinsic tyrosine kinase activity of kinases, such as JAK and SRC rather than a mutation in STAT3 itself.[16,17] As such, intense efforts focusing on the inhibition of kinases that drive STAT3 phosphorylation are underway. In particular, SRC, a tyrosine kinase that has been demonstrated to lie upstream of STAT3,[18] plays key roles in cell growth, division, migration, and survival signalling pathways. Consequently, the ability of compound **2** to inhibit SRC phosphorylation was examined in NCI-H929 and U266B1 cells which were treated with 10 µM lead **2** for 30 minutes, 2, 4 or 8 hours. Next, cells were collected, lysates were prepared, and proteins were separated out on a 12% SDS-PAGE gel. Gels

were probed with anti-total SRC and anti-phospho-SRC (Tyr418) and anti-GAPDH was used as a loading control.

No visible differences were observed in SRC phosphorylated on Tyr418 at any timepoint examined in both the U266B1 and NCI-H929 cell line (Figure 6.5.5). Interestingly, on the total SRC blot, a band approximately 65-70 kDa in size was visible at 4 and 8 hours post treatment with **2** in both the NCI-H929 and U266B1 cell lines, which may be a modified form of SRC such as phosphorylated or ubiquitinated SRC (Figure 6.5.5).

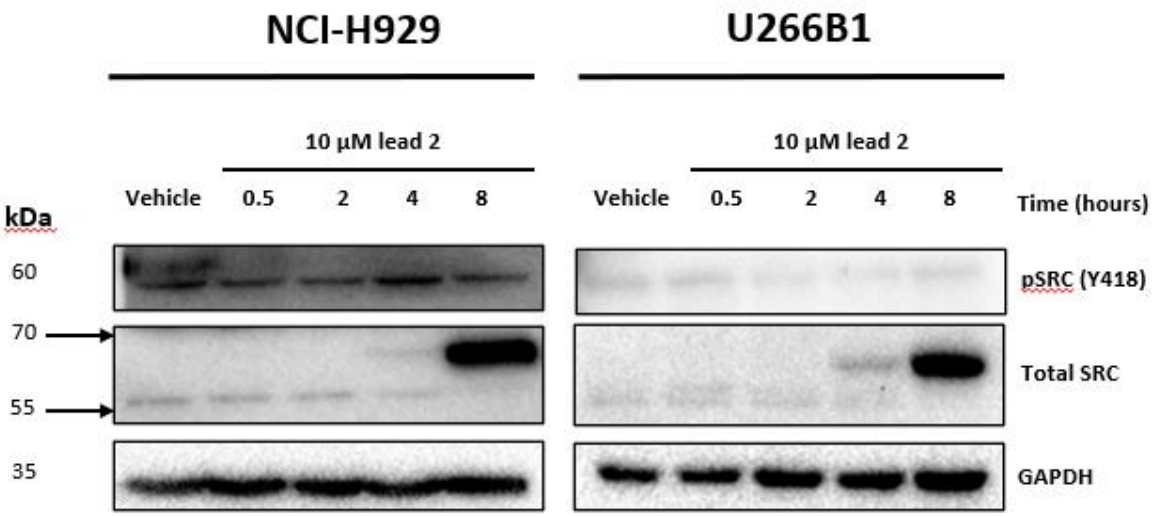

Figure 6.5.5. Compound **2** modulates total SRC but not phospho-SRC in NCI-H929 and U266B1 cells in a time responsive manner.

JAK1 and JAK2 lie upstream of STAT3 and are an essential component of the IL-6R/JAK/STAT3 signalling cascade; moreover, numerous compounds such as ruxolitinib have been shown to inhibit JAK1/2 phosphorylation and consequently STAT3 phosphorylation. Therefore, the effect of lead **2** on JAK1 and JAK2 was also examined. As such, U266B1 cells were treated with 10 µM of compound **2** or 30 µM of ruxolitinib for 4 hours. Then, cells were collected, lysates were prepared, and proteins were separated on a 10% SDS-PAGE gel. Gels were probed with antibodies against JAK1, phospho-JAK1, JAK2, phospho-JAK2, and STAT3 and phospho-STAT3 and anti-GAPDH was used as a loading control.

The effect of **2** and ruxolitinib on phospho-JAK2 was firstly examined. Both compounds were shown to inhibit phospho-JAK2 in the U266B1 cell line (Figure 6.5.6.A). As a result

of time constraints due to a longer optimisation period than expected and technical issues arising with western blots, clear outcomes were obtained only on two occasions. A time course from 0-120 minutes was also carried out showing that JAK2 phosphorylation on Tyr1007/Tyr1008 was inhibited from the time of 15 minutes after treatment with **2**. However, this result is only representative of one experiment as it was not possible to be replicated (Figure 6.5.6.B). Although results from three independent experiments demonstrated inhibition of JAK2 phosphorylation by compound **2,** more studies are required to confirm this considering the technical problems found with the assay.

The effect of **2** on JAK1 and STAT3 was next examined. Interestingly, neither compound **2** nor ruxolitinib elicited any effect on JAK1 phosphorylation in the U266B1 cells (Figure 6.5.7). STAT3 and phosphorylated STAT3 on Tyr705 were also examined finding that both **2** and ruxolitinib inhibited STAT3 phosphorylation with no visible effects on total STAT3 (Figure 6.5.7).

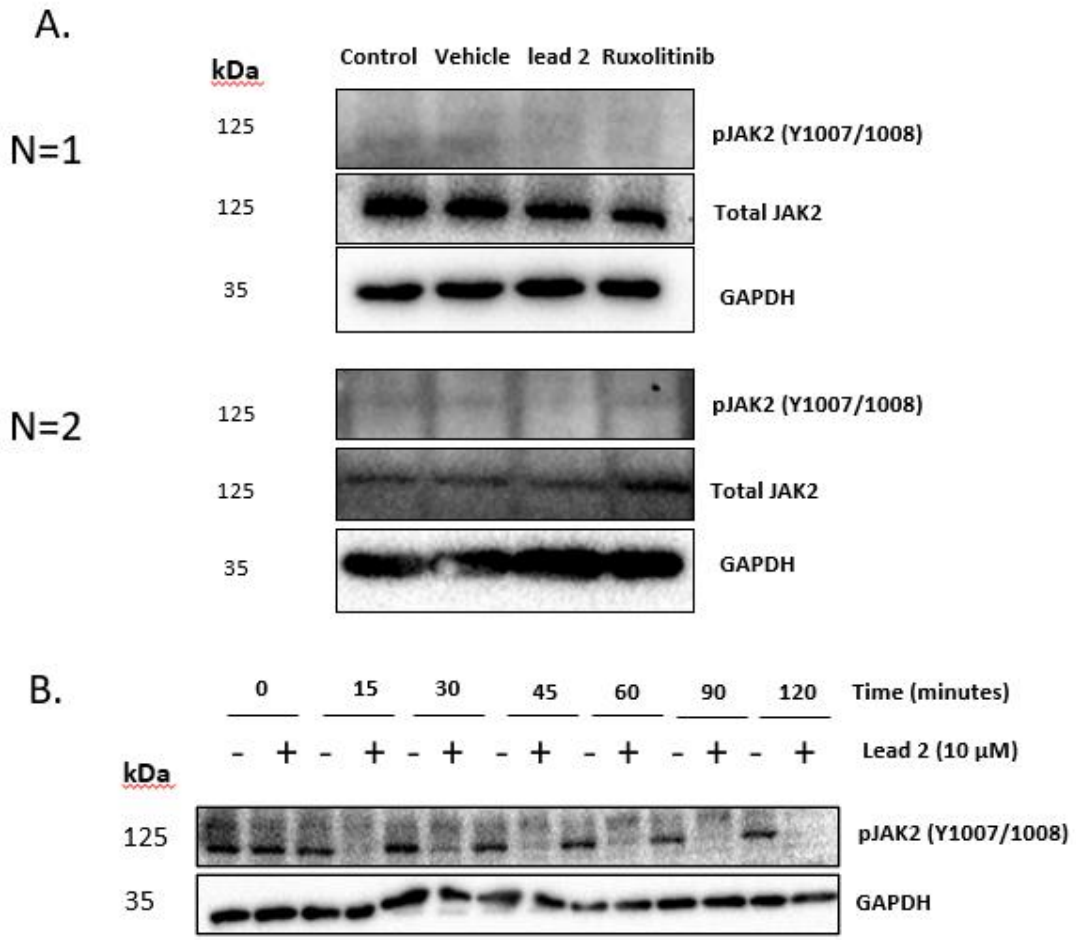

Figure 6.5.6. Compound **2** inhibits JAK2 phosphorylation in U266B1 cells. **A**. Cells were left untreated (control) or treated with either vehicle [0.5% EtOH (v/v) + 0.1% DMSO (v/v)] or 10 µM Lead **2** or 30 µM ruxolitinib for 4 hours or **B**. cells were treated with either vehicle [0.5% EtOH (v/v)] or 10 µM Lead 2 for 0, 15, 30, 45, 60, 90 or 120 minutes. Cells were lysed and 20 µg of protein was loaded and separated on 10% SDS-page gels, transferred to PVDF membrane, and probed with the appropriate antibody. Anti- GAPDH was used as a loading control. Results show 2 independent experiments for **A** and 1 experiment for **B**.

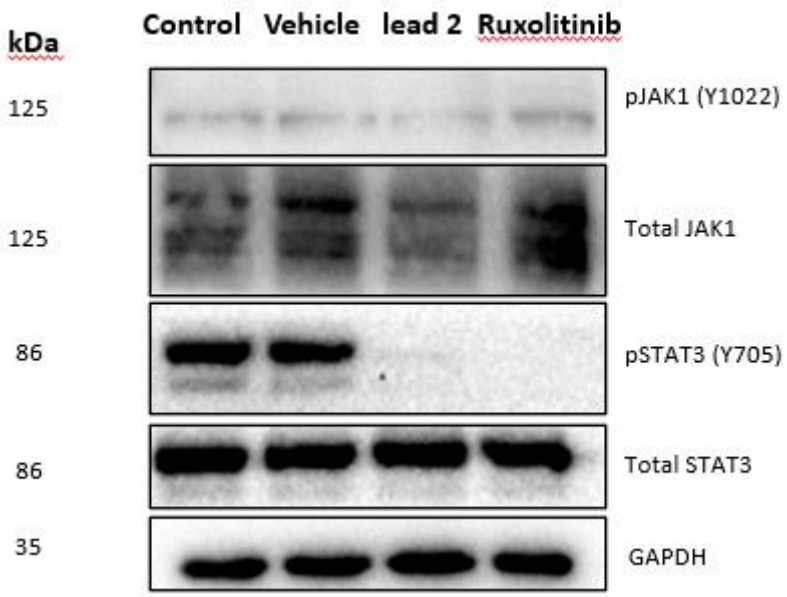

Figure 6.5.7. Compound **2** does not affect JAK1 phosphorylation in U266B1 cells.

6.6. Comparison between the experimental cytotoxicity observed in the NCI-H929 and U266B1 cell lines and predicted binding of derivatives of compound 2 in the JAK2 receptor

The IC_{50} values for the derivatives of lead compound **2** (Figure 6.6.1), were calculated by means of AlamarBlue experiments in NCI-H929 and U266B1 cell lines following similar protocols to those described in the previous Chapter 5. The values obtained (Table 6.6.1) were satisfactory as most of them were still in the low µM range as compared to **2**.

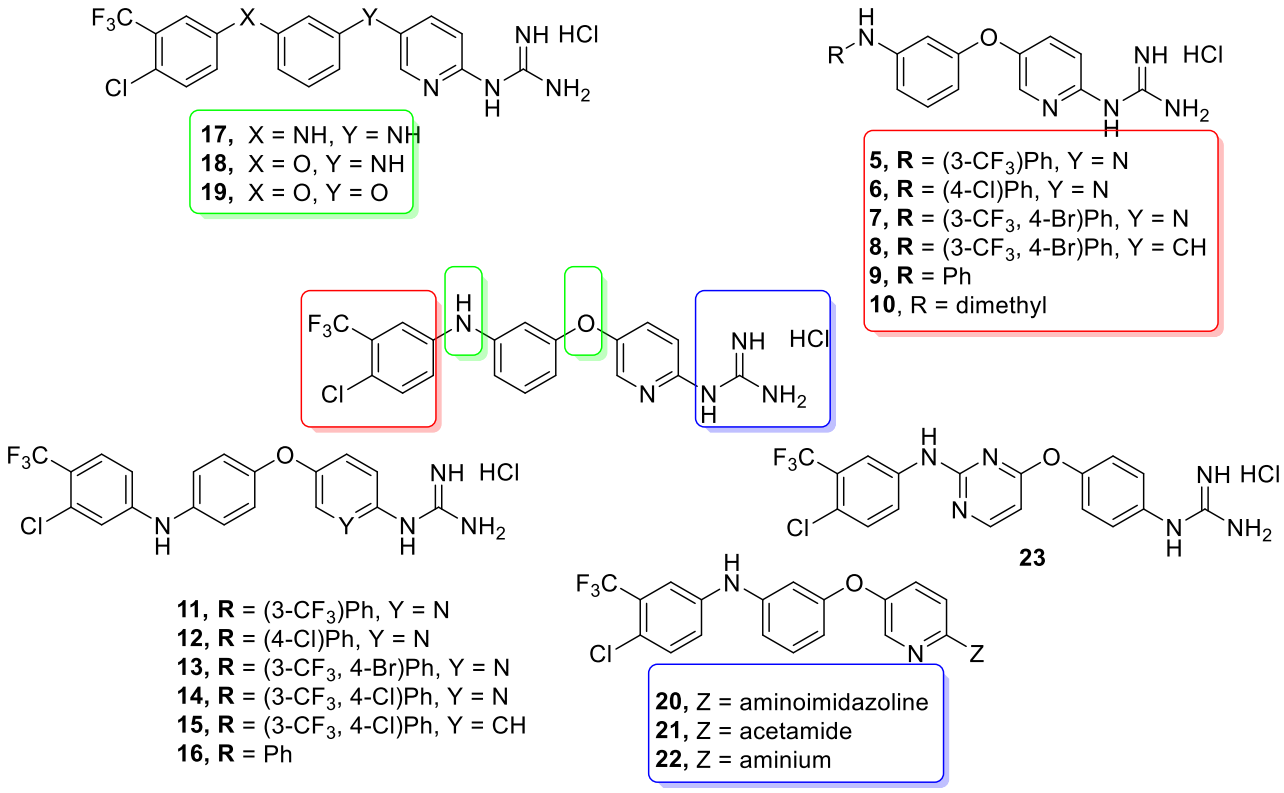

Figure 6.6.1. Structure of all derivatives of compound **2** discussed in this section.

Modifications in the hydrophobic head drive to a variety of IC_{50} values indicating the importance of this moiety for the cell growth inhibitory activity. Thus, in the case of compound **7** [(3-CF_3,4-Br)Ph], the IC_{50} remains similar to that of **2**, with a slight increase in activity in U266B1. For compounds **5** [(3-CF_3)Ph] and **6** [(4-Cl)Ph], a drop in activity is observed, especially for compoun **6**, showing that the 3-CF_3 group is important for the

activity. When the hydrophobic head is not substituted, as in compound **9**, a loss of activity is also achieved. Finally, in the case of compound **10** where there is no hydrophobic head, the IC_{50} is above 10, signifying the importance of this moiety.

Compounds **11-16** show a change in the diaryl substitution pattern and, thus, the hydrophobic head is found in the 4 position. It was found that compounds in this group have relatively good cell growth inhibition in the NCI-H929 cell line, but not so good in U266B1 where none of the compounds improved the activity of lead **2**. In the NCI-H929 cell line, derivative **13** has better activity than **2**; however, derivative **15**, which is structurally similar to **8** except it has a phenyl instead of a pyridyl ring, performs two times worse than **8**, indicating that the pyridine is very important for the activity in this particular cell line.

Those compounds with modified linkers, showed IC_{50} values comparable to **2** in the NCI-H929 line; however, in the U266B1line, derivatives **18** and **19** have a higher IC_{50} value than **2**, showing that in this cell line the HBD linkers are more favourable for the activity.

The results obtained for the compounds with modified polar moiety demonstrate the importance of the guanidinium cation. Thus, in the case of derivative **22**, where the guanidine is substituted by an amino group, the activity is lost and the IC_{50} is >10 μM. For compound **21** where the guanidine is substituted with an acetamide, the cell growth inhibitory activity is not improved in either of the cell lines. Finally, when the guanidinium is replaced by a 2-aminoimidazoline, as in compound **20**, an increase in activity is noticed in both cell lines. These results suggest that the electrostatic, HB and π-cation interactions which can be formed by the guanidine-like system are important for the activity.

From these results we can conclude that the most important modification leading to increased activity in both cell lines is the change from a guanidine to 2-aminoimidazoline (**20**) as it gave the lower IC_{50} compared to compound **2**.

Table 6.6.1. IC_{50} values obtained for derivatives of compound **2** on the alamarBlue® assay for NCI-H929 and U266B1 cell lines and the corresponding Gscore values (kcal/mol) in their 3jy9.

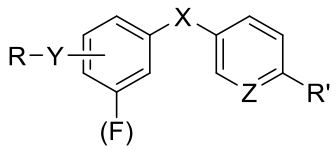

R	Y	X	Z	R’	IC_{50} µM NCI-H929	IC_{50} µM U266	Gscore
(3-CF_3,4-Cl)Ph	(3)NH	O	N	Gua	3.3 ±0.2	3.9 ±0.4	-11.2
(3-CF_3,4-Br)Ph	(3)NH	O	N	Gua	3.37 ±0.4	3.13 ±1.09	-11.9
(3-CF_3,4-Br)Ph	(3)NH	O	CH	Gua	4.59 ± 1.1	5.53 ± 1.03	11.1
(3-CF_3)Ph	(3)NH	O	N	Gua	3.67 ±0.57	4.13 ±0.58	-9.5
(4-Cl)Ph	(3)NH	O	N	Gua	4.47 ±0.64	7.29 ±1.33	-9.5
Ph	(3)NH	O	N	Gua	4.67 ±0.4	5.2 ±0.8	-9.3
Me	(3)NMe	O	N	Gua	>10	>10	-7.8
(3-CF_3,4-Br)Ph	(4)NH	O	N	Gua	3.9 ±1.0	6.04 ±0.8	-8.0
(3-CF_3,4-Cl)Ph	(4)NH	O	N	Gua	2.36 ±0.14	4.91 ±1.04	-7.8
(3-CF_3,4-Cl)Ph	(4)NH	O	CH	Gua	4.32 ±0.60	7.89 ±0.43	-9.1
(3-CF_3)Ph	(4)NH	O	N	Gua	4.12 ±1.0	7.7 ±1.4	-8.8
(4-Cl)Ph	(4)NH	O	N	Gua	5.42 ±1.0	7 ±1.1	-7.4
Ph	(4)NH	O	N	Gua	4.53 ±0.53	7.77 ±0.58	-5.9
(3-CF_3, 4-Cl)Ph	(3)NH	NH	N	Gua	3.72 ± 0.3	3.9 ±0.28	-11.6
(3-CF_3, 4-Cl)Ph	(3)O	O	N	Gua	3.69 ± 0.49	4.12 ±0.44	-9.5
(3-CF_3, 4-Cl)Ph	(3)O	NH	N	Gua	3.73 ± 0.64	4.68 ±0.22	-9.7
(3-CF_3, 4-Cl)Ph	(3)NH	O	N	2-Imi	2.08 ±1.0	1.19 ±0.43	-10.4
(3-CF_3,4-Cl)Ph	(3)NH	O	N	Acetamide	9.1 ±1.7	>10	-12.9
(3-CF_3,4-Cl)Ph	(3)NH	O	N	NH_3^+	>10	>10	-11.9
(3-CF_3,4-Cl)Ph	(3)NH pyrimidine	O	CH	Gua	2.53 ± 0.05	5.32 ±0.41	-9.1

Considering the results obtained in the docking studies of the derivatives of compound **2** into the JAK2 receptor (PDB structure 3JY9), we next compare the predicted binding (i.e. Gscore values) of these derivatives to JAK2 (as described in Chapter 3) with the experimental cell growth inhibitory activity observed in the two MM cell lines analysed

(as seen in the previous section). As mentioned before, JAK2 is of relevance to MM because it has been linked to survival and proliferation of MM cells; therefore, JAK2 inhibition could be explained the good cytotoxicity observed with the MM cell lines.[19] The comparative results are presented in Table 6.6.1.

Looking at derivatives **5-10**, where the hydrophobic moiety has been explored, it can be seen that the Gscore of compound **7**, which is lower than that of **2**, correlates with the slightly lower IC_{50} value obtained. It seems that the substitution of the 4-Cl by the larger 4-Br group is favourable for binding and activity. In derivative **5** there is a significant drop in activity compared to lead **2**, suggesting that the interaction of the 3-CF_3 group with the JAK2 hydrophobic pocket is beneficial for the cell growth inhibitory activity of this series. This seems to be confirmed with the results obtained for compound **6** where only the 4-Cl has been removed.

In compounds **11-16** with a 4,4'-diaryl substitution, the observed trend in cell growth inhibition activity (i.e. IC_{50}) and binding to JAK2 (i.e. Gscore values) was very similar to those compounds with a 3,4'- substitution, indicating that this different substitution in the diaryl core does not seem to play an important role in the activity against the MM cell lines studied.

In the case of compounds **17-19** where the linkers between the aryl rings have been modified, an agreement is found between the binding strength to the JAK2 receptor calculated from the docking studies and the actual IC_{50} measured in the AlamarBlue assays with the NCI-H929 and U266B1 lines. The Gscore values of compounds **17** and **18** optimally correlate with their very good activity in the NCI-H929 cell line. This suggests that the presence of the amino linkers in between de aryl rings leads to higher growth inhibitory activity through inhibition of the JAK2 receptor as hinted by the computational studies.

Looking at compounds **20-22** where the polar moiety was modified, we observe that while the Gscore of the 2-aminoimidazoline **20** was higher than that of **2**, the IC_{50} was lower in the MM cell lines. In the case of **22**, where the guanidine was substituted by an amino group, the activity was significantly reduced, showing that HB donors and electrostatic interactions, as those formed by the guanidine-like cations, are needed to

interact with the target. When the guanidine was replaced with an acetamide, as in compound **21**, the HB donor was replaced with a HB acceptor, what improved the binding to JAK2 (i.e. better Gscore) even though this was not reflected in the activity. Finally, compound **23** shows good activity in the NCI-H929 cell line, but not in the U266B1, while it had better activity in one of the cell lines, the Gscore for **23** is higher than that of **2**. In summary, there is no certainty that the activity of these compounds in MM cell lines involves binding to JAK2.

6.7. Evaluation of the effect of derivatives of lead compound 2 in different cancer cell lines

Considering the good results obtained with lead compound **2** and its derivatives in MM cell lines, a sample of these compounds (i.e. **2, 4-8**, **17-19**, **20**) was submitted to the NCI-DTP to study their effect in the cell growth of a panel of cancer cell lines using a fixed concentration of 10 μM.

6.7.1. Cell growth inhibition effect of derivatives of 2 in leukemia cell lines

The following leukemia cell lines were used for this NCI screening: CCRF-CEM, HL-60, K-562, MOLT-4, RPMI 8226, and SR (details explained in Chapter 5 and Appendix). The results are summarised in Figure 6.7.1.1 and Table 6.7.1.1.

All the compounds tested exert the highest cell death in the HL-60 cell line. Looking at the biological activity of the derivatives of lead compound **2** it can be observed that **19** (where the secondary amine of **2** was replaced with an ether) and **18** (where the diaromatic ether linker of **2** was replaced with an amino) increased cell death in the CCRF-CEM cell line. Surprisingly, we do not see the same effect with compound **17** in which there are two diaromatic amino linkers. Looking at the effect that changes in the polar moiety can exert in the cell death or cell growth inhibition, we noticed that compound **4** where the pyridyl ring present in compound **2** has been changed by a

phenyl, the biological activity changed drastically since this compound causes growth inhibition and not cell death in all leukemia cell lines except in SR. In the case of compound **20**, where the guanidine present in **2** has been substituted by a 2-aminoimidazoline, no notable change is observed, except in some of the cell lines (i.e. CCRF-CEM and MOLT-4) in which cell growth inhibition rather than cell death is observed. For compound **21** only one cell line was screened and there was no cell death or notable growth inhibition.

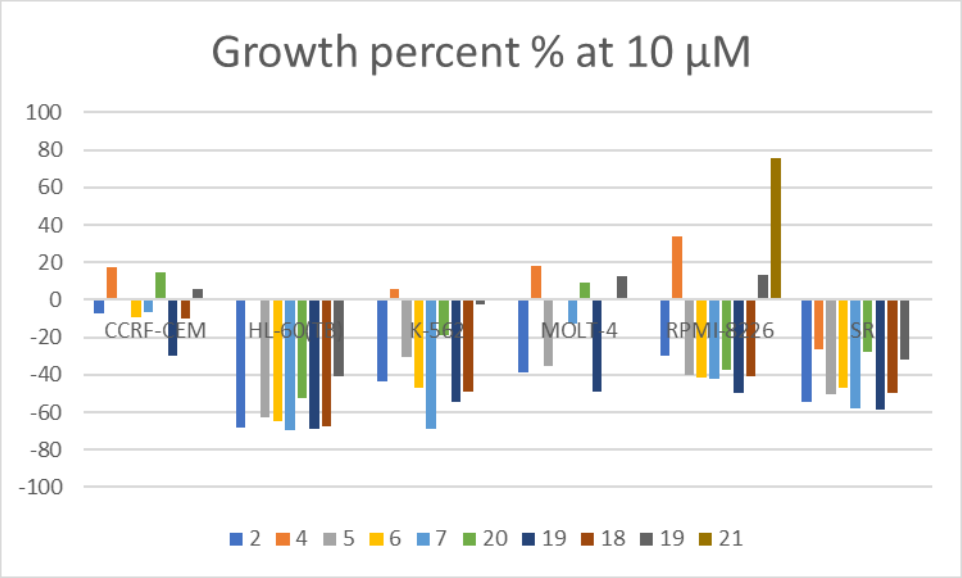

Figure 6.7.1.1. The effect of derivatives of compound **2** on the growth of leukemia cell lines.

Examining the results obtained for those derivatives in which the hydrophobic head was modified, somewhat unexpected activity was found. Thus, compound **5** (containing a (3-CF_3)Ph hydrophobic group) exhibited a slight increase in cell death in two of the cell lines (K-562 and RPMI-8226) and no noticeable effect on the MOLT-4 cell line. For compound **7** (with a 4-Br, 3-CF_3 hydrophobic group) no increase or even a slight decrease in the percentage of cell death is noticed in cell lines like CCRF-CEM and K-562; however, a slight increase in cell death in RPMI-8226 compared to the lead compound **2** is observed.

As mentioned, the GI_{50} indicates the concentration in which 50% of cell growth is inhibited, and in these leukemia cell lines compound **2** showed the best results. When compared these results to those of the derivatives which linkers have been modified, it was found that for **17** the GI_{50} increases (Table 6.7.1.1); however, for **19**, even though a smaller GI_{50} value was obtained, the activity has not increased compared to compound **2**. Compound **21** showed GI_{50} values not as good as those of **2** but better than those obtained for **4**. In the compounds in which the polar moiety has been modified, we observed that **20** as well as **4** performed poorly compared to **2**. In compounds **5**, **6** and **7** the GI_{50} values are poorer than that of **2**. In the cell lines which the TGI was calculated all values were found to be above 4 μM and the LC_{50} values were also found to be high. Compound **21** do not lead to cell death or cell growth inhibition and hence it was not further evaluated.

Table 6.7.1.1. Evaluation of derivatives of compound **2** at five doses in leukemia cell lines.

GI_{50} (μM)									
	2	**4**	**5**	**6**	**7**	**20**	**19**	**18**	**17**
CCRF-CEM	1.82	2.69	2.57	2.04	2.04	2.82	2.04	2.09	2.57
HL-60(TB)	1.91	2	1.62	2.04	2.51	2.09	1.86	1.78	2.29
K-562	1.91	2.51	2.09	1.66	2.63	2.4	1.62	2.14	2.51
MOLT-4	1.78	1.95	2.14	1.95	2.14	3.16	2.09	2.14	2.29
RPMI-8226	1.86	2.63	2.24	1.78	2	2.04	1.91	1.51	2.29
SR	1.62	2.14	2.14	1.82	2.51	2.4	1.82	2.24	2.57
TGI (μM)									
CCRF-CEM		8.91			5.25	14.45			
HL-60(TB)	4.47	4.27	4.17	4.37	4.79	5.5			5.75
K-562	>100	6.46	>100		8.13			>100	>100
MOLT-4		4.57			4.57	14.13			
RPMI-8226					5.13	5.25			
SR									
LC_{50} (μM)									
CCRF-CEM	>100	>100	>100	>100	>100	>100	>100	>100	>100
HL-60(TB)	>100	9.33	21.38	9.33	8.91	>100		>100	>100
K-562	>100	>100	>100	>100	>100	>100	>100	>100	>100
MOLT-4	>100	>100	>100			>100	>100	>100	>100
RPMI-8226	>100	>100	>100	>100	>100	>100	>100	>100	>100

SR	>100	>100	>100	>100	>100	>100	>100	>100	>100

6.7.2. Cell growth inhibition effect of derivatives of 2 in non-small cell lung cancer lines

The following non-small cell lung (NSCL) cancer lines were used in this screening: A549, EKVX, HOP-62, HOP-92, NCI-H226, NCI-H23, NCI-H322M, NCI-H460, NCI-H522. The results are presented in Table 6.7.2.1 and Figure 6.7.2.1.

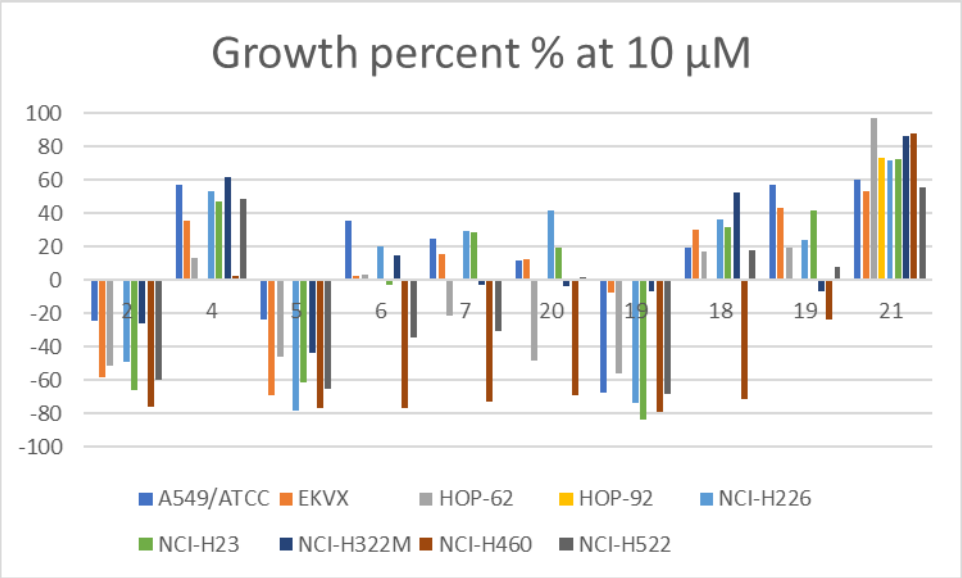

Figure 6.8.2.1. The effect of derivatives of compound **2** on Non-Small Cell Lung cancer cell lines.

In NSCL, compound **2** leads growth inhibition/death in all the screened cell lines, with NCI-H460 being the most affected. When comparing these results with those of the derivatives with the modified diaromatic linkers we can see a drastic difference in activity. Thus, compound **17** showed cell growth inhibition in most of the cell lines, with

the best results seen for A549, but only minor cell death in NCI-H322M and NCI-460. Compound **19** shows an opposite profile that that of **17**, and thus, **19** leads to cell death in all the screened NSCL cell lines, with NCI-H23 almost reaching complete cell death, which is a sharp increase in activity compared to compound **2**. Compound **18** showed similar activity to **17**, leading to the most cell death in the NCI-H460 cell line.

In the derivatives in which the hydrophobic head has been modified, **5** shows comparable activity, and even improved in some cell lines, to that of lead **2**. In derivatives **6** and **7**, the cells do no die but rather exert growth inhibition. In the compounds in which the polar moiety has been changed there is also a drastic change in the activity; for example, in the phenyl derivative (i.e. **4**) none of the cell lines screened died, rather the compound led to growth inhibition. With all the compounds screened the cell line NCI-H460 was found to be most affected. **21** does not lead to cell death or cell growth inhibition.

Table 6.7.2.1. Evaluation of derivatives of compound **2** at five doses in NSCL cancer cell lines

GI_{50} (μM)									
	2	**4**	**5**	**6**	**7**	**20**	**19**	**18**	**17**
A549/ATCC	1.78	1.92	1.78	1.86	1.78	2.34	1.70	1.82	2.29
EKVX	1.48	1.62	1.51	1.58	1.58	2.09	1.62	1.62	1.74
HOP-62	1.70	1.58	1.74	1.74	1.86	2.24	1.86	1.91	1.82
HOP-92	1.12	1.29	1.41	1.07	1.07	6.17	1.23	1.00	1.41
NCI-H226	1.74	1.66	1.70	1.70	1.78	2.04	1.74	1.70	1.78
NCI-H23	1.62	1.70	1.66	1.62	1.66	2.51	1.66	1.58	1.78
NCI-H322M	1.66	1.74	1.66	1.62	1.66	2.40	1.66	1.66	1.62
NCI-H460	1.91	1.86	1.91	1.86	1.86	2.00	1.95	1.91	2.00
NCI-H522	1.62	1.70	1.62	1.55	1.55	1.91	1.55	1.62	1.82
TGI (μM)									
A549/ATCC	3.98	4.07		4.47	4.07	6.31			
EKVX	3.02	3.24	3.02	3.16	3.24	5.50	3.31		3.55
HOP-62	3.55	3.16	3.63	3.63	3.98	6.17	3.63	3.89	4.07
HOP-92	2.51	2.63	2.88	2.45	2.4	5.25	2.63	2.29	2.95
NCI-H226	3.98	3.47	3.63	3.89	4.17	5.37	3.80	3.63	3.89
NCI-H23	3.16	3.24	3.16	3.24	3.24	7.59	3.31		3.63

NCI-H322M	3.09	3.39	3.02	3.02	3.02	6.61	1.95	3.09	3.02
NCI-H460	3.72	3.55		3.55	3.63	3.98		3.80	3.98
NCI-H522	3.39	3.63	3.39	3.31	3.16	4.37	3.31	3.55	3.98
LC_{50} (μM)									
A549/ATCC				>100		89.13			>100
EKVX						27.54			
HOP-62		6.31				46.77			
HOP-92		100			5.37	46.77			
NCI-H226						>100			
NCI-H23		6.03			6.31	46.77			
NCI-H322M		6.61		5.5	5.5	28.18			
NCI-H460		6.76				7.94			
NCI-H522					6.46	9.77			

The GI_{50} values of the all the compounds across the screening are low, the highest being 6.17 μm for compound **20** (Table 6.7.2.1). The total growth inhibition values were also found to be relatively low for all the cells and compounds screened, some even being found to be lower than 2 μM. Thus, these compounds are very promising as potential agents to treat NSCL cancers. Compound **21** do not lead to cell death or cell growth inhibition and hence it was not further evaluated.

6.7.3. Cell growth inhibition effect of derivatives of 2 in colon cancer cell lines

The following colon cancer cell lines were used for this NCI screening: COLO 205, HCC-2998, HCT-116, HCT-15, HT-29, KM12 HCC-2998, SW-620 and the results are presented in Table 6.7.3.1 and Figure 6.7.3.1.

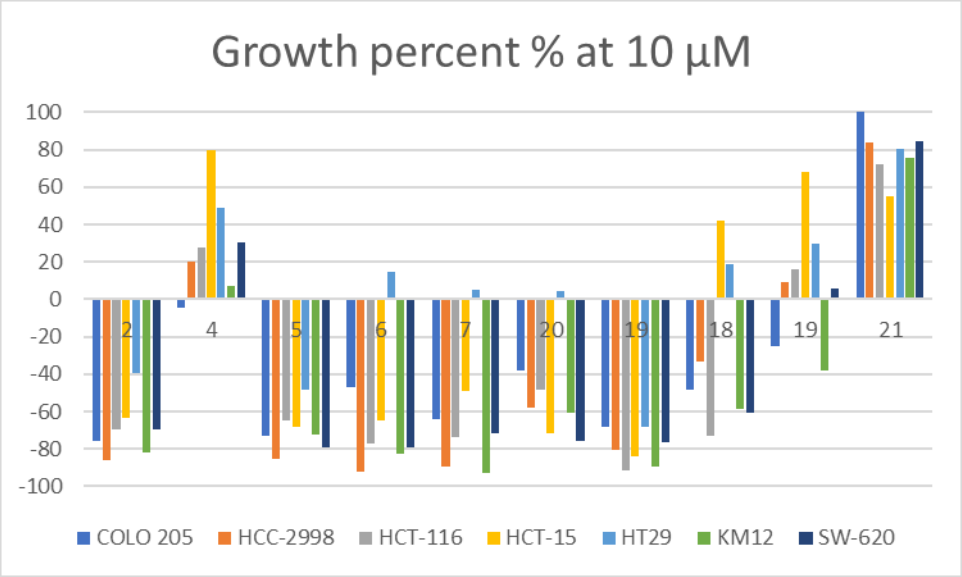

Figure 6.7.3.1. The effect of derivatives of compound **2** on colon cancer cell lines.

Much like with NSCL cells, compound **2** leads to significant cell death in the colon cancer cell lines screened, reaching up to 85% cell death at 10 µM with HCC-2998 cancer cells. In compounds **17-19**, we see the opposite trend as that observed with NSCL cancer cells. In **18** with both diaromatic linkers being ether groups, cell death rather than cell growth inhibition is observed. In fact, these compounds induce up to a 91% cell death in the HCT-116 cancer cell lines, which is a great increase in activity from 69% cell death exerted by **2**. In the case of compound **17** no major cell death effects are observed in these cell lines; however, this compound exerts 68% cell growth inhibition in HCT-15. Derivative **18** activity was maintained in most of the cell lines, although at lower levels than lead **2** in cell lines like KM12 and SW-620. In HCT-15 and HT29 lines, this compound does not produce cell death, but their growth is inhibited by over 50%. In the derivatives with modified hydrophobic head, we found that when we had (4-Br,3-CF_3)Ph, as in compound **5**, comparable activity to compound **2** was observed without drastic changes. This can be seen similarly in compounds **6** and **7**. In the compounds with different polar moieties, we can see that the pyridyl ring is needed for the anticancer activity and when the 2-aminoimidazoline was present as in compound **20**, the cell death activity was maintained except in the HT29 cancer cell line.

The GI_{50} values of the screened compounds (Table 6.7.3.1) are lower than 3 µM, and the total growth inhibition was also found to be reasonably low for the screened compounds. Again, these compounds seem to be very promising anticancer agents. Compound **21** do not lead to cell death or cell growth inhibition and hence it was not further evaluated.

Table 6.7.3.1: Evaluation of derivatives of compound **2** at five doses in colon cancer cell lines.

GI_{50} (µM)									
	2	**4**	**5**	**6**	**7**	**20**	**19**	**18**	**17**
COLO 205	1.58	1.82	1.82	1.62	1.82	1.86	1.95	1.82	1.66
HCC-2998	2.00	1.74	1.74	1.86	1.82	2.00	1.82	2.04	1.82
HCT-116	1.55	1.62	1.62	1.70	1.74	1.74	1.70	1.58	1.86
HCT-15	1.78	1.91	1.66	1.62	1.74	1.66	1.55	1.86	1.95
HT29	1.58	1.86	1.70	1.70	1.48	2.04	1.78	1.66	1.95
KM12	1.58	1.70	2.00	1.74	2.09	2.00	1.78	1.91	1.95
SW-620	1.66	1.82	1.74	1.62	1.82	1.78	1.55	1.66	1.70
TGI (µM)									
COLO 205	3.47	3.63	3.80	3.47	3.72	3.98		3.89	3.80
HCC-2998	3.80	3.24	3.24	3.55	3.39	3.63	3.63		
HCT-116	3.55	3.16		3.31	3.39	3.16	3.16		3.80
HCT-15		4.37	3.16	3.09	3.47	3.31	3.09		4.17
HT29	3.31	3.89	3.55	3.47	2.95	5.13			
KM12	3.24	3.16		3.47	4.57	4.47		3.89	3.89
SW-620	3.24	3.63	3.24	3.24	3.55	3.63			
LC_{50} (µM)									
COLO 205						8.32			
HCC-2998		6.03				6.76			
HCT-116		6.03				5.89			
HCT-15		10				6.61			
HT29						>100			>100
KM12					>100	10			
SW-620					6.92	7.59			

6.7.4. Cell growth inhibition effect of derivatives of 2 in CNS cancer cell lines

The following CNS cancer cell lines were used for this NCI screening: SF-268, SF-295, SF-539, SNB-19, SNB-75, U251 and the results are presented in Table 6.7.4.1 and Figure 6.7.4.1.

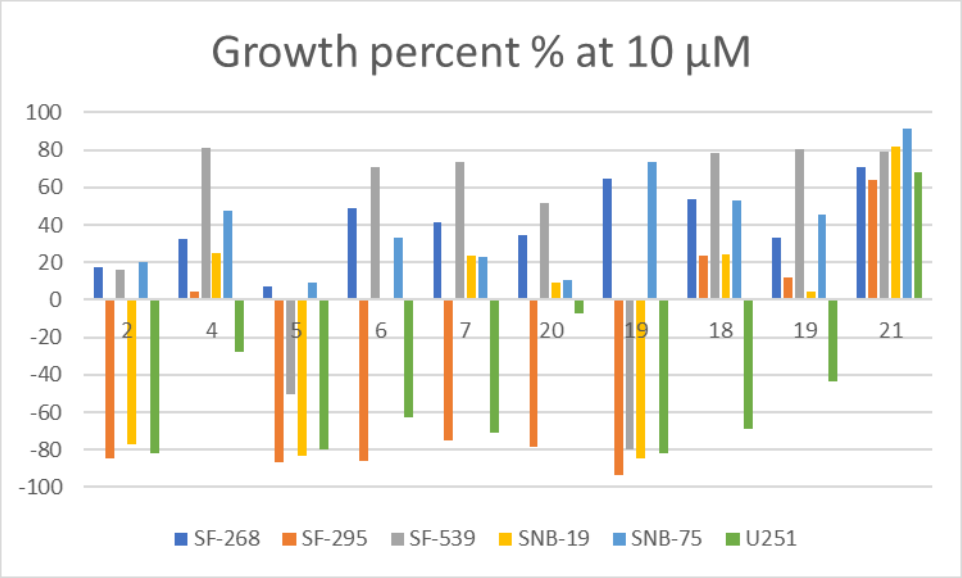

Figure 6.7.4.1. The effect of derivatives of compound **2** on CNS cancer cell lines.

For most of the compounds screened the cell growth inhibition exhibited is not very significant at 10 µM. In Figure 6.7.4.1 it can be seen how compound **2** causes cell death in three of the six CNS cell lines and leads to at least 70% of cell death. Compound **18** has comparable activity to compound **2** except for its effect in the SF-539 cell line in which **18** causes 79% of cell death. Compounds **62** and **60** exert cell death in only one cell line, U251, but both compounds have lower activity than lead **2**. These two compounds show increased cell growth inhibition of SF-539. Looking at the compounds where the hydrophobic head has been modified, it was found that **5** exhibits the same activity than **2** except for the cell lines SF-539 and U251. In the case of derivatives **6** and **7**, the cell growth inhibition increases in the SD-539 cell line; however, they do not show

much activity against SNB-19. In the case of derivatives which polar moiety has been modified, all the compounds screened exert more of an inhibitory effect on the cells' growth than cell death.

Regarding the GI_{50} values obtained (Table 6.7.4.1), all the compounds showed values below 3 µM, except for compound **20** in the SF-268 cell line. However, this compound surprisingly performed the worse compared to lead compound **2** in SF-539, SNB-19 and U251**.** Looking at the calculated LC_{50} values (Table 6.7.4.1), it was found that lead **2** has a value of 5.37 µM in SNB-75, whereas **20** has a wide range of values for all the cell lines screened. The LC_{50} values for all the compounds were found to be like those of compound **2**, and **20** was found to be seven time worse in terms of toxicity (LC_{50}). Compound **21** do not lead to cell death or cell growth inhibition and hence it was not further evaluated.

Table 6.7.4.1. Evaluation of derivatives of compound **2** at five doses in CNS cancer cell lines.

GI_{50} (µM)									
	2	**4**	**5**	**6**	**7**	**20**	**19**	**18**	**17**
SF-268	1.82	1.58	1.86	1.86	1.74	4.17	1.91	1.82	1.95
SF-295	1.70	1.66	1.70	1.70	1.70	1.74	1.74	1.70	1.78
SF-539	1.74	1.70	1.78	1.74	1.66	2.09	1.74	1.78	1.91
SNB-19	1.74	1.51	1.70	1.70	1.51	2.75	1.70	1.78	1.91
SNB-75	1.41	1.20	1.35	1.38	1.26	1.95	1.32	1.58	1.70
U251	1.74	1.70	1.78	1.82	1.62	2.09	1.82	1.78	2.00
TGI (µM)									
SF-268	3.98	3.02	3.80	3.80	3.72	17.78	3.89	3.72	4.07
SF-295	3.31	3.24	3.24	3.24	3.39	3.39	3.31		3.63
SF-539	3.31	3.16	3.39	3.24	3.16	4.57	3.31	3.39	3.72
SNB-19	3.55	3.02	3.47	3.39	2.95	8.71	3.24	3.47	3.89
SNB-75	2.75	2.51	2.63	2.75	2.57	8.32	2.69	3.31	3.55
U251	3.55	3.39	3.55	3.63	3.16	4.79	3.39		4.17
LC_{50} (µM)									
SF-268		5.89			8.13	69.18			
SF-295		6.17				6.61			
SF-539		5.75		6.03	6.03	11.22			
SNB-19						56.23			

SNB-75	5.37	5.13		5.50	5.25	38.90	5.37		
U251						17.78			

6.7.5. Cell growth inhibition effect of derivatives of 2 in melanoma cancer cell lines

The following melanoma cancer cell lines were used for this NCI screening: LOX IMVI, MALME-3M, M14, MDA-MB-435, SK-MEL-2, SK-MEL-28, SK-MEL-5, UACC-257, UACC-62 and the results are presented in Table 6.7.5.1 and Figure 6.7.5.1.

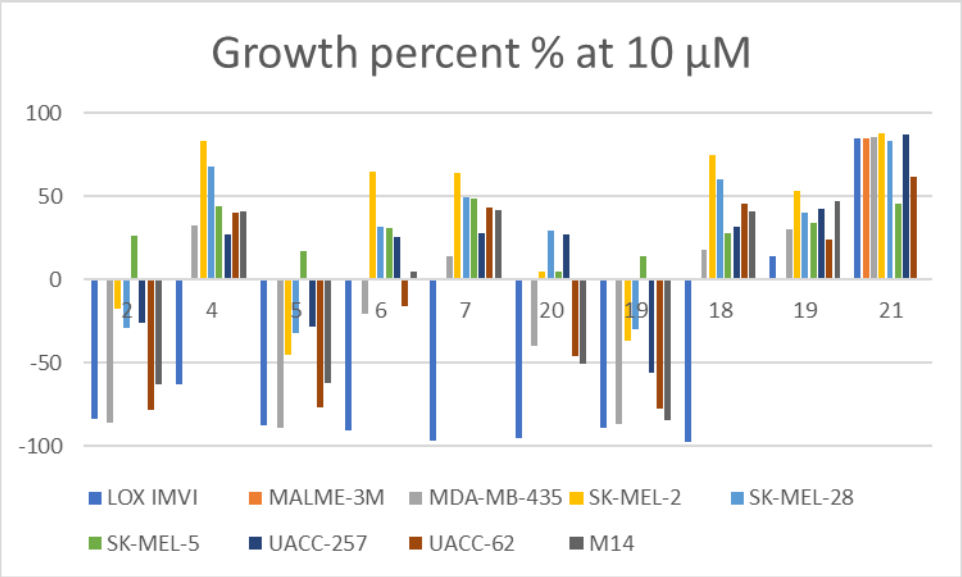

Figure 6.7.5.1.: The effect of amino linked compounds on melanoma cancer cell lines.

In the melanoma cell lines, lead compound **2** causes up to 86% cell death in MDA-MB-435. In the case of compounds which linkers have been modified, **19** leads to cell death in all of the screened cell lines except for SK-MEL-5, which is comparable to the results seen in **2**, additionally, compounds **17** and **18** do not lead to cell death except for **18** which causes major cell death in the LOX IMVI cell line. Compound **17** does not lead to significant cell growth inhibition. Much like in all the cancer cell lines that were screened, compound **5** shows the same activity as the lead compound **2** and both compounds **6** and **7** do not show very good activity in these cell lines. Low activity is also

observed in these cancer cell lines for compounds **4** and **20**. **21** does not cause any cell death or cause significant cell growth inhibition.

Total growth inhibition values calculated for these derivatives in all the melanoma cell lines screened were below 10 µM (Table 6.7.5.1). Moreover, the calculated LC_{50} values were found to be less than 7 µM in most of the melanoma cell lines screened. Compound **21** do not lead to cell death or cell growth inhibition and hence it was not further evaluated.

Table 6.7.5.1. Evaluation of derivatives of compound **2** at five doses in melanoma cell lines.

GI_{50} (µM)									
	2	**4**	**5**	**6**	**7**	**20**	**19**	**18**	**19**
LOX IMVI	1.70	1.70	1.74	1.74	1.74	1.74	1.74	1.74	1.86
MALME-3M	1.91	1.70	1.91	1.91	1.82	2.82	1.86	1.78	2.00
M14	1.74	1.82	1.70	1.74	1.70	1.74	1.78	1.66	1.74
MDA-MB-435	1.62	1.66	1.74	1.58	1.70	1.66	1.66	1.70	1.82
SK-MEL-2	1.95	1.95	1.95	1.86	1.82	2.63	1.91	1.91	1.95
SK-MEL-28	1.74	1.74	1.66	1.70	1.66	1.95	1.70	1.74	1.78
SK-MEL-5	1.82	1.78	1.82	1.82	1.82	1.82	1.82	1.86	1.78
UACC-257	1.82	1.78	1.91	1.82	1.74	3.09	1.78	1.91	2.40
UACC-62	1.86	1.74	1.86	1.78	1.74	2.57	1.82	1.82	1.91
TGI (µM)									
LOX IMVI	3.31	3.16	3.31	3.39	3.39	3.16	3.31		
MALME-3M	4.07	3.72	4.27	4.17	3.98	9.77	3.80	4.07	5.37
M14	3.55	3.47	3.31	3.31	3.31	3.47	3.31	3.24	
MDA-MB-435	3.02	3.09	3.31	3.09	3.16	3.31	3.09	3.24	3.55
SK-MEL-2	3.80	3.63	3.72	3.63	3.47	6.92	3.80	3.72	3.98
SK-MEL-28	3.24	3.16	3.16	3.16	3.09	3.89	3.16	3.31	3.39
SK-MEL-5	3.39	3.24	3.31	3.24	3.39	3.24	3.31		3.24
UACC-257	3.80	3.55	3.98	3.80	3.63	9.55			6.46
UACC-62	3.55	3.24	3.63	3.39	3.31	6.92	3.39	3.63	3.72
LC_{50} (µM)									
LOX IMVI		5.89				5.89			
MALME-3M		7.94				51.29			

M14		6.61		6.31		6.92			
MDA-MB-435		5.62				6.61			
SK-MEL-2						53.70			
SK-MEL-28		5.75		5.89	5.75	7.76			
SK-MEL-5						5.75			
UACC-257						66.07			>100
UACC-62		6.03		6.46	6.17	30.90			

6.7.6. Cell growth inhibition effect of derivatives of 2 in ovarian cancer cell lines

The following ovarian cancer cell lines were used for this NCI screening: OVCAR-3, OVCAR-4, OVCAR-5, OVCAR-8, NCI/ADR-RES, SK-OV-3 and the results are presented in Table 6.7.6.1 and Figure 6.7.6.1.

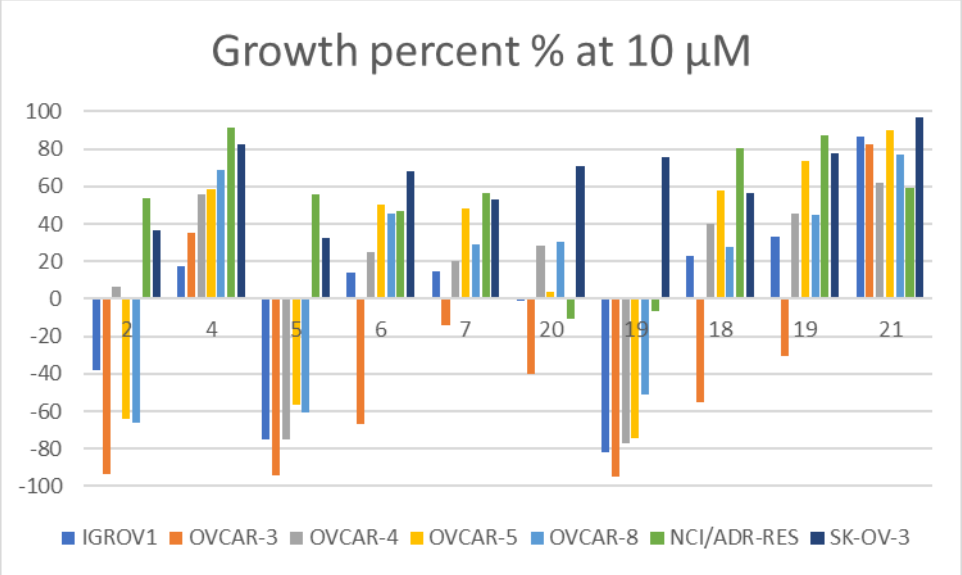

Figure 6.7.6.1. The effect of amino linked compounds on ovarian cancer cell lines.

Lead compound **2** shows an impressive 93% cell death in OVCAR-3 cell line but not in the other ovarian cancer cell lines indicating a degree of selectivity. In the case of compounds with modified linkers, compound **19** has good activity across all these cell lines. Moreover, **17** and **18** exert cell growth inhibition in those ovarian cancer cell lines

in which lead **2** had induced cell death. In the compounds with different hydrophobic moieties, it is found that, as expected, **5** has the same activity as **2** but different to that of compounds **6** and **7**. Compounds **4** and **20** do not exert major cell death, but they lead to cell growth inhibition. **21** does not cause any cell death or cause significant cell growth inhibition.

When the GI_{50} was calculated it was found that there was great fluctuation in the activity shown by all the compounds in the NCI/ADR-RES cell line with the lowest GI_{50} value found for compounds **19** and **20**, which also showed the lowest TGI (Table 6.7.6.1).

Table 6.7.6.1.: Evaluation of derivatives of lead compound **2** at five doses in ovarian cancer cell lines.

GI_{50} (μM)									
	2	**4**	**5**	**6**	**7**	**20**	**19**	**18**	**17**
IGROV1	1.45	1.26	1.51	1.55	1.35	1.82	1.45	1.66	1.66
OVCAR-3	1.74	1.66	1.95	1.66	1.82	2.51	1.74	1.78	1.91
OVCAR-4	1.58	1.70	1.74	1.55	1.62	2.75	1.78	1.62	1.91
OVCAR-5	1.55	1.55	1.62	1.58	1.55	2.51	1.70	1.74	1.82
OVCAR-8	2.04	1.91	2.09	2.09	1.95	2.51	2.09	2.14	2.24
NCI/ADR-RES	3.72	14.79	3.89	4.90	4.07	2.04	1.91	15.49	21.88
SK-OV-3	1.91	2.69	2.04	2.09	2.09	14.79	1.86	3.47	2.82
TGI (μM)									
IGROV1	3.09	2.75	3.16	3.24	2.82	4.27	2.95		3.63
OVCAR-3	3.39	3.24	3.98	3.39	7.24	6.31	3.39	3.55	3.80
OVCAR-4	2.95	3.16	3.16	2.88	3.02	10.96	3.31	3.16	4.17
OVCAR-5	2.95	2.95	3.09	3.02	3.02	6.76	3.16	3.31	3.80
OVCAR-8		4.17		4.90	4.47	6.76			
NCI/ADR-RES	30.20	34.67	29.51	38.02	20.42	4.57	3.89	>100	93.33
SK-OV-3	3.47	6.61	3.72	4.27	4.17	32.36	3.47	13.18	6.92
LC_{50} (μM)									
IGROV1		5.89				9.77			
OVCAR-3					7.24	35.48			
OVCAR-4						60.26			
OVCAR-5		5.50				30.20			
OVCAR-8	>100		>100	>100	>100	81.28	>100	>100	>100
NCI/ADR-RES	>100	79.43	>100	>100	>100	10.00		>100	>100

SK-OV-3	6.17	45.71	6.61	8.71	8.13	69.18		>100	>100

6.7.7. Cell growth inhibition effect of derivatives of 2 in renal cancer cell lines

The following renal cancer cell lines were used for this NCI screening: 786-0, A498, ACHN, CAKI-1, RXF 393, SN12C, TK-10, UO-31 and the results are presented in Table 6.7.7.1 and Figure 6.7.7.1.

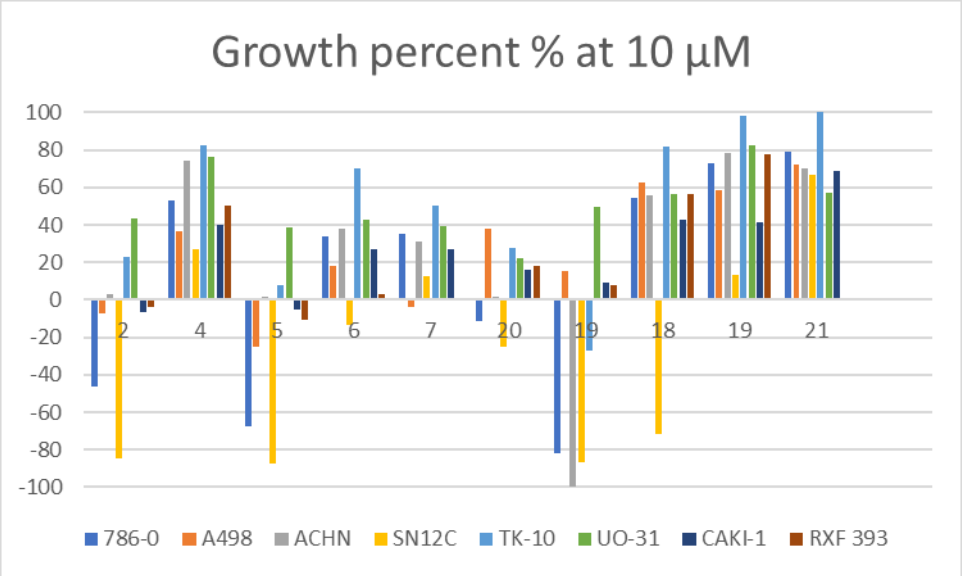

Figure 6.7.7.1. The effect of derivatives of lead compound **2** on renal cancer cell lines.

In the renal cancer cell lines, compound **2** performs relatively poorly compared to the other cell lines screened; the only notable result found in the SN12C cell line with an 84% of cell death. Compound **19** shows a great increase in cytotoxic activity in some of the cell lines, in particular, the activity is almost doubled in the 786-0 cancer cell line. Compound **19** also kills almost all of the ACHN cells while **17** and **18** almost completely inhibit cell growth in 786-0, TK-10, UO-31 and RXD 393 cells. Again, compound **5** shows similar profile to the lead **2**, while compounds **6** and **7** do not exhibit great activity. Surprisingly, derivative **20** does not have significant activity in any of the renal cancer cell lines screened, but **4** seems to inhibit cell growth achieving the highest activity in the TK-10 cell line.

In all the renal cancer cell lines screened the compounds have good activity, the GI_{50} values across all the derivatives showing comparable activity to that of lead compound **2**. The total growth inhibition is low for all compounds studied. Finally, lead compound **2** showed low LC_{50} values in the cell lines screened, but **17** unfortunately had high LC_{50} in the cell lines screened (Table 6.7.7.1).

Table 6.7.7.1. Evaluation of derivatives of lead compound **2** at five doses in renal cancer cell lines.

GI_{50} (μM)									
	2	**4**	**5**	**6**	**7**	**20**	**19**	**18**	**17**
786-0	1.70	1.62	1.74	1.66	1.70	1.78	1.70	1.62	1.86
A498	1.23	1.62	1.41	1.51	1.17	2.29	1.51	1.35	1.70
ACHN	1.74	2.82	1.74	1.70	1.74	2.88	1.66	1.78	3.55
CAKI-1	1.55	1.74	1.74	1.51	1.62	2.75	1.62	1.58	1.70
RXF 393	1.78	1.62	1.78	1.78	1.78	2.04	1.78	1.82	1.91
SN12C	1.74	1.70	1.70	1.66	1.66	1.86	1.66	1.66	1.74
TK-10	1.86	1.95	1.86	1.86	1.70	3.98	1.70	1.74	2.75
UO-31	1.74	2.95	1.74	1.78	1.70	2.19	1.70	1.78	4.37
TGI (μM)									
786-0	3.80	3.16	3.72	3.47	3.47	3.55	3.39	3.39	4.07
A498	2.69	3.16	2.82	3.02	2.63	9.77	3.09	2.82	4.68
ACHN	3.24	8.51	3.24	3.09	3.16	8.71	3.02	3.39	17.38
CAKI-1	3.09	3.55	3.47	3.02	3.16	11.22	3.02	3.16	3.80
RXF 393	3.55	3.02	3.63	3.39	3.39	4.90	3.47	3.55	3.80
SN12C	3.47	3.47	3.39	3.31	3.39	3.80	3.24	3.31	3.55
TK-10	3.80	4.79	3.63	3.63	3.31	16.22	3.31		7.59
UO-31	3.55	11.75	3.63	3.55	3.31	8.71	3.24	3.39	38.02

LC_{50} (µM)									
786-0		6.31				7.24			
A498	5.75	6.31		6.03	6.03	52.48			>100
ACHN	5.89	41.69	5.89		5.62	37.15			>100
CAKI-1		7.41			6.17	44.67			
RXF 393	7.24	5.75		6.61	6.46	19.95	6.61		
SN12C		7.08				7.76			
TK-10		21.88		7.08	6.46	66.07			>100
UO-31		58.88			6.31	45.71			>100

6.7.8. Cell growth inhibition effect of derivatives of 2 in breast cancer cell lines

The following breast cancer cell lines were used for this NCI screening: MCF7, MDA-MB-231/ATCC, MDA-MB-468, HS 578T, BT-549, T-47D and the results are presented in Table 6.7.8.1 and Figure 6.7.8.1.

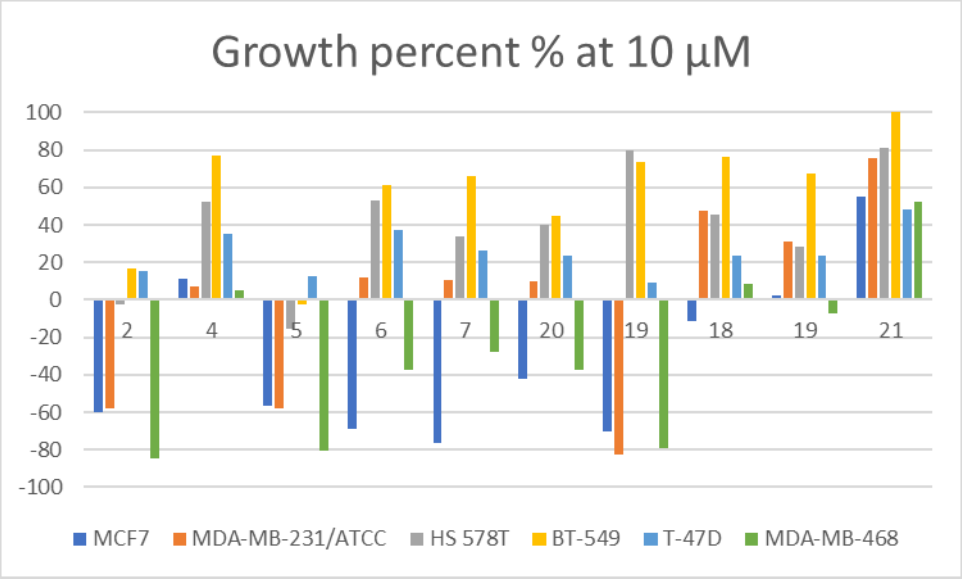

Figure 6.7.8.1. The effect of derivatives of lead compound **2** on breast cancer cell lines.

In the breast cancer cell lines compound **2** performs well, either by causing cell death or cell growth inhibition; in the cell line MDA-MB-468 we see cell death of 84% and in BT-549 16% cell growth. This activity is retained in compound **5**, except in BT-549 where we start to see cell death. In compounds **6** and **7** we only see cell death in two cell lines, MCF-7 in which both perform better than **2** and MDA-MB-468 in which they both perform worse than **2**. Thus, for most of the cell lines a bigger hydrophobic head is favourable. Compound **17** only shows cell death in MDA-MB-468 while in the other cell lines exhibits varying levels of cell growth inhibition. In the case of **19**, it exerts cell death of over 70% in MCF7, MDA-MB-231/ATCC and MDA-MB-468 showing no significant cell growth inhibition in the other cell lines. Compound **18** only leads to minor cell death in MCF7. Again **21** and **4** do not lead to cell death in this cancer category, **20** leads to cell death in MCF7 and MDA-MB-468 at moderate levels. Thus, the guanidine is more favourable.

Table 6.7.8.1. Evaluation of derivatives of lead compound **2** at five doses in breast cancer cell lines.

GI_{50} (μM)									
	2	**4**	**5**	**6**	**7**	**20**	**19**	**18**	**17**
MCF7	1.78	1.74	1.62	1.62	1.74	1.74	1.62	1.55	1.66
MDA-MB-231/ATCC	1.86	1.86	1.91	1.78	1.95	2.19	1.91	1.95	1.95
HS 578T	1.66	1.95	1.91	1.91	2.00	2.00	2.04	2.00	2.04
BT-549	1.78	1.74	1.91	1.78	1.66	3.89	1.91	1.78	1.91
T-47D	1.55	1.74	1.70	1.58	1.62	2.82	1.58	1.62	1.86
MDA-MB-468	1.55	1.48	1.58	1.55	1.38	1.62	1.74	1.51	2.09
TGI (μM)									
MCF7	4.17	3.47	3.72	3.55	3.80	3.72	3.39		3.89
MDA-MB-231/ATCC	3.98	3.98	3.98	3.89	4.27	5.01	3.72	3.98	
HS 578T	3.98	4.57	4.37	4.37	4.57	4.68		4.27	4.90
BT-549	3.39	3.24	3.47	3.31	3.24	16.98	3.55	3.31	3.63
T-47D	3.80	3.98	3.98	3.63	3.63	11.22	3.98	4.57	4.90
MDA-MB-468	3.63	3.47	3.55	3.39	3.16	3.47	3.72		4.47
LC_{50} (μM)									
MCF7		7.08				7.76			
MDA-MB-231/ATCC						20.42			

HS 578T		>100			>100	18.20			>100
BT-549				6.17		54.95			
T-47D		8.91				74.13		>100	>100
MDA-MB-468		8.13				7.41			

6.8. Conclusions and future perspectives

Anticancer activity observed by lead compound **2** was found not to be exerted through the same pathway as lead compound **1** through Western blot experiments. Through the on-going collaboration with Professor Daniela Zisterer, it was possible to evaluate the mechanism of action of lead **2** in the MM cell lines U266B1 and NCI-H929. First, the effect of this compound on the cell cycle was evaluated using flow cytometry. Thus, it was found that **2** leads to cell death without any cell cycle arrest after 72 hours and that over 50% of the cells were in sub G_1/G_0 suggesting that the cells had died. Next, annexin V/PI assays were carried to study if the cells undergo apoptosis or necrosis when treated with lead **2**. It was found that the cells do undergo apoptosis in a dose dependent manner, and that the U266BI cells line undergoes less apoptosis than NCI-H929. Further analysis were carried out finding that lead compound **2** targets the JAK/STAT pathway.

Considering that lead **2** was found to be effective in causing apoptosis in MM cell lines, the newly synthesised derivatives were screened in the two aforementioned MM cell

lines to evaluate their activity. In the instances where the linkers were modified no significant loss in activity was observed. When the hydrophobic head was modified, we saw changes in activity, signifying that some of the components of the head are needed by the compound for activity. This correlates with computational results, since when the CF_3 group was removed there was not only a loss in activity, but also a decrease in the docking Gscore values, suggesting that this group is part of the ligands pharmacophore. Moreover, this was also observed in compound where an SF_5 group was used in the hydrophobic head resulting in improved biding and activity, this can also be seen in **7**, where the Cl substituted for a Br. The change in the substitution pattern also led to no significant changes in activity. The most significant change in the activity was found when the polar group was derivatised. Completely removing the guanidium group, **22**, led to a significant loss in activity, this can also be seen in **21** where the guanidium was substituted for a an acetamide, this suggests that the positive charge as well as multiple hydrogen bonds given by the guanidinium. We saw improved activity when the guanidium was substituted with an aminoimidazoline. From this we can postulate that the positive charge, hydrogen bonds as well as hydrophobic moiety of the aminoimidazoline. Thus from these studies we can conclude that compound **20** has the best activity in the new derivatives, thus it's the new lead compound.

Finally, the new derivatives of **2** prepared were evaluated in 60 cancer cell lines in the NCI-DTP panel; unlike the derivatives of lead compound **1**, it was found that these compounds cause cell death rather than growth inhibition in most cases. This is especially evident in the leukemia cell lines where we can see most of the compounds exert cell death. This is further proof that compounds **1** and **2** have different mode of action. While the GI_{50} was found to be relatively low for most of the compounds tested, the LC_{50} was found to be too high, therefore no further tests were carried out by the NCI with these derivatives.

Lead compound **2** was shown to cause cell death in MM cell lines; furthermore, it was shown to affect key pathways which contribute to the tumorigenesis of MM. Further examination of the effect of lead **2** on key signalling pathways known to play a role in MM pathogenesis should be carried out as well as studies into the translational capacity

of compound 2 by examining its ability to synergise with other therapeutics. The efficacy of lead 2 in a MM mouse model could also be carried out to assess any unwanted cytotoxicity and the ability of this compound to induce cell death in the presence of a cytoprotective environment. Further examination of 2 in ex vivo MM patient samples that represent the wider MM community would be also required to garner further evidence of the anti-myeloma potential of lead compound 2.

6.9. References

(1) Diez-Cecilia, E.; Kelly, B.; Perez, C.; Zisterer, D. M.; Nevin, D. K.; Lloyd, D. G.; Rozas,

I. Guanidinium-Based Derivatives: Searching for New Kinase Inhibitors. *Eur. J. Med. Chem.* **2014**, *81*, 427–441. https://doi.org/https://doi.org/10.1016/j.ejmech.2014.05.025.

(2) Diez-Cecilia, E.; Carson, R.; Kelly, B.; van Schaeybroeck, S.; Murray, J. T.; Rozas, I. Probing a 3,4'-Bis-Guanidinium Diaryl Derivative as an Allosteric Inhibitor of the Ras Pathway. *Bioorg. Med. Chem. Lett.* **2015**, *25* (19), 4287–4292. https://doi.org/https://doi.org/10.1016/j.bmcl.2015.07.082.

(3) Previtali, V.; Mihigo, H. B.; Amet, R.; McElligott, A. M.; Zisterer, D. M.; Rozas, I. Exploring the Anti-Cancer Mechanism of Novel 3,4'-Substituted Diaryl Guanidinium Derivatives. *Pharmaceuticals* . 2020. https://doi.org/10.3390/ph13120485.

(4) MM in Ireland https://www.cancer.ie/cancer-information-and-support/cancer-types/multiple-myeloma.

(5) Catlett-Falcone, R.; Landowski, T. H.; Oshiro, M. M.; Turkson, J.; Levitzki, A.; Savino, R.; Ciliberto, G.; Moscinski, L.; Fernández-Luna, J. L.; Nuñez, G. Constitutive Activation of Stat3 Signaling Confers Resistance to Apoptosis in Human U266 Myeloma Cells. *Immunity* **1999**, *10* (1), 105–115. https://doi.org/https://doi.org/10.1016/S1074-7613(00)80011-4.

(6) Okkenhaug, K.; Graupera, M.; Vanhaesebroeck, B. Targeting PI3K in Cancer: Impact on Tumor Cells, Their Protective Stroma, Angiogenesis, and Immunotherapy. *Cancer Discov.* **2016**, *6* (10), 1090–1105. https://doi.org/10.1158/2159-8290.CD-16-0716.

(7) Xu, J. H.; Pfarr, N.; Endris, V.; Mai, E. K.; Hanafiah, N. H. M.; Lehners, N.; Penzel, R.; Weichert, W.; Ho, A. D.; Schirmacher, P. Molecular Signaling in Multiple Myeloma: Association of RAS/RAF Mutations and MEK/ERK Pathway Activation. *Oncogenesis* **2017**, *6*.

(8) Abramson, H. N. Kinase Inhibitors as Potential Agents in the Treatment of Multiple Myeloma. *Oncotarget* **2016**, *7* (49), 81926–81968. https://doi.org/10.18632/oncotarget.10745.

(9) Dervisis, N.; Klahn, S. Therapeutic Innovations: Tyrosine Kinase Inhibitors in Cancer. *Vet. Sci.* **2016**, *3* (1). https://doi.org/10.3390/vetsci3010004.

(10) Buettner, R.; Mora, L. B.; Jove, R. Activated STAT Signaling in Human Tumors Provides Novel Molecular Targets for Therapeutic Intervention. *Clin. cancer Res. an Off. J. Am. Assoc. Cancer Res.* **2002**, *8* (4), 945–954.

(11) Pene, F.; Claessens, Y.-E.; Muller, O.; Viguié, F.; Mayeux, P.; Dreyfus, F.; Lacombe, C.; Bouscary, D. Role of the Phosphatidylinositol 3-Kinase/Akt and MTOR/P70S6-Kinase Pathways in the Proliferation and Apoptosis in Multiple Myeloma. *Oncogene* **2002**, *21* (43), 6587–6597. https://doi.org/10.1038/sj.onc.1205923.

(12) Menu, E.; Kooijman, R.; Valckenborgh, E. Van; Asosingh, K.; Bakkus, M.; Camp, B. Van; Vanderkerken, K. Specific Roles for the PI3K and the MEK–ERK Pathway in IGF-1-Stimulated Chemotaxis, VEGF Secretion and Proliferation of Multiple Myeloma Cells: Study in the 5T33MM Model. *Br. J. Cancer* **2004**, *90* (5), 1076–1083. https://doi.org/10.1038/sj.bjc.6601613.

(13) Bieghs, L.; Johnsen, H. E.; Maes, K.; Menu, E.; Van Valckenborgh, E.; Overgaard, M. T.; Nyegaard, M.; Conover, C. A.; Vanderkerken, K.; De Bruyne, E. The Insulin-like Growth Factor System in Multiple Myeloma: Diagnostic and Therapeutic Potential. *Oncotarget* **2016**, *7* (30), 48732–48752. https://doi.org/10.18632/oncotarget.8982.

(14) Siveen, K. S.; Sikka, S.; Surana, R.; Dai, X.; Zhang, J.; Kumar, A. P.; Tan, B. K. H.; Sethi, G.; Bishayee, A. Targeting the STAT3 Signaling Pathway in Cancer: Role of Synthetic and Natural Inhibitors. *Biochim. Biophys. Acta* **2014**, *1845* (2), 136–154. https://doi.org/10.1016/j.bbcan.2013.12.005.

(15) Matthes, T.; Manfroi, B.; Huard, B. Revisiting IL-6 Antagonism in Multiple Myeloma. *Crit. Rev. Oncol. Hematol.* **2016**, *105*, 1–4. https://doi.org/10.1016/j.critrevonc.2016.07.006.

(16) Chong, P. S. Y.; Chng, W.-J.; de Mel, S. STAT3: A Promising Therapeutic Target in Multiple Myeloma. *Cancers (Basel).* **2019**, *11* (5), 731. https://doi.org/10.3390/cancers11050731.

(17) Yu, C. L.; Meyer, D. J.; Campbell, G. S.; Larner, A. C.; Carter-Su, C.; Schwartz, J.; Jove, R. Enhanced DNA-Binding Activity of a Stat3-Related Protein in Cells Transformed by the Src Oncoprotein. *Science* **1995**, *269* (5220), 81–83. https://doi.org/10.1126/science.7541555.

(18) Garcia, R.; Bowman, T. L.; Niu, G.; Yu, H.; Minton, S.; Muro-Cacho, C. A.; Cox, C. E.; Falcone, R.; Fairclough, R.; Parsons, S. Constitutive Activation of Stat3 by the Src and JAK Tyrosine Kinases Participates in Growth Regulation of Human Breast Carcinoma Cells. *Oncogene* **2001**, *20* (20), 2499–2513. https://doi.org/10.1038/sj.onc.1204349.

(19) de Oliveira, M. B.; Fook-Alves, V. L.; Eugenio, A. I. P.; Fernando, R. C.; Sanson, L. F. G.; de Carvalho, M. F.; Braga, W. M. T.; Davies, F. E.; Colleoni, G. W. B. Anti-Myeloma Effects of Ruxolitinib Combined with Bortezomib and Lenalidomide: A Rationale for JAK/STAT Pathway Inhibition in Myeloma Patients. *Cancer Lett.* **2017**, *403*, 206–215. https://doi.org/10.1016/j.canlet.2017.06.016.

Chapter 7 – Experimental

7.1. Computational experimental

7.1.1. Autodock

DFT calculations

Density Functional Theory (DFT) was used to optimise the structures of **1, 2, VP-65S** and **VP-A87**. This was performed using the Gaussian16 package[1] at the B3LYP[2] computational level with the 6-311++G** basis set[3] and PCM[4] solvation model.

Molecular Docking: AutoDock

Receptor preparation: The B-Raf model prepared by the Rozas group was used, The model was imported into the AutoDock Vina software.[5] Polar hydrogen atoms were added and the coordinates of the binding site were determined using the AutoGrid function. The Gasteiger charges were added, and the macromolecule was saved as a pdbqt file.

Ligand preparation: The optimised structure was imported into GaussView in Gaussian16, where it was converted to PDB format. The PDB structure was imported to Autodock Vina where its torsions were set. The ligand structure was then converted to pdbqt format which was used for the docking experiment.

Docking: After receptor and ligand preparation, the configuration file was prepared in txt format containing the correct coordinates. The docking experiment was then run

through the command terminal using the Autodock Vina software. Upon completion of the calculation, output files were generated containing binding poses.

Visualisation: Visualisation of the best binding poses was conducted using PyMoL[6] and VMD.[7]

7.1.2. Molecular Docking: Schrodinger

In order to reveal the binding modes of synthesized derivatives of compounds 1 and 2, docking simulation were performed targeting the appropriate crystal structures. Prior to docking, the crystal structures were retrieved from the protein data bank (PDB).[8] The protein structures were prepared using protein preparation wizard and optimized by removing the water molecules, hetero atoms and co-factors. Hydrogen, missing atoms, bonds and charges were computed through Maestro.[9]

All of the compounds to be docked were prepared and optimized using the built ligand preparation, LigPrep module implemented in Maestro. Ligand preparation includes generating various tautomers, assigning bond orders, ring conformations and stereo chemistries. All the conformations generated were minimized using OPLS2005 force field prior to docking study.

Following the preparation of the ligands and protein, the receptor grid box was generated. As PDBs containing a ligand were used, thus this was used as the binding site for docking without changing the size of the grid box, the number of outputs for docking was set to 10.

The induced-fit docking (IFD) is a method for modelling the conformational changes to the receptor induced by ligand binding.[10] This protocol models induced-fit docking ligands using the steps reported by Tutone et al., 2019.[11] Initial docking of each ligand is performed using a softened potential (van der Waals radii scaling). Then, a side-chain prediction within a given distance of any ligand pose is performed. Subsequently, a minimization of the same set of residues and the ligand for each protein/ligand complex pose is performed. After this stage, any receptor structure in each pose reflects an induced fit to the ligand structure and conformation. Finally, the ligand is rigorously

docked, using Glide XP, into the induced-fit receptor structure. Upon completion of the calculation, output files were generated containing binding poses which are ranked based on their theoretical binding affinity in the form of Gscores (Kcal mol^{-1}). The output poses were visualised in Maestro.

7.2. Synthetic chemistry

7.2.1. Materials and Methods

Reagents were purchased at the highest commercial quality and used without further purification, unless otherwise stated. Dry solvents were obtained from PureSolv™ solvent purification system (Innovative Technology, Inc.) or otherwise purchased from Sigma- Aldrich. Solvents for synthesis purposes were used at GPR grade. Yields refer to chromatographically and spectroscopically (1H NMR) homogeneous materials, unless otherwise stated. Reactions were monitored by thin layer chromatography (TLC) using Merck Kieselgel 60 F254 silica gel or aluminium oxide plates. Visualisation was achieved by UV light (254 nm) and basic aqueous potassium permanganate ($KMnO_4$) or ninhydrin and heat as developing agents. Concentration of organic solvents was performed on a rotary evaporator under reduced pressure followed by further evacuation using a two-stage mechanical pump. Deuterated solvents for NMR use were purchased from Apollo and Euriso-top. Chromatographic columns were run using silica gel 60 (230–400 mesh ASTM). NMR spectra were recorded on Bruker DPX–400 Avance and Brucker AV-600 spectrometers, operating at 400.13 MHz and 600.1 MHz for 1H NMR; 100.6 MHz and 150.9 MHz for 13C-NMR. Shifts for 1H and 13C NMR are referenced to the internal solvent signals. NMR data were processed using MestReNova software.

HRMS spectra were measured on a Micromass LCT electrospray TOF instrument with a WATERS 2690 autosampler and methanol/acetonitrile as carrier solvent. Melting points were determined using a Stuart Scientific Melting Point SMP1 apparatus and are uncorrected. Infrared spectra were recorded on a Perkin Elmer Spectrum One FT-IR Spectrometer equipped with a Universal ATR sampling accessory.

HPLC purity analysis was carried out using a Varian ProStar system equipped with a Varian

Prostar 335 diode array detector and a manual injector (20 µL). For purity assessment, UV

detection was performed at 254 nm and peak purity was confirmed using a purity channel.

The stationary phase consisted of an ACE 5 C18-AR column (150 × 4.6 mm), and the mobile

phase used the following gradient system, eluting at 1 mL/min: aqueous formate buffer (30

mM, pH 3.0) for 10 min, linear ramp to 85% methanol buffered with the same system over 25 min, hold at 85% buffered methanol for 10 min. Minimum requirement for purity was set at 95.0 %.

7.2.2. General procedures

Method A: *General procedure for the synthesis of the asymmetric 3,4-bis-Boc-protected guanidino phenyl pyridinyl derivatives.*

To a solution of starting amine (1.00 eq.), *N*,*N*'-bis-(tert-butoxycarbonyl)-S-methylisothiourea) (1.05 eq.) and triethylamine (3.5 eq.) in CH_2Cl_2 (0.193M) at 0 °C, mercury(II) chloride (1.05 eq.) was added. The mixture was stirred at RT until the reaction was complete as adjudged by disappearance of starting material in TLC analysis. The reaction mixture was diluted with EtOAc (100 mL) and filtered through a

pad of Celite® in order to remove the mercury sulphide precipitate formed. The filter cake was rinsed with EtOAc (2 × 25 mL). The organic phase was extracted with water (2 × 30 mL), washed with brine (30 mL), dried over anhydrous $MgSO_4$, and concentrated under vacuum to give a residue. Next, it was purified by flash chromatography on silica gel (eluting with a gradient of hexane:EtOAc) as specified.

Method B: *General procedure for the deprotection of Boc-protected guanidines using hydrochloric acid solutions in organic solvents.*

To a solution of the corresponding Boc-protected guanidine (1 eq.) in 1,4-dioxane, 4M HCl in 1,4-dioxane (6 eq. per Boc group) was added to reach a guanidine final concentration of 0.2M. The mixture was stirred at 55 °C until the reaction was complete (typically 6-8 h, as adjudged by TLC). At the reaction endpoint, solvent and HCl were evaporated under vacuum and the crude salt was dissolved in the minimum volume of $CHCl_3$. It was then purified by flash chromatography (silica gel, $CHCl_3$:MeOH). The purified fractions were evaporated to afford the pure hydrochloride salt.

Method C: *General procedure for N-Arylation*.

An oven-dried round bottom flask was charged with a magnetic stir bar, $Pd_2(dba)_3$ (3 mol%), organophosphorus ligand (3-5 mol%), aniline derivative (1 eq.), base (1.4 eq.) and bromine source (1 eq.). The flask was evacuated and refilled with argon (three times). In the case of liquid bromine source, it was added by syringe under a counterflow of argon, followed by syringe addition of toluene (2 mL/mmol). The mixture was placed in a preheated oil bath at 90 °C and left stirring for 24 h. The reaction mixture was then cooled to room temperature, diluted with EtOAc, filtered through a pad of Celite®, and washed with water. The organic layer was washed with brine, dried over $MgSO_4$, concentrated under vacuum and purified by silica gel chromatography (hexanes:EtOAc) to obtain the desired product.

Method D: *General procedure for nitro reduction using Palladium on carbon (Pd/C).*

To a solution of appropriate nitro derivative (1 eq.) in specified solvent, was added 10% Pd/C mixture (10 mol%), and the reaction mixture was stirred at room temperature

under hydrogen atmosphere (1.0 atm) for 24 h. The reaction mixture was filtered off, and the filtrate was concentrated in vacuo. The residue was purified by silica gel chromatography (hexanes:EtOAc), and the desired fractions were concentrated under reduced pressure to obtain the desired product.

Method E: *General procedure for nitroreduction using $SnCl_2 \cdot 2H_2O$.*

A mixture of appropriate nitro derivative (1 eq.) dissolved in absolute ethanol and $SnCl_2 \cdot 2H2O$ (6/15 eq.) was stirred at 70 °C until the reaction was adjudged complete (typically 3 hrs adjudged by TLC as specified for each compound). The solution was allowed to cool down and then poured onto ice. The solution was basified to pH 7-8 by addition of 5% aqueous $NaHCO_3$. The solution was washed with water, the organic layer extracted with EtOAc, washed with brine, dried over $MgSO_4$, concentrated under vacuum and purified by silica gel chromatography (hexanes:EtOAc) to obtain the desired product.

7.2.3. Synthesis and Characterisation

1-(5-{3-[4-Bromo-3-(trifluoromethyl)phenylamino]phenoxy}pyridin-2-yl)guanidine Hydrochloride (7)

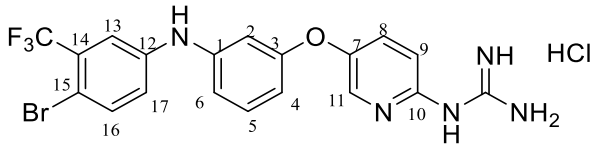

Following Method B, **40** (58 mg, 0.09 mmol) was dissolved in 4M HCl in 1, 4-dioxane (0.26

mL, 1.04 mmol) and in additional dioxane (0.17 mL) until a final concentration of 0.2M was

reached. After 8 h stirring at 55 °C, the reaction was adjudged complete (TLC), solvents were

evaporated and the residue was purified by silica gel chromatography ($CHCl_3$:MeOH) to

afford **3**, the pure hydrochloride salt as a white solid (40 mg, 76%) **Mp:** 90-91 ℃

^{1}H NMR (400 MHz, MeOD) δ 8.16 (d, *J* = 2.6 Hz, 1H, H-11), 7.62 (dd, *J* = 8.9, 2.9 Hz, 1H, H-8), 7.59 (d, *J* = 8.7 Hz, 1H, H-16), 7.40 (d, *J* = 2.8 Hz, 1H, H-13), 7.32 (t, *J* = 8.1 Hz, 1H, H-5), 7.19 (dd, *J* = 8.7, 2.7 Hz, 1H, H-17), 7.08 (d, *J* = 9.1 Hz, 1H, H-9), 6.93 (dd, *J* = 7.8, 1.8 Hz, 1H, H-6), 6.77 (t, *J* = 2.2 Hz, 1H, H-2), 6.64 (dd, *J* = 8.2, 1.7 Hz, 1H, H-4) ppm.

^{13}C NMR (101 MHz, MeOD) δ 160.2 (qC), 152.6 (qC), 149.6 (qC), 146.3 (qC), 145.6 (qC), 139.6 (CH Ar, C-11), 137.7 (CH Ar, C-16), 132.9 (CH Ar, C-5), 132.6 (CH Ar, C-8), 122.7 (CH Ar, C-17),117.4 (qC) 116.3 (CH Ar, C-13), 115.7 (CH Ar, C-9), 113.1 (CH Ar, C-4), 109.6 (CH Ar, C-2) ppm.

^{19}F NMR (376 MHz, MeOD) δ -64.15 (s) ppm.

HRMS (m/z ESI$^-$): Found 464.0333 $(M - H)^-$, C19H14BrF3N5O requires: 464.0339.

ν_{max} (ATR)/cm^{-1}: 3264 (NH), 2923, 2863, 1684, 1629, 1595, 1474 (C=N), 1400, 1332, 1229 (C-O), 1129 (CF_3), 1115 (C-Cl), 977, 998.

HPLC: 96.82% (*t*R 33.72 min).

1-(4-{3-[4-Bromo-3-(trifluoromethyl)phenylamino]phenoxy}phenyl)guanidine Hydrochloride (15)

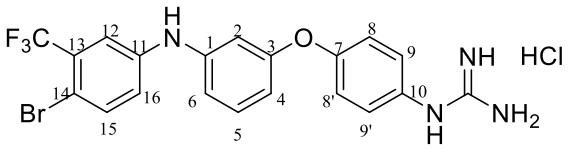

Following Method B (53 mg, 0.08 mmol), **40a** was dissolved in 4M HCl in dioxane (0.24 mL, 0.96 mmol) and in additional dioxane (0.16 mL) until a final concentration of 0.2M was reached. After 8 h stirring at 55 °C, the reaction was adjudged complete (TLC), solvents were evaporated and the residue was purified by flash chromatography to afford **3a**, the pure hydrochloride salt as a white-brown solid (34.9 mg, 78%) **Mp**: 59-60 °C

^{1}H NMR (400 MHz, MeOD) δ 7.55 (d, *J* = 8.7 Hz, 1H, H-15), 7.37 (d, *J* = 2.8 Hz, 1H, H-12), 7.32 – 7.25 (m, 3H, H-5, H-9, and H-9'), 7.16 (dd, *J* = 8.7, 2.8 Hz, 1H, H-16), 7.13 – 7.09 (m, 2H, H-8 and H-8'), 6.90 (dd, *J* = 8.1, 2.1 Hz, 1H, H-6), 6.78 (t, *J* = 2.2 Hz, 1H, H-2), 6.63 (dd, *J* = 8.1, 2.3 Hz, 1H, H-4) ppm.

^{13}C NMR (101 MHz, MeOD) δ 157.7 (qC), 156.99 (qC), 156.8 (qC), 143.8 (qC), 143.5 (qC), 135.4 (qC), 130.4 (CH Ar, C-15), 130.2 (CH Ar, C-5),), 129.9 (qC), 129.5 (qC), 127.4 (2 CH Ar, C- and C-9'), 124.4 (qCF3), 121.6 (qC), 120.1 (CH Ar, C-16), 119.5 (2 CH Ar, C-8 and C-8'), 115.0 (q, *J* = 5.6 Hz, CH Ar, C-12), 113.6 (CH Ar, C-6), 111.7 (CH Ar, C-4), 108.4 (CH Ar, C-2) ppm.

^{19}F NMR (376 MHz, MeOD) δ -64.15 (s) ppm.

HRMS (m/z ESI^{+}): found : 465.0546 $(M + H)^{+}$, C20H17BrF3N4O requires: 465.0538.

ν_{max} (ATR)/cm^{-1}: 3295 (NH), 3163, 2923, 2853, 2400, 1664 (C=O), 1595 (C=N), 1504, 1482,

1441,1333, 1258, 1217 (CF3), 1127, 1112 (C-Br), 1027, 999, 977, 825.

HPLC: 97.22% (*t*R 34.80 min)

1-(4-{3-[3-(Trifluoromethyl)phenylamino] pyridin-2-yl })guanidine hydrochloride (5)

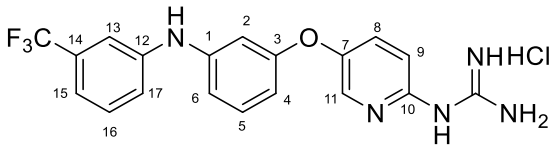

Following Method B, **41** (371mg, 0.34 mmol) was dissolved in 4M HCl in 1, 4-dioxane (1.90

mL, 7.56 mmol) and in additional dioxane (1.25 mL) until a final concentration of 0.2M was

reached. After 6 h stirring at 55 °C, the reaction was adjudged complete (TLC), solvents were

evaporated and the residue was purified by flash chromatography to afford, **5**, the pure

hydrochloride salt as a white solid (242 mg, 80%) **Mp**: 92-94 ℃.

^{1}H NMR (400 MHz, MeOD) δ 8.11 (d, *J* = 2.9 Hz, 1H, H-11), 7.57 (dd, *J* = 8.9, 2.9 Hz, 1H, H-8), 7.36 (t, *J* = 8.3 Hz, 1H, H-13), 7.26 (m, 3H, H-9, -15 and H-17), 7.06 (t, *J* = 8.3 Hz, 2H, H-5 and H-16), 6.88 (dd, *J* = 8.1, 2.0 Hz, 1H, H-6), 6.73 (t, *J* = 2.2 Hz, 1H, H-2), 6.55 (dd, *J* = 8.1, 2.3 Hz, 1H, H-4)ppm.

^{13}C NMR (101 MHz, MeOD) δ 160.2 (qC), 157.8 (qC), 152.7 (qC), 149.5 (qC), 146.9 (qC), 146.3 (qC), 139.5 (CH Ar, C-11), 132.7 (CH Ar, C-8), 132.6 (CH Ar, C-5 or C-16),), 131.9 (CH Ar, C-5 or C-16),), 122.3 (CH Ar, C-17), 118.3 (CH Ar, C-13), 116.3 (qC), 115.2 (CH Ar, C-9), 114.9 (CH Ar, C-6), 112.5 (CH Ar, C-4), 109.1 (CH Ar, C-2) ppm.

^{19}F NMR (377 MHz, MeOD) δ -64.39 (s) ppm.

HRMS (m/z ESI^{+}): found : 388.1379 (M+ H)$^{+}$, C19H17F3N5O, requires: 388.1380

ν_{max} (ATR)/cm^{-1}: 3301 (NH), 3135 (NH), 1665, 1587 (C=N), 1490, 1486, 1335 (C-N), 1216 (C-O), 1161, 1116 (CF_3), 1067 (C-Cl), 976, 836, 785, 689.

HPLC: 98.02% (*t*R 32.87 min)

1-(4-{3-[3-(Trifluoromethyl)phenylamino] pyridin-2-yl })guanidine hydrochloride (6)

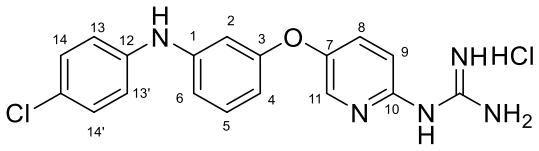

Following Method B, **41** (97mg, 0.18 mmol) was dissolved in 4M HCl in 1, 4-dioxane (0.53

mL, 2.10 mmol) and in additional dioxane (0.9 mL) until a final concentration of 0.2M was

reached. After 6 h stirring at 55 °C, the reaction was adjudged complete (TLC), solvents were

evaporated and the residue was purified by flash chromatography to afford, **5**, the pure

hydrochloride salt as a white solid (58 mg, 78%) **Mp**: 50-52 ℃.

^{1}H NMR (400 MHz, MeOD) δ 8.11 (d, *J* = 2.9 Hz, 1H, H-11), 7.57 (dd, *J* = 8.9, 2.9 Hz, 1H, H-8), 7.25 – 7.17 (m, 3H, H-5, H-14 and H-14'), 7.10 – 7.04 (m, 2H, H-13 and H-13'), 6.88 (dd, *J* = 8.1, 2.0 Hz, 1H, H-6), 6.73 (t, *J* = 2.2 Hz, 1H, H-2), 6.55 (dd, *J* = 8.1, 2.3 Hz, 1H, H-4) ppm.

^{13}C NMR (101 MHz, MeOD) δ 158.1 (qC), 156 (qC), 150.9 (qC), 147.6 (qC), 145.9 (qC), 142.1 (CH Ar, C-11), 137.3 (CH Ar, C-8), 130.7 (CH Ar, C-5), 130.4 (qC), 129.8 (CH Ar, C-14 and C-14'), 125.2 (qC), 119.1 (CH Ar, C-13 and C-13'), 114.3 (CH Ar, C-9), 112.5 (CH Ar, C-6), 109.7 (CH Ar, C-4), 106.7 (CH Ar, C-2) ppm.

HRMS (m/z ESI^{+}): Found : 354.1116 $(M + H)^{+}$, C18H17ClN5O requires: 354.1116.

ν_{max} (ATR)/cm^{-1}: 3297 (N-H), 3126 (N-H), 1688, 1586 (C=N), 1502, 1485 (C-N), 1325, 1216 (C-O), 1142 (C-Cl), 997, 972, 823, 770, 689, 604, 588, 570.

HPLC: 98.94% (*t*R 33.72 min)

1-(5-(3-(phenylamino) phenoxy) pyridin-2-yl) guanidine hydrochloride (9)

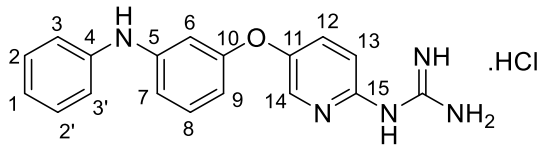

43 (130.5 mg, 0.25 mmol) was dissolved in 4M HCl in dioxane (0.35 mL, 1.4 mmol) and in additional dioxane (0.35 mL) until a final concentration of 0.2 M was reached. After 8 h stirring at 55 °C, the reaction was adjudged complete (TLC), solvents were evaporated and the residue was purified by silica gel (CH_3Cl:MeOH) chromatography to afford the pure hydrochloride salt **7** as a white-yellow solid (41.5 mg, 52 %). **Mp**: > 120˚C.

^{1}H NMR (600 MHz, CD_3OH) δ 8.08 (d, *J*= 2.8 Hz, 1H, H-14), 7.53 (dd, *J*= 2.8, 5.9 Hz, 1H, H-12), 7.26-7.16 (m, 3H, H-1, H-3 & H-3'), 7.13-7.06 (m, 3H, H-2, H-2' & H-13), 6.88 (m, 2H, H-7 & H-8), 6.73 (t, *J*= 2.2 Hz, 1H, H-6), 6.43 (dd, *J*= 2.2, 5.8 Hz, 1H, H-9) ppm.

^{13}C NMR (101 MHz, CD_3OH) δ 158.1 (C=N), 155.5 (qC, C-10), 151 (qC, C-15), 147.4 (qC, C-11), 146.6 (qC, C-5), 143.1 (qC, C-4), 137.3 (CH Ar, C-14), 130.6 (CH Ar, C-1), 130.2 (CH Ar, C-12), 129.1 CH Ar, C-3 & C-3'), 121.7 (CH Ar, C-8), 118.4 (CH Ar, C-2 & C-2'), 114.4 (CH Ar, C-13), 112.3 (CH Ar, C-7), 109.2 (CH Ar, C-9), 106.2 (CH Ar, C-6) ppm.

HRMS (*m/z* ESI^+): Found: 320.1501 $(M + H)^+$, C18H18N5Orequires 320.1506.

ν_{max} (ATR)/cm^{-1}: 3373 (N-H), 3130, 2985, 1769 (C=O), 1624, 1565, 1458, 1387, 1286 (C-N), 1219 (C-O), 1144 (C-O), 1100, 862, 754, 687.

HPLC: 95.9 % (tR 31.44 min).

1-(5-(3-(dimethylamino)phenoxy)pyridin-2-yl)guanidine hydrochloride (10)

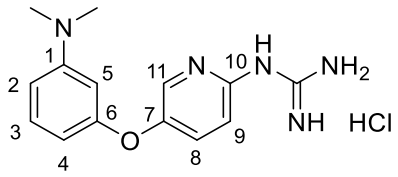

44 (122.6 mg, 0.26 mmol) was dissolved in 4M HCl in 1,4-dioxane (0.75 mL) and an additional dioxane (0.55 mL) until the final concentration of 0.2 M was reached. After 8 h stirring at 55˚C the reaction was adjudged complete by TLC. The crude product was dried and purified by silica gel chromatography ($CHCl_3$: MeOH) to afford **8**, a brown oil (21.5 mg, 27%).

^{1}H NMR (400 MHz, $CDCl_3$) δ 8.08 (d, *J*= 2.9 Hz, 1H, H-11), 7.53 (dd, *J*= 5.9, 2.9 Hz, 1H, H-2), 7.21 (t, *J*= 8.2 Hz, 1H, H-3), 7.06 (d, *J*= 8.9 Hz, 1H, H-9), 6.60 (dd, *J*= 6.3, 2.1 Hz, 1H, H-4), 6.44 (t, *J*= 2.3 Hz, 1H, H-5), 6.31 (dd, *J*= 6.1, 1.1 Hz, 1H, H-8) ppm.

^{13}C NMR (101 MHz, $CDCl_3$) δ 155.7 (C=N), 152.8 (C-6), 151.9 (C-7), 147.2 (C-1), 136.5 (C-11), 130.3 (C-10), 129.8 (C-3), 129.7 (C- 2), 113.9 (C-9), 109.4 (C-4), 105.4 (C-8), 102.8 (C-5), 39.1 (CH_3) ppm.

HRMS (*m/z* ESI$^+$): found: 272.1516, $(M + H)^+$, C14H18N5O, Requires: 272.1506

ν_{max} (ATR)/cm^{-1}: 3200, 2923 (N-H), 2367, 1672, 1598, 1477, 1379, 1232 (C-N), 1141, 999, 826, 669.

HPLC: 98.81 % (tR 20.36 min).

1-(5-{4-[4-Bromo-3-(trifluoromethyl)phenylamino]phenoxy}pyridin-2-yl)guanidine Hydrochloride (13)

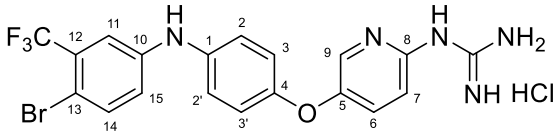

Following Method B, **45 (** 201mg, 0.34 mmol) was dissolved in 4M HCl in 1, 4-dioxane (1.02

mL, 7.56 mmol) and in additional dioxane (0.66 mL) until a final concentration of 0.2M was

reached. After 6 h stirring at 55 °C, the reaction was adjudged complete (TLC), solvents were

evaporated and the residue was purified by flash chromatography to afford, **8**, the pure

hydrochloride salt as a white solid (126 mg, 88%) **Mp**: 89-90 °C

^{1}H NMR (400 MHz, MeOD) δ 8.12 (d, *J* = 2.9 Hz, 1H, H-9), 7.59 – 7.53 (m, 2H, H-6 and H-14), 7.34 (d, *J* = 2.9 Hz, 1H, H-11), 7.24 (m, 2H, H-2 and H-2'), 7.14 (dd, *J* = 8.7, 2.8 Hz, 1H, H-15), 7.07 (dd, *J* = 7.2, 4.8 Hz, 3H, H-3, H-3' and H-7) ppm.

^{13}C NMR (101 MHz, MeOD) 13C NMR 155.4 (qC), 151.5 (qC), 151.1 (qC), 146.8 (qC), 144.5 (qC), 138.4 (qC), 136.2 (CH Ar, C-9), 135.3 (CH Ar, C-6), 129.2 (CH Ar, C-14), 120.9 (CH Ar, C-2, C-2' and C-7), 119.9 (CH Ar, C-3 and C-3'), 118.8 (CH Ar, C-15), 114.0 (CH Ar, C-11) ppm.

^{19}F NMR (377 MHz, MeOD) δ -64.17 (s) ppm.

HRMS (m/z ESI^{+}): Found : 466.0488 $(M + H)^{+}$, C19H16BrF3N5O requires: 466.0485.

ν_{max} (ATR)/cm^{-1}: 3264 (NH), 2923, 2863, 1684, 1629, 1595, 1474 (C=N), 1400, 1332, 1229 (C-O), 1129 (CF3), 1115 (C-Br), 977, 998.

HPLC: 97.94 % (tR 35.64 min).

1-(5-{4-[4-chloro-3-(trifluoromethyl)phenylamino]phenoxy}pyridin-2-yl)guanidine Hydrochloride (14)

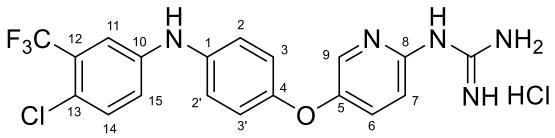

Following Method B, **46** (200 mg, 0.32 mmol) was dissolved in 4M HCl in dioxane (0.96 mL, 3.86 mmol) and in additional dioxane (0.65 mL) until a final concentration of 0.2M was

reached. After 8 h stirring at 55 °C, the reaction was adjudged complete (TLC), solvents were

evaporated and the residue was purified by silica gel chromatography ($CHCl_3$:MeOH) to afford the pure hydrochloride salt as a white solid (136 mg, 93%). **Mp**: 89 - 91 °C

1H NMR (400 MHz, MeOD) δ 8.07 (dd, *J* = 3.0, 0.5 Hz, 1H, H-9), 7.52 (dd, *J* = 8.9, 3.0 Hz, 1H, H-6), 7.32 (m, 2H, H-11 and H-14), 7.19 – 7.13 (m, 3H, H-15, H-3 and H-3'), 7.07 – 6.99 (m, 3H, H-7, H-2 and H-2') ppm.

^{13}C NMR (101 MHz, DMSO) δ 155.4 (qC-18), 151.4 (qC-13), 150.6 (qC-17), 147.7 (qC-12), 144.4 (qC-2), 138.2 (qC- 7), 137.1 (C-14), 132.9 (C-3), 130.5 (C-15), 127.6 (qC-6), 124.3 (C-19), 121.4 (C-10 and C-11), 120.3 (C-8 and C-9), 119.4 (C-5), 118.8 (qC-1), 115.1 (C-16), 114.1 (C-4) ppm.

^{19}F NMR (376.5 MHz, MeOD) δ - 64.1 (s) ppm.

HRMS (*m/z* ESI$^+$): Found: 422.0996, $(M + H)^+$, C19H16ClF3N5O requires: 422.0990.

ν_{max} (ATR)/cm^{-1}: 3297.24 (N-H stretch), 1681.37 (C=N stretch), 1605.21 (N-H bend),1473.80 (N-O stretch), 1229.95 (C-F stretch), 1172.14 (C-N stretch), 823.09 (C-Cl stretch).

HPLC: 98.35 % (tR 33.83 min).

1-(5-{4-[4-chloro-3-(trifluoromethyl)phenylamino]phenoxy}pyridin-2-yl)guanidine Hydrochloride (15)

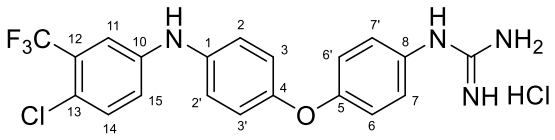

Following Method B, **46** (200 mg, 0.32 mmol) was dissolved in 4M HCl in dioxane (0.96 mL, 3.86 mmol) and in additional dioxane (0.65 mL) until a final concentration of 0.2M was

reached. After 8 h stirring at 55 °C, the reaction was adjudged complete (TLC), solvents were

evaporated and the residue was purified by silica gel chromatography ($CHCl_3$:MeOH) to afford the pure hydrochloride salt as a white solid (136 mg, 93%). **Mp**: 94 - 96 °C

^{1}H NMR (400 MHz, MeOD) δ 7.37 (d, *J* = 8.8 Hz, 1H, H-14), 7.33 (d, *J* = 2.7 Hz, 1H, H-11), 7.30 – 7.26 (m, 2H, H-7 and H-7'), 7.22 – 7.17 (m, 3H, H-15, H-2 and H-2'), 7.11 – 7.03 (m, 4H, H-3, H-3', H-6 and H-6') ppm.

^{13}C NMR (101 MHz, MeOD) δ 155.4 (qC-18), 151.4 (qC-13), 150.6 (qC-17), 147.7 (qC-12), 144.4 (qC-2), 138.2 (qC- 7), 137.1 (C-14), 132.9 (C-3), 130.5 (C-15), 127.6 (qC-6), 124.3 (C-19), 121.4 (C-10 and C-11), 120.3 (C-8 and C-9), 119.4 (C-5)m 118.8 (qC-1), 115.1 (C-16), 114.1 (C-4) ppm.

^{19}F NMR (376.5 MHz, MeOD) δ – 64.15 (s) ppm.

HRMS (*m/z* ESI$^+$): Found: 421.1044, (M + H)$^+$, C19H16ClF3N5O requires: 421.1043.

ν_{max} (ATR)/cm^{-1}: 3297 (N-H stretch), 1681 (C=N stretch), 1605 (N-H bend), 1473 (N-O stretch), 1229 (C-F stretch), 1172 (C-N stretch), 823 (C-Cl stretch).

HPLC: 99 % (tR 33.13 min).

1-(5-{4-[3-(trifluoromethyl)phenylamino]phenoxy}pyridin-2-yl)guanidine Hydrochloride (11)

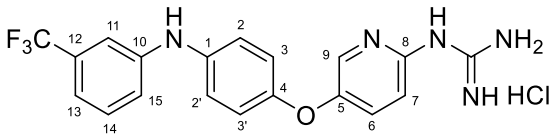

Following Method B, **47** (363mg, 0.34 mmol) was dissolved in 4M HCl in 1, 4-dioxane (1 mL, 7.56 mmol) and in additional dioxane (0.61 mL) until a final concentration of 0.2M was reached. After 6 h stirring at 55 °C, the reaction was adjudged complete (TLC), solvents were evaporated and the residue was purified by flash chromatography to afford, **10**, the pure hydrochloride salt as a white solid (238 mg, 79%) **Mp**: 92-94 ℃

^{1}H NMR (400 MHz, MeOD) δ 8.11 (d, *J* = 2.9 Hz, 1H, H-11), 7.57 (dd, *J* = 8.9, 2.9 Hz, 1H, H-8), 7.36 (t, *J* = 8.3 Hz, 1H, H-13), 7.26 (m, 3H, H-9, -15 and H-17), 7.06 (t, *J* = 8.3 Hz, 2H, H-5 and H-16), 6.88 (dd, *J* = 8.1, 2.0 Hz, 1H, H-6), 6.73 (t, *J* = 2.2 Hz, 1H, H-2), 6.55 (dd, *J* = 8.1, 2.3 Hz, 1H, H-4) ppm.

^{13}C NMR (101 MHz, MeOD) δ 160.2 (qC), 157.8 (qC), 152.7 (qC), 149.5 (qC), 146.9 (qC), 146.3 (qC), 139.5 (CH Ar, C-11), 132.7 (CH Ar, C-8), 132.6 (CH Ar, C-5 or C-16), 131.9 (CH Ar, C-5 or C-16), 122.3 (CH Ar, C-17), 118.3 (CH Ar, C-13), 116.3 (s), 115.2 (CH Ar, C-9), 114.9 (CH Ar, C-6), 112.5 (CH Ar, C-4), 109.1 (CH Ar, C-2) ppm.

^{19}F NMR (377 MHz, MeOD) δ -64.31 (s) ppm.

HRMS (m/z ESI^{+}): found : 388.1380 $(M + H)^{+}$, C19H17F3N5O requires: 388.1380.

ν_{max} (ATR)/cm^{-1}: 3263 (NH), 3135, 2929, 1680, 1630, 1594, 1477 (CN), 1335, 1229, 1117 (CF_3), 1058, 998, 977, 832, 784, 692, 611.

HPLC: 99.15% (*t*R 33.72 min)

1-(5-{4-[4-chloro-phenylamino]phenoxy}pyridin-2-yl)guanidine Hydrochloride (12)

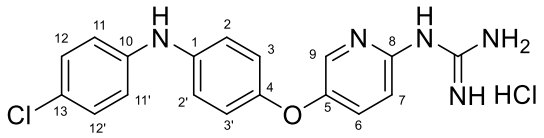

Following Method B, **48** (95mg, 0.34 mmol) was dissolved in 4M HCl in 1, 4-dioxane (0.48

mL, 1.98 mmol) and in additional dioxane (0.66 mL) until a final concentration of 0.2M was

reached. After 6 h stirring at 55 °C, the reaction was adjudged complete (TLC), solvents were

evaporated and the residue was purified by flash chromatography to afford, **11**, the pure

hydrochloride salt as a white solid (62 mg, 85%) **Mp**: 51-53 ℃

^{1}H NMR (400 MHz, MeOD) δ 8.08 (d, *J* = 2.8 Hz, 1H, H-9), 7.52 (dd, *J* = 8.9, 2.8 Hz, 1H, H-6), 7.22 – 7.17 (m, 2H, H-12 and 12'), 7.16 – 7.12 (m, 2H, H-11 and H-11'), 7.08 – 6.98 (m, 5H, H-7, H-2, H-2', H-3 and H-3') ppm.

^{13}C NMR (101 MHz, MeOD) δ 155.7 (s), 151.4 (s), 149.7 (s), 146.6 (s), 143.5 (s), 140.1 (s), 135.9 (CH Ar, C-9), 128.8 (CH Ar, C-6), 128.6 (s), 123.8 (s), 119.9 (s), 119.2 (s), 117.4 (s), 113.9 (s) ppm.

HRMS (m/z ESI^{+}): Found : 354.1120 $(M + H)^{+}$, C18H17ClN5O requires: 354.1116.

ν_{max} (ATR)/cm^{-1}: 3263 (NH), 3135, 2929, 1680, 1630, 1594, 1477 (CN), 1335, 1229, 1117 (CF_3), 1058, 998, 977, 832, 784, 692, 611.

HPLC: 95.53% (*t*R 34.71 min)

1-(5-{4-[phenylamino]phenoxy}pyridin-2-yl)guanidine Hydrochloride (16)

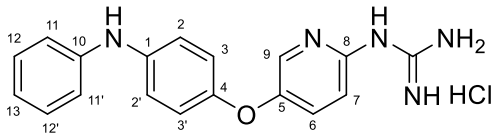

Following Method B, **29** (201mg, 0.34 mmol) was dissolved in 4M HCl in 1, 4-dioxane (1.02

mL, 7.56 mmol) and in additional dioxane (0.66 mL) until a final concentration of 0.2M was

reached. After 6 h stirring at 55 °C, the reaction was adjudged complete (TLC), solvents were

evaporated and the residue was purified by flash chromatography to afford, **12**, the pure

hydrochloride salt as a white solid (126 mg, 88%) **Mp**: 92-94 ℃

^{1}H NMR (400 MHz, MeOD) δ 6.49 (d, *J* = 2.8 Hz, 1H, H-9), 5.93 (dd, *J* = 8.9, 2.8 Hz, 1H, H-6), 5.65 (m, 2H, H-12 and H-12'), 5.58 – 5.54 (m, 2H, H-2 and H-2'), 5.51 – 5.45 (m, 3H, H-11, H-11' and H-7), 5.42 – 5.37 (m, 2H, H-3 and H-3'), 5.27 (t, *J* = 7.3 Hz, 1H, H-13) ppm.

^{13}C NMR (101 MHz, MeOD) δ 156.3 (qC), 152.4 (qC), 149.5 (qC), 146.8 (qC), 144.5 (qC), 141.3 (qC), 136.1 (CH Ar, C-9), 129.1 (CH Ar, C-12 and C-13'), 129.8 (CH Ar, C-6), 120.3 (CH Ar, C-3 and C-3'), 120.1 (CH Ar, C-13), 118.9 (CH Ar, C-2 and C-2'), 117.7 (CH Ar, C-11 and C-11'), 114.3 (CH Ar, C-7) ppm.

HRMS (m/z ESI^{+}): Found : 320.1507 $(M + H)^{+}$, C18H18N5O requires: 320.1506.

ν_{max} (ATR)/cm^{-1}: 3263 (NH), 3135, 2929, 1680, 1630, 1594, 1477 (CN), 1335, 1229, 1117 (CF_3), 1058, 998, 977, 832, 784, 692, 611.

HPLC: 95.06% (*t*R 32.17 min)

3-(dimethylamino)phenol (44)

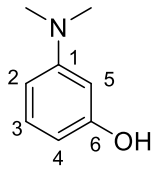

A solution of 3-aminophenol (200 mg, 1.83 mmol), MeI (320 mg 2.25 mmol) and Na_2CO_3 (220 mg, 2.08 mmol) in ethanol (6 mL) was stirred at 90˚C for 8 h. the reaction adjudged complete by TLC and the usual work up completed. The crude product was purified by silica gel chromatography (Hex:EtOAc) and **13a** was obtained as a purple solid (201.5 mg, 92%) **Mp**: 83-85 ℃, (lit. 83 °C).[12]

^{1}H NMR (400 MHz, $CDCl_3$) δ 7.07 (t, *J* = 8.07 Hz, 1H, H-3), 6.36-6.30 (m, 1H, H-2), 6.23-6.15 (m, 2H, H-4 and H-5), 2.90 (s, 6H, NMe_2) ppm.

3-((6-Nitropyridin-3-yl)oxy)aniline (25)[13]

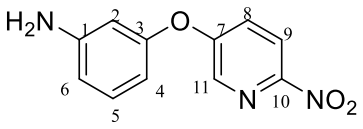

5-Bromo-2-nitropyridine (500 mg, 2.45 mmol, 1eq.), 3-aminophenol (295 mg, 2.7 mmol, 1.1 eq.) and Cs_2CO_3 (1.2 g, 3.7 mmol, 1.5 eq.) were dissolved in acetonitrile (5 mL) and stirred at 80 °C for 12 h. The mixture was cooled to room temperature, washed with water and the organic layer extracted with EtOAc, washed with brine, dried over MgSO4, concentrated under vacuum and purified by flash chromatography (hexanes: EtOAc) to get **15** as orange crystals (327 mg, 58 %). **Mp**: 118-120 °C.

^{1}H NMR (400 MHz, $CDCl_3$) δ 8.32 (d, *J* = 2.6 Hz, 1H, H-11), 8.22 (d, *J* = 8.9 Hz, 1H, H-9), 7.42 (dd, *J* = 8.9, 2.6 Hz, 1H, H-8), 7.20 (t, *J* = 8.1 Hz, 1H, H-5), 6.58 (d, *J* = 8.1 Hz, 1H, H-6), 6.45 (d, *J* = 8.1 Hz, 1H, H-4), 6.40 (s, 1H, H-2), 3.83 (s, 2H, NH_2) ppm.

3-(4-Nitrophenoxy)aniline (31)

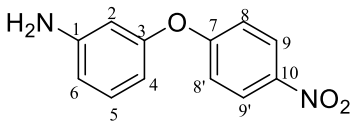

1-Fluoro-4-nitrobenzene(200 mg, 1.42 mmol, 1 eq.), 3-aminophenol (109 mg, 1.42 mmol, 1 eq.) and K_2CO_3 (294.4 mg, 2.13 mmol, 1.5 eq.) were dissolved in DMF (1.5 mL) and stirred at 80 ˚C for 12 h.The mixture was cooled to room temperature, washed with water and the organic layer extracted with EtOAc, washed with brine, dried over $MgSO_4$, concentrated under vacuum and purified by flash chromatography (silica gel, hexanes: EtOAc) to get **76** as a yellow solid (190 mg, 58%). **Mp**: 76-79 °C (lit. 79 °C).[14]

^{1}H NMR (400 MHz, $CDCl_3$) δ 8.23 – 8.11 (m, 2H, H-9, H-9’), 7.18 (t, *J* = 8.1 Hz, 1H, H-5), 7.06 – 6.98 (m, H-8 and H-8’), 6.57 (dd, *J* = 8.0, 2.1 Hz, 1H, H-4 or H-6), 6.46 (dd, *J* = 8.0, 2.1 Hz, 1H, H-4 or H-6), 6.41 (t, *J* = 2.1 Hz, 1H), 3.94 (s, 2H, NH) ppm.

_N_-(4-((6-nitropyridin-3-yl)oxy)phenyl)acetamide (28)[15]

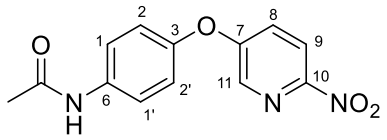

To a solution of 5-bromo-2-nitropyridine (2.03 g, 10.0 mmol) in DMF (30 mL) at 0 °C was added Cs_2CO_3 (4.9 g, 15.0 mmol) followed by 4-acetylaminophenol (1.66 g, 11.0 mmol) in DMF (30 mL), and the mixture was then stirred at rt overnight. The mixture was extracted with EtOAc. The organic layer was washed with water and brine and dried over Na_2SO_4. After solvent removal and sequence purification on silica gel column and then recrystallization from EtOAc, **18** (1.78 g, 65%) was obtained. **Mp**: 154-156 °C.

1H NMR (400 MHz, $CDCl_3$) δ 8.31 (d, *J* = 2.8 Hz, 1H, H-11), 8.23 (d, *J* = 8.9 Hz, 1H, H-9), 7.60 (d, J = 8.9 Hz, 2H, H-2 and H-2'), 7.39 (dd, *J* = 8.9, 2.8 Hz, 1H, H-8), 7.24 (s, 1H, NH), 7.08 (d, *J* = 8.9 Hz, 2H, H-1 and H-1'), 2.21 (s, 3H, CH_3) ppm.

4-((6-nitropyridin-3-yl)oxy)aniline (29)

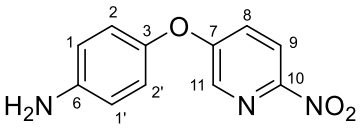

18 (100 mg) was refluxed in 1.25 M HCl/MeOH overnight. The solvent was removed under vacuum, the crude product was dissolved in water, drops of 5% $NaHCO_3$ were added until the product crushed out. The product was dissolved in EtOAc and washed with water to remove any remaining impurities, the solvent was removed under vacuum to give **19** (87.7 mg, 90%) **Mp**: 136-138 ℃.

^{1}H NMR (400 MHz, $CDCl_3$) δ 8.27 (d, *J* = 2.8 Hz, 1H, H-11), 8.19 (d, *J* = 8.9 Hz, 1H, H-9), 7.34 (dd, *J* = 9.0, 2.8 Hz, 1H, H-8), 6.96 – 6.85 (m, 2H, H-1 and H-1'), 6.74 (dd, *J* = 6.9, 5.0 Hz, 2H, H-2 and H-2'), 3.74 (s, 2H, NH) ppm.

^{13}C NMR (101 MHz, $CDCl_3$) δ 160.3 (qC), 146.0 (qC), 145.0 (qC), 138.2 (CH Ar, C-11), 124.8 (CH Ar, C-9), 121.8 (CH Ar, C3- and C-3'), 120.0 (CH Ar, C-8), 116.7 (CH Ar, C2- and C-2') ppm.

HRMS (m/z ESI$^+$): found: 232.0717 $(M + H)^+$, C11H10N3O3, requires: 232.0717

ν_{max} (ATR)/cm^{-1}: 3360 (NH), 2979, 2930, 1719 (C=O), 1598 (C=N), 1482, 1406, 1304, 1233 (C-O), 1047, 818, 772.

4-(4-Nitrophenoxy)aniline (32)[16]

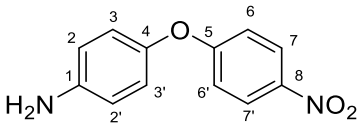

4-Fluoro-nitrophenyl (500 mg, 2.45 mmol, 1eq.), 4-aminophenol (295 mg, 2.7 mmol, 1.1 eq.) and Cs2CO3 (1.2 mg, 3.7 mmol, 1.5 eq.) were dissolved in DMF (5 mL) and stirred at 80 °C for 12 h. The mixture was cooled to room temperature, washed with water and the organic layer extracted with EtOAc, washed with brine, dried over MgSO4, concentrated under vacuum and purified by flash chromatography (hexanes: EtOAc) to get **19a** as yellow/orange crystals (311 mg, 55 %). **Mp**: 135-136 °C (Lit. 135-137 °C)

^{1}H NMR (400 MHz, $CDCl_3$) δ 8.19 – 8.14 (m, 2H, H-7 and H-7'), 6.98 – 6.93 (m, 2H, H-2 and H-2'), 6.92 – 6.86 (m, 2H, H-6 and H-6'), 6.75 – 6.69 (m, 2H, H-3 and H-3'), 3.70 (s, 2H, NH_2) ppm.

4-Bromo-*N*-(3-((6-nitropyridin-3-yl) oxy) phenyl-)-3-(trifluoromethyl)aniline (33)

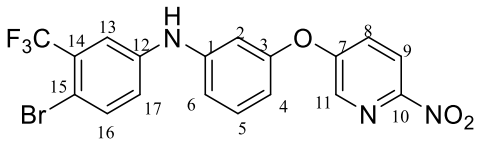

Following Method C, $Pd_2(dba)_3$ (3 mol%, 25.6 mg), Xantphos (3 mol%, 16.4 mg), compound **15** (200 mg, 0.88 mmol), Cs_2CO_3 (390.8 mg, 0.31 mmol) and 1,4-dibromo-2-(trifluoromethyl) benzene (267.4 mg, 0.88 mmol) were mixed, followed by addition of toluene (1.9 mL). The mixture was heated at 90 °C for 24 h and worked up as par method C and flash chromatography afforded **20** as a yellow oil (311 mg, 78%).

^{1}H NMR (400 MHz, $CDCl_3$) δ 8.33 (d, *J* = 2.8 Hz, 1H, H-11), 8.24 (d, *J* = 8.9 Hz, 1H, H-9), 7.56 (d, *J* = 8.6 Hz, 1H, H-13), 7.46 (dd, *J* = 8.9, 2.8 Hz, 1H, H-8), 7.38 – 7.33 (m, 2H, H-16, H-5), 7.10 (dd, *J* = 8.6, 2.7 Hz, 1H, H-17), 6.96 (dd, *J* = 8.1, 2.2 Hz, 1H, H-6), 6.80 (t, *J* = 2.2 Hz, 1H, H-2), 6.70 (dd, *J* = 8.1, 2.2 Hz, 1H, H-4), 6.09 (bs, 1H, NH).

^{13}C NMR (101 MHz, $CDCl_3$) δ 158.6 (qC), 155.4 (qC), 144.1 (qC), 141.5 (qC), 138.6 (CH Ar, C-11), 135.9 (CH Ar, C-13), 131.6 (CH Ar, C-5 or C-16), 125.9 (CH Ar, C-8), 121.8 (CH Ar, C-17), 119.8 (CH Ar, C-9), 117.2 (CH Ar, C-5 or C-16), 115.3 (CH Ar, C-6), 113.1 (CH Ar, C-4), 109.4 (CH Ar, C-2) ppm.

^{19}F NMR (377 MHz, $CDCl_3$) δ -62.93 (s) ppm.

HRMS (m/z ESI^-): found: 451.9859 $(M - H)^-$, C18H10BrF3N3O3, requires: 451.9863.

ν_{max} (ATR)/cm^{-1}: 3385 (NH), 3064, 2924, 1724, 1599, 1567, 1531 (NO_2), 1483 (NO_2), 1459,

1347, 1332, 1236 (CF_3), 1130 (C-O), 1111 (C-Br), 1028, 999, 975, 868, 823, 786.

4-Bromo-N-(3-(4-nitrophenoxy)phenyl)-3-(trifluoromethyl)aniline (34)

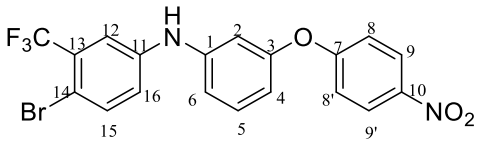

$Pd_2(dba)_3$ (23.8 mg, 3mol%), BINAP (16.2 mg, 3 mol%), compound **15a** (200 mg, 0.87 mmol), NaO^tBu (117.2 mg, 1.22 mmol) and 1,4-dibromo-2-(trifluoromethyl)benzene (264.4 mg, 0.87 mmol) were mixed, followed by addition of toluene (4 mL). The mixture was heated at 90 °C for 24 h and usual work up and flash chromatography afforded **20a** as a yellow oil (262 mg, 72%).

^{1}H NMR (400 MHz, $CDCl_3$) δ 8.24 – 8.19 (m, 2H, H-9 and H-9'), 7.55 (d, *J* = 8.5 Hz, 1H, H-15), 7.35 (m, 2H, H-5 and H-12), 7.09 (d, *J* = 2.8 Hz, 1H, H-16), 7.08 – 7.03 (m, 2H, H8 and H-8'), 6.93 (dd, *J* = 8.1, 1.8 Hz, 1H, H-6), 6.78 (t, *J* = 2.2 Hz, 1H, H-2), 6.71 (dd, *J* = 8.2, 1.8 Hz, 1H, H-4), 5.94 (s, 1H, NH) ppm.

^{13}C NMR (101 MHz, $CDCl_3$) δ 162.9 (qC), 156.0 (qC), 143.6 (qC), 142.8 (qC), 141.9 (qC), 135.8 (CH Ar, C-15), 131.3 (CH Ar, C-5), 129.2 (qC) 125.9 (2 CH Ar, C-9 and C-9'), 124.0 (qC, C-14), 121.4 ((2 CH Ar, C-16), 117.4 ((2 CH Ar, C-8 and C-8'), 116.9 (d, *J* = 5.5 Hz, CH Ar, C-12), 115.0 (CH Ar, C-6), 113.8 (CH Ar, C-4), 110.0 (CH Ar, C-2) ppm.

^{19}F NMR (377 MHz, $CDCl_3$) δ -62.91 (s) ppm.

HRMS (m/z ESI$^+$): Found 453.0905 $(M)^+$, C19H12BrF3N2O3 requires: 453.0056.

ν_{max} (ATR)/cm^{-1}: 3381 (NH), 1481 (NO_2), 1338, 1328, 1236 (C-O), 1131 (CF_3), 1110 (C-N), 847 (C-Cl),749.

3-((6-Nitropyridin-3-yl)oxy)-*N*-(3-(trifluoromethyl)phenyl)aniline (35)

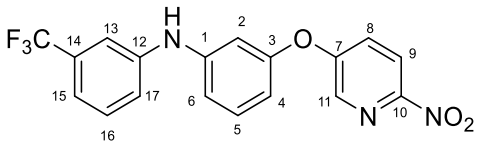

Following Method C, $Pd_2(dba)_3$ (3 mol%, 27.5 mg), Xantphos (3 mol%, 17.4 mg), compound **15** (200 mg, 0.87 mmol), Cs_2CO_3 (391 mg, 1.2 mmol) and 3-bromobenzotrifluoride (195.8 mg, 0.87 mmol) were mixed, followed by addition of toluene (2 mL/mmol). The mixture was heated at 90 °C for 24 h and worked up as par method C and flash chromatography afforded **21** as a yellow oil (265 mg, 78%).

^{1}H NMR (400 MHz, $CDCl_3$) δ 8.35 (d, *J* = 2.8 Hz, 1H, H-11), 8.26 (d, *J* = 8.9 Hz, 1H, H-9), 7.49 (dd, *J* = 8.9, 2.8 Hz, 1H, H-8), 7.44 – 7.32 (m, 3H, H-13, H-15 and H-17), 7.30 – 7.21 (m, 2H, H-5 and H-16), 7.00 (dd, *J* = 8.2, 2.0 Hz, 1H, H-6), 6.83 (t, *J* = 2.0 Hz, 1H, H-2), 6.70 (dd, *J* = 8.2, 2.0 Hz, 1H, H-4), 6.04 (s, 1H, NH) ppm.

^{13}C NMR (101 MHz, $CDCl_3$) δ 158.7 (qC), 155.3 (qC), 151.10 (qC), 144.7 (qC), 142.5 (qC), 138.6 (CH Ar, C-11), 132.1 (qC), 131.4 (CH Ar, C-5 or C-16), 130.1 (CH Ar, C-5 or C-16), 125.8 (CH Ar, C-8), 121.3 (CH Ar, C-17), 119.7 (CH Ar, C-9), 118.4 (q, CH Ar, C-15), 115.0 (CH Ar, C-6), 114.8 (q, CH Ar, C-13), 112.6 (CH Ar, C-4), 108.9 (CH Ar, C-2) ppm.

^{19}F NMR (377 MHz, $CDCl_3$) δ -62.88 (s) ppm.

HRMS (m/z ESI$^+$): Found 398.0718 $(M + Na)^+$, C18H12F3N3O3 Requires: 398.0831

ν_{max} (ATR)/cm^{-1}: 3385 (NH), 3064, 2924, 1724, 1599, 1567, 1531 (NO_2), 1483 (NO_2), 1459,

1347, 1332, 1236 (CF_3), 1130 (C-O), 1028, 999, 975, 868, 823, 786.

_N_-(4-Chlorophenyl)-3-((6-nitropyridin-3-yl)oxy)aniline (36)

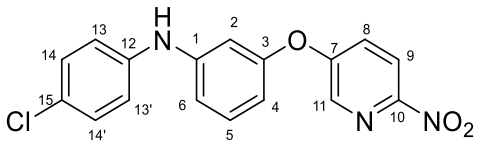

Following Method C, $Pd_2(dba)_3$ (3 mol%, 27.5 mg), Xantphos (3 mol%, 17.4 mg), compound **15** (200 mg, 0.87 mmol), Cs_2CO_3 (391 mg, 1.2 mmol) and 1-Bromo, 4-Chloro-benzotrifluoride (166.6 mg, 0.87 mmol) were mixed, followed syringe addition of toluene (1.8 mL). The mixture was heated at 90 °C for 24 h and worked up as par method C and flash chromatography afforded **22** as a yellow oil (126 mg, 42%).

^{1}H NMR (400 MHz, $CDCl_3$) δ 8.34 (d, *J* = 2.7 Hz, 1H, H-11), 8.26 (d, *J* = 8.9 Hz, 1H, H-9), 7.47 (dd, *J* = 8.9, 2.7 Hz, 1H, H-8), 7.33 (t, *J* = 8.1 Hz, 1H, H-5), 7.28 (d, *J* = 8.6 Hz, 2H, H-14 and H-14'), 7.07 (d, *J* = 8.6 Hz, 2H, H-13 and H-13'), 6.92 (d, *J* = 6.9 Hz, 1H, H-6), 6.78 (s, 1H, H-2), 6.63 (d, *J* = 8.0 Hz, 1H, H-4), 5.84 (s, 1H, NH) ppm.

^{13}C NMR (101 MHz, $CDCl_3$) δ 158.9 (qC), 155.3 (qC), 145.7 (qC), 140.2 (qC), 138.5 (CH Ar, C-11), 131.3 (CH Ar, C-5), 129.6 (CH Ar, C-14 and C-14'), 127.3 (qC), 125.7 (CH Ar, C-8), 120.6 (CH Ar, C-13 and C-13'), 119.8 (CH Ar, C-9), 114.3 (CH Ar, C-6), 111.8 (CH Ar, C-4), 108 (CH Ar, C-2) ppm.

HRMS (m/z ESI$^-$): Found : 340.0498 $(M - H)^-$, C17H11ClN3O3 requires: 340.0494.

ν_{max} (ATR)/cm^{-1}: 3396 (NH), 3083, 1591, 1563, 1489 (NO_2), 1346, 1246, 1146, 1105, 1091 (C-Cl), 849, 767, 688.

3-((6-nitropyridin-3-yl) oxy)-N-phenylaniline (37)

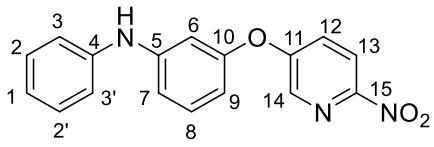

$Pd_2(dba)_3$ (3 mol%, 18.3 mg), Xantphos (3 mol%, 11.8 mg), compound **15** (162.3 mg, 0.70 mmol), Cs_2CO_3 (384.5 mg, 1.18 mmol) and remaining liquid bromo-benzene(0.07 mL, 0.7 mmol) were mixed, followed syringe addition of toluene (2.0 mL). The mixture was heated at 90 °C for 24 h and usual work up and flash chromatography afforded **23** as a yellow oil (100.7 mg, 47%).

^{1}H NMR (600 MHz, $CDCl_3$) δ 8.35 (d, *J*= 2.5 Hz, 1H, H-14), 8.26 (d, *J*= 6.3 Hz, 1H, H-13), 7.46 (dd, *J*= 2.5, 6.3 Hz, 1H, H-12), 7.37-7.25 (m, 3H, H-3, H-3' and H-1), 7.14 (d, *J*= 8.0 Hz, 2H, H-2 and H-2'), 7.04 (t, *J*= 7.3 Hz, 1H, H-8), 6.94 (dd, *J*= 1.7, 7.3 Hz, 1H, H-7), 6.81 (t, *J*= 1.7 Hz, 1H, H-6), 6.61 (dd, *J*= 1.7, 7.3 Hz, 1H, H-9) ppm.

^{13}C NMR (101 MHz, $CDCl_3$) δ 158.9 (qC), 155.2 (qC), 150.9 (qC), 146.1 (qC), 141.5 (qC), 138.5 (CH Ar, C-14), 131.2 (CH Ar, C-1), 129.5 (CH Ar, C-3 & C-3'), 125.6 (CH Ar, C-12), 122.6 (CH Ar, C-8), 119.8 (CH Ar, C-13), 119.5 (CH Ar, C-2 & C-2'), 114.1 (CH Ar, C-7), 111.3 (CH Ar, C-9), 10.68 (CH Ar, C-6) ppm..

HRMS (*m/z* ESI$^+$): Found 308.1030 $(M + H)^+$, C12H12N2O2 requires 308.0957.

ν_{max} (ATR)/cm^{-1}: 3390 (N-H), 3058, 2921, 1593, 1566, 1529 (N-O), 1488, 1457, 1437, 1235 (C-N), 1140 (C-O), 1111, 968, 844, 743, 686.

_N_,_N_'-dimethyl-3-((6-nitropyridin-3-yl)oxy)aniline (45)

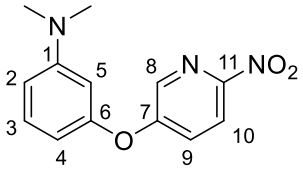

A solution of **13a** (39.4 mg, 0.29 mmol, 1.0 eq), 1-bromo-4-nitropyridine (64.1 mg, 0.32 mmol, 1.1 eq) and Cs_2CO_3 (140 mg, 0.43 mmol, 1.5 eq) in DMF (1 mL) was stirred overnight at 90˚C. The reaction was adjudged complete by TLC. The usual work up was completed, and the crude product was purified by silica gel chromatography (Hex:EtOAc) and **24** was obtained as an orange amorphous solid (96 mg, 78%) **Mp**: 84-85 °C.

^{1}H NMR (400 MHz, $CDCl_3$) δ 8.30 (d, 1H, H-10), 8.19 (d, 1H, H-9), 7.39 (dd, 1H, H-4), 7.28-7.23 (m, 1H, H-3), 6.61 (m, 1H, H-8), 6.40-6.36 (m, 2H, H-2 and H-5), 2.95 (s, 6H, 2x CH_3) ppm.

^{13}C NMR (101 MHz, $CDCl_3$) δ 159.5 (qC), 155.2 (C), 152 (CH Ar, C-11), 150.3 (qC), 138.3 (CH Ar,C-10), 130.7 (CH Ar, C-3), 125.3 (CH Ar, C-4), 119.6 (CH Ar, C-9), 109.7 (CH Ar, C-8), 107.1 (CH Ar, C-5), 103.5 (CH Ar, C-2), 40.3 (CH_3) ppm.

HRMS (*m/z* ESI$^+$): Found: 260.1032 $(M + H)^+$, C13H13N3O3 requires: 260.0957.

ν_{max} (ATR)/cm^{-1}: 3411, 3279, 3045, 2919, 1610 (C-H ar.), 1578, 1501 (N-O), 1486, 1253 (C-N), 1093 (C-O), 840.

4-bromo-*N*-(4-((6-nitropyridin-3-yl)oxy)phenyl)-3-(trifluoromethyl)aniline (38)

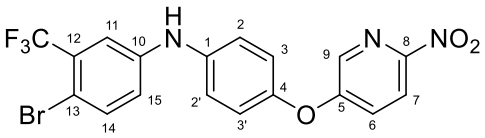

Following Method C, $Pd_2(dba)_3$ (3 mol%, 5.49 mg), Xantophos (3 mol%, 4.1 mg), compound **19** (50 mg, 0.22 mmol), Cs_2CO_3 (97.75 mg, 0.3 mmol) and 1,4-dibromo-2-(trifluoromethyl)benzene (0.03 mL, 0.22 mmol) were mixed, followed syringe addition of toluene (0.5 mL). The mixture was heated at 90 °C for 24 h and worked up as par method C and flash chromatography afforded **25** as a yellow oil (70 mg, 80%).

^{1}H NMR (400 MHz, $CDCl_3$) δ 8.34 (d, *J* = 2.7 Hz, 1H, H-9), 8.27 (d, *J* = 8.9 Hz, 1H, H-7), 7.57 (d, *J* = 8.6 Hz, 1H, H-14), 7.46 (dd, *J* = 8.9, 2.7 Hz, 1H, H-6), 7.35 (d, *J* = 2.8 Hz, 1H, H-11), 7.22 – 7.16 (m, 2H, H-2 and H-2‘), 7.13 – 7.05 (m, 3H, H-3,H-3‘ and H-16) ppm.

^{13}C NMR (111 MHz, $CDCl_3$) δ 159.2 (qC), 149.0 (qC), 142.7 (qC), 139.4 (qC), 138.2 (CH Ar, C-9), 135.8 (CH Ar, C-14), 125.2 (CH Ar, C-6), 121.6 (CH Ar, C-3 and C-3’), 121 (CH Ar, C-2 and C2’), 120.5 (CH Ar, C-15), 119.8 (CH Ar, C-7), 116 (CH Ar, C-11) ppm.

^{19}F NMR (377 MHz, $CDCl_3$) δ -62.88 (s) ppm.

HRMS (m/z ESI^-): found: 451.9867 $(M)^-$, C18H10BrF3N3O3 requires: 451.9836.

ν_{max} (ATR)/cm^{-1}: 3385 (NH), 3064, 2924, 1724, 1599, 1567, 1531 (NO_2), 1483 (NO_2), 1459,

1347, 1332, 1236 (CF_3), 1130 (C-O), 1111 (C-Br), 1028, 999, 975, 868, 823, 786.

4-Chloro-*N*-(4-((6-nitropyridin-3-yl)oxy)phenyl)-3-(trifluoromethyl)aniline (39)

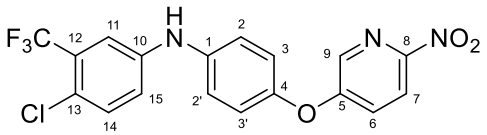

Following Method C, $Pd_2(dba)_3$ (3 mol%, 55 mg), Xantophos (3 mol%, 37 mg), compound **19** (460 mg, 2 mmol), Cs_2CO_3 (736 mg, 3.2 mmol) and 4-bromo-1-chloro-2-(trifluoromethyl)benzene (0.28 mL, 2 mmol) were mixed, followed syringe addition of toluene (4 mL). The mixture was heated at 90 °C for 24 h and worked up as par method C and flash chromatography afforded **26** as a yellow oil (698 mg, 77%).

^{1}H NMR (600 MHz, $CDCl_3$) δ 8.34 (s, 1H, H-9), 8.27 (d, *J* = 8.8 Hz, 1H, H-7), 7.45 (dd, *J* = 8.8, 2.5 Hz, 1H, H-6), 7.39 (d, *J* = 8.7 Hz, 1H, H-14), 7.35 (d, *J* = 2.4 Hz, 1H, H-11), 7.18 (d, *J* = 8.7 Hz, 2H, H-2 and H-2'), 7.15 (dd, *J* = 8.6, 2.5 Hz, 1H, H-15), 7.10 (d, *J* = 8.7 Hz, 2H, H-3 and H-3'), 5.90 (s, 1H, NH) ppm.

^{13}C NMR (151 MHz, $CDCl_3$) δ 159.6 (qC), 151.3 (qC), 149.3 (qC), 142.4 (qC), 140 (qC), 138.5 ((CH Ar, C-9), 132.8 ((CH Ar, C-14), 129.6 (q, *J* = 31.3 Hz, qC), 125.6 ((CH Ar, C-6), 123.9 (qC), 123.4 (qC), 122 ((CH Ar, C-3 and C-3'), 121.2 (CH Ar, C-2 and C-2'), 120.9 (CH Ar, C-15), 120.2 (CH Ar, C-7), 116.2 (q, *J* = 5.4 Hz, CH Ar, C-11) ppm.

^{19}F NMR (377 MHz, $CDCl_3$) δ -62.85 (s) ppm.

HRMS (m/z ESI$^+$): Found : 410.0521 $(M + H)^+$, C18H12ClF3N3O3 requires: 410.0514.

ν_{max} (ATR)/cm^{-1}: 3381 (NH), 1481 (NO2), 1338, 1328, 1236 (C-O), 1131 (CF3), 1110 (C-N), 847 (C-Cl),749.

4-Chloro-*N*-(4-((6-nitropyridin-3-yl)oxy)phenyl)-3-(trifluoromethyl)aniline (40)

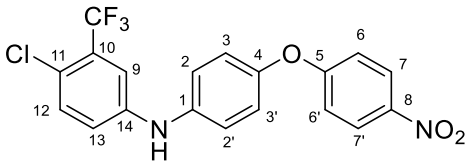

Following Method C, $Pd_2(dba)_3$ (3 mol%, 5.49 mg), Xantophos (3 mol%, 4.1 mg), compound **19a** (50 mg, 0.22 mmol), Cs_2CO_3 (97.75 mg, 0.3 mmol) and 4-bromo-1-chloro-2- (trifluoromethyl)benzene (0.03 mL, 0.22 mmol) were mixed, followed syringe addition of toluene (0.5 mL). The mixture was heated at 90 °C for 24 h and worked up as par method C and flash chromatography afforded **26a** as a yellow oil (77 mg, 87%).

^{1}H NMR (400 MHz, $CDCl_3$) δ 8.24 – 8.18 (m, 2H, H-7 and H-7'), 7.36 (d, *J* = 8.7 Hz, 1H, H-9), 7.31 (d, *J* = 2.8 Hz, 1H, H-12), 7.17 – 7.00 (m, 7H, H-2, H-2', H-3, H-3', H-6, H-6' and H-13), 5.83 (bs, 1H, NH)

^{13}C NMR (101 MHz, $CDCl_3$) δ 150.1 (qC), 139.2 (qC), 132.7 (CH Ar, C-9), 126.3 (CH Ar, C7- and C-7'), 122.2 (CH Ar, C2- and C-2'), 121.4 (CH Ar, C6- and C-6'), 120.5 (CH Ar, C-13), 117.1 (CH Ar, C3- and C-3'), 115.8 (CH Ar, C-12)

^{19}F NMR (377 MHz, $CDCl_3$) δ -62.84 (s).

HRMS (m/z ESI$^+$): found : 409.0557 (M + H)$^+$, C19H12ClF3N2O3, requires: 409.0489

ν_{max} (ATR)/cm^{-1}: 3468.6 (NH), 3068.2, 2929.6, 2852.6, 1605, 1514.11, 1499.36, 1485.98 (NO), 1454.45, 1336.89, 1250.87, 1134.97, 1107.66 (C-Cl), 876.27, 689.

_N_-(4-((6-nitropyridin-3-yl)oxy)phenyl)-3-(trifluoromethyl)aniline (41)

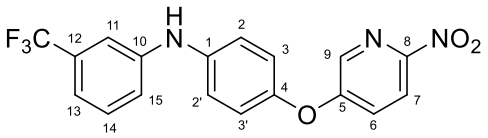

Following Method C, $Pd_2(dba)_3$ (3 mol%, 6 mg), Xantophos (3 mol%, 4 mg), compound **19** (50 mg, 0.22 mmol), Cs_2CO_3 (97.75 mg, 0.3 mmol) and 3-bromo-1-trifluoromethylbenzene (0.03 mL, 0.22 mmol) were mixed, followed syringe addition of toluene (0.5 mL). The mixture was heated at 90 °C for 24 h and worked up as par method C and flash chromatography afforded **27** as a yellow oil (70 mg, 77%).

^{1}H NMR (400 MHz, $CDCl_3$) δ 8.35 (d, *J* = 2.8 Hz, 1H, H-9), 8.27 (d, *J* = 8.9 Hz, 1H, H-7), 7.45 (dd, *J* = 8.9, 2.8 Hz, 1H, H-6), 7.41 (t, *J* = 7.9 Hz, 1H, H-14), 7.30 (s, 1H, H-11), 7.25 – 7.18 (m, 4H, H-13, H-15, H-2 and H-2'), 7.12 – 7.07 (m, 2H, H-3 and H-3') ppm.

^{13}C NMR (101 MHz, $CDCl_3$) δ 159.3 (s, qC), 148.5 (s, qC), 143.5 (s, qC), 140.1 (s, qC), 138.21 (s, CH Ar, C-9), 130 (s, CH Ar, C-14), 125.1 (s, CH Ar, C-6), 121.6 (s, CH Ar, C-3 and C-3'), 120.5 (s, CH Ar, C-2 and C-2'), 120.1 (s, CH Ar, C-14), 119.8 (s, CH Ar, C-7), 117.6 (d, J = 3.8 Hz, CH Ar, C-13), 113.5 (d, J = 4.0 Hz, CH Ar, C-11) ppm.

HRMS (m/z ESI^-): Found: 374.0764 $(M - 1)^-$, C18H11F3N3O3 requires: 374.0831.

ν_{max} (ATR)/cm^{-1}: 3385 (NH), 3064, 2924, 1724, 1599, 1567, 1531 (NO_2), 1483 (NO_2), 1459,

1347, 1332, 1236 (CF_3), 1130 (C-O), 1028, 999, 975, 868, 823, 786.

4-chloro-*N*-(4-((6-nitropyridin-3-yl)oxy)phenyl)aniline (42)

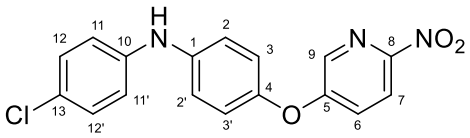

Following Method C, $Pd_2(dba)_3$ (3 mol%, 7.5 mg), Xantophos (3 mol%, 11 mg), compound **19** (100 mg, 0.43 mmol), Cs_2CO_3 (97.75 mg, 0.3 mmol) and 4-bromochlorobenzene (82.8 mg, 0.43 mmol) were mixed, followed syringe addition of toluene (1 mL). The mixture was heated at 90 °C for 24 h and worked up as par method C and flash chromatography afforded **28** as a yellow oil (68 mg, 52%).

^{1}H NMR (400 MHz, $CDCl_3$) δ 8.34 (d, *J* = 2.8 Hz, 1H, H-9), 8.26 (d, *J* = 8.9 Hz, 1H, H-7), 7.43 (dd, *J* = 8.9, 2.8 Hz, 1H, H-6), 7.30 – 7.25 (m, 2H, H-12 and H-12'), 7.13 (m, 2H, H-2 and H-2'), 7.08 – 7.01 (m, 4H, H-11, H-11', H-3 and H-3') ppm.

^{13}C NMR (151 MHz, $CDCl_3$) δ 158.9 (qC), 155.3 (qC), 145.7 (qC), 140.2 (qC), 138.5 (CH Ar, C-11), 131.3 (CH Ar, C-5), 129.6 (CH Ar, C-12 and C-12'), 127.3 (qC), 125.7 (CH Ar, C-8), 121.60 (s, CH Ar, C-3 and C-3'), 120.6 (s, CH Ar, C-2 and C-2'), 120.4 (CH Ar, C-11 and C-11'), 119.8 (CH Ar, C-9), 114.3 (CH Ar, C-6) ppm.

HRMS (m/z ESI$^-$): Found: 340.0496 $(M - H)^-$, C17H11ClN3O3 requires: 340.0494.

ν_{max} (ATR)/cm^{-1}: 3396 (NH), 3083, 1591, 1563, 1489 (NO_2), 1346, 1246, 1146, 1105, 1091 (C-Cl), 849, 767, 688.

4-((6-nitropyridin-3-yl)oxy)-*N*-phenylaniline (43)

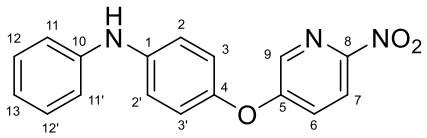

Following Method C, $Pd_2(dba)_3$ (3 mol%, 11.9 mg), Xantophos (3 mol%, 7.5 mg), compound **19** (100 mg, 0.22 mmol), Cs_2CO_3 (211.78 mg, 0.3 mmol) and bromobenzene (0.05 mL, 0.22 mmol) were mixed, followed syringe addition of toluene (0.5 mL). The mixture was heated at 90 °C for 24 h and worked up as par method C and flash chromatography afforded **29** as a yellow oil (70 mg, 51%).

^{1}H NMR (400 MHz, $CDCl_3$) δ 8.34 (d, *J* = 2.8 Hz, 1H, H-9), 8.25 (d, *J* = 8.9 Hz, 1H, H-7), 7.42 (dd, *J* = 9.0, 2.9 Hz, 1H, H-6), 7.36 – 7.31 (m, 1H, H-13), 7.20 – 7.10 (m, 4H, H-2, H-2', H-12 and H-12'), 7.07 – 6.99 (m, 4H, H-11, H-11', H-3 and H-3') ppm.

^{13}C NMR (101 MHz, $CDCl_3$) δ 159.8 (qC), 150.9 (qC), 147.6 (qC), 138.1 (CH Ar, C-9), 129.5 (CH Ar, C-13), 124.8 (CH Ar, C-6), 121.9 (CH Ar, CH Ar, C-11 and H-11'), 121.4 (CH Ar, C-2 and H-2'), 119.7 (CH Ar, C-7), 119.2 (CH Ar, C-12 and H-12'), 118.3 (CH Ar, C-3 and H-3') ppm.

HRMS (m/z ESI$^-$): Found : 306.0887 $(M - H)^-$, C12H12N2O2 requires: 306.0957.

ν_{max} (ATR)/cm^{-1}: 3390 (N-H), 3058, 2921, 1593, 1566, 1529 (N-O), 1488, 1457, 1437, 1235 (C-N), 1140 (C-O), 1111, 968, 844, 743, 686.

5-(3-((3-(Trifluoromethyl)phenyl)amino)phenoxy)pyridin-2-amine (46)

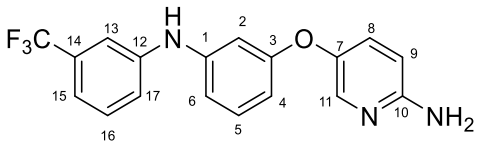

Following Method D, to a solution of nitro derivative **21** (265 mg, 0.71 mmol) in absolute ethanol (10 mL) was added 10% Pd/C mixture (10 mol%, 7.55 mg). After 24 h, usual work up followed by silica gel chromatography afforded **30** as brown oil (197 mg, 80 %).

^{1}H NMR (400 MHz, $CDCl_3$) δ 7.93 (d, *J* = 2.4 Hz, 1H, H-11), 7.35 (t, *J* = 7.9 Hz, 1H, H-5), 7.30 – 7.13 (m, 5H, H-8, H-13, H-15, H-16 and H-17), 6.78 (dd, *J* = 8.0, 1.6 Hz, 1H, H-6), 6.66 (t, *J* = 2.2 Hz, 1H, H-2), 6.59 – 6.51 (m, 2H, H-4 and H-9), 6.03 (s, 1H, NH), 4.27 (s, 2H, NH_2) ppm.

^{13}C NMR (101 MHz, $CDCl_3$) δ 160.0 (qC), 155.4 (qC), 145.3 (qC), 143.9 (qC), 143.6 (qC), 139.6 (CH Ar, C-11), 131.6 (CH Ar, C-8), 130.9 (CH Ar, C-16), 130.2 (CH Ar, C-5), 125.6 (qC), 122.9 (qC), 120.8 (CH Ar, C-17), 117.7 (d, *J* = 3.9 Hz, CH Ar, C-13), 114.1 (d, *J* = 3.8 Hz, CH Ar, C-15), 112.6 (CH Ar, C-6), 110.5 (CH Ar, C-4), 109.9 (CH Ar, C-9), 106.9 (CH Ar, C-2) ppm.

^{19}F NMR (377 MHz, $CDCl_3$) δ -62.82 (s) ppm.

HRMS (m/z ESI$^+$): Found 346.1166 $(M + H)^+$, C18H15F3N3O requires: 346.1162.

ν_{max} (ATR)/cm^{-1} : 3352 (NH), 2943, 2847, 1595, 1480, 1327, 1258, 1225, 1172, 1135 (CF_3), 872, 723.

5-(3-(phenylamino) phenoxy) pyridin-2-amine (47)

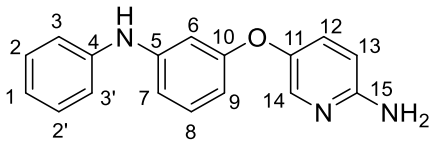

To a solution of **23** (100.7 mg, 0.33 mmol) in ethanol (0.7 mL), was added 10% Pd/C mixture (10 mol%). The reaction mixture was stirred at room temperature under hydrogen atmosphere (1.0 atm) for 24 h. The reaction mixture was filtered off, and the filtrate was concentrated in vacuo. The residue was purified by silica gel chromatography (hexane:EtOAc) to obtain **31** as a brown oil (88.6 mg, 97 %).

^{1}H NMR (600 MHz, $CDCl_3$) δ 7.92 (d, *J*= 2.7 Hz, 1H, H-14), 7.33-7.20 (m, 3H, H-3, H-5 & H-1), 7.15 (t, *J*= 8.1 Hz, 1H, H-12), 7.09 (dd, *J*= 1.7, 7.3 Hz, 2H, H-2 & H-2'), 6.95 (t, *J*= 6.2 Hz, 1H, H-8), 6.75 (dd, *J*=2.2, 6.2 Hz, 1H, H-7), 6.66 (t, *J*= 2.2 Hz, 1H, H-6), 6.52 (d, *J*= 8.7 Hz, 1H, H-13), 6.44 (dd, *J*= 2.2, 6.0 Hz, 1H, H-9) ppm.

^{13}C NMR (101 MHz, $CDCl_3$) δ 159.6 (qC), 155 (qC), 145.2 (qC), 145 (qC), 142.3 (qC), 139.6 (CH Ar, C-14), 131 (CH Ar, C-8), 130.2 (CH Ar, C-12), 129.3 (CH Ar, C-1, C-3 &C-3'), 121.4 (CH Ar,, C-8), 118.5 (CH Ar,, C-2 & C-2'), 111.13 (CH Ar, C-7), 109.35 (CH Ar,, C-13), 108.77 (CH Ar,, C-9), 105.71 (CH Ar, C-6) ppm.

HRMS (*m/z* ESI$^+$): Found: 278.1288 $(M + H)^+$, C17H16N3Orequires 278.1288.

ν_{max} (ATR)/cm^{-1}: 3376 (N-H), 3120, 2911, 1796, 1631, 1566, 1486, 1398, 1306, 1259 (C-N), 1050 (C-O), 932, 800, 770, 686.

5-(3-(dimethylamino)phenoxy)pyridin-2-amine (48)

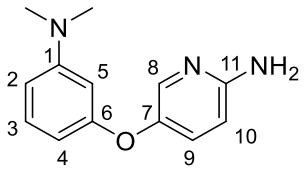

To a solution of **24** (216 mg, 0.83 mmol, 1.0 eq) in ethanol (2 mL), 10% Pd/C mixture (10 mol%, excess) was added, and the mixture was stirred, at room temperature, under hydrogen overnight. The crude product was filtered using Celite and the filtrate was concentrated to obtain **32** as a brown oil (164.1 mg, 85%).

^{1}H NMR (400 MHz, $CDCl_3$) δ 8.88 (d, *J* = 2.3 Hz ,1H, H-8), 7.18 (dd, *J* = 8.6, 2.3 Hz 1H, H-9), 7.10 (t, *J* = 2.1 Hz, 1H, H-5), 6.47 (d, *J* = 8.6 Hz, 1H, H-10), 6.40 (dd, *J* = 8.4, 2.1 Hz, 1H, H-2), 6.31 (t, *J* = 8.1 Hz, 1H, H-3), 6.20 (dd, *J* = 8.4, 2.1 Hz, 1H, H-4), 2.89 (s, 6H, NMe_2) ppm.

^{13}C NMR (101 MHz, $CDCl_3$) δ 159.6 (qC), 154.9 (qC), 145.7 (qC), 139.7 (qC),139.76 (CH Ar, C-8), 130.6 (CH Ar, C-9), 129.9 (CH Ar, C-3), 109.2 (CH Ar, C-10), 107.08 (CH Ar, C-2), 104.73 (CH Ar, C-4), 101.55 (CH Ar, C-5), 40.34 (CH_3) ppm.

HRMS (*m/z* ESI$^+$): found: 230.1289 $(M + H)^+$, C13H16N3O3 requires: 229.1288.

***ν*max (ATR)/cm-1** : 3289 (N-H), 2895 (C-H), 1667 (N=C), 1314 (C-N).

5-(4-((3-(trifluoromethyl)phenyl)amino)phenoxy)pyridin-2-amine (49)

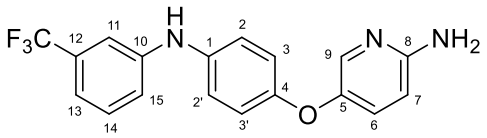

Tin (II) chloride (784 mg, 3.2 mmol) was added to a solution of **27** (260 mg, 0.70 mmol) was dissolved in ethanol (10 mL), the mixture was stirred at 70 ℃ for 24hrs. the solvent was removed under a vacuum. The residue was dissolved in EtOAc and poured onto ice, the pH was adjusted to 8 with 5% $NaHCO_3$, the product was extracted with EtOAc, washed with water, brine, dried over dry $MgSO_4$ and concentrated under reduced pressure. Purified by flash chromatography over silica (hexane: EtOAc: Et_3N) to give the product, **33**, as a brown oil (203 mg, 88%).

^{1}H NMR (400 MHz, $CDCl_3$) δ 7.94 (d, *J* = 2.8 Hz, 1H, H-9), 7.32 (t, *J* = 7.9 Hz, 1H, H-14), 7.23 (dd, *J* = 8.8, 2.9 Hz, 1H, H-6), 7.16 (s, 1H, H-11), 7.11 – 7.06 (m, 4H, H-13, H-16, H-2 and H-2'), 6.96 – 6.90 (m, 2H, H-3 and H-3'), 6.54 (d, *J* = 8.8 Hz, 1H,H-7), 5.82 (bs, 2H, NH_2), 4.41 (s, 1H, NH) ppm.

^{13}C NMR (101 MHz, $CDCl_3$) δ 154.9 (s, qC), 154.1 (s, qC), 146.0 (s, qC), 145.1 (s, qC), 139.7 (s, CH Ar, C-9), 136.4 (s, qC), 131.9 (s, qC), 131.6 (s, qC), 130.3 (s, CH Ar, C-6), 129.8 (s, CH Ar, C-14), 122.2 (s, CH Ar, C-3 and C-3'), 118.5 (s, CH Ar, C-15), 118.3 (s, CH Ar, C-13), 116.2 (s, C-2 and C-2'), 111.9 (q, J = 4.0 Hz, CH Ar, C-11), 109.2 (s, CH Ar, C-7) ppm.

^{19}F NMR (377 MHz, $CDCl_3$) δ -62.88 (s) ppm.

HRMS (m/z APCI$^+$): Found : 346.1161 $(M + H)^+$, C18H15F3N3O requires: 346.1162.

vmax (ATR)/$cm^{-1:}$ 3352 (NH), 2943, 2847, 1595, 1480, 1327, 1258, 1225, 1172, 1135 (CF_3), 872, 723.

5-(4-(phenylamino)phenoxy)pyridin-2-amine (50)

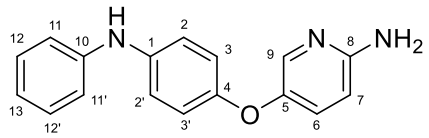

Tin (II) chloride (784 mg, 3.2 mmol) was added to a solution of **29** (100mg, 0.3mmol) was dissolved in ethanol (1 mL), the mixture was stirred at 70 ℃ for 24hrs. the solvent was removed under a vacuum. The residue was dissolved in EtOAc and poured onto ice, the pH was adjusted to 8 with 5% $NaHCO_3$, the product was extracted with EtOAc, washed with water, brine, dried over dry $MgSO_4$ and concentrated under reduced pressure. Purified by flash chromatography over silica (hexane: EtOAc: Et_3N) to give the product, **34**, as a brown oil (87mg, 95%).

^{1}H NMR (400 MHz, $CDCl_3$) δ 7.91 (d, *J* = 2.5 Hz, 1H. H-9), 7.26 – 7.21 (m, 2H, H-12 and H-12’), 7.19 (dd, *J* = 8.8, 2.5 Hz, 1H, H-6), 7.08 – 7.01 (m, 2H, H-2 and H-2’), 6.97 (d, J = 8.3 Hz, 2H, H-11 and H-11’), 6.87 (m, 3H, H-3, H-3’ and H-13), 6.50 (d, *J* = 8.8 Hz, 1H, H-7), 5.62 (s, 1H, NH), 4.36 (s, 2H, NH_2) ppm.

^{13}C NMR (101 MHz, $CDCl_3$) δ 154.8 (qC), 153 (qC), 146.6 (qC), 144.2 (qC), 139.5 (s, CH Ar, C-9), 138.1 (qC), 130.1 (s, CH Ar, C-6), 129.4 (s, CH Ar, C-12 and C-12’), 120.8 (s, CH Ar, C-2 and C-2’), 120.4 (s, CH Ar, C-13), 118.5 (s, CH Ar, C-3 and C-3’), 116.8 (s, CH Ar, C-11 and C-11’), 109.7 (s, CH Ar, C-7) ppm.

HRMS (m/z APCI$^+$): Found : 278.1293 $(M + H)^+$, C17H16N3O requires: 278.1288.

vmax (ATR)/cm^{-1}: 3352 (NH), 2933, 2857, 1597, 1486, 1327, 1258, 1225, 1172, 1135, 872, 723.

5-(3-((4-Bromo-3-(trifluoromethyl)phenyl)amino)phenoxy)pyridin-2-amine (51)

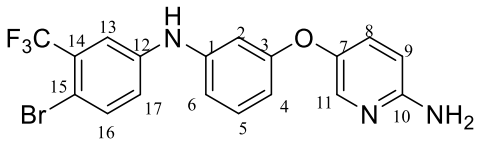

Tin (II) chloride (820 mg, 3.6 mmol) was added to a solution of Compound **20** (110 mg, 0.24 mmol) dissolved in ethanol (1mL) The mixture was stirred at 70 ℃ for 24h. the solvent was removed under vacuum. The residue was dissolved in EtOAc and poured onto ice, the pH was adjusted to 8 with 5% $NaHCO_3$, the product was extracted with EtOAc, washed with water, brine, dried over dry $MgSO_4$ and concentrated under reduced pressure. Purified by flash chromatography over silica (hexane: EtOAc: Et_3N) to give the product, **35** as a brown oil (70 mg, 69%).

^{1}H NMR (400 MHz, $CDCl_3$) δ 7.92 (d, *J* = 2.7 Hz, 1H, H-11), 7.52 (d, *J* = 8.7 Hz, 1H, H-16), 7.34 (d, *J* = 2.6 Hz, 1H, H-13), 7.23 (m, 2H, H-5, H-8), 7.05 (dd, *J* = 8.7, 2.6 Hz, 1H, H-17), 6.78 – 6.73 (m, 1H, H-6), 6.63 (s, 1H, H-2), 6.58 (dd, *J* = 8.2, 1.8 Hz, 1H, H-4), 6.54 (d, *J* = 8.8 Hz, 1H, H-9), 6.11 (s, 1H, NH), 4.47 (s, 2H, NH) ppm.

^{13}C NMR (101 MHz, $CDCl_3$) δ 160.2 (qC), 155.5 (qC), 145.2 (qC), 143.2 (qC), 142.7 (qC), 140.3 (CH Ar, C-11), 136.0 (CH Ar, C-16), 131.4 (CH Ar, C-5 or C-8), 131.0 (CH Ar, C-5 or C-8), 124.4 (qC), 121.7 (qC), 121.2 (CH Ar, C-17), 116.6 (q, *J* = 5.6 Hz, CH Ar, C-13), 112.9 (CH Ar, C-6), 111.0 (CH Ar, C-4), 109.7 (CH Ar, C-9), 107.3 (CH Ar, C-2) ppm.

^{19}F NMR (377 MHz, $CDCl_3$) δ -62.86 (s) ppm.

HRMS (m/z APCI$^+$): Found : 424.0270 $(M + H)^+$, C18H13BrF3N3O requires: 424.0267.

ν_{max} (ATR)/cm^{-1}: 3352 (NH), 2943, 2847, 1595, 1480, 1327, 1258, 1225, 1172,1125 (CF_3), 872, 723.

5-(3-((4-Bromo-3-(trifluoromethyl)phenyl)amino)phenoxy)pyridin-2-amine (52)

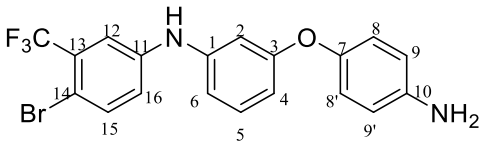

Tin (II) chloride (412 mg, 1.83 mmol) was added to a solution of Compound **20a** (138 mg, 0.3 mmol) dissolved in ethanol (1mL) The mixture was stirred at 70 °C for 24h. the solvent was removed under vacuum. The residue was dissolved in EtOAc and poured onto ice, the pH was adjusted to 8 with 5% $NaHCO_3$, the product was extracted with EtOAc, washed with water, brine, dried over dry $MgSO_4$ and concentrated under reduced pressure. Purified by flash chromatography over silica (hexane: EtOAc: Et_3N) to give the product, **35** as a brown oil (85 mg, 64%).

^{1}H NMR (400 MHz, $CDCl_3$) δ 7.47 (d, *J* = 8.7 Hz, 1H, H-15), 7.30 (d, *J* = 2.6 Hz, 1H, H-12), 7.20 (t, *J* = 8.0 Hz, 1H, H-5), 6.99 (dd, *J* = 8.7, 2.6 Hz, 1H, H-16), 6.89 (d, *J* = 8.7 Hz, 2H, H-8 and H-8'), 6.69 (m, 3H, H-9, H-9' and H-6), 6.61 (m, 2H, H-2 and H-4), 5.94 (s, 1H, NH), 3.66 (s, 2H, NH_2) ppm.

^{13}C NMR (101 MHz, $CDCl_3$) δ 160.6 (qC, C-3), 148.3 (qC, C-7), 143.2 (qC, C-10), 142.9 (d, *J* = 3.9 Hz, qC), 135.9 (CH Ar, C-15),), 130.8 (CH Ar, C-5), 124.4 (qC), 121.7 (2 CH Ar, C-8 and C-8'), 121.0 (CH Ar, C-16), 116.6 (2 CH Ar, C-9 and C-9'), 116.3 (q, *J* = 5.6 Hz, q, *J* = 5.4 Hz, CH Ar, C-12), 112.6 (CH Ar, C-6), 111.5 (CH Ar, C-4), 107.6 (CH Ar, C-2) ppm.

^{19}F NMR (377 MHz, $CDCl_3$) δ -62.82 (s) ppm.

HRMS (m/z ESI$^+$): Found : 423.0305 $(M + H)^+$, C19H14BrF3N2O requires: 423.0320.

ν_{max} (ATR)/cm^{-1}: 3373 (NH), 2928, 1725, 1594, 1504 (C-N), 1482 (C-N), 1329, 1250, 1172 (C-Cl), 1130 (C-O), 1122 (CF_3), 925, 691, 666.

5-(3-((4-Chlorophenyl)amino)phenoxy)pyridin-2-amine (53)

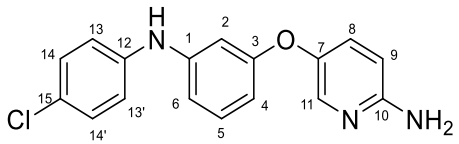

Tin (II) chloride (784 mg, 3.2 mmol) was added to a solution of **22** (110 mg, 0.24 mmol) was dissolved in ethanol (1 mL), the mixture was stirred at 70 ℃ for 24hrs. the solvent was removed under a vacuum. The residue was dissolved in EtOAc and poured onto ice, the pH was adjusted to 8 with 5% $NaHCO_3$, the product was extracted with EtOAc, washed with water, brine, dried over dry $MgSO_4$ and concentrated under reduced pressure. Purified by flash chromatography over silica (hexane: EtOAc: Et_3N) to give the product, **36** as a brown oil (70 mg, 69%).

^{1}H NMR (400 MHz, $CDCl_3$) δ 7.93 (d, *J* = 2.6 Hz, 1H, H-9), 7.25 – 7.20 (m, 3H, H-8, H-14 and H-14), 7.20 – 7.15 (t, 7.9 Hz, 1H, H-5), 7.03 – 6.99 (m, 2H, H-13 and H-13'), 6.73 (dd, *J* = 8.1, 2.2 Hz, 1H, H-6), 6.62 (t, *J* = 2.3 Hz, 1H, H-2), 6.54 (d, *J* = 8.8 Hz, 1H, H-9), 6.47 (dd, *J* = 8.2, 2.4, 1H, H-4), 5.85 (s, 1H, NH), 4.3 (bs, NH_2) ppm.

^{13}C NMR (101 MHz, $CDCl_3$) δ 159.8 (qC), 155.16 (qC), 145.2 (qC), 144.4 (qC), 141.1 (qC), 140.1 (CH Ar, C-11), 130.9 (CH Ar, C-8), 130.4 (CH Ar, C-5), 129.3 (2C, CH Ar, C-14 and C-14'), 126.1 (qC), 119.5 (2C, CH Ar, C-13 and C-13'), 111.5 (CH Ar, C-6), 109.2 (s, 2C, CH Ar, C-4 and C-9), 105.9 (CH Ar, C-2) ppm.

HRMS (m/z ESI$^+$): Found: 312.0904 (M + H) $^+$, C17H15ClN3O requires: 312.0825.

ν_{max} (ATR)/cm^{-1}: 3409 (NH), 3286 (NH), 3377 (NH), 1588, 1527, 1484 (C-O), 1324 (C-N), 1250, 1206, 1139 (C-Cl), 994, 972, 760.

5-(4-((4-bromo-3-(trifluoromethyl)phenyl)amino)phenoxy)pyridin-2-amine (54)

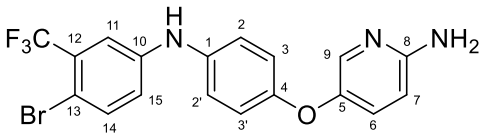

Tin (II) chloride (1222 mg, 5.4 mmol) was added to a solution of **25** (164mg, 0.36mmol) was dissolved in ethanol (10 mL), the mixture was stirred at 70 ℃ for 24hrs. the solvent was removed under a vacuum. The residue was dissolved in EtOAc and poured onto ice, the pH was adjusted to 8 with 5% $NaHCO_3$, the product was extracted with EtOAc, washed with water, brine, dried over dry $MgSO_4$ and concentrated under reduced pressure. Purified by flash chromatography over silica (hexane: EtOAc: Et_3N) to give the product, **37** as a brown oil (86mg, 80%).

^{1}H NMR (400 MHz, $CDCl_3$) δ 7.93 (d, *J* = 2.7 Hz, 1H, H-9), 7.49 (d, *J* = 8.7 Hz, 1H, H-14), 7.26 – 7.19 (m, 2H, H-6 and H-11), 7.11 – 7.04 (m, 2H, H-2 and H-2'), 6.98 – 6.89 (m, 3H, H-15, H-3 and H-3'), 6.55 (d, *J* = 8.8 Hz, 1H, H-7), 5.81 (s, 1H, NH), 4.43 (s, 2H, NH_2) ppm.

^{13}C NMR (101 MHz, $CDCl_3$) δ 155.0 (qC), 154.6 (qC), 145.8 (qC), 144.2 (qC), 139.81 (CH Ar, C-9), 135.7 (qC), 135.5 (CH Ar, C-14), 130.4 (CH Ar, C-6), 122.6 (CH Ar, C2 and C2'), 119 (CH Ar, C-15), 118.3 (CH Ar, C-3 and C3'), 114.6 (d, *J* = 5.6 Hz, H-11), 109.32 (CH Ar, C-7) ppm.

^{19}F NMR (377 MHz, $CDCl_3$) δ -62.83 (s) ppm.

HRMS (m/z APCI$^+$): Found : 424.0260 $(M + H)^+$, C18H14BrF3N3O requires: 424.0267.

vmax (ATR)/cm^{-1}: 3352 (NH), 2943, 2847, 1595, 1480, 1327, 1258, 1225, 1172,1125 (CF_3), 872, 723.

5-(4-((4-chloro-3-(trifluoromethyl)phenyl)amino)phenoxy)pyridin-2-amine (55)

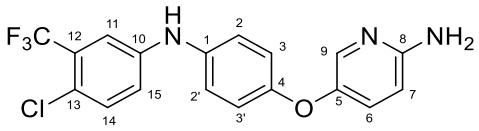

Tin (II) chloride (1.93g, 8.56mmol) was added to a solution of **26** (233.2 mg, 0.57 mmol) was dissolved in ethanol (1 mL), the mixture was stirred at 70 ℃ for 24hrs. the solvent was removed under a vacuum. The residue was dissolved in EtOAc and poured onto ice, the pH was adjusted to 8 with 5% $NaHCO_3$, the product was extracted with EtOAc, washed with water, brine, dried over dry $MgSO_4$ and concentrated under reduced pressure. Purified by flash chromatography over silica (hexane: EtOAc: Et_3N) to give the product, **38**, as a brown oil (180mg, 83%).

^{1}H NMR (400 MHz, $CDCl_3$) δ 7.90 (d, *J* = 2.8 Hz, 1H, H-9), 7.29 (d, *J* = 8.7 Hz, 1H, H-14), 7.22 (dd, *J* = 8.8, 2.8 Hz, 1H, H-6), 7.19 (d, *J* = 2.8 Hz, 1H, H-11), 7.08 – 7.02 (m, 2H, H-2 and H-2'), 6.98 (dd, *J* = 8.7, 2.8 Hz, 1H, H-15), 6.95 – 6.89 (m, 2H, 2H, H-3 and H-3'), 6.54 (d, *J* = 8.8 Hz, 1H, H-7), 5.74 (s, 1H, NH), 4.43 (bs, 2H, NH).

^{13}C NMR (101 MHz, $CDCl_3$) δ 155.2 (qC), 154.8 (qC), 146.2 (qC), 143.9 (qC), 139.7 (CH Ar, C-9), 136.3 (qC), 132.5 (CH Ar, C-14), 130.9 (CH Ar, C-6), 129.5 (qC), 129.2 (qC), 124.5 (qC), 122.8 (2C, CH Ar, C-2 and C-2'), 121.7 (qC), 119.3 (CH Ar, C-15), 118.7 (2C, CH Ar, C-3 and C-3'), 114.6 (q, *J* = 5.5 Hz, CH Ar, C-11), 109.7 (CH Ar, C-7) ppm.

^{19}F NMR (377 MHz, $CDCl_3$) δ -62.81 (s) ppm.

HRMS (m/z APCI$^+$): Found : 380.0778 $(M + H)^+$, C18H14ClF3N3O requires: 380.0772.

ν_{max} (ATR)/cm^{-1}: 3332 (NH), 2923 (C-H), 2847 (C-H), 1595, 1480, 1327, 1258, 1225, 1172, 1125 (CF_3), 1111 (C-Cl), 820, 711, 665.

***N*-(4-(4-Aminophenoxy)phenyl)-4-chloro-3-(trifluoromethyl)aniline (56)**

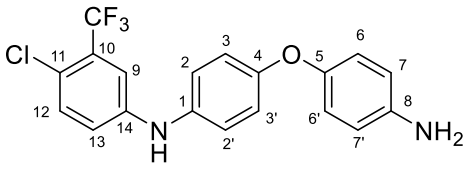

Tin (II) chloride (327.19 mg, 1.45 mmol) was added to a solution of compound **26a** (99 mg, 0.24 mmol) in ethanol (1 mL). the mixture was stirred at 70 ℃ for 6 h after which completion of the reaction was adjudged by TLC. The solvent was removed under vacuum, the residue was then dissolved in EtOAc and then poured onto ice, 5% $NaHCO_3$ was added until the pH reached 7-8, the crude product was the extracted with EtOAc, washed with water, brine and dried over dry $MgSO_4$. The solvent was removed under vacuum, the residue was purified by silica column chromatography (hexane: EtOAc) to yield compound **38a** as a brown oil (70 mg, 77%)

^{1}H NMR (400 MHz, $CDCl_3$) δ 7.31 – 7.27 (m, 1H, H-9), 7.20 (d, *J* = 2.8 Hz, 1H, H-12), 7.08 – 7.03 (m, 2H, m, 2H, H-2 and H-2’), 6.99 (dd, *J* = 8.7, 2.8 Hz, 1H, H-13), 6.96 – 6.92 (m, 2H, H-6, H-6’), 6.92 – 6.87 (m, 2H, H-3, H-3’), 6.73 – 6.68 (m, 2H, H-7 and H-7’), 5.81 (s, 1H, NH) ppm.

^{13}C NMR (101 MHz, $CDCl_3$) δ 155.36 (qC), 149.2 (qC), 144.2 (qC), 142.9 (qC), 135.7 (qC), 132.4 (CH Ar, C-9), 123.0 (CH Ar, C2- and C-2’), 121.0 (CH Ar, C6- and C-6’), 119.0 (CH Ar, C-13), 118.8 (CH Ar, C3- and C-3’), 116.6 (CH Ar, C-12), 114.4 (CH Ar, C7- and C-7’) ppm.

^{19}F NMR (377 MHz, $CDCl_3$) δ -62.79 (s) ppm.

ν_{max} (ATR)/cm^{-1}: 3383 (NH), 2926, 1725, 1594, 1504 (C-N), 1482 (C-N), 1329, 1250, 1172 (C-Cl), 1130 (C-O), 1112 (CF_3), 825, 681, 666.

HRMS (m/z ESI^+): Found : 379.0815 $(M + H)^+$, C19H14ClF3N2O requires: 379.0825.

5-(4-((4-chlorophenyl)amino)phenoxy)pyridin-2-amine (57)

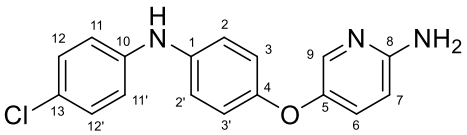

Tin (II) chloride (1050 mg, 4.7 mmol) was added to a solution of **28** (107mg, 107mmol) was dissolved in ethanol (1 mL), the mixture was stirred at 70 ℃ for 24hrs. the solvent was removed under a vacuum. The residue was dissolved in EtOAc and poured onto ice, the pH was adjusted to 8 with 5% $NaHCO_3$, the product was extracted with EtOAc, washed with water, brine, dried over dry $MgSO_4$ and concentrated under reduced pressure. Purified by flash chromatography over silica (hexane: EtOAc: Et_3N) to give the product, **39**, as a brown oil (72mg, 64%).

^{1}H NMR (400 MHz, $CDCl_3$) δ 7.88 (d, *J* = 2.8 Hz, 1H, H-9), 7.26 (dd, *J* = 8.9, 2.8 Hz, 1H, H-6), 7.23 – 7.18 (m, 2H, H-2 and H-2'), 7.07 – 7.01 (m, 2H, H-11 and H-11'), 6.95 – 6.88 (m, 4H, H-3, H-3', H-12 and H-12'), 6.57 (d, *J* = 8.9 Hz, 1H, H-7), 5.59 (s, 1H, NH), 4.57 (s, 2H, NH_2) ppm.

^{13}C NMR (101 MHz, $CDCl_3$) δ 154.5 (qC), 153.1 (qC), 146.4 (qC), 142.9 (qC), 138.1 (s, CH Ar, C-9), 137.7 (qC), 130.7 (s, CH Ar, C-6), 129.2 (CH Ar, C-12 and C-12'), 124.9 (qC), 121.8 (CH Ar, C-3 and C-3'), 118.6 (CH Ar, C-2 and C-2), 117.6 (CH Ar, C-11 and C11'), 109.7 (s, CH Ar, C-7) ppm.

HRMS (m/z APCI$^+$): Found : 312.0904 (M + H) $^+$, C18H15ClF3N3O requires: 312.0825.

vmax (ATR)/cm^{-1}: 3409 (NH), 3286 (NH), 3377 (NH), 1588, 1527, 1484 (C-O), 1324 (C-N), 1250, 1206, 1139 (C-Cl), 994, 972, 760.

1,2-Di-(*tert*-butoxycarbonyl)-3-(4-{3-[4-bromo-3-(trifluoromethyl)phenylamino]phenoxy} pyridin-2-yl)guanidine (58)

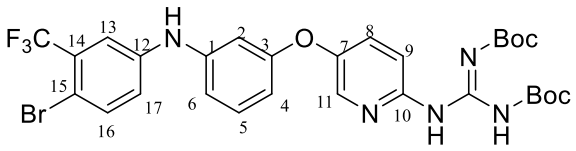

Following Method A, $HgCl_2$ (49 mg, 0.18 mmol, 1.04 eq) was added to a solution of **35** (70 mg, 0.17 mmol, 1 eq), *N,N'*-bis-(*tert*-butoxycarbonyl)-*S*-methylisothiourea (52.3 mg, 0.18 mmol, 1.04 eq), and triethylamine (0.08 mL, 0.6 mmol, 3.5 eq) in CH_2Cl_2. the mixture was stirred for 24 hrs, then work-up and purification on silica gel (hexane: EtOAc) to give **40** as a white solid (68 mg, 88%) **Mp**: 69-70 ℃.

^{1}H NMR (400 MHz, $CDCl_3$) δ 11.52 (s, 1H, NH), 10.87 (s, 1H, NH), 8.37 (d, *J* = 8.7 Hz, 1H, H-9), 8.10 (d, *J* = 2.7 Hz, 1H, H-11), 7.51 (d, *J* = 8.7 Hz, 1H, H-16), 7.37 (dd, *J* = 8.7, 2.7 Hz, 1H, H-8), 7.33 (d, *J* = 2.7 Hz, 1H, H-13), 7.23 (t, *J* = 8.1 Hz, 1H, H-5), 7.06 (dd, *J* = 8.7, 2.7 Hz, 1H, H-17), 6.81 (dd, *J* = 8.1, 1 Hz, 1H, H-6), 6.66 (t, *J* = 2.1 Hz, 1H, H-2), 6.58 (dd, *J* = 8.2, 2.2 Hz, 1H, H-4), 6.00 (s, 1H, NH), 1.56 (s, 11H, $(CH_3)_6$) ppm.

^{13}C NMR (101 MHz, $CDCl_3$) δ 158.9 (qC), 149.9 (qC), 143.4 (qC), 142.5 (CH Ar, C-2), 136 (CH Ar, C-16), 131 (CH Ar, C-5), 129 (CH Ar, C-8), 124.4 (qC), 121.7 (qC), 121.3 (CH Ar, C-17), 117.2 (CH Ar, C-9), 116.9 (d, *J* = 5.7 Hz, CH Ar, C-13), 113.6 (CH Ar, C-6), 111.9 (CH Ar, C-4), 108.4 (CH Ar, C-2), 84.5 (qC, $\underline{C}(CH_3)_3$), 80.6 (qC, $\underline{C}(CH_3)_3$), 28.4 ($(CH_3)_6$) ppm.

^{19}F NMR (377 MHz, $CDCl_3$) δ -62.89 (s) ppm.

HRMS (m/z ESI$^+$): Found : 666.1527 $(M + H)^+$, C29H32BrF3N4O5 requires: 665.1533.

ν_{max}(ATR)/cm^{-1}:3263 (N-H), 2980, 1741 (C=O), 1587 (C=N), 1561, 1477, 1290 (C-O), 1122 (CF_3), 1140 (C-N), 1110,978, 784, 664.

1,2-Di-(tert-butoxycarbonyl)-3-(4-{3-[4-bromo-3-(trifluoromethyl)phenylamino] phenoxy}phenyl)guanidine (59)

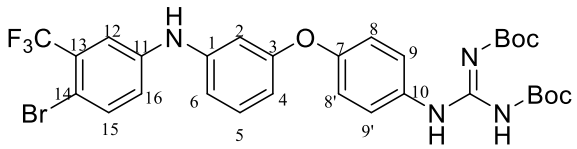

$HgCl_2$ (149.3 mg, 0.55 mmol) was added over a solution of **35a** (219 mg, 0.52 mmol), *N,N'-bis*-(*tert*-butoxycarbonyl)-*S*-methylisothiourea (160.1 mg, 0.55 mmol) and NEt_3 (0.27 mL, 1.82 mmol) in CH_2Cl_2. The reaction was stirred at room temperature for 24 h, then work up and silica gel chromatography (hexanes: EtOAc) afforded **40a** as a white solid (265 mg, 88%) **Mp**: 91-93 ℃.

^{1}H NMR (400 MHz, $CDCl_3$) δ 11.67 (s, 1H, NH), 10.32 (s, 1H, NH), 7.61 – 7.56 (m, 2H, H-9 and H-9'), 7.53 (d, *J* = 8.7 Hz, 1H, H-15), 7.34 (d, *J* = 2.8 Hz, 1H, H-12), 7.25 (t, *J* = 8.1 Hz, 1H, H-5), 7.07 (dd, *J* = 8.7, 2.8 Hz, 1H, H-16), 7.03 – 6.97 (m, 2H, H-8 and H-8'), 6.81 (dd, *J* = 8.0, 1.5 Hz, 1H, H-6), 6.69 – 6.63 (m, 2H, H-2 and H-4), 5.94 (s, 1H, NH), 1.56 (s, 11H, $(CH_3)_3$), 1.51 (s, 18H, $(CH_3)_3$) ppm.

^{13}C NMR (101 MHz, $CDCl_3$) δ 163.8 (qC), 159.3 (qC), 154.0 (qC), 153.6 (qC), 143.2 (qC), 142.9 (qC), 135.9 (qC), 132.9 (CH Ar, C-15), 130.9 (CH Ar, C-5), 124.3 (2 CH Ar, C-9 and C-9'), 121.0 (CH Ar, C-16), 120.1 (2 CH Ar, C-8 and C-8'), 116.7 (CH Ar, C-12), 113.3 (CH Ar, C-6), 112.5 (CH Ar, C-4), 108.9 (CH Ar, C-2), 84.2 (qC, $\underline{C}(CH_3)_3$), 80.0 (qC, $\underline{C}(CH_3)_3$), 28.5 ($(CH_3)_3$), 28.4 ($(CH_3)_3$) ppm.

^{19}F NMR (377 MHz, $CDCl_3$) δ -62.86 (s) ppm.

HRMS (m/z ESI$^+$): found : 665.1580 $(M + H)^+$, C30H33BrF3N4O5 requires: 665.1586.

ν_{max} (ATR)/cm^{-1}: 3260 (NH), 2979, 2930, 1719 (C=O), 1596 (C=N), 1482, 1406, 1304, 1233 (C-O), 1213, 1141 (CF_3), 1109 (C-Br), 1027, 818, 772.

1,2-Di-(*tert*-butoxycarbonyl)-3-(4-{3-[3-(trifuoromethyl)phenylamino]phenoxy} pyridin-2-yl) guanidine (60)

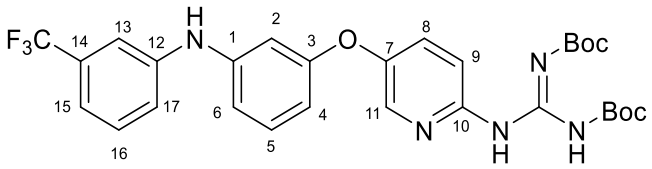

Following Method A, $HgCl_2$ (57.7 mg, 0.58 mmol) was added over a solution of **30** (197 mg,

0.57 mmol), *N*,*N'*-bis-(*tert*-butoxycarbonyl)-*S*-methylisothiourea (168.4 mg, 0.58 mmol), and NEt_3 (0.16 mL, 2 mmol) in CH_2Cl_2 (2 mL). The reaction was stirred at room temperature

for 24 h, then work up and silica gel chromatography (hexanes:EtOAc) afforded **41** as a

white amorphous solid (250 mg, 83%) **Mp**: 70-73 °C.

^{1}H NMR (400 MHz, $CDCl_3$) δ 11.54 (bs, 1H, NH), 10.91 (bs, 1H, NH), 8.39 (bs, 1H, NH), 8.14 (d, *J* = 2.8 Hz, 1H, H-11), 7.42 (dd, *J* = 9.1, 3.0 Hz, 1H, H-8), 7.37 (t, *J* = 7.9 Hz, 1H, H-16), 7.31 – 7.22 (m, 3H,), 7.19 (d, *J* = 7.7 Hz, 1H, H-9), 6.85 (dd, *J* = 8.0, 1.8 Hz, 1H, H-6), 6.72 (t, *J* = 2.2 Hz, 1H, H-2), 6.59 (dd, *J* = 8.1, 2.2 Hz, 1H, H-4), 5.93 (bs, 1H, NH), 1.55 (s, 18H, $(CH_3)_6$) ppm.

^{13}C NMR (101 MHz, $CDCl_3$) δ 163.5 (qC), 158.8 (qC), 153.2 (qC), 150.1 (qC), 146.6 (qC), 144.1 (qC), 143.4 (qC), 140 (CH Ar, C-11), 131 (CH Ar, C-14), 130 (CH Ar, C-16), 125.6 (CH Ar, C-8), 122.9 (qCF_3), 120.9 (q, *J* = 3.9 Hz, CH Ar, C-17), 118 (q, *J* = 3.8 Hz, q, *J* = 3.9 Hz, CH Ar, C-15), 117.2 (CH Ar, C-9), 114.5 (q, *J* = 3.9 Hz, CH Ar, C-13), 113.3 (CH Ar, C-6), 111.4 (CH Ar, C-4), 108.1 (CH Ar, C-2), 84.3 (qC, $\underline{C}(CH_3)_3$), 80.3 (qC, $\underline{C}(CH_3)_3$), 28.4 ($(CH_3)_6$) ppm.

^{19}F NMR (377 MHz, $CDCl_3$) δ -62.88 (s) ppm.

HRMS (m/z ESI$^+$): Found 588.2245 $(M + H)^+$, C29H33F3N5O5 requires: 588.2434.

vmax (ATR)/cm^{-1}: 3371 (NH), 3268 (NH), 2991, 2929, 1728 (C=O), 1595 (C=N), 1471, 1369, 1223, 1119 (CF3), 1110 (C-O), 771, 692.

1,2-Di-(*tert*-butoxycarbonyl)-3-(4-{3-[3-(trifuoromethyl)phenylamino]phenoxy} pyridin-2-yl) guanidine (61)

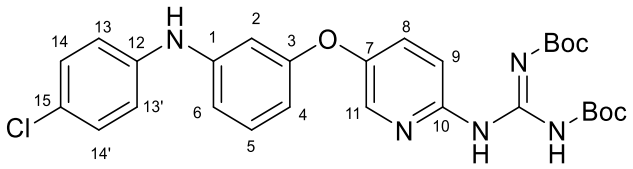

Following Method A, $HgCl_2$ (57.7 mg, 0.58 mmol) was added over a solution of **36** (197 mg, 0.57 mmol), *N*,*N'*-bis-(*tert*-butoxycarbonyl)-*S*-methylisothiourea (168.4 mg, 0.58 mmol), and NEt_3 (0.16 mL, 2 mmol) in CH_2Cl_2 (2 mL). The reaction was stirred at room temperature for 24 h, then work up and silica gel chromatography (hexanes:EtOAc) afforded **42** as a white amorphous solid (221 mg, 78%). **Mp**: 120 °C

^{1}H NMR (600 MHz, $CDCl_3$) δ 8.13 (d, *J* = 2.7 Hz, 1H, H-11), 7.43 (dd, *J* = 9.0, 2.7 Hz, 1H, H-8), 7.27 – 7.20 (m, 3H, H-5, H-14 and H-14'), 7.04 (m, 2H, H-13 and H-13'), 6.79 (d, *J* = 7.9 Hz, 1H, H-4), 6.68 (s, 1H, H-12), 6.53 (d, *J* = 8.0 Hz, 1H, H-6), 5.75 (s, 1H, NH), 1.61 – 1.51 (m, 18H, $(CH_3)_6$) ppm.

^{13}C NMR (101 MHz, $CDCl_3$) δ 144.8 (qC), 140.8 ((CH Ar, C-11), 130.6 ((CH Ar, C-5), 129.41 ((CH Ar, C-8, C-14, and C-14'), 126.5 (qC), 120.7 (qC), 120.2 (qC), 119.8 ((CH Ar, C-13 and C-13'), 112.3 (CH Ar, C-4), 110.6 (CH Ar, C-6), 107 (CH Ar, C-12), 84.3 (qC, $\underline{C}(CH_3)_3$), 80.3 (qC, $\underline{C}(CH_3)_3$), 28.4 ($(CH_3)_6$) ppm.

HRMS (m/z APCI$^+$): Found: 554.2168 $(M + H)^+$, C28H33ClN5O5 requires: 554.2165.

ν_{max} (ATR)/cm^{-1}: 3296 (NH), 2925, 1718 (C=O), 1649, 1628 (C=O), 1589 (C=N), 1485, 1390, 1367, 1330, 1310, 1258, 1148 (C-O), 1113 (C-N), 1096 (C-Cl), 829, 765.

2,3-(di-tert-butoxycarbonyl)-1-(5-(3-(phenylamino) phenoxy) pyridin-2-guanidine (62)

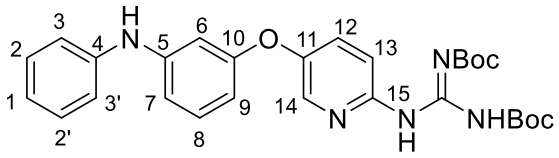

$HgCl_2$ (89.5 mg, 0.33 mmol) was added over a solution of **31** (88.6 mg, 0.32 mmol), 1,3-Bis(methoxycarbonyl)-2-methyl-2-thiopseudourea (93 mg, 0.34 mmol) and NEt_3 (0.16 mL, 0.33 mmol) in CH_2Cl_2 (1.7 mL). the reaction was allowed to stir at room temperature for 24 h. The reaction mixture was filtered off, extracted using ethyl acetate and washed with water and brine. The residue was purified by silica gel chromatography (hexane:EtOAc) to obtain **43** as a white solid (132.5 mg, 77 %). **Mp**: 40-44 ˚C.

^{1}H NMR (600 MHz, DMSO-d_6) δ 8.13 (d, *J* = 2.7 Hz, 1H, H-14), 7.43 (dd, *J*= 2.7, 6.1 Hz, 1H, H-12), 7.33- 7.30 (m, 1H, H-13), 7.21 (t, *J* = 8.1 Hz, 2H, H-2 & H-2'), 7.11 (m, 3H, H-1, H-3 and H-3'), 6.91 (t, *J* = 6.2 Hz, 1H, H-8), 6.82 (dd, *J* = 2.2, 6.2 Hz, 1H, H-7), 6.72 (t, *J* = 2.2 Hz, 1H, H-6), 6.51 (dd, *J* = 2.2, 6.2 Hz, 1H, H-9) 1.49 (d, 18H,$(CH_3)_6$) ppm.

^{13}C NMR (101 MHz, DMSO-d_6) δ 159.4 (qC), 151.2 (qC), 146.4 (qC), 142.1 (qC), 136.5 (qC), 130.6 (CH Ar, C-2 & C-2'), 129.5 (CH Ar, C-13), 128.7 (CH Ar, C-12), 123.4 (CH Ar, C-8), 119.2 (CH Ar, C-1), 118.9 (CH Ar, C-3 & C-3'), 112.2 (CH Ar, C-7), 110.1 (CH Ar, C-9), 106.8 (CH Ar, C-6), 28.1 ($(CH_3)_6$) ppm..

HRMS (*m/z* ESI$^+$): Found: 520.2554 $(M + H)^+$, C28H34N5O5 requires 520.2554.

ν_{max} (ATR)/cm^{-1}: 3373 (N-H), 3130, 2985, 1769 (C=O), 1624, 1565, 1458, 1387, 1286 (C-N), 1219 (C-O), 1144 (C-O), 1100, 862, 754, 687.

5-((3-(dimethylamino)phenoxy)pyridin-2-amine)guanidine (63)

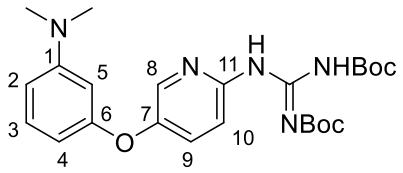

$HgCl_2$ (149.3 mg, 0.55 mmol, 1.05 eq) was added over a solution of **32** (121.2 mg, 0.52 mmol, 1.0 eq), *N,N'-bis*-(*tert*-butoxycarbonyl)-*S*- methylisothiourea (159.7 mg, 0.55 mmol, 1.05 eq) and NEt_3 (187.2 mg, 1.85 mmol, 3.5) in CH_2Cl_2. The reaction was stirred at room temperature for 24 h, the usual wok up and purified using silica gel chromatography (Hex:EtoAc) to afford **44** as a brown oil (212.2 mg, 88%).

^{1}H NMR (400 MHz, $CDCl_3$) δ 8.30 (d, = 8.6 Hz, 1H, H-8), 8.08 (d, J = 2.7 Hz, 1H, H-10), 7.34 (dd, J = 8.6, 2.7 Hz, 1H,),7.13 (t, J = 8.1 Hz, 1H, H-3), 6.45 (dd, J = 8.1, 1.8 Hz, 1H, H-10), 6.32 (t, J = 1.8 Hz, 1H, H-5), 6.26 (dd, J = 8.1, 1.8 Hz, 1H, H-4), 2.89 (s, 6H, NMe_2), 1.49 (d, 18H,$(CH_3)_6$) ppm.

HRMS (*m/z* ESI$^+$): found: 472.2557 $(M + H)^+$, C24H34N5O5 requires: 471.2554.

ν_{max} (ATR)/cm^{-1}: 2965, 2924, 2853, 1980 (C-H Ar), 1719 (C=O), 1608, 1573, 1588, 1503, 1488, 1452, 1390, 1229 (C-N), 1142 (C-O), 834, 733.

1,2-Di-(*tert*-butoxycarbonyl)-4-(4-{3-[4-bromo-3-(trifluoromethyl)phenylamino]phenoxy} pyridin-2-yl)guanidine (64)

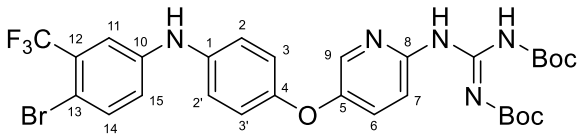

Following Method A, $HgCl_2$ (30 mg, 0.1 mmol) was added over a solution of **37** (44 mg, 0.1 mmol), *N*,*N'*-bis-(*tert*-butoxycarbonyl)-*S*-methylisothiourea (32 mg, 0.1 mmol), and NEt_3 (0.05 mL, 0.35 mmol) in CH_2Cl_2 (1 mL). The reaction was stirred at room temperature for 24 h, then work up and silica gel chromatography (hexanes:EtOAc) afforded **45** as a white amorphous solid (55 mg, 80%). **Mp**: 93 °C

^{1}H NMR (400 MHz, $CDCl_3$) δ 11.55 (s, 1H, NH), 10.87 (s, 1H, NH), 8.34 (d, *J* = 7.5 Hz, 1H, H-7), 8.10 (d, *J* = 2.6 Hz, 1H, H-9), 7.48 (d, *J* = 8.7 Hz, 1H, H-11), 7.32 (dd, *J* = 7.5, 2.6 Hz, 1H, H-6), 7.25 (d, *J* = 2.8 Hz, 1H, H-14), 7.11 – 7.06 (m, 2H, H-2 and H-2'), 6.99 – 6.94 (m, 3H, H-15, H-3 and H-3'), 6.05 (s, 1H, NH), 1.53 (m, 18H, $(CH_3)_6$) ppm.

^{13}C NMR (151 MHz, $CDCl_3$) δ 163.6 (qC), 153.2 (qC), 152.6 (qC), 152.5 (qC), 150.3 (qC), 145.8 (qC), 143.3 (qC), 138.9 (CH Ar, C-9), 137.5 (qC), 135.5 (CH Ar, C-11), 130.7 (q, J = 31.0 Hz, qC), 127.8 (CH Ar, C-6), 125.5 (qC), 123.7 (qC), 121.9 (CH Ar, C-2 and C-2'), 119.7 (CH Ar, C-3, C-3' and C-15), 119.3 (qC), 117.4 (CH Ar, C-7), 115.2 (CH Ar, C-14), 108.5 (qC), 845 (qC, $\underline{C}(CH_3)_3$), 80.3 (qC, $\underline{C}(CH_3)_3$), 28.8 ($(CH_3)_6$) ppm.

^{19}F NMR (377 MHz, $CDCl_3$) δ -62.81 (s) ppm.

HRMS (m/z APCI$^+$): Found : 666.1527 $(M + H)^+$, C29H32BrF3N5O5, requires: 666.1533.

vmax (ATR)/cm^{-1}: :3253 (N-H), 2980 (C-H), 1721 (C=O), 1597 (C=N), 1561, 1477, 1386, 1368,

1290 (C-O), 1122 (CF3), 1140 (C-N), 1110, 1056 (C-Br), 1027, 998, 978, 764, 664.

1,2-Di-(*tert*-butoxycarbonyl)-4-(4-{3-[4-bromo-3-(trifluoromethyl)phenylamino]phenoxy} pyridin-2-yl)guanidine (65)

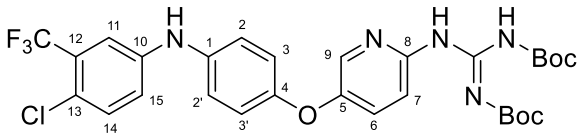

Following Method A, $HgCl_2$ (27.2 mg, 0.1 mmol) was added over a solution of **38** (150 mg, 0.1 mmol), *N,N'*-bis-(*tert*-butoxycarbonyl)-*S*-methylisothiourea (125 mg, 0.1 mmol), and NEt_3 (0.05 mL, 0.35 mmol) in CH_2Cl_2 (1 mL). The reaction was stirred at room temperature for 24 h, then work up and silica gel chromatography (hexanes:EtOAc) afforded **46** as a white amorphous solid (109 mg, 76%). **Mp**: 94 °C

^{1}H NMR (400 MHz, $CDCl_3$) δ 11.52 (s, 1H, NH), 10.86 (s, 1H, NH), 8.34 (d, *J* = 7.7 Hz, 1H, H-7), 8.09 (d, *J* = 2.7 Hz, 1H, H-9), 7.34 (dd, *J* = 7.7, 2.7 Hz, 1H, H-6), 7.30 (d, *J* = 8.7 Hz, 1H, H-14), 7.23 (d, *J* = 2.7 Hz, 1H, H-11), 7.10 – 7.04 (m, 2H, H-2 and H-2'), 7.02 (dd, *J* = 8.7, 2.7 Hz, 1H, H-15), 6.99 – 6.94 (m, 2H, H-3 and H-3'), 5.88 (s, 1H, NH), 1.52 (s, 18H, $(CH_3)_6$) ppm.

^{13}C NMR (101 MHz, $CDCl_3$) δ 163.4 (qC), 153.1 (qC), 152.7 (qC), 150.8 (qC), 146.1 (qC), 143.3 (qC), 139.1 (CH Ar, C-9), 137.2 (qC), 132.3 (CH Ar, C-14), 129.3 (qC), 128.9 (qC), 128.1 (CH Ar, C-6), 124.2 (qC), 122.7 (CH Ar, C-2 and C-2'), 121.8 (qC), 121.5 (qC), 119.9 (CH Ar, C-3 and C-3'), 119.4 (CH Ar, C-15), 117.0 (CH Ar, C-7), 114.8 (q, *J* = 5.5 Hz, CH Ar, C-11), 84.2 (qC, $\underline{C}(CH_3)_3$), 80.2 (qC, $\underline{C}(CH_3)_3$), 28.5 $(CH_3)_6$) ppm.

^{19}F NMR (377 MHz, $CDCl_3$) δ -62.81 (s) ppm.

HRMS (m/z APCI$^+$): found : 622.2028 $(M + H)^+$, C29H32ClF3N5O5, requires: 622.2039.

vmax (ATR)/cm^{-1}: 3407 (NH), 3256, 2978, 2932, 1717 (CO), 1637 (CN), 1584, 1546, 1461, 1409, 1368, 1293, 1233, 1148, 1106, 1057, 941, 848, 804, 758, 691.

1,2-Di-(tert-butoxycarbonyl)-3-(4-{4-[4-chloro-3-(trifluoromethyl)phenylamino] phenoxy}phenyl)guanidine (66)

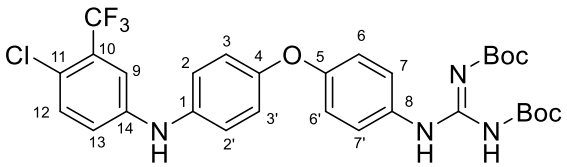

Following Method G, $HgCl_2$ (59.82 mg, 0.22 mmol) was added over a solution of **38a** (81 mg, 0.2 mmol), *N*,*N'*-bis-(*tert*-butoxycarbonyl)-*S*- methylisothiourea (63.88 mg, 0.22 mmol), and NEt_3 (0.11 mL, 0.7 mmol) in CH_2Cl_2 (1 mL). The reaction was stirred at room temperature for 24 h, then work up and silica gel chromatography (hexanes:EtOAc) afforded **46a** as a white amorphous solid (89 mg, 76%). **Mp**: 96 °C

^{1}H NMR (400 MHz, $CDCl_3$) δ 11.65 (s, 1H), 10.29 (s, 1H), 7.54 (d, *J* = 8.9 Hz, 2H, H-7 and H-7'), 7.29 (d, *J* = 8.7 Hz, 1H, H-9), 7.21 (d, *J* = 2.7 Hz, 1H, H-12), 7.06 (d, *J* = 8.8 Hz, 2H, H-6 and H-6'), 7.01 (dd, *J* = 8.7, 2.7 Hz, 1H, H-13), 6.99 – 6.93 (m, 4H, H-2, H-2', H-3 and H-3'), 5.83 (bs, 1H, NH), 1.54 (s, 9H, $CH_3)_3$), 1.48 (s, 9H, $CH_3)_3$) ppm.

^{13}C NMR (101 MHz, $CDCl_3$) δ 163.9 (qC), 154.7 (qC), 154.0 (qC), 153.6 (qC), 153.4 (qC), 143.79 (qC), 136.9 (qC), 132.4 (CH Ar, C-12), 132.3 (qC), 129.4 (qC), 124.3 (2 CH Ar, C-7 and C-7'), 122.3 (2 CH Ar, C-2 and C-2'), 121.7 (qC), 120.4 (2 CH Ar, C-6 and C-6'), 119.4 (CH Ar, C-13), 119.2 (2 CH Ar, C-3 and C-3'), 114.8 (q, *J* = 5.6 Hz, CH Ar, C-9), 84.1 (qC, $C(CH_3)_3$), 80.0 (qC, $\underline{C}(CH_3)_3$), 28.4 (($CH_3)_6$) ppm.

^{19}F NMR (377 MHz, $CDCl_3$) δ -62.80 (s) ppm.

HRMS (m/z ESI$^+$): Found 621.2102 $(M + H)^+$, C30H33ClF3N4O5 requires: 621.2086.

ν_{max} (ATR)/cm^{-1}: 3260 (NH), 2979, 2930, 1719 (C=O), 1596 (C=N), 1482, 1406, 1304, 1233 (C-O), 1213, 1141 (CF_3), 1027, 818, 772.

1,2-Di-(tert-butoxycarbonyl)-3-(4-{4-[3-(trifluoromethyl)phenylamino] phenoxy}phenyl)guanidine (67)

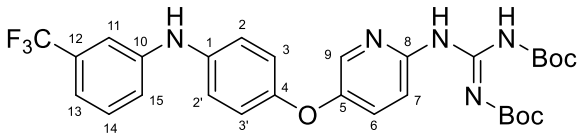

Following Method A, $HgCl_2$ (46.2 mg, 0.1 mmol) was added over a solution of **33** (55 mg, 0.1 mmol), *N*,*N'*-bis-(*tert*-butoxycarbonyl)-*S*-methylisothiourea (49.4 mg, 0.1 mmol), and NEt_3 (0.05 mL, 0.35 mmol) in CH_2Cl_2 (1 mL). The reaction was stirred at room temperature for 24 h, then work up and silica gel chromatography (hexanes:EtOAc) afforded **47** as a white amorphous solid (74 mg, 81%). **Mp**: 65 °C

^{1}H NMR (400 MHz, $CDCl_3$) δ 11.55 (s, 1H, NH), 10.89 (s, 1H, NH), 8.38 (d, *J* = 9.2 Hz, 1H, H-9), 8.13 (d, *J* = 2.8 Hz, 1H, H-7), 7.42 – 7.32 (m, 2H, H-6 and H-11), 7.20 (s, 1H, H-14), 7.17 – 7.09 (m, 4H, H-13, H-15, H-3 and H-3'), 7.04 – 6.97 (m, 2H, H-2 and H-2'), 5.79 (s, 1H, NH), 1.58 – 1.52 (m, 18H, $(CH_3)_6$) ppm.

^{13}C NMR (101 MHz, $CDCl_3$) δ 163.5 (qC), 158.8 (qC), 153.2 (qC), 150.1 (qC), 146.6 (qC), 144.1 (qC), 143.4 (qC), 140.0 (CH Ar, C-11), 131.0 (CH Ar, C-14), 130.2 (CH Ar, C-14), 125.6 (CH Ar, C-8), 122.9 (qCF_3), 120.9 (q, *J* = 3.9 Hz, CH Ar, C-15), 118.0 (q, *J* = 3.8 Hz, q, *J* = 3.9 Hz, CH Ar, C-13), 117.2 (CH Ar, C-9), 114.5 (q, *J* = 3.9 Hz, CH Ar, C-11), 113.3 (CH Ar, C-6), 111.4 (CH Ar, C-4), 108.1 (CH Ar, C-2 and C-2'), 84.3 (qC, $\underline{C}(CH_3)_3$), 80.3 (qC, $\underline{C}(CH_3)_3$), 28.4 ($(CH_3)_6$) ppm.

^{19}F NMR (377 MHz, $CDCl_3$) δ -62.89 (s) ppm.

HRMS (m/z APCI$^+$): Found: 588.2434 $(M^+ + H)^+$, C29H33F3N5O5, requires: 588.2428.

ν_{max} (ATR)/cm^{-1}: : 3303 (NH), 2979, 1719 (C=O), 1594 (C=N), 1486, 1486, 1407, 1303, 1293, 1213, 1146 (C-N), 1110 (C-O).

1,2-Di-(tert-butoxycarbonyl)-3-(4-{4-[4-chloro)phenylamino] phenoxy}phenyl)guanidine (68)

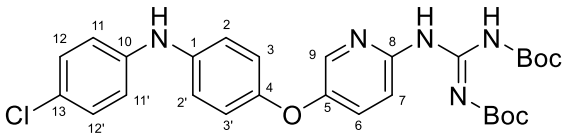

Following Method A, $HgCl_2$ (29.9 mg, 0.1 mmol) was added over a solution of **39** (34 mg, 0.1 mmol), *N*,*N'*-bis-(*tert*-butoxycarbonyl)-*S*-methylisothiourea (31 mg, 0.1 mmol), and NEt_3 (0.05 mL, 0.35 mmol) in CH_2Cl_2 (1 mL). The reaction was stirred at room temperature for 24 h, then work up and silica gel chromatography (hexanes:EtOAc) afforded **48** as a white amorphous solid (55 mg, 82%). **Mp**: 125 °C

^{1}H NMR (400 MHz, $CDCl_3$) δ 11.54 (s, 1H, NH), 10.87 (s, 1H, NH), 8.37 (d, *J* = 8.3 Hz, 1H, H-9), 8.11 (d, *J* = 2.8 Hz, 1H, H-7), 7.37 (dd, *J* = 8.3, 2.8 Hz, 1H, H-6), 7.25 – 7.19 (m, 2H, H-2 and H-2'), 7.11 – 7.04 (m, 2H, H-11 and H-11'), 6.96 (m, 4H, H-2, H-2', H-12 and H-12'), 5.63 (s, 1H, NH), 1.54 (m, 18H, $(CH_3)_6$) ppm.

^{13}C NMR (101 MHz, $CDCl_3$) δ 159.6 (qC), 151.3 (qC), 149.2 (qC), 142.4 (qC), 139.9 (qC), 138.54 ((CH Ar, C-9), 132.7 ((CH Ar, C-12 and C-12'), 129.5 (q, *J* = 31.3 Hz, qC), 125.5 ((CH Ar, C-6), 123.9 (qC), 123.3 (qC), 122.0 ((CH Ar, C-3 and C-3'), 121.2 (CH Ar, C-2 and C-2'), 120.9 (CH Ar, C-15), 120.1 (CH Ar, C-7), 116.1 (CH Ar, C-11 and C-11'), 83.9 (q, $C(CH_3)_3$), 80.0 (q, $C(CH_3)_3$), 28.3 ($(CH_3)_3$), 28.0 ($(CH_3)_3$) ppm.

HRMS (m/z APCI$^+$): found : 554.2167 $(M + H)^+$, C28H33ClN5O5, requires: 554.2165.

vmax (ATR)/cm^{-1}: 3407 (NH), 3285, 2978, 2932, 1718 (CO), 1596 (CN), 1555, 1490, 1408, 1367, 1331, 1289, 1233, 1143, 1105, 1056, 946, 804, 752, 690.

1,2-Di-(tert-butoxycarbonyl)-3-(4-{4-phenylamino] phenoxy}phenyl)guanidine (69)

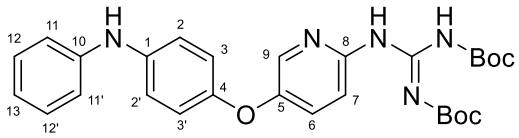

Following Method A, $HgCl_2$ (29.9 mg, 0.1 mmol) was added over a solution of **34** (25 mg, 0.1 mmol), *N*,*N'*-bis-(*tert*-butoxycarbonyl)-*S*-methylisothiourea (31.9 mg, 0.1 mmol), and NEt_3 (0.05 mL, 0.35 mmol) in CH_2Cl_2 (1 mL). The reaction was stirred at room temperature for 24 h, then work up and silica gel chromatography (hexanes:EtOAc) afforded **49** as a white amorphous solid (41 mg, 81%). **Mp**: 118 °C

^{1}H NMR (400 MHz, $CDCl_3$) δ 11.54 (s, 1H, NH), 10.87 (s, 1H, NH), 8.36 (d, *J* = 8.6 Hz, 1H, H-7), 8.12 (d, *J* = 2.8 Hz, 1H, H-7), 7.36 (dd, *J* = 8.6, 2.8 Hz, 1H, H-6), 7.31 – 7.25 (m, 2H, H-13 and H-13'), 7.13 – 7.07 (m, 2H, H-2 and H-2'), 7.05 (m, 2H, H-12 and H-12'), 6.99 – 6.92 (m, 3H, H-13, H-3 and H-3'), 5.67 (s, 1H, NH), 1.55 (m, 18H, $(CH_3)_6$) ppm.

^{13}C NMR (101 MHz, $CDCl_3$) δ 163.7 (qC), 153.6 (qC), 152.7 (qC), 151.9 (qC), 151.1 (qC), 145.7 (qC), 143.8 (qC), 139.3 (qC), 138.8 (CH Ar, C-9), 129.5 (s, CH Ar, C-12 and H-12'), 127.6 (CH Ar, C-6), 120.8 (s, CH Ar, C-1), 120.3 (CH Ar, C-2 and C-2'), 120.4 (CH Ar, C-3 and C-3'), 118.6 (s), 117.1 (CH Ar, C-11 and C-11'), 116.9 (CH Ar, C-7), 116.7 (qC), 84.6 (qC, $\underline{C}(CH_3)_3$), 80.3 (qC, $\underline{C}(CH_3)_3$), 28.4 $(CH_3)_6$) ppm.

HRMS (*m/z* ESI$^+$): Found: 520.2553 $(M + H)^+$, C28H34N5O5 requires 520.2554.

ν_{max} (ATR)/cm^{-1}: 3373 (N-H), 3130, 2985, 1769 (C=O), 1624, 1565, 1458, 1387, 1286 (C-N), 1219 (C-O), 1144 (C-O), 1100, 862, 754, 687.

1-(5-{3-[4-Chloro-3-(trifluoromethyl)phenylamino]phenylamino}pyridin-2-yl)guanidine hydrochloride (17)

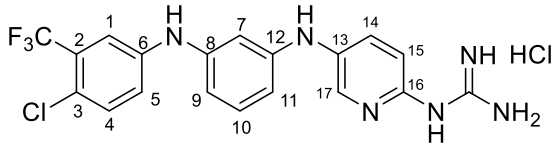

Following Method B, **78** (58 mg, 0.09 mmol) was dissolved in 4M HCl in 1, 4-dioxane (0.26 mL, 1.04 mmol) and in additional dioxane (0.17 mL) until a final concentration of 0.2M was reached. After 8 h stirring at 55 °C, the reaction was adjudged complete (TLC), solvents were evaporated and the residue was purified by silica gel chromatography ($CHCl_3$:MeOH) to afford **60**, the pure hydrochloride salt as a white solid (40 mg, 83%) **Mp:** 90-91 ℃

^{1}H NMR (400 MHz, MeOD) δ 8.13 (d, *J* = 2.7 Hz, 1H, H-17), 7.59 (dd, *J* = 8.8, 2.8 Hz, 1H, H-14), 7.39 (dd, *J* = 7.7, 5.9 Hz, 2H, H-1 and H-4), 7.24 (dd, *J* = 8.7, 2.7 Hz, 1H, H-5), 7.19 (t, *J* = 8.0 Hz, 1H, H-10), 6.97 (d, *J* = 8.8 Hz, 1H, H-15), 6.83 (t, *J* = 2.1 Hz, 1H, H-7), 6.70 – 6.63 (m, 2H, H-9 and H-11) ppm.

^{13}C NMR (101 MHz, MeOD) δ 146.8 (qC), 144.54 (qC), 143.6 (qC), 143.1 (qC), 136.3 (qC), 135.6 (CH Ar, C-17), 131.8 (CH Ar, C-4), 129.9 (CH Ar, C-10), 128.6 (CH Ar, C-14), 124.4 (qC), 121.7 (qC), 119.8 (CH Ar, C-5), 114.1 (CH Ar, C-1), 110.8 (CH Ar, C-11), 110.2 (CH Ar, C-9), 106.3 (CH Ar, C-7) ppm.

^{19}F NMR (377 MHz, MeOD) δ -64.08 (s) ppm.

HRMS (m/z ESI$^+$): Found: 421.1156 $(M + H)^+$, C19H17ClF3N6 requires: 421.1150.

vmax (ATR)/cm^{-1}: 3264 (NH), 2923, 2863, 1684, 1629, 1595, 1474 (C=N), 1400, 1332, 1229

(C-O), 1129 (CF3), 1115 (C-Cl), 977, 998.

HPLC: 95.06 % (*t*R 33.55 min)

1-(5-{3-[4-Chloro-3-(trifluoromethyl)phenoxy]phenoxy}pyridin-2-yl)guanidine hydrochloride (19)

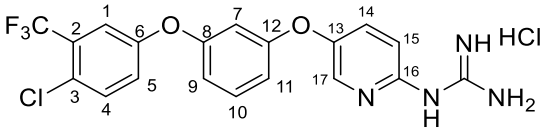

Following Method B, **76** (55 mg, mmol) was dissolved in 4M HCl in 1, 4-dioxane (mL, mmol) and in additional dioxane (mL) until a final concentration of 0.2M was reached. After 8 h stirring at 55 °C, the reaction was adjudged complete (TLC), solvents were evaporated and the residue was purified by silica gel chromatography ($CHCl_3$:MeOH) to afford **61**, the pure hydrochloride salt as a white solid (42 mg, 86%) **Mp:** 92 ℃

^{1}H NMR (400 MHz, MeOD) δ 8.14 (d, *J* = 2.6 Hz, 1H, H-17), 7.64 – 7.56 (m, 2H, H-14 and H-4), 7.43 (t, *J* = 8.3 Hz, 1H, H-10), 7.37 (d, *J* = 2.9 Hz, 1H, H-1), 7.23 (dd, *J* = 8.8, 2.9 Hz, 1H, H-5), 7.11 (d, *J* = 8.3 Hz, 1H, H-15), 6.90 – 6.81 (m, 2H, H-9 and H-11), 6.74 (t, *J* = 2.3 Hz, 1H, H-7) ppm.

^{13}C NMR (101 MHz, MeOD) δ 158.4 (qC), 157.3 (qC), 155.8 (qC), 155.4 (qC), 149.8 (qC), 147.7 (qC), 137.5 (CH Ar, C-17), 132.9 (CH Ar, C-4), 131.1 (CH Ar, C-10), 130.6 (CH Ar, C-14), 129. (qC), 128.8 (qC), 128.5 (qC), 125.6 (qC), 123.8 (qC), 122.8 (CH Ar, C-5), 121.8 (qC), 117.3 (q, *J* = 5.5 Hz, CH Ar, C-1), 114.1 (CH Ar, C-9 and C-15), 113.7 (CH Ar, C-11), 109.1 (CH Ar, C-7) ppm.

^{19}F NMR (377 MHz, MeOD) δ -64.27 (s) ppm.

HRMS (m/z APCI$^+$): found : 423.0833 (M + H)$^+$, C19H15ClF3N4O2 requires: 423.0830.

vmax (ATR)/cm^{-1}: 2923, 2863, 1684, 1629, 1595, 1474 (C=N), 1400, 1332, 1229 (C-O), 1129 (CF_3), 1115 (C-Cl), 977, 998.

HPLC: 99.79 % (*t*R 35.39 min)

1-(5-{3-[4-Chloro-3-(trifluoromethyl)phenoxy]phenylamino}pyridin-2-yl)guanidine hydrochloride (18)

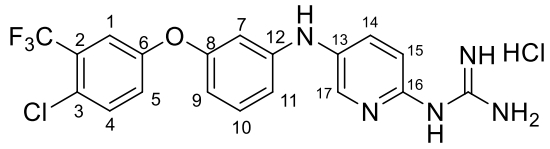

Following Method B, **77** (55 mg, mmol) was dissolved in 4M HCl in 1, 4-dioxane (mL, mmol) and in additional dioxane (mL) until a final concentration of 0.2M was reached. After 8 h stirring at 55 °C, the reaction was adjudged complete (TLC), solvents were evaporated and the residue was purified by silica gel chromatography ($CHCl_3$:MeOH) to afford **62**, the pure hydrochloride salt as a white solid (mg, 83 %) **Mp:** 87 ℃

^{1}H NMR (400 MHz, MeOD) δ 8.15 (d, *J* = 2.7 Hz, 1H, H-17), 7.63 (dd, *J* = 8.8, 2.7 Hz, 1H, H-14), 7.57 (d, *J* = 8.8 Hz, 1H, H-4), 7.36 (d, *J* = 2.9 Hz, 1H, H-1), 7.29 (t, *J* = 8.1 Hz, 1H, H-10), 7.22 (dd, *J* = 8.8, 2.9 Hz, 1H, H-5), 6.96 (d, *J* = 8.8 Hz, 1H, H-15), 6.93 – 6.88 (m, 1H, H-9), 6.72 (t, *J* = 2.2 Hz, 1H, H-7), 6.58 – 6.54 (m, 1H, H-11) ppm.

^{13}C NMR (101 MHz, MeOD) δ 156.8 (qC), 145.1(qC), 136.5 (qC), 135.8 (CH Ar, C-17), 132.6 (CH Ar, C-4), 130.5 (CH Ar, C-10), 128.7 (CH Ar, C-14), 122.4 (CH Ar, C-5), 116.8 (q, *J* = 5.5 Hz, CH Ar, C-1), 113.3 (CH Ar, C-15), 112.2 (CH Ar, C-9), 110.7 (CH Ar, C-11), 107.0 (CH Ar, C-7) ppm.

^{19}F NMR (377 MHz, MeOD) δ -64.26 (s) ppm.

HRMS (m/z APCI$^+$): Found : 422.0990 $(M + H)^+$, C19H16ClF3N5O requires: 422.0990.

vmax (ATR)/cm^{-1}: 3264 (NH), 2923, 2863, 1684, 1629, 1595, 1474 (C=N), 1400, 1332, 1229
(C-O), 1129 (CF_3), 1115 (C-Cl), 977, 998.

HPLC: 95.04 % (*t*R 34.04 min)

3-(4-chloro-3-(trifluoromethyl)phenoxy)aniline (72)

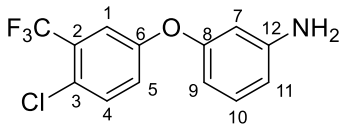

Following Method F, CuI (10 mol%, 17.6 mg), picolinic acid (20 mol%, 22.8 mg), 3-aminophenol (200 mg, 1.82 mmol), Cs_2CO_3 (382 mg, 1.82 mmol) and 4-bromo-1-chloro-2- (trifluoromethyl)benzene (0.14 mL, 0.9 mmol) were mixed, followed by addition of toluene (3.5 mL). The mixture was heated at 90 °C for 24 h and usual work up and flash chromatography afforded **63** as a brown oil (198 mg, 75%).

^{1}H NMR (400 MHz, $CDCl_3$) δ 7.41 (d, *J* = 8.8 Hz, 1H, H-4), 7.33 (d, *J* = 2.9 Hz, 1H, H-1), 7.14 (t, *J* = 8.0 Hz, 1H, H-10), 7.08 (dd, *J* = 8.8, 2.9 Hz, 1H, H-5), 6.49 (dd, *J* = 8.0, 1.9 Hz, 1H, H-9), 6.37 (dd, *J* = 8.0, 1.9 Hz, 1H, H-11), 6.33 (t, *J* = 1.9 Hz, 1H, H-7), 3.75 (s, 2H, NH_2) ppm.

^{13}C NMR (101 MHz, $CDCl_3$) δ 157.1 (qC), 156.3 (qC), 148.4 (qC), 132.6 (CH Ar, C-4), 130.8 (CH Ar, C-10), 129.5 (q, *J* = 31.8 Hz, CF_3), 125.6 (qC), 123.9(qC), 122.5 (CH Ar, C-5), 121.2 (qC), 117.9 (q, *J* = 5.4 Hz, CH Ar, C-1), 111.3 (CH Ar, C-9), 109.2 (CH Ar, C-11), 106.6 (CH Ar, C-7) ppm.

^{19}F NMR (377 MHz, $CDCl_3$) δ -62.87 (s) ppm.

HRMS (m/z ESI$^+$): Found : 288.0393 (M + H)$^+$, C13H10ClF3NO requires: 288.0398.

ν_{max} (ATR)/cm^{-1}: 3473 (NH), 3378 (NH), 3064, 2924, 1724, 1599, 1567, 1459, 1347, 1332, 1236 (CF3), 1111 (C-Cl), 1028, 999, 975.

3-(4-chloro-3-(trifluoromethyl)phenoxy)phenol (73)

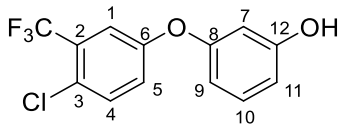

Following Method F, CuI (10 mol%, 17.6 mg), picolinic acid (20 mol%, 22.8 mg), resorcinol (200 mg, 1.82 mmol), Cs_2CO_3 (382 mg, 1.82 mmol) and 4-bromo-1-chloro-2-(trifluoromethyl)benzene (0.14 mL, 0.9 mmol) were mixed, followed by addition of toluene (3.5 mL). The mixture was heated at 90 °C for 24 h and usual work up and flash chromatography afforded **64** as a colourless oil (114 mg, 56%).

^{1}H NMR (400 MHz, $CDCl_3$) δ 7.44 (d, *J* = 8.8 Hz, 1H, H-4), 7.34 (d, *J* = 2.9 Hz, 1H, H-1), 7.23 (t, *J* = 8.2 Hz, 1H, H-10), 7.10 (dd, *J* = 8.8, 2.9 Hz, 1H, H-5), 6.64 (dd, *J* = 8.1, 2.3 Hz, 1H, H-9), 6.58 (dd, *J* = 8.2, 2.0 Hz, 1H, H-11), 6.51 (t, *J* = 2.3 Hz, 1H, H-7), 5.00 (bs, 1H, OH) ppm.

^{13}C NMR (101 MHz, $CDCl_3$) δ 157.3 (qC), 157.1 (qC), 155.9 (qC), 132.8 (CH Ar, C-4), 130.9 (CH Ar, C-10), 125.9 (qC), 123.8 (qC), 122.8 (CH Ar, C-5), 121.7 (qC), 118.1 (CH Ar, C-1), 111.6 (CH Ar, C-9 and C-11), 106.8 (CH Ar, C-7) ppm.

^{19}F NMR (377 MHz, $CDCl_3$) δ -62.92 (s) ppm.

HRMS (m/z ESI^-): Found : 287.0096 $(M - H)^-$, C13H7ClF3O2 requires: 287.0092.

ν_{max} (ATR)/cm^{-1}: 3295 (OH), 2983, 1658, 1589, 1556, 1505, 1461, 1203, 1140 (CF3), 1092 (C-Cl), 835, 772.

_N_-(3-((4-chloro-3-(trifluoromethyl)phenyl)amino)phenyl)acetamide (76)

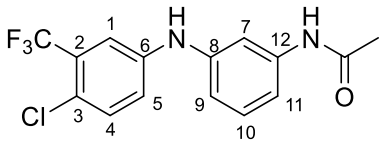

Following Method C, $Pd_2(dba)_3$ (3 mol%, 18.3 mg), Xantophos (3 mol%, 11.6 mg), N-(3-aminophenyl)acetamide (100 mg, 0.0.67 mmol), Cs_2CO_3 (306.3mg, 0.94 mmol) and 4-bromo-1-chloro-2-(trifluoromethyl)benzene (0.1 mL, 0.67 mmol) were mixed, followed syringe addition of 1,4-dioxane (1.5 mL). The mixture was heated at 90 °C for 24 h and usual work up and flash chromatography afforded **66** as a yellow oil (126 mg, 57%).

^{1}H NMR (400 MHz, $CDCl_3$) δ 7.50 (m, 2H, H-10 and NH), 7.35 – 7.29 (m, 2H, H-1 and H-4), 7.23 (t, *J* = 8.0 Hz, 1H, H-10), 7.15 (dd, *J* = 8.7, 2.7 Hz, 1H, H-5), 6.94 (dd, *J* = 8.0, 1.6 Hz, 1H, H-9), 6.84 (dd, *J* = 8.0, 1.6 Hz, 1H, H-11), 2.19 (s, 3H, CH_3) ppm.

^{13}C NMR (101 MHz, $CDCl_3$) δ 168.7 (qC), 142.3 qC), 141.9 (qC), 139.1 (qC), 132.2 (CH Ar, C-4), 129.9 (CH Ar, C-10), 120.7 (CH Ar, C-5), 116.1 (CH Ar, C-1), 114.1 (CH Ar, C-11), 113.4 (CH Ar, C-9), 110.3 (CH Ar, C-10), 24.6 (s, CH_3) ppm.

^{19}F NMR (377 MHz, $CDCl_3$) δ -62.79 (s) ppm.

HRMS (m/z ESI$^+$): found: 351.0482 $(M + H)^+$, C15H12ClF3N2NaO requires: 351.0488.

ν_{max} (ATR)/cm^{-1}: 3491 (NH), 2924, 1595, 1488 (C-N), 1512 (C-O), 769, 681, 667.

_N_-1-(4-chloro-3-(trifluoromethyl)phenyl)benzene-1,3-diamine (74)

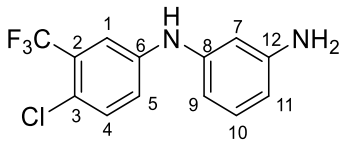

66 (100 mg) was refluxed in 1.25 M HCl/MeOH overnight. The solvent was removed under vacuum, the crude product was dissolved in water, drops of 5% $NaHCO_3$ were added until the product crushed out. The product was dissolved in EtOAc and washed with water to remove any remaining impurities, the solvent was removed under vacuum to give **19** (72 mg, 74%) **Mp**: 136-138 ℃.

^{1}H NMR (600 MHz, DMSO-d_6) δ 9.02 (s, 1H, NH), 7.53 (d, *J* = 8.8 Hz, 1H, H-4), 7.43 (d, *J* = 2.5 Hz, 1H), 7.41 – 7.33 (m, 2H, H-1, H-), 7.07 (d, *J* = 8.1 Hz, 2H), 6.85 (d, *J* = 8.2 Hz, 1H) ppm.

^{13}C NMR (151 MHz, DMSO-d_6) δ 143.85 – 143.29 (m), 142.75 (d, *J* = 18.0 Hz), 134.11 (d, *J* = 77.2 Hz), 133.23 – 132.55 (m), 131.65 – 130.39 (m), 128.15 – 127.32 (m), 126.15 – 120.46 (m), 121.10 (d, *J* = 17.1 Hz), 120.34 (d, *J* = 12.5 Hz), 116.57 (d, *J* = 19.3 Hz), 116.01 – 115.66 (q, *J* = 5.36 Hz, CH Ar, C-1), 115.27 (d, *J* = 10.4 Hz), 111.48 (d, *J* = 11.7 Hz) ppm.

^{19}F NMR (377 MHz, DMSO-d_6) δ -61.55 (s) ppm.

HRMS (m/z ESI^-): Found: 285.0495 $(M - H)^-$, C13H9ClF3N2 requires: 285.0412.

ν_{max} (ATR)/cm^{-1}: 3361 (NH), 3256 (NH), 1629, 1601, 1578, 1505, 1474, 1322 (CF3), 1259, 1110 (C-F), 1004 (C-Cl), 822, 748, 670.

5-(3-(4-chloro-3-(trifluoromethyl)phenoxy)phenoxy)-2-nitropyridine (77)

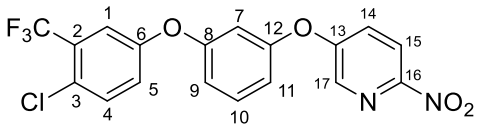

5-Bromo-2-nitropyridine (73 mg, 0.36 mmol, 1eq.), **64** (114 mg, 0.4 mmol, 1.1 eq.) and Cs_2CO_3 (162.9 mg, 3.7 mmol, 1.5 eq.) were dissolved in DMF (2 mL) and stirred at 80 °C for 12 h. The mixture was cooled to room temperature, washed with water and the organic layer extracted with EtOAc, washed with brine, dried over MgSO4, concentrated under vacuum and purified by flash chromatography (hexanes: EtOAc) to get **69** as colourless oil (65 mg, 40 %).

^{1}H NMR (400 MHz, $CDCl_3$) δ 8.33 (d, *J* = 2.8 Hz, 1H, H-17), 8.25 (d, *J* = 8.7 Hz, 1H,H-15), 7.50 (m, H-14 and H-4), 7.45 (t, *J* = 8.7 Hz, 1H, H-10), 7.36 (d, *J* = 2.9 Hz, 1H, H-1), 7.14 (dd, *J* = 8.7, 2.9 Hz, 1H, H-5), 6.94 – 6.89 (m, 2H, H-9 and H-11), 6.78 (t, *J* = 2.3 Hz, 1H, H-7) ppm.

^{13}C NMR (101 MHz, $CDCl_3$) δ 158.5 (qC), 158.4 (qC), 155.9 (qC), 155.2 (qC), 151.6 (qC), 139.5 (CH Ar, C-17), 133.3 (CH Ar, C-14), 132.8 (CH Ar, C-10), 126.4 (CH Ar, C-5), 123.5 (CH Ar, C-5), 120.1 (CH Ar, C-15), 118.7 (d, *J* = 5.4 Hz, CH Ar, C-1), 116.3 (CH Ar, C-9 or C11), 115.7 (CH Ar, C-9 or C-11), 111.2 (CH Ar, C-7) ppm.

^{19}F NMR (377 MHz, $CDCl_3$) δ -62.99 (s) ppm.

HRMS (m/z ESI^-): Found: 409.0202 $(M - H)^-$, C18H9ClF3N2O4 requires: 409.0209.

ν_{max} (ATR)/cm^{-1}: 3064, 2924, 1724, 1599, 1567, 1531 (NO_2), 1483 (NO2), 1459,

1347, 1332, 1236 (CF_3), 1130 (C-O), 1111 (C-Cl), 1028, 999, 975, 868, 823, 786.

***N*-(3-(4-chloro-3-(trifluoromethyl)phenoxy)phenyl)-6-nitropyridin-3-amine (79)**

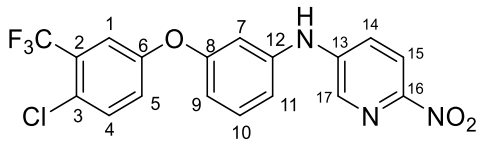

Following Method C, $Pd_2(dba)_3$ (3 mol%, 18.3 mg), Xantophos (3 mol%, 11.6 mg), **63** (162 mg, 0.56 mmol), Cs_2CO_3 (254.1 mg, 0.78 mmol) and 5-Bromo-2-nitropyridine (113.7 mg, 0.56 mmol) were mixed, followed syringe addition of toluene (1 mL). The mixture was heated at 90 °C for 24 h and usual work up and flash chromatography afforded **71** as a yellow oil (180 mg, 78%).

^{1}H NMR (400 MHz, $CDCl_3$) δ 8.21 (d, *J* = 2.8 Hz, 1H, H-17), 8.18 (d, *J* = 8.9 Hz, 1H, H-15), 7.52 – 7.45 (m, 2H, H-14 and H-4), 7.39 (t, *J* = 8.1 Hz, 1H, H-10), 7.35 (d, *J* = 2.9 Hz, 1H, H-1), 7.13 (dd, *J* = 8.7, 2.9 Hz, 1H, H-5), 7.03 (dd, *J* = 8.1, 1.8 Hz, 1H, H-9), 6.86 (t, *J* = 1.8 Hz, 1H, H-7), 6.80 (dd, *J* = 8.1, 1.8 Hz, 1H, H-11), 6.59 (s, 1H, NH) ppm.

^{13}C NMR (101 MHz, $CDCl_3$) δ 157.7 (qC), 155.5 (qC), 145.1 (qC), 140.9 (qC), 136.1 (CH Ar, C-17), 133.0 (CH Ar, C-1), 131.5 (CH Ar, C-10), 123.1 (CH Ar, C-5), 121.7 (CH Ar, C-14), 120.2 (CH Ar, C-15), 118.5 (CH Ar, C-1), 116.6 (CH Ar, C-9), 115.2 (CH Ar, C-11), 111.7 (CH Ar, C-7).

^{19}F NMR (377 MHz, $CDCl_3$) δ -62.95 (s) ppm.

HRMS (m/z ESI$^-$): Found: 408.0375 $(M - H)^-$, C18H10ClF3N3O3, requires: 408.0368.

ν_{max} (ATR)/cm^{-1}: 3385 (NH), 3064, 2934, 1724, 1599, 1557, 1531 (NO2), 1483 (NO2), 1459,
1347, 1342, 1233 (CF3), 1130 (C-O), 1110 (C-Cl), 1028, 999, 975, 868, 823, 786.

_N_1-(4-chloro-3-(trifluoromethyl)phenyl)-N3-(6-nitropyridin-3-yl)benzene-1,3-diamine (80)

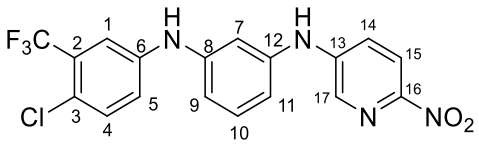

Following Method C, $Pd_2(dba)_3$ (3 mol%, 45.8 mg), Xantophos (3 mol%, 28.9 mg), **67** (470 mg, 1.75 mmol), Cs_2CO_3 (798.3 mg, 2.45 mmol) and 5-Bromo-2-nitropyridine (355.2 mg, 1.75 mmol) were mixed, followed syringe addition of toluene (3.5 mL). The mixture was heated at 90 °C for 24 h and usual work up and flash chromatography afforded **72** as a yellow oil (574 mg, 80%).

^{1}H NMR (400 MHz, $CDCl_3$) δ 8.17 (m, 2H, H-17 and H-15), 7.47 (dd, *J* = 9.0, 2.9 Hz, 1H, H-14), 7.40 – 7.36 (m, 2H, H-1 and H-4), 7.33 (t, *J* = 8.3 Hz, 1H, H-10), 7.16 (dd, *J* = 8.7, 2.7 Hz, 1H, H-5), 6.91 – 6.82 (m, 3H, H-7, H-9 and H-11), 6.44 (s, 1H, NH), 5.94 (s, 1H, NH) ppm.

^{13}C NMR (101 MHz, $CDCl_3$) δ 149.4 (qC), 145.4 (qC), 143.6 (qC), 141.5 (qC), 140.3 (qC), 135.9 (CH Ar, C-17), 132.6 (CH Ar, C-4), 131.3 (CH Ar, C-10), 129.5 (qC), 124.2 (qC), 123.7 (qC), 121.7 (CH Ar, C-5), 121.3 (CH Ar, C-14), 120.2 (CH Ar, C-1), 116.8 (CH Ar, C-1), 115.0 (2C, CH Ar, C-9 and C-11), 110.8 (CH Ar, C-7) ppm.

^{19}F NMR (377 MHz, $CDCl_3$) δ -62.82 (s) ppm.

HRMS (m/z ESI$^+$): found: 431.0490 $(M + H)^+$, C18H12ClF3N4O2Na, requires: 431.0499.

ν_{max} (ATR)/cm^{-1}: 3395 (NH), 3064, 2954, 1724, 1605, 1567, 1541 (NO_2), 1483 (NO_2), 1469,1347, 1332, 1236 (CF_3), 1130 (C-O), 1111 (C-Cl), 1028, 1000, 975, 868, 823, 786.

5-(3-(4-chloro-3-(trifluoromethyl)phenoxy)phenoxy)pyridin-2-amine (81)

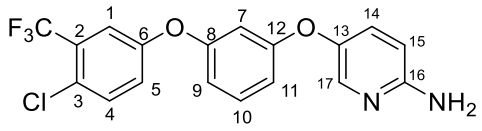

Tin (II) chloride (521 mg, 2.3 mmol) was added to a solution of **70** (63 mg, 0.15 mmol) was dissolved in ethanol (1 mL), the mixture was stirred at 78 ℃ for 6 h. the solvent was removed under a vacuum. The residue was dissolved in EtOAc and poured onto ice, the pH was adjusted to 8 with 5% $NaHCO_3$, the product was extracted with EtOAc, washed with water, brine, dried over dry $MgSO_4$ and concentrated under reduced pressure. Purified by flash chromatography over silica (hexane: EtOAc: Et_3N) to give the product, **73** as a brown oil (43 mg, 75%).

^{1}H NMR (400 MHz, $CDCl_3$) δ 7.94 (d, *J* = 2.7 Hz, 1H, H-17), 7.45 (d, *J* = 8.8 Hz, 1H, 4), 7.35 (d, *J* = 2.9 Hz, 1H, H-1), 7.26 (t, *J* = 8.1 Hz, 1H, H-10), 7.23 (dd, *J* = 8.8, 2.8 Hz, 1H, H-14), 7.11 (dd, *J* = 8.8, 2.9 Hz, 1H, H-5), 6.74 (dd, *J* = 8.1, 2.4 Hz, 1H), 6.68 (dd, *J* = 8.1, 2.4 Hz, 1H), 6.62 (t, *J* = 2.4 Hz, 1H), 6.55 (d, *J* = 8.8 Hz, 1H), 4.47 (s, 2H, NH) ppm.

^{13}C NMR (101 MHz, $CDCl_3$) δ 157.3 (qC), 155.7 (qC), 155.6 (qC), 144.8 (qC), 140.6 (CH Ar, C-17), 132.8 (CH Ar, C-4), 131.0 (CH Ar, C-14), 130.9 (CH Ar, C-10), 129.7 (d, *J* = 31.8 Hz, qC), 126.2 (qC), 123.8 (qC), 122.7 (CH Ar, C-5), 121.1 (qC), 118.1 (CH Ar, C-1), 113.0 (CH Ar, C-9), 112.6 (CH Ar, C-11), 109.4 (CH Ar, C-15), 108.1 (CH Ar, C-7) ppm.

^{19}F NMR (377 MHz, $CDCl_3$) δ -62.94 (s) ppm.

HRMS (m/z APCI$^+$): Found: 379.0470 $(M - H)^-$, C18H11ClF3N2O2 requires: 379.0467.

ν_{max} (ATR)/cm^{-1}: 3361 (NH), 3256 (NH), 1649, 1621, 1578, 1505, 1474, 1322 (CF_3), 1269, 1110 (C-F), 1014 (C-Cl), 822, 748, 670.

N5-(3-(4-chloro-3-(trifluoromethyl)phenoxy)phenyl)pyridine-2,5-diamine (82)

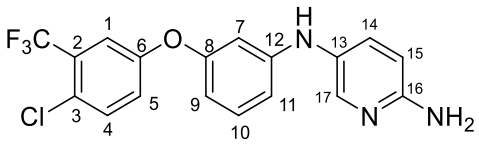

Tin (II) chloride (1410 mg, 6.2 mmol) was added to a solution of **71** (170 mg, 0.41 mmol) was dissolved in ethanol (2 mL), the mixture was stirred at 78 ℃ for 6 h. the solvent was removed under a vacuum. The residue was dissolved in EtOAc and poured onto ice, the pH was adjusted to 8 with 5% $NaHCO_3$, the product was extracted with EtOAc, washed with water, brine, dried over dry $MgSO_4$ and concentrated under reduced pressure. Purified by flash chromatography over silica (hexane: EtOAc: Et_3N) to give the product, **74** as a brown oil (101 mg, 65%).

^{1}H NMR (400 MHz, $CDCl_3$) δ 7.97 (d, *J* = 2.6 Hz, 1H, H-17), 7.42 (d, *J* = 8.8 Hz, 1H, H-4), 7.37 – 7.32 (m, 2H, H-14 and H-1), 7.18 (t, *J* = 8.1 Hz, 1H, H-10), 7.09 (dd, *J* = 8.8, 2.8 Hz, 1H, H-5), 6.59 (dd, *J* = 8.1, 2.2 Hz, 1H, H-9), 6.55 – 6.51 (m, 1H, H-15), 6.44 (t, *J* = 2.2 Hz, 1H, H-7), 6.41 (dd, *J* = 8.1, 2.2, Hz, 1H, H-11), 5.54 (s, 1H, NH), 4.57 (s, 2H, NH) ppm.

^{13}C NMR (101 MHz, $CDCl_3$) δ 157.3 (qC), 156.2 (qC), 155.6 (qC), 148.2 (qC), 143.8 (CH Ar, C-17), 134.5 (CH Ar, C-14), 132.6 (CH Ar, C-4), 130.9 (CH Ar, C-10), 129.2 (qC), 125.6 (qC), 124.8 (qC), 122.4 (CH Ar, C-5), 121.2 (qC), 117.7 (d, *J* = 5.4 Hz, CH Ar, C-1), 110.7 (CH Ar, C-9), 109.6 (CH Ar, C-11), 109.1 (CH Ar, C-15), 105.2 (CH Ar, C-7) ppm.

^{19}F NMR (377 MHz, $CDCl_3$) δ -62.88 (s) ppm.

HRMS (m/z APCI$^+$): found: 380.0772 $(M + H)^+$, C18H14ClF3N3O, requires: 380.0772.

ν_{max} (ATR)/cm^{-1}: 3368 (NH), 3356 (NH), 1629, 1609, 1578, 1505, 1474, 1342 (CF_3), 1259, 1120 (C-F), 1004 (C-Cl), 852, 748, 670.

N5-(3-((4-chloro-3-(trifluoromethyl)phenyl)amino)phenyl)pyridine-2,5-diamine (83)

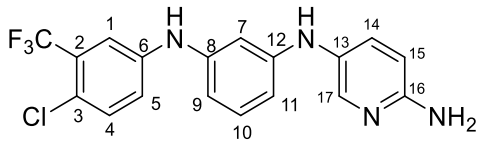

Tin (II) chloride (1740 mg, 7.7 mmol) was added to a solution of **72** (524 mg, 1.28 mmol) was dissolved in ethanol (5 mL), the mixture was stirred at 78 ℃ for 6 h. the solvent was removed under a vacuum. The residue was dissolved in EtOAc and poured onto ice, the pH was adjusted to 8 with 5% $NaHCO_3$, the product was extracted with EtOAc, washed with water, brine, dried over dry $MgSO_4$ and concentrated under reduced pressure. Purified by flash chromatography over silica (hexane: EtOAc:Et_3N) to give the product, **75** as a brown oil (232 mg, 48%).

^{1}H NMR (400 MHz, $CDCl_3$) δ 7.93 (d, *J* = 2.4 Hz, 1H, H-17), 7.37 (dd, *J* = 8.7, 2.5 Hz, 1H, H-14), 7.35 – 7.27 (m, 2H, H-1 and H-4), 7.14 (t, *J* = 7.8 Hz, 1H, H-10), 7.09 (dd, *J* = 8.7, 2.5 Hz, 1H, H-5), 6.50 (m, 2H, H-7, H-9, H-11 and H-15), 5.96 (s, 1H, NH), 5.46 (s, 1H, NH), 4.67 (bs, 2H, NH) ppm.

^{13}C NMR (101 MHz, $CDCl_3$) δ 155.3 (qC), 147.5 (qC), 143.1 (qC), 142.7 (CH Ar, C-17), 142.5 (qC), 134.7 (CH Ar, C-14), 132.2 (CH Ar, C-4), 130.68 (CH Ar, C-10), 129.6 (qC), 129.1 (qC), 128.7 (qC), 122.2 (qC), 120.7 (CH Ar, C-5), 115.7 (CH Ar, C-1), 109.8 (CH Ar, C-9), 109.4 (CH Ar, C-11), 109.2 (CH Ar, C-15), 104.5 (CH Ar, C-7) ppm.

^{19}F NMR (377 MHz, $CDCl_3$) δ -62.73 (s) ppm.

HRMS (m/z ESI$^+$): Found: 377.0791 (M - H)$^-$, C18H13ClF3N4 requires: 377.0786.

ν_{max} (ATR)/cm^{-1}: 3419 (NH), 3296 (NH), 3477 (NH), 1588, 1577, 1494 (C-O), 1324 (C-N), 1250, 1306, 1149 (C-Cl), 994, 972, 760.

1,2-Di-(tert-butoxycarbonyl)-3-(5-{3-[4-chloro-3-(trifluoromethyl)phenoxy] phenoxy}pyridin-2-yl)guanidine (84)

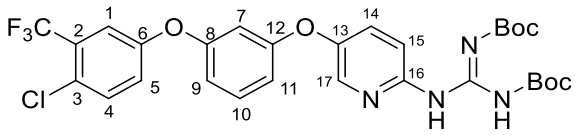

Following Method A, $HgCl_2$ (27.2 mg, 0.1 mmol) was added over a solution of **73** (42 mg, 0.1 mmol), *N*,*N*'-bis-(*tert*-butoxycarbonyl)-*S*-methylisothiourea (39 mg, 0.1 mmol), and NEt_3 (0.05 mL, 0.35 mmol) in CH_2Cl_2 (1 mL). The reaction was stirred at room temperature for 24 h, then worked up and separated on column(hexanes:EtOAc), which afforded **76** as a white amorphous solid (55 mg, 86%). **Mp:** 68-70 °C

^{1}H NMR (600 MHz, $CDCl_3$) δ 11.52 (s, 1H, NH), 10.89 (s, 1H, NH), 8.41 (d, *J* = 8.0 Hz, 1H, H-15), 8.11 (d, *J* = 2.6 Hz, 1H, H-17), 7.44 (d, *J* = 8.8 Hz, 1H, H-4), 7.41 (dd, *J* = 9.0, 2.7 Hz, 1H, H-14), 7.34 (d, *J* = 2.8 Hz, 1H, H-1), 7.30 (t, *J* = 8.2 Hz, 1H, H-10), 7.09 (dd, *J* = 8.7, 2.7 Hz, 1H, H-5), 6.77 (dd, *J* = 8.2, 2.2 Hz, 1H, H-9), 6.72 (dd, *J* = 8.1, 2.1 Hz, 1H, H-11), 6.66 (t, *J* = 2.2 Hz, 1H, H-7), 1.53 (s, 9H, $CH_3)_3$), 1.52 (s, 9H, $(CH_3)_3$) ppm.

^{13}C NMR (151 MHz, $CDCl_3$) δ 163.2 (qC), 159.0 (qC), 157.4 (qC), 155.6 (qC), 153.0 (qC), 152.8 (qC), 149.4 (qC), 146.8 (qC), 140.0 (CH Ar, C-17), 132.9 (CH Ar, C-4), 131.1 (CH Ar, C-10), 130.18 – 129.43 (qC), 129.3 (CH Ar, C-14), 126.4 (qC), 125.2 (qC), 123.4 (qC), 122.7 (CH Ar, C-5), 121.5 (qC), 119.7 (qC), 118.2 (q, *J* = 5.3 Hz, CH Ar, C-1), 117.0 (CH Ar, C-15), 113.9 (CH Ar, C-11), 113.6 (CH Ar, C-9), 109.2 (CH Ar, C-7), 84.2 (qC, $\underline{C}(CH_3)_3$), 80.1 (qC, $\underline{C}(CH_3)_3$), 28.3 ($(CH_3)_3$), 28.1 ($(CH_3)_3$) ppm.

^{19}F NMR (377 MHz, $CDCl_3$) δ -62.95 (s) ppm.

HRMS (m/z APCI$^+$): Found : 623.1890 $(M + H)^+$, C29H31ClF3N4O6 requires: 623.1879.

ν_{max} (ATR)/cm^{-1}: 3409 (NH), 3386 (NH), 3277 (NH), 1588, 1527, 1484 (C-O), 1424 (C-N), 1250, 1206, 1239 (C-Cl), 998, 982, 764.

1,2-Di-(tert-butoxycarbonyl)-3-(5-{3-[4-chloro-3-(trifluoromethyl)phenoxy] phenylamino}pyridin-2-yl)guanidine (85)

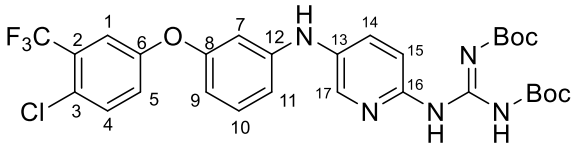

Following Method A, $HgCl_2$ (73.4 mg, 0.27 mmol) was added over a solution of **74** (100 mg, 0.26 mmol), *N*,*N'*-bis-(*tert*-butoxycarbonyl)-*S*-methylisothiourea (78.4 mg, 0.27 mmol), and NEt_3 (0.13 mL, 0.91 mmol) in CH_2Cl_2 (2 mL). The reaction was stirred at room temperature for 24 h, then work up and silica gel chromatography (hexanes:EtOAc) afforded **77** as a yellowish amorphous solid (108 mg, 67%). **Mp:** 68-71 °C

^{1}H NMR (400 MHz, $CDCl_3$) δ 11.53 (s, 1H, NH), 10.82 (s, 1H, NH), 8.29 (d, *J* = 8.5 Hz, 1H, H-15), 8.10 (d, *J* = 2.7 Hz, 1H, H-17), 7.51 (dd, *J* = 8.5, 2.7 Hz, 1H, H-14), 7.42 (d, *J* = 8.8 Hz, 1H, H-4), 7.33 (d, *J* = 2.9 Hz, 1H, H-1), 7.22 (t, *J* = 8.1 Hz, 1H, H-10), 7.08 (dd, *J* = 8.8, 2.9 Hz, 1H, H-5), 6.80 – 6.72 (m, 1H, H-9), 6.63 (t, *J* = 2.2 Hz, 1H, H-7), 6.56 – 6.46 (m, 1H. H-11), 5.77 (s, 1H, NH), 1.53 (s, 9H, $(CH_3)_3$), 1.51 (s, 9H, $(CH_3)_3$) ppm.

^{13}C NMR (151 MHz, $CDCl_3$) δ 163.2 (qC), 157.21 (qC), 156.11 (qC), 152.9 (qC), 145.5 (qC), 140.1 (CH Ar, C-17), 135.1 (qC), 132.8 (CH Ar, C-4), 131.1 (CH Ar, C-10), 129.7 (qC), 129.57 (qC), 129.2 (CH Ar, C-14), 125.8 (qC), 123.4 (qC), 122.49 (CH Ar, C-5), 121.6 (qC), 119.7 (qC), 117.8 (q, *J* = 5.4 Hz, CH Ar, C-1), 116.8 (CH Ar, C-15), 112.4 (CH Ar, C-9), 111.3 (CH Ar, C-11), 107.2 (CH Ar, C-7), 84.0 (qC, $C(CH_3)_3$), 80.1 (qC, $C(CH_3)_3$), 28.3 ($(CH_3)_3$), 28.1 ($(CH_3)_3$).

^{19}F NMR (377 MHz, $CDCl_3$) δ -62.90 (s) ppm.

HRMS (m/z APCI$^+$): Found: 622.2051 $(M + H)^+$, C29H32ClF3N5O5 requires: 622.2039.

ν_{max} (ATR)/cm^{-1}: 3262 (NH), 2974, 2928, 2284, 2165, 2050, 1981, 1722 (CO), 1638 (CN), 1592, 1542, 1485, 1438, 1420, 1390, 1366, 1334, 1287, 1245, 1209, 1148, 1089, 1015, 966, 919, 853, 804, 767, 750, 689.

1,2-Di-(tert-butoxycarbonyl)-3-(5-{3-[4-chloro-3-(trifluoromethyl)phenylamino] phenylamino}pyridin-2-yl)guanidine (86)

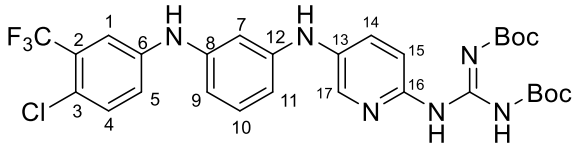

Following Method A, $HgCl_2$ (163.1 mg, 0.6 mmol) was added over a solution of **75** (210 mg, 0.6 mmol), *N*,*N'*-bis-(*tert*-butoxycarbonyl)-*S*-methylisothiourea (174.2 mg, 0.6 mmol), and NEt_3 (0.3 mL, 2.1 mmol) in CH_2Cl_2 (2 mL). The reaction was stirred at room temperature for 24 h, then work up and silica gel chromatography (hexanes:EtOAc) afforded **78** as a white solid (260 mg, 70%). **Mp:** 72-74 °C

^{1}H NMR (400 MHz, $CDCl_3$) δ 11.52 (s, 1H, NH), 10.77 (s, 1H, NH), 8.20 (d, *J* = 6.6 Hz, 1H, H-15), 8.06 (d, *J* = 2.6 Hz, 1H, H-17), 7.44 (dd, *J* = 6.6, 2.6 Hz, 1H), 7.33-7.28 (m, 2H, H-1 and H-4), 7.15 (t, *J* = 8.0 Hz, 1H, H-10), 7.10 (dd, *J* = 8.7, 2.6 Hz, 1H, H-5), 6.61 (m, 3H, H-7, H-9 and H-11), 6.01 (s, 1H, NH), 5.83 (s, 1H, NH), 1.51 (s, 18H, $(CH_3)_6$) ppm.

^{13}C NMR (101 MHz, $CDCl_3$) δ 153.2 (qC), 144.6 (qC), 142.9 (qC), 142.3 (qC), 139.6 (CH Ar, C-17), 135.7 (qC), 132.2 (CH Ar, C-4), 130.7 (CH Ar, C-10), 129.5 (qC), 129.2 (qC), 128.8 (qC), 128.5 (CH Ar, C-14), 127.0 (qC), 124.2 (qC), 122.3 (qC), 121.5 (qC), 120.7 (CH Ar, C-5), 117.0 (CH Ar, C-15), 115.9 (q, *J* = 5.4 Hz, CH Ar, C-1), 111.2 (CH Ar, C-9), 110.9 (CH Ar, C-11), 106.6 (CH Ar, C-7), 84.2 (qC, $\underline{C}(CH_3)_3$), 80.2 (qC, $\underline{C}(CH_3)_3$), 28.22 ($(CH_3)_6$) ppm.

^{19}F NMR (377 MHz, $CDCl_3$) δ -62.76 (s) ppm.

HRMS (m/z ESI^-): Found: 619.2049 $(M - H)^-$, C29H31ClF3N6O4 requires: 619.2053.

vmax (ATR)/cm^{-1}: 3411(NH), 3264, 2978, 2932, 1718 (CO), 1636 (CN), 1590, 1559, 1481, 1461, 1408, 1337, 1305, 1230, 1211, 1145, 1095, 1056, 835, 806, 750, 690.

5-{3-[4-Chloro-3-(trifluoromethyl)phenyl]aminophenyloxy}-2-nitropyridine (87)

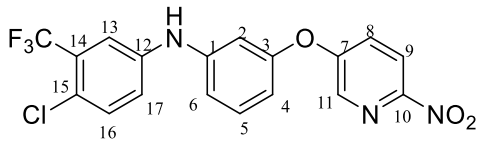

Following Method D, $Pd_2(dba)3$ (3 mol%, 6 mg), Xantphos (3 mol%, 4 mg), compound **15** (50 mg, 0.22 mmol), Cs_2CO_3 (100 mg, 0.31 mmol) and remaining liquid 4-bromo-1-chloro-2- (trifluoromethyl)benzene (0.03 mL, 0.22 mmol) were mixed, followed syringe addition of toluene (0.5 mL). The mixture was heated at 90 °C for 24 h and usual work up and flash chromatography afforded **79** as a yellow oil (82 mg, 91%).

^{1}H NMR (400 MHz, $CDCl_3$) δ 6.01 (bs, 1H, NH), 6.70 (dd, *J* = 8.1, 2.2 Hz, 1H, H-4), 6.79 (t, *J* = 2.2 Hz, 1H, H-2), 6.96 (dd, *J* = 7.9, 1.8 Hz, 1H, H-6), 7.18 (dd, *J* = 8.5, 2.8 Hz, 1H, H-17), 7.34 –

7.39 (m, 3H, H-13, H-16 and H-5), 7.46 (dd, *J* = 8.9, 2.8 Hz, 1H, H-8), 8.24 (d, *J* = 8.9 Hz,

1H, H-9), 8.33 (d, *J* = 2.8 Hz, 1H, H-11) ppm.

^{13}C NMR (100 MHz, CDCl3) δ 109.4 (CH Ar, C-2), 113.2 (CH Ar, C-4), 115.3 (CH Ar, C-6), 117.2

(q, *J* = 5.5 Hz, CH Ar, C-13), 119.9 (CH Ar, C-9), 122.0 (CH Ar, C-17), 122.7 (d, J = 273.4

Hz, qCF3), 124.1 (qC, C-15), 126.0 (CH Ar, C-8), 129.4 (d, *J* = 31.2 Hz, qC, C-14), 131.7

(CH Ar, C-5 or C-16), 132.6 (CH Ar, C-5 or C-16), 138.8 (CH Ar, C-11), 141.1 (qC), 144.5

(qC), 151.3 (qC), 155.5 (qC), 158.8 (qC) ppm.

^{19}F NMR (377 MHz, $CDCl_3$) δ -62.89 (s).

HRMS (m/z ESI+): Found: 410.0520 $(M + H)^+$, C18H12N3O3ClF3 requires: 410.0519.

ν_{max} (ATR)/cm-1: 3385 (NH), 3064, 2924, 1724, 1599, 1567, 1531 (NO_2), 1483 (NO_2), 1459,

1347, 1332, 1236 (CF3), 1130 (C-O), 1111 (C-Cl), 1028, 999, 975, 868, 823, 786.

2-Amino-5-{3-[4-chloro-3-(trifluoromethyl)phenyl]aminophenyloxy}pyridine (88)

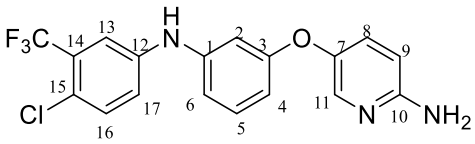

Following Method F, a mixture of **79** (66 mg, 0.16 mmol) and $SnCl_2 \cdot 2H_2O$ (218 mg, 0.97 mmol) in 1 mL of absolute ethanol were heated at 70°C for 3 h. Usual work up and flash chromatography afforded **80** as a brown oil (48 mg, 80%).

^{1}H NMR (400 MHz, CDCl3) δ 4.41 (s, 2H, NH2), 5.88 (s, 1H, NH), 6.53 (d, J = 8.8 Hz, 1H, H-9),

6.56 (dd, *J* = 8.3, 2.2 Hz, 1H, H-4), 6.61 (t, *J* = 2.0 Hz, 1H, H-2), 6.73 (dd, *J* = 8.0, 1.7 Hz,

1H, H-6), 7.11 (dd, *J* = 8.6, 2.7 Hz, 1H, H-17), 7.19 – 7.23 (m, 2H, H-5 and H-8), 7.32 – 7.34

(m, 2H, H-13 and H-16), 7.91 (d, *J* = 2.1 Hz, 1H, H-11) ppm.

^{13}C NMR (100 MHz, CDCl3) δ 107.0 (CH Ar, C-2), 109.4 (CH Ar, C-9), 110.8 (CH Ar, C-4), 112.6(CH Ar, C-6), 116.2 (q, *J* = 5.4 Hz, CH Ar, C-13), 121.1 (CH Ar, C-17), 122.8 (d, *J* = 273.3

Hz, CF_3), 123.0 (qC, C-15), 129.2 (d, *J* = 31.1 Hz, CH Ar, C-14), 130.8 (CH Ar, C-5 or C-

8), 131.1 (CH Ar, C-5 or C-8), 132.4 (CH Ar, C-16), 140.5 (CH Ar, C-11), 142.0 (qC), 143.2 (qC), 145.1 (qC), 155.4 (qC), 160.1 (qC) ppm.

^{19}F NMR (377 MHz, $CDCl_3$) δ -62.85 (s).

HRMS (m/z ESI$^-$): Found: 378.0629 $(M - H)^-$, C18H12N3OF3Cl requires: 378.0621.

ν_{max} (ATR)/cm^{-1}: 3332 (NH), 2923 (C-H), 2847 (C-H), 1595, 1480, 1327, 1258, 1225, 1172, 1125 (CF3), 1111 (C-Cl), 820, 711, 665.

1,3-Di(*tert*-butoxycarbonyl)imidazolidine-2-thione (89)[17]

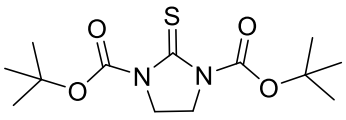

To a cooled solution of the imidazolidine-2-thione (500 mg, 4.92 mmol) in dry tetrahydrofuran (40 mL) under argon, NaH as a 60% suspension in mineral oil (882 mg, 22.1 mmol) was added. After 5 min, the ice-bath was removed and the reaction was stirred for 10 min at room temperature. The reaction mixture was again cooled to 0 °C and di-*tert*-butyldicarbonate (2.38 g, 10.78 mmol) was added neat. After 30 min, the ice-bath was removed and the reaction mixture was stirred overnight h at room temperature (reaction progress adjudged by TLC). The reaction was quenched by the dropwise addition of saturated NaHCO3 solution (5 mL) and extracted with EtOAc (3 × 40 mL). The organic phase was washed with brine (25 mL), dried over $MgSO_4$, filtered, and concentrated under vacuum. The product was purified by flash chromatography using alumina column (eluting with hexane:EtOAc) and recrystallised from hexane slowly (1 to 2 days), to afford the title compound as lustrous yellow needles (1.24 g, 89%). **Mp**: 115 °C (lit.: 117- 119 °C).

^{1}H NMR (400 MHz, CDCl3) δ 1.47 (s, 18H, $(CH_3)_6$), 3.90 (s, 4H, CH_2) ppm.

di-tert-butyl-2-((5-(3-((4-chloro-3-(trifluoromethyl)phenyl)amino)phenoxy)pyridin-2-yl)imino)imidazolidine-1,3-dicarboxylate (90)

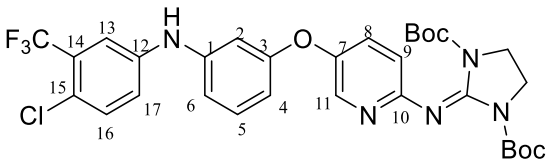

Following Method A, $HgCl_2$ (163.1 mg, 0.6 mmol) was added over a solution of **81** (210 mg, 0.6 mmol), **81** (174.2 mg, 0.6 mmol), and NEt_3 (0.3 mL, 2.1 mmol) in CH_2Cl_2 (2 mL). The reaction was stirred at room temperature for 24 h, then work up and silica gel chromatography (hexanes:EtOAc) afforded **82** as a white amorphous solid (260 mg, 83%). **Mp**: 84-85 °C

^{1}H NMR (400 MHz, $CDCl_3$) δ 8.07 (d, *J* = 2.8 Hz, 1H, H-11), 7.36 – 7.27 (m, 3H, H-13, H-16 and H-8), 7.25 – 7.18 (m, 1H, H-5), 7.14 (dd, *J* = 8.2, 4.1 Hz, 1H, H-17), 6.79 (dd, *J* = 8.0, 1.7 Hz, 1H, H-4), 6.65 (t, *J* = 1.7 Hz, 1H, H-2), 6.57 (dd, *J* = 8.0, 1.7 Hz, 1H, H-6), 6.22 (s, 1H, NH), 3.82 (s, 4H, $(CH_2)_2$), 1.55 (s, 18H, $(CH_3)_6$) ppm.

^{13}C NMR (101 MHz, $CDCl_3$) δ 159.5 (qC), 147.6 (qC), 143.3 (qC), 141.8 (qC), 139.6 (CH Ar, C-11), 132.2 (CH Ar, C-16), 130.6 (CH Ar, C-5), 129.7 (CH Ar, C-13), 129.2 (qC), 129 (qC), 124.2 (qC), 122.4 (qC), 120.8 (CH Ar, C-17), 116.4 (q, *J* = 5.6 Hz, CH Ar, C-13), 112.7 (CH Ar, C-4), 110.8 (CH Ar, C-6), 107.4 (CH Ar, C-2), 45.2 (s, $CH_2)_2$), 28.2 ($(CH_3)_6$)) ppm.

^{19}F NMR (377 MHz, CDCl3) δ -62.80 (s) ppm.

HRMS (m/z ESI-): Found: 647.2112 $(M - H)^-$, C31H33ClF3N5O5 requires: 647.2122.

ν_{max} (ATR)/cm-1: 2977, 2929, 1754 (CO), 1695 (CN), 1596, 1477, 1457, 1366, 1297, 1247, 1143, 974, 848, 765, 695.

4-chloro-*N*-(3-((6-(imidazolidin-2-ylideneamino)pyridin-3-yl)oxy)phenyl)-3-(trifluoromethyl)aniline trifluoroacetate (20)

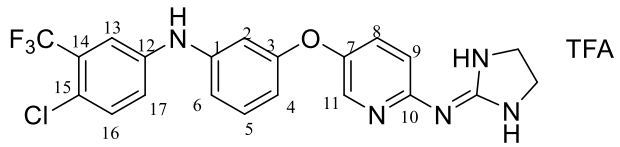

A solution of the corresponding Boc-protected precursor **82** (100 mg, 0.13 mmol) in 10 mL

of a 50% v/v solution of TFA and CH_2Cl_2 was stirred at room temperatura for 24 h.

The excess of TFA and CH_2Cl_2 were removed under vacuum to generate the trifluoroacetate salt. afforded **83** as a white amorphous solid (260 mg, 83%). **Mp**: 146-150 °C.

^{1}H NMR (400 MHz, MeOD) δ 8.16 (d, *J* = 2.8 Hz, 1H, H-11), 7.59 (dd, *J* = 8.9, 2.9 Hz, 1H, H-8), 7.39 (m, 2H, H-13 and H-16), 7.31 (t, *J* = 8.1 Hz, 1H, H-5), 7.26 (dd, *J* = 8.7, 2.7 Hz, 1H, H-17), 7.11 – 7.07 (m, 1H, H-9), 6.92 (dd, *J* = 8.1, 1.5 Hz, 1H, H-4), 6.76 (t, *J* = 2.2 Hz, 1H, H-2), 6.61 (dd, *J* = 8.0, 2.0 Hz, 1H, H-6), 3.87 (s, 1H, $(CH_2)_2$) ppm.

^{13}C NMR (101 MHz, MeOD) δ 158.8 (qC), 156.5 (qC), 150.4 (qC), 146.4 (qC), 144.3 (qC), 142.7 (qC), 137.9 (CH Ar, C-11), 132.1 (CH Ar, C-16), 130.6 (CH Ar, C-5), 130.2 (CH Ar, C-8), 128.4 (qC), 128.7 (qC), 124.2 (qC), 121.5 (qC), 120.9 (qC), 120.3 (CH Ar, C-17), 114.8 (q, J = 5.6 Hz, CH Ar, C-13), 113.3 (CH Ar, C-4 or C-9), 113.2 (CH Ar, C-4 or C-9), 110.6 (CH Ar, C-6), 107.2 (CH Ar, C-2), 42.4 ($(CH_2)_2$) ppm.

^{19}F NMR (377 MHz, MeOD) δ -64.14 (CF_3), -76.97 (TFA) ppm.

HRMS (m/z ESI-): Found: 448.1146 $(M + H)^+$, C21H18ClF3N5Orequires: 448.1074

ν_{max} (ATR)/cm-1: 3138 (NH), 2898, 1644 (CN), 1585, 1513, 1435, 1381, 1281, 1282,

1201, 1083, 1018, 983.

HPLC: 98.60 % (*t*R 34.16 min)

1-(4-((2-((4-chloro-3-(trifluoromethyl)phenyl)amino)pyrimidin-4-yl)oxy)phenyl)guanidine hydrochloride (23)

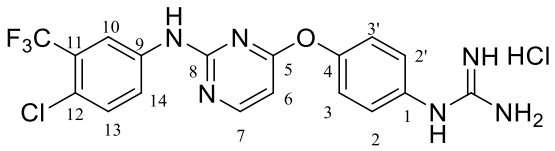

Following Method B, **98** (58 mg, 0.09 mmol) was dissolved in 4M HCl in 1, 4-dioxane (0.26

mL, 1.04 mmol) and in additional dioxane (0.17 mL) until a final concentration of 0.2M was

reached. After 8 h stirring at 55 °C, the reaction was adjudged complete (TLC), solvents were

evaporated and the residue was purified by silica gel chromatography (CHCl3:MeOH) to

afford **92**, the pure hydrochloride salt as a white solid (40 mg, 88%) **Mp:** 90-91 ℃

^{1}H NMR (400 MHz, MeOD) δ 8.38 (d, *J* = 5.8 Hz, 1H, H-6), 7.97 (d, *J* = 2.5 Hz, 1H, H-10), 7.71 (dd, *J* = 8.8, 2.5 Hz, 1H, H-14), 7.43 – 7.38 (m, 2H, H-3 and C-3'), 7.35 (m, 3H, H-2, C-2' and C-13), 6.57 (d, *J* = 5.8 Hz, 1H, H-7) ppm.

^{13}C NMR (101 MHz, MeOD) δ 170.0 (qC), 158.9 (CH Ar, C-6), 158.6 (qC), 156.8 (qC), 151.6 (qC), 138.9 (qC), 132.1 (CH Ar, C-13), 131.1 (qC), 127.6 (d, *J* = 31.1 Hz), 126.7 (CH Ar, C-2 and C-2'), 124.2 (qC), 123.5 (CH Ar, C-14), 123.2 (CH Ar, C-3 and C3'), 121.5 (qC), 117.8 (d, *J* = 5.7 Hz, H-10), 99.4 (CH Ar, C-7).

^{19}F NMR (377 MHz, MeOD) δ -63.89 (s) ppm.

ν_{max} (ATR)/cm^{-1}: 3289 (NH), 3127 (NH), 1659 (CN), 1582, 1508, 1505, 1331, 1238, 1167, 880.

HRMS (m/z APCI^{+}): Found : 423.0942 (M)$^{+}$, C18H15ClF3N6O requires: 423.0942.

HPLC: 99.83% (*t*R 31.67 min)

2-chloro-4-(4-nitrophenoxy)pyrimidine (95)[18]

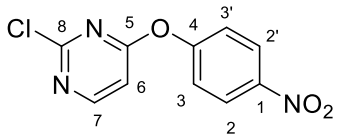

4-nitro-phenol **(**500 mg, 2.45 mmol, 1eq.), 2,6-dichloropyrimidine (295 mg, 2.7 mmol, 1.1 eq.) and K_2CO_3 (1.2 g, 3.7 mmol, 1.5 eq.) were dissolved in DMF (5 mL) and stirred at 80 °C for 12 h. The mixture was cooled to room temperature, washed with water and the organic layer extracted with EtOAc, washed with brine, dried over $MgSO_4$, concentrated under vacuum and purified by flash chromatography (hexanes: EtOAc) to get **15** as orange crystals (339 mg, 68 %).

1H NMR (400 MHz, $CDCl_3$) δ 8.53 (d, *J* = 5.6 Hz, 1H, H-6), 8.36 – 8.29 (m, 2H, H-2 and H-2'), 7.40 – 7.33 (m, 2H, H-3 and H-3'), 6.96 (d, *J* = 5.6 Hz, 1H, H-7) ppm.

^{13}C NMR (151 MHz, $CDCl_3$) δ 169.9 (qC), 161 (qC), 160.4 (CH Ar, C-7), 156.4 (qC), 145.4 (qC), 125.7 (CH Ar, C-2 and C-2'), 122.4 (CH Ar, C-3 and C-3'), 107.5 (CH Ar, C-6) ppm.

_N_-(4-chloro-3-(trifluoromethyl)phenyl)-4-(4-nitrophenoxy)pyrimidin-2-amine (96)

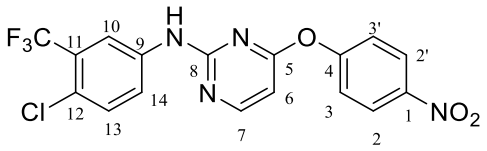

Following Method C, $Pd_2(dba)_3$ (3 mol%, 25.6 mg), Xantphos (3 mol%, 16.4 mg), compound **95** (200 mg, 0.88 mmol), Cs_2CO_3 (390.8 mg, 0.31 mmol) and 4-chloro-3-trifluoromethyl-aniline (267.4 mg, 0.88 mmol) were mixed, followed by addition of toluene (1.9 mL). The mixture was heated at 90 °C for 24 h and worked up as par method C and flash chromatography afforded **96** as a yellow oil (311 mg, 82%).

^{1}H NMR (400 MHz, DMSO-d_6) δ 10.17 (s, 1H, NH), 8.53 (d, *J* = 5.6 Hz, 1H, H-6), 8.39 – 8.30 (m, 2H, H-2 and H-2'), 8.06 (s, 1H, H-10), 7.73 (d, *J* = 7.9 Hz, 1H, H-14), 7.56 (m, 2H, H-3 and H-3'), 7.48 (d, *J* = 8.8 Hz, 1H, H-13), 6.73 (d, *J* = 5.6 Hz, 1H, H-7) ppm.

^{13}C NMR (151 MHz, DMSO-d_6) δ 168.9 (qC), 160.6 (CH Ar, C-6), 159.3 (qC), 157.8 (qC), 145.2 (qC), 139.8 (qC), 132.4 (CH Ar, C-13), 126.2 (CH Ar, C-2 and C-2'), 124.2 (CH Ar, C-14), 123.3 (CH Ar, C-3 and C-3'), 122.5 (qC), 122.2 (qC), 117.8 (d, *J* = 5.6 Hz, CH Ar, C-10), 100.6 (CH Ar, C-7) ppm.

^{19}F NMR (377 MHz, DMSO) δ -61.61 (s) ppm.

HRMS (m/z ESI$^-$): Found: 409.0327 $(M - H)^-$, C17H9ClF3N4O3 requires: 409.0321.

ν_{max} (ATR)/cm-1: 3160 (NH), 2979, 2933, 1718 (CO), 1628 (CN), 1598, 1567, 1506, 1450, 1407, 1367, , 1306, 1290, 1233, 123, 1143, 1106, 1055, 879, 804, 769, 686.

4-(4-aminophenoxy)-N-(4-chloro-3-(trifluoromethyl)phenyl)pyrimidin-2-amine (97)

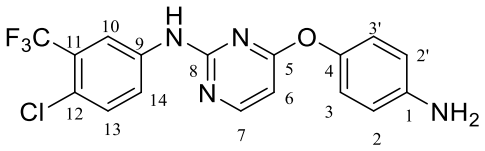

Tin (II) chloride (820 mg, 3.6 mmol) was added to a solution of Compound **96** (110 mg, 0.24 mmol) dissolved in ethanol (1mL) The mixture was stirred at 70 ℃ for 24h. the solvent was removed under vacuum. The residue was dissolved in EtOAc and poured onto ice, the pH was adjusted to 8 with 5% $NaHCO_3$, the product was extracted with EtOAc, washed with water, brine, dried over dry $MgSO_4$ and concentrated under reduced pressure. Purified by flash chromatography over silica (hexane: EtOAc: Et_3N) to give the product, **97** as a brown oil (70 mg, 62%).

^{1}H NMR (400 MHz, $CDCl_3$) δ 8.23 (d, *J* = 5.4 Hz, 1H, H-13), 7.72 (d, i = 2.3 Hz, 1H, H-10), 7.62 (dd, *J* = 8.8, 2.5 Hz, 1H, H-14), 7.37 (s, 1H, NH), 7.27 (d, *J* = 8.8 Hz, 1H, H-7), 6.96 – 6.87 (m, 2H, H-2 and H-2'), 6.75 – 6.67 (m, 2H, H-3 and H3'), 6.34 (d, *J* = 8.8 Hz, 1H, H-6) ppm.

^{13}C NMR (151 MHz, $CDCl_3$) δ 168.9 (qC), 160.9 (CH Ar, C-6), 159.3 (qC), 157.8 (qC), 145.2 (qC), 139.8 (qC), 132.4 (CH Ar, C-13), 126.2 (qC), 124.2 (CH Ar, C-14), 123.3 (CH Ar, C-3 and C-3'), 122.5 (qC), 122.2 (CH Ar, C-2 and C-2'), 117.8 (d, *J* = 5.6 Hz, CH Ar, C-10), 100.6 (CH Ar, C-7) ppm.

HRMS (m/z ESI+): Found: 379.0577 $(M - H)^-$, C17H11ClF3N4O requires: 379.0579.

ν_{max} (ATR)/cm-1: 3383 (NH), 2926, 1725, 1594, 1504 (C-N), 1482 (C-N), 1329, 1250, 1172 (C-Cl), 1130 (C-O), 1112 (CF3), 825, 681, 666.

1,2-Di-(tert-butoxycarbonyl)-3-(4-((2-((4-chloro-3 (trifluoromethyl)phenyl)amino)pyrimidin-4-yl)oxy)phenyl)guanidine (98)

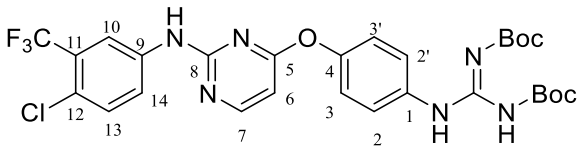

$HgCl_2$ (49 mg, 0.18 mmol, 1.04 eq) was added to a solution of **97** (70 mg, 0.17 mmol, 1 eq), *N,N'*-bis-(*tert*-butoxycarbonyl)-*S*-methylisothiourea (52.3 mg, 0.18 mmol, 1.04 eq), and triethylamine (0.08 mL, 0.6 mmol, 3.5 eq) in CH_2Cl_2. the mixture was stirred for 24 hrs, then work-up and purification on silica gel (hexane: EtOAc) to give **98** as a white solid (66 mg, 83%) **Mp**: 69-70 °C.

^{1}H NMR (400 MHz, $CDCl_3$) δ 11.67 (s, 1H, NH), 10.40 (s, 1H, NH), 8.32 (d, *J* = 5.6 Hz, 1H, H-6), 7.83 – 7.61 (m, 4H, H-10, H-11, H-2 and H-2'), 7.36 (d, *J* = 8.6 Hz, 1H, H-13), 7.14 (d, J = 8.1 Hz, 2H, H-3 and H-3'), 6.44 (d, *J* = 5.6 Hz, 1H, H-7), 1.55 (s, 18H, $(CH_3)_6$) ppm.

^{13}C NMR (101 MHz, CDCl3) δ 170.1 (qC), 158.9 (CH Ar, C-6), 154.2 (qC), 153.3 (qC), 149.7 (qC), 138.1 (qC), 134.2 (qC), 131.7 (CH Ar, C-13), 128.6 (qC), 128.3 (qC), 124.3 (CH Ar, C-2 and C-2'), 122.7 (CH Ar, C-14), 122.4 (CH Ar, C-3 and C-3'), 117.8 (CH Ar, C-10), 100.6 (CH Ar, C-7), 84.4 (qC, $\underline{C}(CH_3)_3$), 80.9 (qC, $\underline{C}(CH_3)_3$), 28.1 ($(CH_3)_6$) ppm.

^{19}F NMR (377 MHz, $CDCl_3$) δ -63.40 (s) ppm.

HRMS (m/z APCI$^+$): Found : 623.1990 $(M + H)^+$, C28H31ClF3N6O5 requires: 623.1991.

ν_{max} (ATR)/cm^{-1}: 3259 (NH), 3135 (NH), 2979, 2933, 1719 (CO), 1633 (CN), 1599, 1552, 1407, 1368, 1336, 1297, 1230, 1148, 1099, 1056, 1028, 941, 881, 845, 805, 757.

7.3. Biochemistry

7.3.1. Materials

All reagents were purchased from Sigma Aldrich or Gibco (Life Technologies) and sterile when required. Sorafenib was purchased from LC laboratories. Buffers where prepared when needed according to the following recipes: 20X Annexin Binding Buffer (pH 7.4 – 50 mL: 2.60 g HEPES 10.9 mM, 8.18 g NaCl 140 mM, 0.28 g CaCl2 2.5 mM); 1X Annexin Binding Buffer (40 mL: 2 mL 20X Binding Buffer, 38 mL PBS); Annexin V (600 µL: 18 µL Annexin V, 582 µL 1X Annexin Binding Buffer); Propidium Iodide (3 µL propidium iodide, 6 mL 1X Annexin Binding Buffer); Laemmli buffer [Tris-HCl 50 mM (pH 6.7), glycerol 10% (w/v), sodium dodecyl sulphate 2% (w/v), bromophenol blue 0.02% (w/v)]; Radioimmunoprecipitation assay buffer (RIPA buffer) was purchased from SigmaAldrich and protease inhibitors freshly added before use; running buffer 10 X for wester blotting (250 mM Tris base, 2 M glycine, 5% v/v SDS); transfer buffer 10 X for wester blotting (250 mM Tris base, 2 M glycine).

7.3.2. General Procedures

7.3.2.1. Cell Storage/Cryopreservation

When an aliquot of cells was required, the cells were quickly removed from the liquid nitrogen and thawed at 37 °C for 2 min. Just before the samples had fully thawed, their contents were gently pipetted into a sterile 20 mL tube containing growing medium. The cells were then centrifuged at 300 x *g* for 5 min. The supernatant was discarded, and the pellet was resuspended in 5 mL of medium. This solution was then added to a T25 flask and the cells monitored closely over a period of time depending on the cell line.

The growth medium was stored at 4 °C and heated to 37 °C prior to culture work. Cells were grown at 37 °C in a humidified environment with 5% CO_2 and passaged at least twice weekly when the cells have reached 70% confluency. When required for sub-culturing, if in suspension, cells were transferred to a sterile tube and centrifuged at 300 x *g* for 5 min. Otherwise, if adherent cells, cells were washed with PBS, trypsinised and

transferred to a sterile tube and centrifuged at 300 x *g* for 5 min. The supernatant was discarded, and the cell pellet was resuspended in 15 mL of fresh medium.

7.3.2.2. Use of Haemocytometer

A haemocytometer is a modified microscope slide containing an accurately sub-divided grid that enables the counting of cells in suspension. Each grid (there are two) consists of nine large squares, each measuring 1 mm^2. Each of these primary squares contains 16 medium squares, each measuring 0.04 mm^2. When a particular seeding density of cells was required, a clean cover slip was placed on the haemocytometer; 10 µL of the cell suspension is then pipetted into the groove at the end of the plane. The cell suspension is then drawn across the grid by capillary action. The number of cells within the four outer primary squares is counted. Those that touched the sides of the grid were counted and those that were outside the four squares were not counted. As each medium square is 0.04 mm^3, the total volume per primary square is 1×10^{-4} mL. This implies that the total cell concentration in the original suspension (cells/mL) is = average cell count/primary square $\times 1 \times 10^4$.

7.3.2.3. Preparation of the Drugs' Solutions

Stock solutions (10 mM) of the compounds were prepared in sterile EtOH, DMSO or water and were then sterile filtered (0.2 µM filters). Required concentration ranges (10-0.01 mM) of each drug were prepared in sterile EtOH, DMSO or H_2O and stored at -20 °C until required. Sorafenib was purchased from LC Laboratories and dissolved in 100% ethanol to make a 10 mM stock. Working dilutions were made up with ethanol to the concentration required. All stock concentrations and dilutions in ethanol were stored at 4°C.

7.3.2.4. Growth and Maintenance of the Cell Lines

NCI-H929 and U266B1 Cell Line

The NCI-H929 and U266B1 (human bone marrow myeloma) cell lines were obtained from Prof. Daniela Zisterer's group (School of Biochemistry and Immunology, TCD). They were maintained in Roswell Park Memorial Institute (RPMI) 1640 medium with stable glutamate (GlutaMax I) supplemented with 10% (v/v) fetal bovine serum (FBS) and 1% penicillin/ streptomycin (pen-strep).

HL-60 Cell Line

The HL-60 (human caucasian promyelocytic leukemia) cell line was obtained from European

Collection of Cell Cultures (Porton Down, Wiltshire, U.K.). It was maintained between

200,000 and 2,000,000 cells/mL in Roswell Park Memorial Institute (RPMI) 1640 medium

with stable glutamate (GlutaMax I) supplemented with 10% (v/v) fetal bovine serum (FBS)

and 1% penicillin/ streptomycin (pen-strep).

7.3.3. AlamarBlue® Cell Viability Assay

Cells were counted and seeded at a density of 2 × 10^5 cells/mL for HL-60, 2.5× 10^4 cells/mLfor MCF-7, MCF10A and 2.5 × 10^5cells/mL for NCI-H929 and U266B1, all of them in complete medium. The 96 well plates were then treated with a 1:100 dilution of stock concentrations of drugs or EtOH (1% v/v) as vehicle control in triplicate. Three blank wells containing 200 µL RPMI with no cells were also set-up as blanks. After a 72 h incubation, 20 µL of AlamarBlue was added to each well. The plates were incubated in darkness at 37 °C for 4-5 h. Using a Molecular Devices microplate reader, the fluorescence (F) was then read at an excitation wavelength of 544 nm and an emission wavelength of 590 nm. Cell viability was then determined by subtracting the mean blank fluorescence (Fb) from the treated sample fluorescence (Fs) and expressing this as a percentage of the fluorescence of the blanked vehicle control (Fc). This is demonstrated in the equation below. The results were then plotted as a nonlinear regression,

sigmoidal dose-response curves on Prism, from which the IC50 value for each drug was determined.

$$\frac{Fs - Fb}{Fc - Fb} X\ 100 = \%\ Cell\ Viability$$

7.3.4. NCI cancer screening panel

The cancer screening panel human tumor cell lines are grown in RPMI 1640 medium containing 5% fetal bovine serum and 2 mM L-glutamine. For a typical screening experiment, cells in 96-well microtiter plates are inoculated in 100 µl at plating densities in the range of 5,000 to 40,000 cells / well, depending on the doubling time of the individual cell lines. After the cell inoculation, the microtiter plates are incubated at 37 ° C., 5% CO_2, 95% air and 100% relative humidity for 24 h before the experimental drugs are added.

After 24 hours, two plates of each cell line are fixed in situ with TCA to provide a measurement of the cell population for each cell line at the time of drug addition (Tz). Experimental drugs are solubilized in dimethyl sulfoxide at 400 times the desired maximum final concentration of the test and stored frozen prior to use. At the time of drug addition, an aliquot of the frozen concentrate is thawed and diluted to twice the desired maximum test concentration with complete medium containing 50 µg / ml gentamicin. Additional four, 10-fold, or ½ log serial dilutions are made to provide a total of five drug concentrations plus control. Aliquots of 100 µl of these different drug dilutions are added to the appropriate microtiter wells, which already contain 100 µl of medium, which results in the required final drug concentrations.

After the drug has been added, the plates are incubated for a further 48 hours at 37° C., 5% CO_2, 95% air and 100% relative humidity. In the case of adherent cells, the assay is terminated by adding cold TCA. The cells are fixed in situ by gently adding 50 µl of cold 50% (w / v) TCA (final concentration, 10% TCA) and incubating at 4° C. for 60 minutes. The supernatant is discarded and the plates are washed five times with tap water and air dried. Sulforhodamine B (SRB) solution (100 µl) containing 0.4% (w / v) in 1% acetic acid is added to each well and the plates are incubated for 10 minutes at room

temperature. After staining, unbound dye is removed by washing five times with 1% acetic acid and the panels are air dried. Bound dye is then solubilized with 10 mM Trizma base and the absorbance read on an automatic plate reader at a wavelength of 515 nm. For suspension cells, the methodology is the same, except that the assay is terminated by fixing settled cells to the bottom of the wells by carefully adding 50 µl of 80% TCA (final concentration 16% TCA). Using the seven absorbance measurements [time zero, (Tz), control growth, (C), and test growth in the presence of drug at the five concentration levels (Ti)], the percent growth at each of the drug concentration levels is calculated. The percentage growth inhibition is calculated as follows:

[(Ti-Tz)/(C-Tz)] x 100 for concentrations for which Ti>/=Tz

[(Ti-Tz)/Tz] x 100 for concentrations for which Ti<Tz.

For each experimental agent, three dose-response parameters are calculated. The growth inhibition of 50% (GI50) is calculated from [(Ti-Tz) / (C-Tz)] x 100 = 50, which corresponds to the active ingredient concentration that leads to a 50% reduction in net protein gain (measured by SRB staining) in control cells during drug incubation. The drug concentration that leads to total growth inhibition (TGI) is calculated from Ti = Tz. The LC50 (concentration of the drug which results in a 50% reduction in the measured protein at the end of drug treatment compared to that at the beginning), which indicates a net loss of cells after treatment, is calculated from [(Ti-Tz) / Tz] x 100 = -50. Values are calculated for each of these three parameters when the activity level is reached; however, if the effect is not achieved or exceeded, the value for this parameter is given as greater or less than the maximum or minimum concentration tested.

7.3.5. Flow cytometry

7.3.5.1. Cell cycle analysis by propidium iodide staining

Propidium iodide (PI) is a DNA intercalating agent which binds stoichiometrically to DNA. PI fluorescence intensity increases 20-fold when bound to DNA (excitation 488 nm and emission 600 nm). Following treatment, cells were harvested and fixed in 70% ethanol/30% phosphate buffered saline (PBS) and stored at -20°C until required. When samples were required 5 µL of FBS was added to each sample and samples were centrifuged at 1000 x g for 10 minutes to obtain a cell pellet. The ethanol containing supernatant was discarded and the pellet was resuspended in 200 µL of PBS supplemented with 10 µg/mL of RNase A (Sigma Aldrich, St Louis, MO, USA) and 100 µg/mL propidium iodide (Sigma Aldrich, St Louis, MO, USA). Cells were incubated in the dark at 37°C for 30 minutes. Analysis was performed using a BD Accuri C6 flow cytometer using BD Accuri C6 software. Samples were first gated on vehicle controls to remove debris and cell aggregates. Cells (1 x 10^4) from each sample were counted and results were visualised on histograms. PI was detected using 585/40 bandpass filter.

7.3.5.2. Detection of cell death by annexin V/PI staining

Cells were seeded in 12 well plates at a density of 3 x 105 cells/mL in a total volume of 2 mL, allowed to rest for 1 hour and then treated for the required amount of time. Following treatment, cells were transferred to a 30 mL falcon tube. Cells were

centrifuged at 300 x g for 5 minutes to obtain a cell pellet. The cell pellet was then washed with 0.5 mL of annexin V Binding Buffer (20X Binding buffer: 0.1 M HEPES, 1.4M NaCl, 25 mM $CaCl_2$ pH 7.4, diluted 1 in 20 in PBS to give 1 X solution) and centrifuged at 300 x g for 5 minutes to obtain a pellet. The supernatant was discarded, and the pellet stained with 50 µL of annexin V-FITC (1:33.3 dilution in 1X annexin binding buffer) for 30 minutes in the dark on ice. 0.5 mL of annexin V binding buffer was added, and the samples centrifuged at 300 x g for 5 minutes at 4oC. The supernatant was discarded, and the pellet resuspended in 2.5 mL PI (1 mg/mL diluted 1:2000 in annexin V binding buffer). The samples were then analysed immediately on a BD Accuri C6 flow cytometer using BD Accuri C6 software. Samples were first gated on vehicle controls (unstained, annexin V-FITC only, PI only and annexin V+/PI+) to remove debris and cell aggregates. These gates were then analysed on an annexin V-FITC (535 nm – FL1 channel using a 530/30 bandpass filter) vs PI (488 nm – FL2 using a 585/40 bandpass filter) dot plot.

7.3.6. Western blotting

7.3.6.1. Preparation of cell lysates

NCI-H929 and U266B1 cells were seeded at a density of 3 x 10^5 cells/mL in 25 cm^2 flasks in

10 mL of media. Cells were treated with the required concentration of each drug for varying

amounts of time. Cells and media were transferred to universal tubes and flasks were

washed with 1 mL PBS. Samples were centrifuged at 600 x g for 5 minutes. The supernatant

was discarded, and samples were resuspended in 1 mL non-sterile PBS. The resuspended

pellet was centrifuged at 600 x g for 5 minutes at 4°C. After centrifugation the supernatant

was removed, and pellets were stored at -70°C until required.

Cell pellets were removed from the -70°C freezer and kept on ice during the lysis process.

The lysis of the samples was performed using ice-cold radioimmunoprecipitation (RIPA) buffer supplemented with 10% (v/v) protease inhibitor and 1% (v/v) phosphatase inhibitor cocktail 2 and 3. RIPA lysis buffer was obtained from Sigma. A 10 X concentrated protease inhibitor cocktail was prepared by diluting 1 tablet (complete™ tablets mini EASY pack) in 1 mL of dH_2O. This solution was distributed into 100 µL aliquots and stored at -20 °C until required. The 10 X protease inhibitor cocktail was diluted to 1 X concentration in RIPA buffer.

Phosphatase inhibitor cocktails 2 and 3 (Sigma) were also added to lysis buffer at a dilution of 1 in 100. RIPA buffer was kept on ice until required.

Sample pellets were resuspended in an appropriate volume of RIPA buffer and left on ice for 30 minutes. Following incubation with RIPA lysis buffer protein concentration was quantified by BCA assay.

7.3.6.2. Determination of protein concentration

Protein concentration was determined using a BCA assay kit from Pierce. BSA standards were prepared as described in Table 2.1 from a 2 mg/mL stock. BCA working reagent was prepared by diluting reagent B 1:50 with reagent A. 20 µL of each standard or diluted sample was added to a 96 well plate followed by 200 µL of the BCA working reagent. This was performed in duplicate. The plate was wrapped in tinfoil and left for 30 minutes at 37°C in a

non-sterile incubator. Absorbance was read at 562 nm using a molecular devices microplate
reader and the mean of the standards was determined and a standard curve was constructed (Figure 2.4). The standard curve was used to determine the protein concentration of each sample and the volume of sample required to make 100 ug/100 µL
lysate was determined to ensure equal loading.

Table 8.6.2.1. Preparation of BSA standards.

Vial	Volume of Diluent (µL)	Volume and Source of BSA (µL)	Final concentration BSA mg/Ml
1	0	Stock solution	2
2	250	250 of 1	1
3	250	250 of 2	0.5
4	250	251 of 3	0.25
5	250	252 of 4	0.125
6	250	253 of 5	0.0625
7	250	0	0

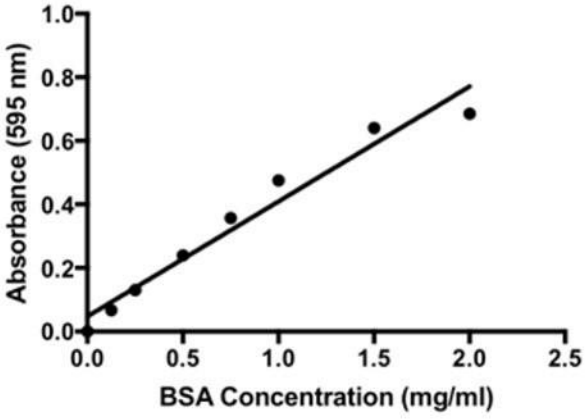

Figure 8.6.2.1. BSA standard curve.[19]

BSA standards from a 2 mg/mL stock were prepared as described in Table 2.1. 20 µL of each standard or diluted sample was added to a 96 well plate in duplicate followed by 200 µL of the BCA working reagent. Absorbance was read at 562 nm and the mean of the standards was determined and a standard curve was constructed.

2.7.3. Sodium dodecylsulphate-polyacrylamide gel electrophoresis (SDS-PAGE)

Cell lysates were boiled with 5x Laemmli sample buffer [Tris-HCl 62.5 mM (pH 6.7), glycerol
10% (v/v), sodium dodecyl sulphate 2% (w/v), bromophenol blue 0.002% (w/v) containing
DTT (50 µM)] for 10 minutes at 80°C. Following boiling, lysates were vortexed and placed on
ice or frozen until required.

Bio-rad 1.5 mm glass plates were washed, dried and assembled. Resolving gel was prepared
as in Table 2.2, 7.5 mL of the resolving gel mix was pipetted between the plates 1 mL at a
time to minimise bubbles. 200 µL of iso-propanol was pipetted onto the gel to prevent bubbles and even out the surface layer of the gel. Once the resolving gel had set, the isopropanol was poured off and the top of the gel was washed with deionised water. The
stacking gel was prepared as per Table 2.2 and was poured on top of the resolving gel. A comb was then placed into the gel to create wells in the gel. Once the gel had set it was ready for use. If not needed immediately, the gel was wrapped in wet tissue paper and clingfilm and stored at 4°C.

When ready to use, the 2 gels were placed into a Bio-rad rig (mini-PROTEAN II) creating a
chamber and the chamber was then filled with 1X running buffer diluted from 10X solution
(25 mM Tris, 192 mM glycine, 0.1 % (v/v) SDS in dH_2O). The comb in the gel was then

removed to create wells in which the lysate would be added. Molecular weight marker (7
µL) was loaded into the first well. Lysate samples were then added to each well (10-20 µg of
protein). The chamber was then filled with 1X running buffer and a current was applied. The
gel was run at 80 V for 30 minutes to allow samples to travel through the stacking gel and
then the voltage was increased to 120 V. The gel was run until samples reached the bottom
of the resolving gel.

Components (mL)	6% Resolving Gel	8% Resolving Gel	10% Resolving Gel	12% Resolving Gel	15% Resolving Gel	5% stacking
H_2O	15.9	13.9	11.9	9.9	6.9	6.8
30 % acrylamide mix	6	8	10	12	15	1.7
1.5 M Tris (pH 8.8)	7.5	7.5	7.5	7.5	7.5	N/A
10% SDS	0.3	0.3	0.3	0.3	0.3	0.1
10% ammonium persulfate	0.3	0.3	0.3	0.3	0.3	0.1
TEMED	0.024	0.018	0.012	0.012	0.012	0.1
1 M Tris (pH 6.8)	N/A	N/A	N/A	N/A	N/A	1.25

Table 8.3.6.2.1. Solutions for preparing 30 mL resolving and stacking 10 mL gels used in SDS-PAGE.

7.3.6.3. Transfer

Polyvinylidene difluoride (PVDF) membrane was activated in methanol for 2 minutes and
left soaking in 1 X transfer buffer diluted from 10X solution (25 mM Tris, 192 mM glycine in
dH_2O) along with 4 pieces of filter paper. A sponge was placed on a transfer cassette, followed by 2 pieces of filter paper. The gel was removed from the gasket and was carefully
Components excised from in-between the glass plates. The gel was then placed on the filter paper followed by activated PVDF membrane, taking care to avoid bubbles forming between the gel and PVDF. Two pieces of filter paper were then placed on top of the PVDF followed by a sponge. The assembled cassette was then placed into the transfer rig (Bio-rad) and filled to
50% with 1X transfer buffer, an icepack was placed in the rig and the 1X transfer buffer was
topped up. The gel was transferred for 60-100 minutes at 150 mA depending on protein size.

7.3.6.4. Probing membranes for proteins

Following transfer of proteins onto a PVDF membrane, non-specific binding sites on the membrane were blocked by washing the membrane in 5% non-fat dried milk (Marvel) in TBST (20 mM Tris, 0.15 mM NaCl, 0.1% Tween, pH 7.6) for 1 hour at room temperature. Following blocking membranes were washed once in TBST and incubated overnight in primary antibody at 4°C. Antibodies were diluted in either 5% (w/v) dried milk for total proteins or 5% (w/v) BSA for phosphorylated proteins in TBST. Dilution factors varied for each antibody ranging from 1:500 – 1:5000. Following incubation, the membrane was washed in TBST 3 for 10 minutes each time. The membrane was then incubated in secondary
antibody (anti-rabbit or anti-mouse, conjugated to horseradish peroxidase (HRP)) for 1 hour

at room temperature and was then washed 3 times in TBST to remove any non-bound secondary antibody. The presence of bound antibodies on the membrane was detected by
electrochemiluminescence (ECL). The membrane was covered in ECL detection reagent which consists of luminol and peroxide. The presence of HRP and peroxide results in the oxidation of luminol and the release of light that can be detected with the Bio-rad Gel Doc
TM XR + system with Image Lab software. GAPDH, beta-actin and alpha-tubulin were used as
loading controls in order to ensure equal loading of protein across the gel. If a protein was
a similar size to the loading control, the membrane was stripped for 15 minutes in stripping
buffer (Thermo Fisher), washed X3 times in TBST and blocked in 5% (w/v) dried milk as before. The membrane was then re-probed with anti-GAPDH (1:5000), for 1 hour at room
temperature. Following incubation, the membrane was washed X3 in TBST and placed in anti-mouse secondary (1:5000) for 1 hour at room temperature. The membrane was then
washed X3 in TBST and proteins were detected as above.

7.4. References

(1) G16_c01.

(2) Becke, A. D. A New Mixing of Hartree–Fock and Local Density-functional Theories. *J. Chem. Phys.* **1993**, *98* (2), 1372–1377. https://doi.org/10.1063/1.464304.

(3) Hehre, W. J.; Ditchfield, R.; Pople, J. A. Self—Consistent Molecular Orbital Methods. XII. Further Extensions of Gaussian—Type Basis Sets for Use in Molecular Orbital Studies of Organic Molecules. *J. Chem. Phys.* **1972**, *56* (5), 2257–2261. https://doi.org/10.1063/1.1677527.

(4) Tomasi, J.; Mennucci, B.; Cammi, R. Quantum Mechanical Continuum Solvation Models. *Chem. Rev.* **2005**, *105* (8), 2999–3094. https://doi.org/10.1021/cr9904009.

(5) Trott, O.; Olson, A. J. AutoDock Vina: Improving the Speed and Accuracy of Docking with a New Scoring Function, Efficient Optimization, and Multithreading. *J. Comput. Chem.* **2010**, *31* (2), 455–461. https://doi.org/https://doi.org/10.1002/jcc.21334.

(6) The PyMOL Molecular Graphics System, Version 1.2r3pre, Schrödinger, LLC. https://pymol.org/2/.

(7) Humphrey, W.; Dalke, A.; Schulten, K. VMD: Visual Molecular Dynamics. *J. Mol. Graph.* **1996**, *14* (1), 33–38. https://doi.org/https://doi.org/10.1016/0263-7855(96)00018-5.

(8) Protein Data Bank https://www.rcsb.org/.

(9) Schrödinger Release 2021-3: Maestro, Schrödinger, LLC, New York, NY, 2021.

(10) Sherman, W.; Day, T.; Jacobson, M. P.; Friesner, R. A.; Farid, R. Novel Procedure for Modeling Ligand/Receptor Induced Fit Effects. *J. Med. Chem.* **2006**, *49* (2), 534–553. https://doi.org/10.1021/jm050540c.

(11) Tutone, M.; Pibiri, I.; Lentini, L.; Pace, A.; Almerico, A. M. Deciphering the Nonsense Readthrough Mechanism of Action of Ataluren: An in Silico Compared

Study. *ACS Med. Chem. Lett.* **2019**, *10* (4), 522–527. https://doi.org/10.1021/acsmedchemlett.8b00558.

(12) Agashe, M. S.; Jose, C. I. Analysis of Complex Hydroxyl Absorptions of Amino- and Dimethylamino-Phenols. *J. Chem. Soc. Faraday Trans. 2 Mol. Chem. Phys.* **1977**, *73* (7), 1227–1231. https://doi.org/10.1039/F29777301227.

(13) Patent. WO2008/46216, 2008.

(14) Okaniwa, M.; Hirose, M.; Imada, T.; Ohashi, T.; Hayashi, Y.; Miyazaki, T.; Arita, T.; Yabuki, M.; Kakoi, K.; Kato, J. Design and Synthesis of Novel DFG-Out RAF/Vascular Endothelial Growth Factor Receptor 2 (VEGFR2) Inhibitors. 1. Exploration of [5,6]-Fused Bicyclic Scaffolds. *J. Med. Chem.* **2012**, *55* (7), 3452–3478. https://doi.org/10.1021/jm300126x.

(15) Hasegawa, M.; Nishigaki, N.; Washio, Y.; Kano, K.; Harris, P. A.; Sato, H.; Mori, I.; West, R. I.; Shibahara, M.; Toyoda, H. Discovery of Novel Benzimidazoles as Potent Inhibitors of TIE-2 and VEGFR-2 Tyrosine Kinase Receptors. *J. Med. Chem.* **2007**, *50* (18), 4453–4470. https://doi.org/10.1021/jm0611051.

(16) Avery, C. A.; Pease, R. J.; Smith, K.; Boothby, M.; Buckley, H. M.; Grant, P. J.; Fishwick, C. W. G. (±) Cis-Bisamido Epoxides: A Novel Series of Potent FXIII-A Inhibitors. *Eur. J. Med. Chem.* **2015**, *98*, 49–53. https://doi.org/https://doi.org/10.1016/j.ejmech.2015.05.019.

(17) Dardonville, C.; Goya, P.; Rozas, I.; Alsasua, A.; Martín, M. I.; Borrego, M. J. New Aromatic Iminoimidazolidine Derivatives as A1-Adrenoceptor Antagonists: A Novel Synthetic Approach and Pharmacological Activity. *Bioorg. Med. Chem.* **2000**, *8* (7), 1567–1577. https://doi.org/https://doi.org/10.1016/S0968-0896(00)00089-4.

(18) Guo-Rui Gaoa, Meng-Yuan Lib,d, Yong-Cong Lvc, Su-Fen Caoa, Lin-Jiang Tongb, Li-Xin Weid, Jian Dingb, Hua Xieb, Wen-Hu Duana, c. Design, Synthesis and Biological Evaluation of Biphenylurea Derivatives as VEGFR-2 Kinase Inhibitors (Ⅱ). *Chinese Chem. Lett.* **2016**, *27* (02), 200–204.

(19) Brzica, H.; Abdullahi, W.; Reilly, B. G.; Ronaldson, P. T. A Simple and Reproducible

Method to Prepare Membrane Samples from Freshly Isolated Rat Brain Microvessels. *J. Vis. Exp.* **2018**, No. 135. https://doi.org/10.3791/57698.

Appendix

Leukemia cell lines

Leukemia is a cancer of the blood and bone marrow, according to the WHO in 2020 there was an estimated 474,519 new cases of leukemia in both male and females of all ages, as this cancer affects everyone in society including children, there is a great amount of effort to find therapeutics that target it. The NCI screening panel uses six cell lines derived from patients with leukemia from a variety of age.

CCRF-CEM [CCRF CEM] human T lymphoblasts are isolated from the peripheral blood of a female, Caucasian 4 year old with acute lymphoblastic leukemia (ALL). CCRF-CEM grow in suspension culture with a doubling time is 26.7 hours and the density of inoculation is 40000 cells/well.

The HL-60 cell line is a human caucasian promyelocytic leukaemia. Peripheral blood leukocytes were first obtained by leukopheresis from a 36-year-old Caucasian female with acute promyelocytic leukemia. HL-60 cells grow in suspension culture with a doubling time of 28.6 hours and the density of inoculation is 40000 cells/well.

K-562 cells are lymphoblasts isolated from the bone marrow of a 53-year-old chronic myelogenous leukemia patient. K-562 cells grow in suspension culture with a doubling time of 19.6 hours and the density of inoculation is 5000 cells/well.

MOLT-4 are derived from a 19 year old male with acute lymphoblastic leukaemia, the leukemic cells were taken whilst in relapse. Cells grow in suspension culture with a doubling time of 27.9 hours and the density of inoculation is 30000 cells/well.

RPMI 8226 are B lymphocytes isolated from the peripheral blood derived from a 61-year-old, male, plasmacytoma patient in 1966. Cells grow in suspension culture with a doubling time of 33.5 hours and the density of inoculation is 20000 cells/well.

SR is a human lymphoma cell line originated in 1983 from an 11 year old white male. Cells grow in suspension culture with a doubling time of 28.7 hours and the density of inoculation is 20000 cells/well.

Non-Small Cell Lung Cancer cell lines

According to the American Cancer Society 80-85% of lung cancers are Non-Small Cell Lung Cancers (NSCLC)[11] and according to the WHO over 2 million new cases of lung cancer were reported in 2020 in both sexes and all ages. Nine NSCLC cell lines were used in the NCI screening, which are described as follows:

A549 cells are isolated from the lung tissue of a 58 year old Caucasian male with lung cancer. Cells grow in adherent culture with a doubling time of 22.9 hours and the density of inoculation is 7500 cells/well.

EKVX cells are isolated from the lung tissue of a male of unspecified age with lung cancer. Cells grow in adherent culture with a doubling time of 43.6 hours and the density of inoculation is 20000 cells/well.

HOP-62 cells are isolated from the lung tissue of a 60 year old female with lung cancer. Cells grow in adherent culture with a doubling time of 39 hours and the density of inoculation is 10000 cells/well.

HOP-92 cells are isolated from the lung tissue of a 62 year old male with lung cancer. Cells grow in adherent culture with a doubling time of 79.5 hours and the density of inoculation is 20000 cells/well.

NCI-H226 cells are isolated from the lung tissue of a male of unspecified age with lung cancer. Cells grow in adherent culture with a doubling time of 61 hours and the density of inoculation is 20000 cells/well.

NCI-H23 cells are isolated from the lung tissue of a 51 year old black male with lung cancer. Cells grow in adherent culture with a doubling time of 33.4 hours and the density of inoculation is 20000 cells/well.

NCI-H322M cells are isolated from the lung tissue of a 52 year old male with lung cancer. Cells grow in adherent culture with a doubling time of 35.3 hours and the density of inoculation is 20000 cells/well.

NCI-H460 cells are isolated from the lung tissue of a male of unspecified age with lung cancer. Cells grow in adherent culture with a doubling time of 17.8 hours and the density of inoculation is 7500 cells/well.

NCI-H522 cells are isolated from the lung tissue of a 58 year old white male with lung cancer. Cells grow in adherent culture with a doubling time of 38.2 hours and the density of inoculation is 20000 cells/well.

Colon cancer cell lines

Colorectal cancer, also known as colon or rectal cancer depending on where it starts, is a cancer of the large intestine. There was almost 2 million cases of colorectal cancer in 2020 of both sexes and all ages. In our case, seven cell lines were screened by the NCI.

COLO 205 cell line is made up of epithelial cells isolated from a 70 year old, Caucasian man with colon cancer. Cells grow in a mix suspension and adherent culture with a doubling time of 23.8 hours and the density of inoculation is 15000 cells/well.

HCC-2998 cell line are cells from an unspecified source (age or sex). Cells grow in an adherent culture with a doubling time of 31.5 hours and the density of inoculation is 15000 cells/well.

HCT-116 cell line was isolated from the colon of an adult male, colon cancer patient. Cells grow in an adherent culture with a doubling time of 17.4 hours and the density of inoculation is 5000 cells/well.

HCT-15 cells are isolated from the large intestine of a male with Dukes C colorectal cancer. Cells grow in an adherent culture with a doubling time of 20.6 hours and the density of inoculation is 10000 cells/well.

HT-29 cell line is made up of cells isolated from a 44 year old, Caucasian female with colon cancer. Cells grow in a mix suspension and adherent culture with a doubling time of 19.5 hours and the density of inoculation is 5000 cells/well.

KM12 HCC-2998 cell line are cells from an unspecified source (age or sex). Cells grow in an adherent culture with a doubling time of 23.7 hours and the density of inoculation is 15000 cells/well.

SW-620 cells are isolated from the large intestine of a 51 year old male Dukes C colorectal cancer patient. Cells grow in an adherent culture with a doubling time of 20.4 hours and the density of inoculation is 10000 cells/well.

CNS cancer cell lines

Brain and CNS cancers are found in the brain and spinal cord. The brain is protected by the blood-brain barrier which prevents many cancer treatments from reaching the cancer cells, thus new treatments are always being researched. The NCI utilised six cell lines derived from patients with CNS cancer with our compounds.

SF-268 are derived from a 24 year old female astrocytoma patient. Cells grow in adherent culture with a doubling time of 33.1 hours and the density of inoculation is 15000 cells/well.

SF-295 are derived from a 65 year old female Glioblastoma patient. Cells grow in adherent culture with a doubling time of 29.5 hours and the density of inoculation is 10000 cells/well.

SF-539 are derived from a 34 year old female Glioblastoma patient. Cells grow in adherent culture with a doubling time of 35.4 hours and the density of inoculation is 15000 cells/well.

SNB-19 are derived from a 47 year old male Glioblastoma patient. Cells grow in adherent culture with a doubling time of 34.6 hours and the density of inoculation is 15000 cells/well.

SNB-75 are derived from a 75 year old female Astrocytoma patient. Cells grow in adherent culture with a doubling time of 62.8 hours and the density of inoculation is 20000 cells/well.

U251 are derived from a 75 year old male Glioblastoma patient. Cells grow in adherent culture with a doubling time of 23.8 hours and the density of inoculation is 7500 cells/well.

Melanoma

Melanoma is a type of skin cancer with an estimated number of cases over 300,000 reported in 2020. The NCI utilised nine cell lines derived from patients with melanoma cancer in the screening of our compounds.

LOX IMVI cells are derived from a 58 year old male Amelanotic melanoma patient. Cells grow in semi-adherent culture with a doubling time of 20.5 hours and the density of inoculation is 7500 cells/well.

MALME-3M cells are derived from a 43 year old male malignant melanoma patient. Cells grow in suspension and adherent culture with a doubling time of 46.2 hours and the density of inoculation is 20000 cells/well.

M14 cells are derived from a 33 year old male malignant melanoma patient. Cells grow in adherent culture with a doubling time of 26.3 hours and the density of inoculation is 15000 cells/well.

MDA-MB-435 cells are derived from a 33 year old male Adenocarcinoma patient. Cells grow in adherent culture with a doubling time of 25.8 hours and the density of inoculation is 15000 cells/well.

SK-MEL-2 cells are derived from a 60 year old male Melanoma patient. Cells grow in adherent culture with a doubling time of 45.5 hours and the density of inoculation is 20000 cells/well.

SK-MEL-28 cells are derived from a 51 year old male Cutaneous melanoma patient. Cells grow in adherent culture with a doubling time of 35.1 hours and the density of inoculation is 10000 cells/well.

SK-MEL-5 cells are derived from a 24 year old female Cutaneous melanoma patient. Cells grow in adherent culture with a doubling time of 25.2 hours and the density of inoculation is 10000 cells/well.

UACC-257 cells are derived from an unspecified (age and sex) patient with melanoma. Cells grow in adherent culture with a doubling time of 38.5 hours and the density of inoculation is 20000 cells/well.

UACC-62 cells are derived from an unspecified (age and sex) patient with melanoma. Cells grow in adherent culture with a doubling time of 31.3 hours and the density of inoculation is 10000 cells/well.

Overian cancer cell lines

Ovarian cancer is one of the most common types of cancer in women, with over 300,000 cases reported in 2020. In the screening performed by the NCI, seven cell lines derived from patients with ovarian cancer were used.

IGR-OV1 cells are derived from a 47 year old female ovarian endometrioid adenocarcinoma patient. Cells grow in adherent culture with a doubling time of 31 hours and the density of inoculation is 10000 cells/well.

OVCAR-3 cells are derived from a 60 year old female high grade ovarian serous adenocarcinoma patient. Cells grow in adherent culture with a doubling time of 34.7 hours and the density of inoculation is 10000 cells/well.

OVCAR-4 cells are derived from a 42 year old female high grade ovarian serous adenocarcinoma patient. Cells grow in adherent culture with a doubling time of 41.4 hours and the density of inoculation is 15000 cells/well.

OVCAR-5 cells are derived from a 67 year old female high grade ovarian serous adenocarcinoma patient. Cells grow in adherent culture with a doubling time of 48.8 hours and the density of inoculation is 20000 cells/well.

OVCAR-8 cells are derived from a 64 year old female high grade ovarian serous adenocarcinoma patient. Cells grow in adherent culture with a doubling time of 26.1 hours and the density of inoculation is 10000 cells/well.

NCI/ADR-RES cells are derived from a 64 year old female high grade ovarian serous adenocarcinoma patient. Cells grow in adherent culture with a doubling time of 34 hours and the density of inoculation is 15000 cells/well.

SK-OV-3 cells are derived from a 64 year old female ovarian serous cystadenocarcinoma patient. Cells grow in adherent culture with a doubling time of 48.7 hours and the density of inoculation is 20000 cells/well.

Renal cancer cell lines

Renal cancer is cancer of the kidneys, according to the National Health Services in the United Kingdom,[12] it usually effects adults in there 60 and is rare in people under 50. The NCI uses seven cell lines derived from patients with renal cancer from different age groups.

786-0 cells are derived from a 58 year old male with renal cell carcinoma. Cells grow in adherent culture with a doubling time of 22.4 hours and the density of inoculation is 10000 cells/well.

A498 cells are derived from a 52 year old male with renal cell carcinoma. Cells grow in adherent culture with a doubling time of 66.8 hours and the density of inoculation is 25000 cells/well.

ACHN cells are derived from a 22 year old male with papillary renal cell carcinoma. Cells grow in adherent culture with a doubling time of 27.5 hours and the density of inoculation is 10000 cells/well.

CAKI-1 cells are derived from a 49 year old male with clear cell renal cell carcinoma. Cells grow in adherent culture with a doubling time of 39 hours and the density of inoculation is 10000 cells/well.

RXF 393 cells are derived from a 54 year old male with renal cell carcinoma. Cells grow in adherent culture with a doubling time of 62.9 hours and the density of inoculation is 15000 cells/well.

SN12C cells are derived from male with renal cell carcinoma. Cells grow in adherent culture with a doubling time of 62.9 hours and the density of inoculation is 15000 cells/well.

TK-10 cells are derived from a 43 year old male with clear cell renal cell carcinoma. Cells grow in adherent culture with a doubling time of 51.3 hours and the density of inoculation is 15000 cells/well.

UO-31 cells are derived from female of unspecified age with renal cell carcinoma. Cells grow in adherent culture with a doubling time of 41.7 hours and the density of inoculation is 15000 cells/well.

Breast cancer cell lines

Breast cancer is one of the most common and aggressive types of cancer in women, with an estimated over 2 million cases reported in 2020 in which this was the most occurring cancer worldwide amongst both sexes and all age groups. In their screening, the NCI uses seven cell lines derived from patients with breast cancer.

MCF7 cells are derived from a 69 year old female with invasive breast carcinoma of no special type. Cells grow in adherent culture with a doubling time of 25.4 hours and the density of inoculation is 10000 cells/well.

MDA-MB-231/ATCC cells are derived from a 51 year old female with breast adenocarcinoma. Cells grow in adherent culture with a doubling time of 41.9 hours and the density of inoculation is 20000 cells/well.

MDA-MB-468 MDA-MB-231/ATCC cells are derived from a 51 year old female with breast adenocarcinoma. Cells grow in adherent culture with a doubling time of 62 hours and the density of inoculation is 2000 cells/well.

HS 578T cells are derived from a 74 year old female with invasive breast carcinoma of no special type. Cells grow in adherent culture with a doubling time of 53.8 hours and the density of inoculation is 20000 cells/well.

BT-549 cells are derived from a 72 year old female with invasive breast carcinoma of no special type. Cells grow in adherent culture with a doubling time of 53.9 hours and the density of inoculation is 20000 cells/well.

T-47D cells are derived from a 54 year old female with invasive breast carcinoma of no special type. Cells grow in adherent culture with a doubling time of 45.5 hours and the density of inoculation is 20000 cells/well.

List and Description of NCI-60 Cancer Cell Lines

Name	**Species**	**Organ of Origin**	**Doubling Time (Hrs)**	**Disease**	**Culture**
BT549	Human	Breast	53.9	Ductal Carcinoma	Adherent
HS 578T	Human	Breast	53.8	Carcinoma	Adherent
MCF7	Human	Breast	25.4	Adenocarcinoma	Adherent
MDA-MB-231	Human	Breast	41.9	Adenocarcinoma	Adherent
MDA-MB-468	Human	Breast	62	Adenocarcinoma	Adherent
T-47D	Human	Breast	45.5	Ductal Carcinoma	Adherent

Name	Species	Organ of Origin	Doubling Time (Hrs)	Disease	Culture
SF268	Human	CNS	33.1	Anaplastic Astrocytoma	Adherent
SF295	Human	CNS	29.5	Glioblastoma-Multiforme	Adherent
SF539	Human	CNS	35.4	Glioblastoma	Adherent
SNB-19	Human	CNS	34.6	Glioblastoma	Adherent
SNB-75	Human	CNS	62.8	Astrocytoma	Adherent
U251	Human	CNS	23.8	Glioblastoma	Adherent
Colo205	Human	Colon	23.8	Dukes' type D, Colorectal adenocarcinoma	Adherent & Suspension
HCC 2998	Human	Colon	31.5	Carcinoma	Adherent
HCT-116	Human	Colon	17.4	Carcinoma	Adherent
HCT-15	Human	Colon	20.6	Dukes' type C, Colorectal adenocarcinoma	Adherent
HT29	Human	Colon	19.5	Colorectal adenocarcinoma	Adherent
KM12	Human	Colon	23.7	Adenocarcinoma, Grade III	Adherent

Name	Species	Organ of Origin	Doubling Time (Hrs)	Disease	Culture
SW620	Human	Colon	20.4	Adenocarcinoma	Adherent
786-O	Human	Kidney	22.4	renal cell adenocarcinoma	Adherent
A498	Human	Kidney	66.8	Adenocarcinoma	Adherent
ACHN	Human	Kidney	27.5	renal cell adenocarcinoma	Adherent
CAKI	Human	Kidney	39	clear cell carcinoma	Adherent
RXF 393	Human	Kidney	62.9	Poorly Differentiated Hypernephroma	Adherent
SN12C	Human	Kidney	29.5	Carcinoma	Adherent
TK-10	Human	Kidney	51.3	Spindle Cell carcinoma	Adherent
UO-31	Human	Kidney	41.7	Carcinoma	Adherent
CCRF-CEM	Human	Leukemia	26.7	acute lymphoblastic leukemia	Suspension
HL-60	Human	Leukemia	28.6	acute promyelocytic leukemia	Suspension
K562	Human	Leuke	19.6	chronic	Suspensio

Name	Species	Organ of Origin	Doubling Time (Hrs)	Disease	Culture
		mia		myelogenous leukemia	n
MOLT-4	Human	Leukemia	27.9	acute lymphoblastic leukemia	Suspension
RPMI-8226	Human	Leukemia	33.5	plasmacytoma, myeloma	Suspension
SR	Human	Leukemia	28.7	Large Cell, Immunoblastic	Suspension
A549	Human	Lung	22.9	Adenocarcinoma	Adherent
EKVX	Human	Lung	43.6	Adenocarcinoma	Adherent
HOP-62	Human	Lung	39	Adenocarcinoma	Adherent
HOP-92	Human	Lung	79.5	Large Cell, Undifferentiated	Adherent & Suspension
NCI-H226	Human	Lung	61	squamous cell carcinoma; mesothelioma	Adherent
NCI-H23	Human	Lung	33.4	adenocarcinoma; non-small cell lung cancer	Adherent
NCI-H322M	Human	Lung	35.3	Small Cell Bronchioalveolar	Suspension

Name	Species	Organ of Origin	Doubling Time (Hrs)	Disease	Culture
				Carcinoma	
NCI-H460	Human	Lung	17.8	carcinoma; large cell lung cancer	Adherent
NCI-H522	Human	Lung	38.2	adenocarcinoma; non-small cell lung cancer	Adherent
LOX IMVI	Human	Melanoma	20.5	Malignant Amelanotic melanoma	Semi-Adherent
M14	Human	Melanoma	26.3	malignant melanoma	Adherent
MALME-3M	Human	Melanoma	46.2	malignant melanoma	Adherent & Suspension
MDA-MB-435	Human	Melanoma	25.8	Adenocarcinoma	Adherent
SK-MEL-2	Human	Melanoma	45.5	malignant melanoma	Adherent
SK-MEL-28	Human	Melanoma	35.1	malignant melanoma	Adherent
SK-MEL-5	Human	Melanoma	25.2	malignant melanoma	Adherent
UACC-257	Human	Melanoma	38.5	malignant melanoma	Adherent

Name	Species	Organ of Origin	Doubling Time (Hrs)	Disease	Culture
UACC-62	Human	Melanoma	31.3	malignant melanoma	Adherent
IGROV1	Human	Ovary	31	Cystoadenocarcinoma	Adherent
OVCAR-3	Human	Ovary	34.7	Adenocarcinoma	Adherent
OVCAR-4	Human	Ovary	41.4	Adenocarcinoma	Adherent
OVCAR-5	Human	Ovary	48.8	Adenocarcinoma	Adherent
OVCAR-8	Human	Ovary	26.1	Adenocarcinoma	Adherent
SK-OV-3	Human	Ovary	48.7	Adenocarcinoma	Adherent
NCI-ADR-RES	Human	Ovary	34	Adenocarcinoma	Adherent

NCI-60 Breast Cell Lines

Shown below are stained trypan blue images and Cellometer counted images of NCI-60 breast cell lines. Counted live cells are outlined in green while the dead trypan blue positive cells are outlined in red.

BT-549 cells

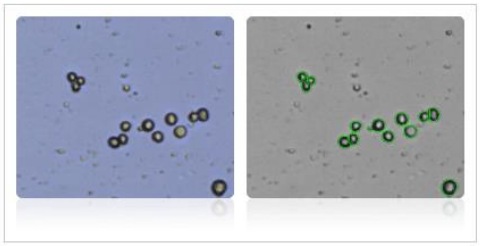

Hs 578T

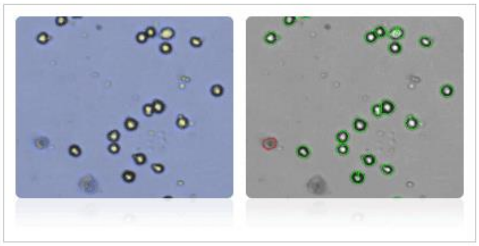

MCF7

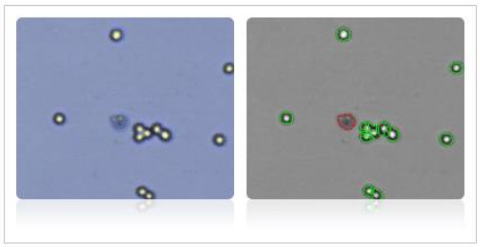

MDA-MB-231

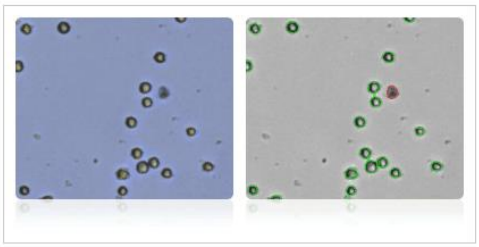

MDA-MB-468

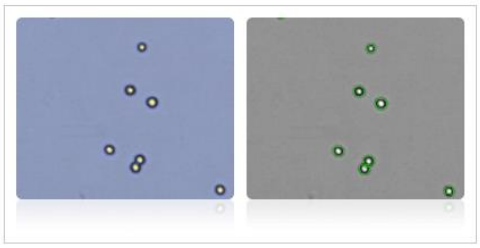

T-47D

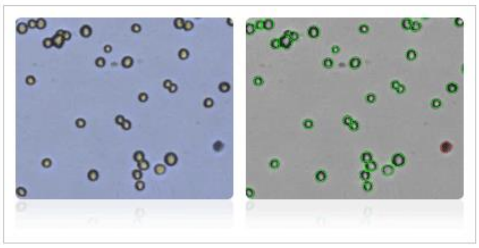

NCI-60 Central Nervous System Cell Lines

Shown below are stained trypan blue images and Cellometer counted images of NCI-60 central nervous system cell lines. Counted live cells are outlined in green while the dead trypan blue positive cells are outlined in red.

SF-268

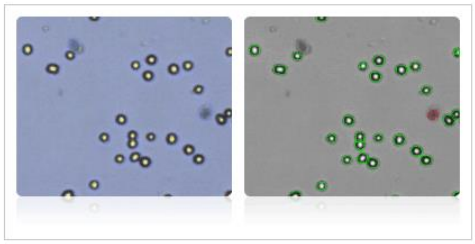

SF-295

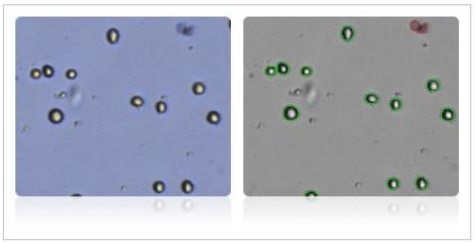

SF-539

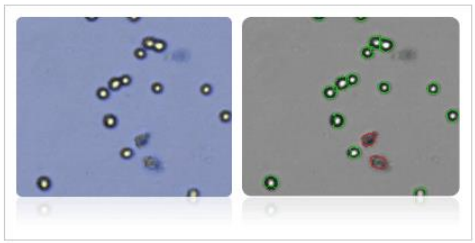

SNB-19

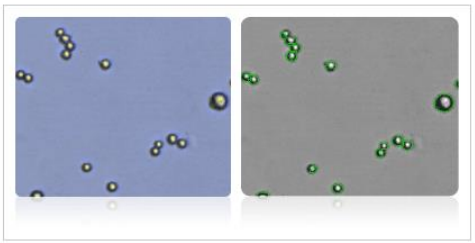

SNB-75

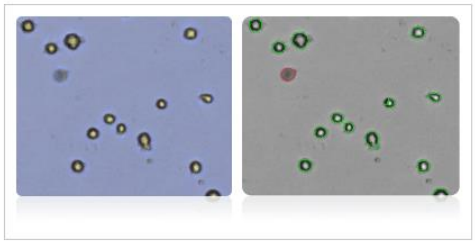

U251

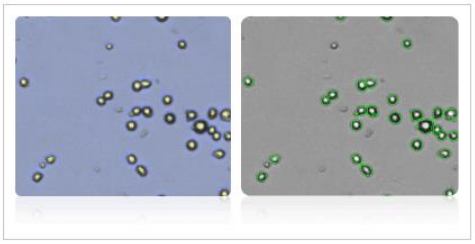

NCI-60 Colon Cell Lines

Shown below are stained trypan blue images and Cellometer counted images of NCI-60 colon cell lines. Counted live cells are outlined in green while the dead trypan blue positive cells are outlined in red.

Colo205

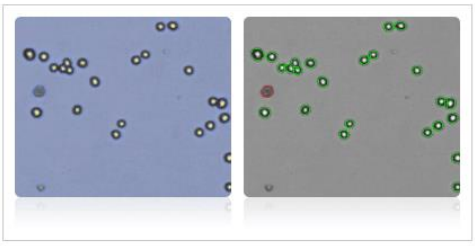

HCC-2998

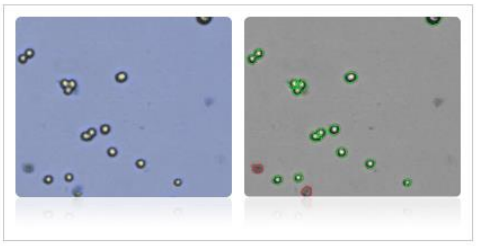

HCT-116

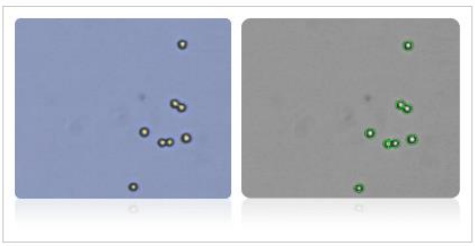

HCT-15

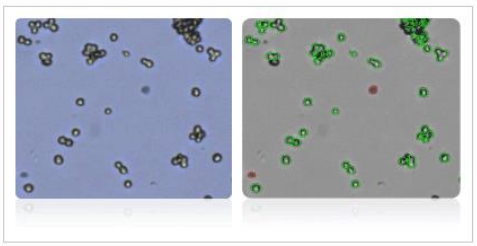

HT29

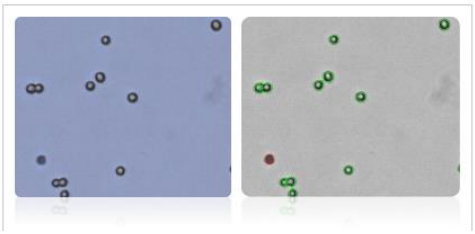

KM12

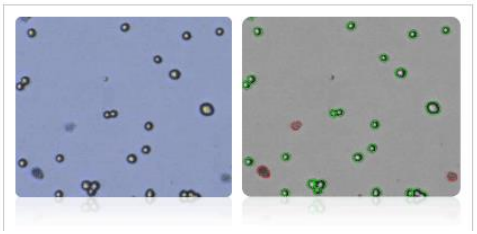

SW-620

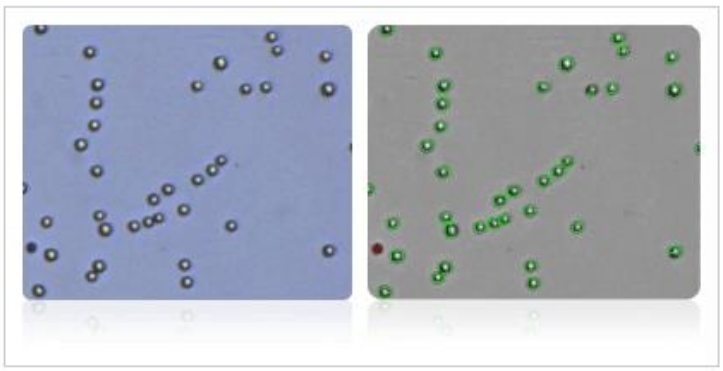

NCI-60 Kidney Cell Lines

Shown below are stained trypan blue images and Cellometer counted images of NCI-60 kidney cell lines. Counted live cells are outlined in green while the dead trypan blue positive cells are outlined in red.

786-O

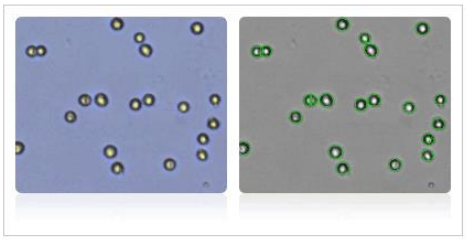

A498

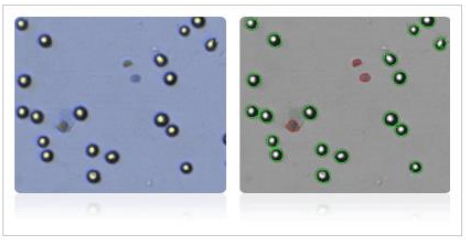

ACHN

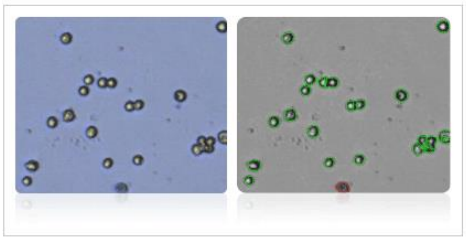

CAKI-1

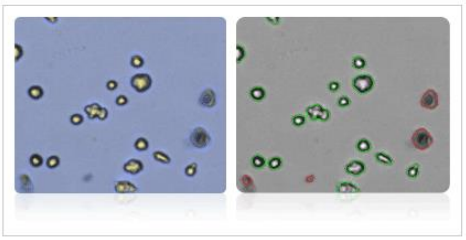

RXF 393

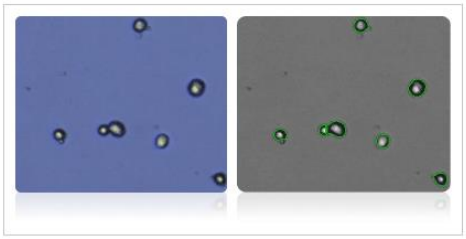

SN12C

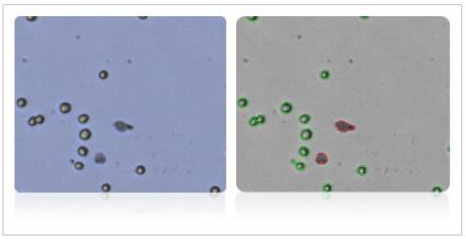

TK-10

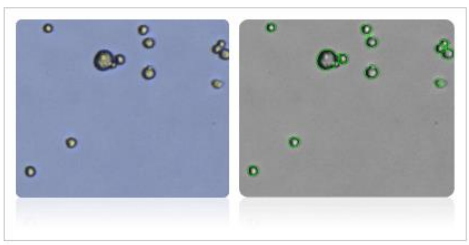

UO-31

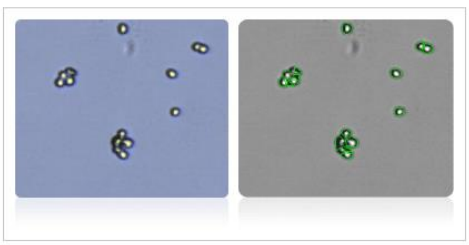

NCI-60 Leukemia Cell Lines

Shown below are stained trypan blue images and Cellometer counted images of NCI-60 leukemia cell lines.. Counted live cells are outlined in green while the dead trypan blue positive cells are outlined in red.

CCRF-CEM

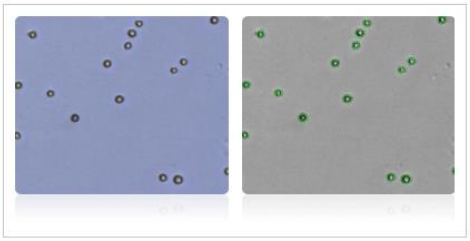

HL-60

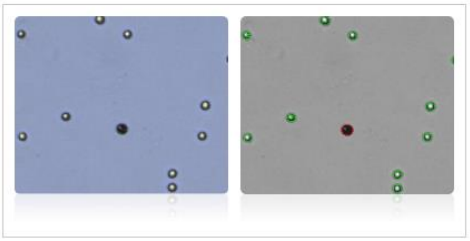

K-562

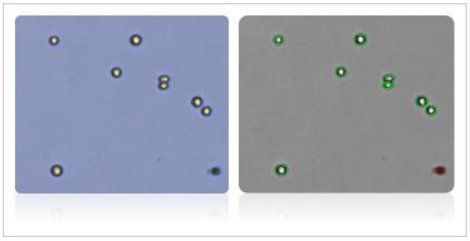

MOLT-4

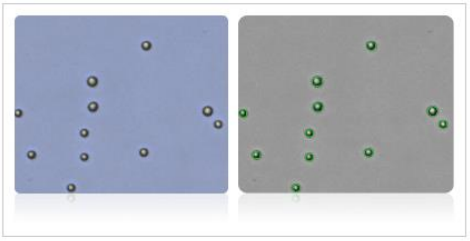

RPMI-8226

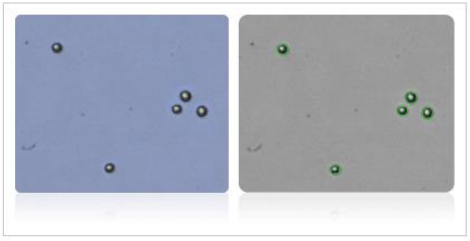

SR

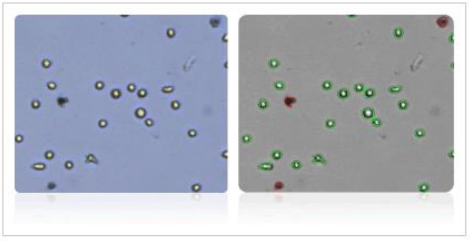

NCI-60 Lung Cell Lines

Shown below are stained trypan blue images and Cellometer counted images of NCI-60 lung cell lines. Counted live cells are outlined in green while the dead trypan blue positive cells are outlined in red.

A549

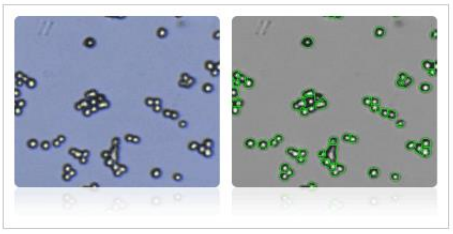

EKVX

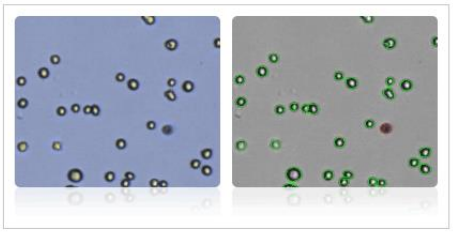

HOP-62

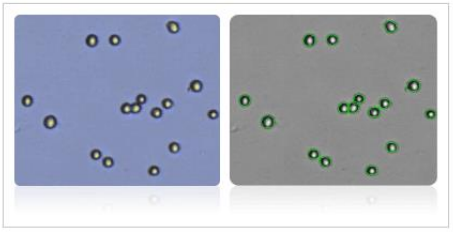

HOP-92

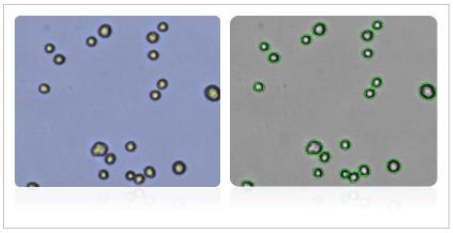

NCI-H226

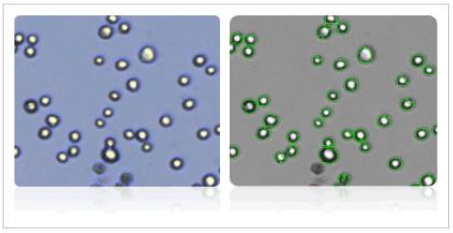

NCI-H23

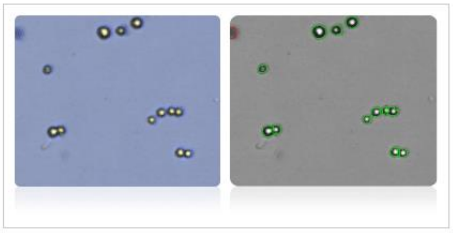

NCI-H322M

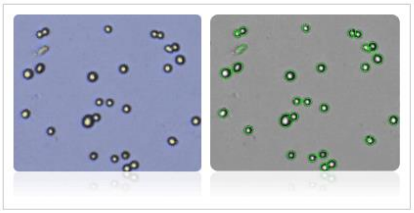

NCI-H460

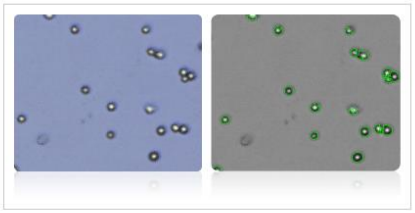

NCI-H522

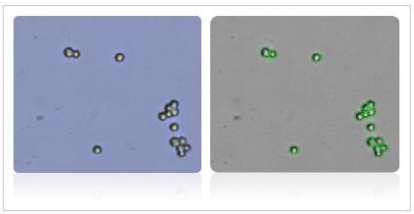

NCI-60 Melanoma Cell Lines

Shown below are stained trypan blue images and Cellometer counted images of NCI-60 melanoma cell lines. Counted live cells are outlined in green while the dead trypan blue positive cells are outlined in red.

LOX-IMVI

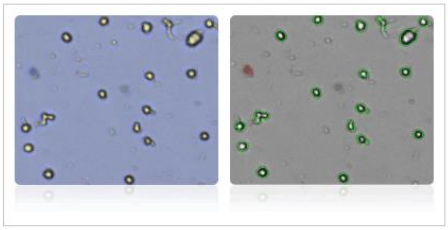

M14

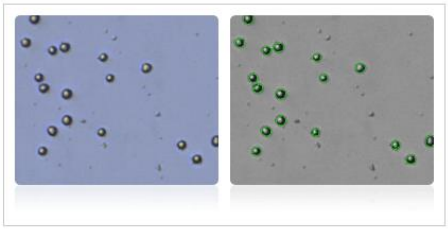

MALME-3M

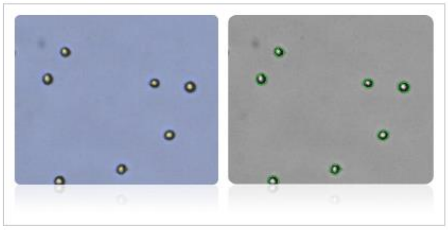

MDA-MB-435

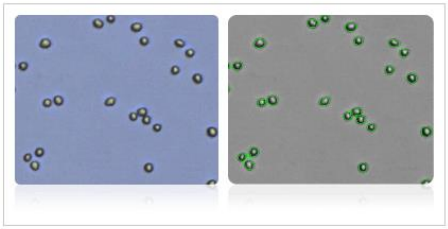

SK-MEL-2

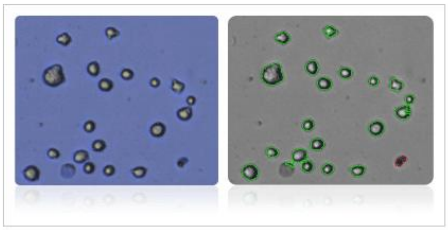

SK-MEL-28

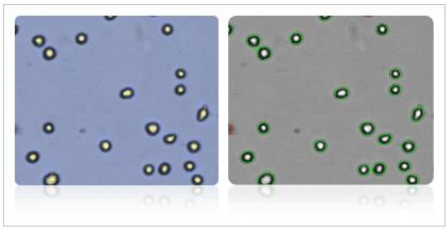

SK-MEL-5

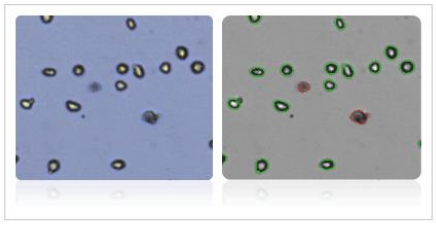

UACC-257

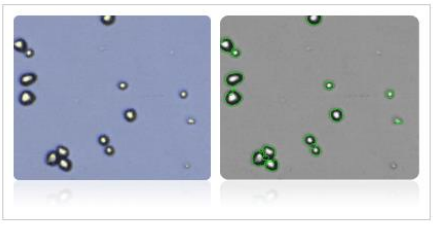

UACC-62

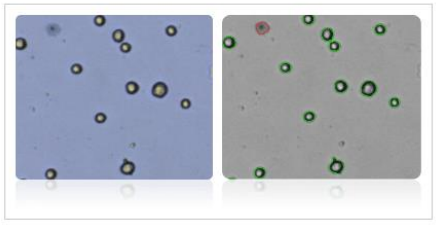

NCI-60 Ovarian Cell Lines

Shown below are stained trypan blue images and Cellometer counted images of NCI-60 ovarian cell lines. Counted live cells are outlined in green while the dead trypan blue positive cells are outlined in red.

IGROV1

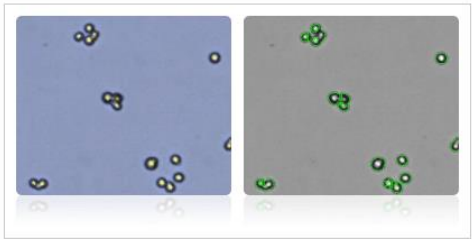

NCI/ADR-RES

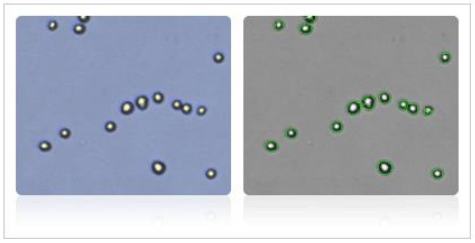

OVCAR-3

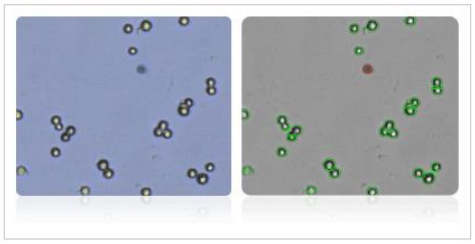

OVCAR-4

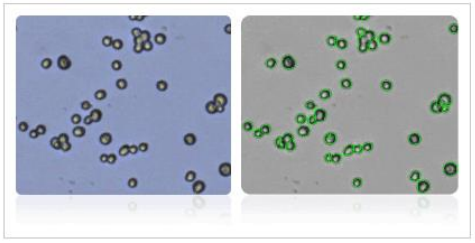

OVCAR-5

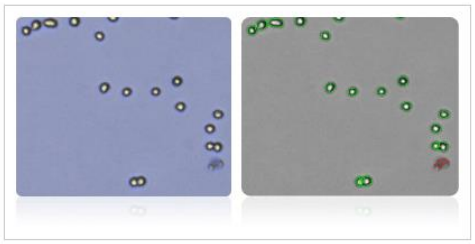

OVCAR-8

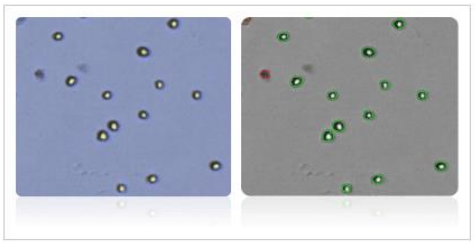

SK-OV-3